Journal of Research of the National Bureau of Standards Vol. 49, No. 3, September 1952 Research Paper 2350

Thermodynamics of Some Simple Sulfur-Containing Molecules

William H. Evans and Donald D. Wagman

The thermodynamic functions $(F^\circ - H_o^\circ)/T$, $(H^\circ - H_o^\circ)/T$, S° $(H^\circ - H_o^\circ)$, and C_p° are calculated to high temperatures for gaseous sulfur (monatomic and diatomic), sulfur monoxide, sulfur dioxide, sulfur trioxide, and hydrogen sulfide from molecular and spectroscopic data. Values of the heats of formation of the various atomic and molecular species are selected from published experimental data, and certain industrially important equilibria are calculated.

1. Introduction

The calculation of the thermodynamic properties of a number of simple gaseous sulfur-containing molecules has been carried out as a part of the Bureau's program on the compilation of tables of Selected Values of Chemical Thermodynamic Properties. The data on a large number of inorganic sulfur compounds had been critically evaluated by K. K. Kelley in 1936 [1].[1] Since that date, sufficient new information has been reported in the literature to warrant a reevaluation and recalculation of the properties of gaseous monatomic and diatomic sulfur, sulfur monoxide, sulfur dioxide, sulfur trioxide, and hydrogen sulfide.[2]

The calculations are divided into two parts: (a) Calculation of the thermodynamic functions, $(F^\circ - H_o^\circ)/T$, $(H^\circ - H_o^\circ)/T$, S°, $(H^\circ - H_o^\circ)$, and C_p°, for the various molecules in the ideal gaseous state; and (b) selection of "best" values for the heats of formation of the various compounds.

2. Units

The calorie used in these calculations is the thermochemical calorie, defined as 4.1840 abs j. The gas constant R is taken as 1.98719 cal/mole °K. The atomic weights used are H, 1.0080; O, 16.0000; S, 32.066 [2]. The standard states chosen for the elements are O_2 (g), H_2 (g), both in the ideal gas state at 1-atm pressure, and S (c, rhombic). As is customary, nuclear spin and isotopic mixing contributions to the entropy and free-energy functions have been omitted.

3. Calculation of the Thermodynamic Functions

The translational contributions to the free-energy function, $(F^\circ - H_o^\circ)/T$; the heat-content function, $(H^\circ - H_o^\circ)/T$; entropy, S°; and heat capacity, C_p°, were calculated for all the molecules, using the equations given by Wagman et al. [3].

For monatomic sulfur gas the only other contribution is from the electronic excitation. The electronic functions were calculated by direct summation of the energy levels, using term values and multiplicities (table 1) from Moore [4] and the conversion factor 1 cm^{-1}=2.85851 cal/mole. Only the five lowest levels are significant below 5,000°K.

TABLE 1. *Spectroscopic energy levels for* S (g)

Term designation	Energy	Multiplicity
	cm^{-1}	
$^3P_2$	0.0	5
$^3P_1$	396.8	3
$^3P_0$	573.6	1
$^1D_2$	9239.0	5
$^1S_0$	22181.4	1

For diatomic sulfur gas the rotational and vibrational constants selected by Herzberg [5] for the isotopic S_2^{32} molecule were corrected to the naturally occurring isotopic mixture, using the relations given by Herzberg [6]:

$$\sqrt{\frac{\mu}{\mu_i}}=\rho=\frac{\omega_{e_i}}{\omega_e} \quad \text{and} \quad x_{e_i}\omega_{e_i}=\rho^2 x_e\omega_e,$$

where ω_e is the fundamental equilibrium vibrational frequency, x_e the anharmonicity constant, and μ the reduced mass. These corrected values, ω_e=724.62 cm^{-1} and $x_e\omega_e$=2.844 cm^{-1}, were used to calculate approximate thermodynamic functions, assuming a rigid rotator of symmetry number 2 and an independent harmonic oscillator of frequency $\omega_e - 2x_e\omega_e$. In the rigid rotator calculation the equations given by Wagman et al. [3] were used. The harmonic oscillator calculations were carried out, using the tables of the Planck-Einstein functions calculated by Johnston, Savedoff, and Belzer [7]. The triplet electronic ground state required the addition of R ln 3 to the entropy and $-R$ ln 3 to the free-energy function.

Corrections for rotational stretching, vibrational anharmonicity, and rotational-vibrational interaction were calculated by using the second-order expansions given by Mayer and Mayer [8] at 300, 500, 1,000, 1,500, and 2,000°K; values at intermediate temperatures were obtained by graphical interpolation. At

[1] Figures in brackets indicate the literature references given at the end of this paper.

[2] The higher polymeric forms of sulfur, S_4, S_6, and S_8, are not included in this report. The necessary molecular data on S_4 and S_8 are not available; indeed the existence of S_4, which has been assumed in the interpretation of the most recent gas density measurements [53], is still unproved. Dr. George Guthrie of the U. S. Bureau of Mines, Bartlesville, Okla., has recently completed calculations of the thermodynamic functions of gaseous S_6 [54].

1,500°K these corrections amounted to −0.03 cal/mole °K for the free-energy function, 0.04 for the heat-content function, and 0.09 for the heat capacity.

For sulfur monoxide gas the rotational and vibrational constants taken from Herzberg [5] were corrected for isotopic composition to give the constants $\omega_e=1123.09$ cm^{-1} and $x_e\omega_e=6.109$ cm^{-1}, which were used in the rigid rotator-harmonic oscillator calculation. The triplet ground state required the addition of R ln 3 to the entropy and $-R$ ln 3 to the free-energy function. Anharmonicity and stretching corrections were evaluated as for diatomic sulfur gas. At 1,500° K these corrections were −0.02, 0.02, and 0.05 cal/mole °K for the free-energy function, heat-content function, and heat capacity, respectively.

For sulfur dioxide gas, the product of the moments of inertia was taken as the average of the microwave measurements of Dailey, Golden, and Wilson [9], who obtained 106.403×10^{-117} g^{3}cm^6, Sirvetz [10], 107.007×10^{-117} g^{3}cm^6, and Crable and Smith [11], 106.996×10^{-117} g^{3}cm^6. This product of the moments of inertia, 106.80×10^{-117} g^{3}cm^6, and the vibrational frequencies given by Herzberg [12] were used in a rigid rotator-harmonic oscillator calculation. As the available data do not permit the calculation of the anharmonicities, these were estimated from the relation, based on the data for sulfur monoxide, $X_{ij}=0.003\ (\nu_i+\nu_j)$, where X_{ij} is the anharmonicity arising from the interaction of the two fundamental frequencies ν_i and ν_j [13]. These were used to correct the rigid rotator-harmonic oscillator calculation by the method developed by Stockmayer, Kavanagh, and Mickley [13]. In this treatment the vibrational levels of a molecule with nondegenerate fundamental frequencies are taken as

$$\frac{E_v-E_0}{hc}=\sum v_i\nu_i-\sum_i X_{ii}(v_i-1)-\sum_{i<j}X_{ij}v_iv_j,$$

where ν_i are the observed fundamentals, in cm^{-1}, v_i are quantum numbers, and X_{ii} are the anharmonicities, in cm^{-1}, as calculated above. If the anharmonicities are considered to be small, their contribution to the Boltzmann factor can be expanded and the vibrational partition function Q_v readily summed:

$$Q_v=\Pi_i[1-e^{-u_i}]^{-1}\Big[1+\sum_{i\le j}f_{ij}+\ldots\Big],$$

where

$$u_i=hc\nu_i/kT$$
$$f_{ii}=2X_{ii}hc[kT(e^{u_i}-1)^2]^{-1}$$
$$f_{ij}=X_{ij}hc[kT(e^{u_i}-1)\ (e^{u_j}-1)]^{-1}.$$

This expression is equivalent to Q'_vQ_e, where Q'_v is the partition function for a harmonic oscillator with frequencies ν_i, and Q_e is the partition function containing the anharmonicities. Q_e may then be written as

$$Q_e=1+\sum_{i\le j}f_{ij}.$$

From this the correction to the free-energy function is given by $-F_e/T=R\ln Q_e$. Differentiation with respect to T gives the corrections to the heat-content function, $H_e/T=RT(d\ln Q_e/dT)$, and the heat capacity, $C_e=Rd(T^2d\ln Q_e/dT)/dT$. In this way corrections to the free energy function, heat content function, and heat capacity (amounting to −0.05, 0.10, and 0.23 cal/mole °K at 1,500°K, respectively,) were calculated at 300°, 500°, 1,000°, and 1,500°K; intermediate values were interpolated graphically.

The value 59.29 cal/mole °K for the entropy at 298.16 °K may be compared with 59.24 ±0.10 [14] obtained from the low-temperature calorimetric data of Giauque and Stephenson [15].

In the case of sulfur trioxide gas, the recent calculations of Stockmayer, Kavanagh, and Mickley [13] were checked and converted to the values of the fundamental constants used in this paper.

For hydrogen sulfide gas, the rigid rotator-harmonic oscillator calculations and corrections, made in the same way as for sulfur dioxide, were based upon the recent complete vibrational analysis of Allen, Cross, and King [16], which gives the anharmonicity terms. Moments of inertia were taken from the work of Allen, Cross, and Wilson [17], Grady, Cross, and King [18], and Hainer and King [19] and corrected to approximate equilibrium values by comparison with water vapor. These gave a product $I_xI_yI_z$ equal to 49.25×10^{-120} g^3 cm^6. A stretching correction, insignificant in the case of the other polyatomic molecules, was applied by using the method of Wilson [20]. The corrections to the rigid rotator-harmonic oscillator at 1,500 °K were −0.06, 0.08, and 0.22 cal/mole °K for the free-energy function, heat-content function, and heat capacity.

The calculated value of the entropy at 298.16 °K, 49.17 cal/mole °K, may be compared with the value [14] 49.11 ±0.10 obtained from the low-temperature calorimetric data of Clusius and Frank [21] and Giauque and Blue [22].

To correct values of $\Delta Hf°$ and $\Delta Ff°$ between 0 °K and 298.16 °K, it was necessary to know the thermodynamic functions at the latter temperature for crystalline rhombic sulfur. These were obtained by graphical integration of the heat-capacity data of Eastman and McGavock [23] as follows:

TABLE 2. *Thermodynamic functions for* S (c, rhombic)

	298.16° K	300° K
	cal/mole °K	*cal/mole °K*
$(F°-H°_0)/T$	−4.086	−4.097
$(H°-H°_0)/T$	3.532	3.544
$C°_p$	5.401	5.412

4. Selection of the "Best" Values for the Heats of Formation

The heat of formation of sulfur dioxide gas is based upon the combustion measurements of Eckman and Rossini [24], who burned excess sulfur in

oxygen under conditions precluding the formation of sulfur trioxide. Their data, when corrected for the atomic weight of sulfur, give for the selected value:

$$S\ (c, \text{rhombic}) + O_2\ (g) = SO_2\ (g)$$

$$\Delta H^\circ_{298.16} = -70.947 \pm 0.050 \text{ kcal/mole.}^3$$

The earlier combustion measurements at constant pressure of Thomsen [26], which yield $\Delta H^\circ_{298.16} = -71.04 \pm 0.50$ kcal/mole, confirm this value. Berthelot [27, 28], in two sets of combustions at constant volume using two different analytical techniques, obtained $\Delta H^\circ_{298.16} = -69.46 \pm 1.00$ kcal/mole. The data of Giran [29], who obtained heats of combustion at various high oxygen pressures, give $\Delta H^\circ_{298.16} = -70.5 \pm 0.8$ kcal/mole.

The value for the heat of formation of hydrogen sulfide gas is based upon: (a) the heat of combustion of hydrogen sulfide gas obtained by Zeumer and Roth [30] and by Thomsen [26], together with the value for the heat of formation of SO_2 (g) selected above and that for water given by Rossini et al. [25]; (b) the heat of reaction of H_2S (g) with a solution of iodine in aqueous hydriodic acid [26], combined with the appropriate values of the heats of formation given in Rossini et al.; and (c), the heat of reaction derived from the equilibrium measurements of Pollitzer [31] on the reaction of H_2S (g) with crystalline iodine to give hydrogen iodide gas and rhombic sulfur, together with the heat of formation of HI (g) given by Rossini et al. These results, as summarized in table 3, lead to

$$S\ (c, \text{rhombic}) + H_2\ (g) = H_2S\ (g)$$

$$\Delta H^\circ_{298.16} = -4.82 \pm 0.10 \text{ kcal/mole.}$$

TABLE 3. *Heat of formation of* H_2S (g)

Observer	Method	$\Delta H^\circ_{298.16}$
		kcal/mole
Thomsen [26]	Combustion of H_2S	[a] -2.61 ± 0.50
Thomsen [26]	Reaction with HI-I_2 (aqueous).	-4.82 ± 0.20
Pollitzer [31]	Reaction with I_2 (c)	-4.81 ± 0.20
Zeumer and Roth [30]	Combustion of H_2S	-4.82 ± 0.14

[a] Omitted in obtaining "best" value.

For sulfur trioxide several sets of high-temperature measurements of the equilibrium between sulfur dioxide, sulfur trioxide, and oxygen are available. These were combined with the appropriate free-energy functions [32] and the heat of formation of sulfur dioxide to calculate the values of ΔH°_0 for the reaction

$$2SO_2\ (g) + O_2\ (g) = 2SO_3\ (g)$$

and $\Delta Hf^\circ_{298.16}$ for sulfur trioxide gas given in table 4.

A value of -94.35 ± 0.12 kcal/mole for the heat of formation of sulfur trioxide gas was obtained from

TABLE 4. *Heats of dissociation of* SO_3 (g) [a]

Observer	Number of measurements	ΔH°_0	$\Delta Hf^\circ_{298.16}$ SO_3 (g)
		kcal	*kcal*
Bodländer and Koppen [33]	6	-46.28 ± 0.36	-94.87 ± 0.60
Knietsch [34]	11	-44.23 ± 0.50	-93.84 ± 0.80
Lunge and Reinhardt [35]	39	-45.25 ± 0.25	-94.36 ± 0.20
Bodenstein and Pohl [36]	49	-45.57 ± 0.04	-94.52 ± 0.04
Lucas [37]	7	-49.33 ± 0.65	-95.40 ± 1.40
Taylor and Lenher [40]	4	-45.45 ± 0.10	-94.46 ± 0.12
Kapustinskii and Shamovskii [38, 39]	11	-45.57 ± 0.08	-94.52 ± 0.07

[a] The uncertainties given for ΔH°_0 represent the probable error of the mean of the measurements. Those given for $\Delta Hf^\circ_{298.16}$, as elsewhere in this paper, are the estimated over-all uncertainties.

calorimetric measurements of Roth and coworkers [41–43] through a series of reactions involving the heat of solution of liquid sulfur trioxide in water [42], the heat of solution of gaseous sulfur dioxide in aqueous hydrogen peroxide [41], the heat of decomposition of hydrogen peroxide [41], the heat of dilution of sulfuric acid [25, 42], and the heat of vaporization of sulfur trioxide [25].

As the best value a weighted average was taken to give

$$S\ (c, \text{rhombic}) + 3/2\ O_2\ (g) = SO_3\ (g)$$

$$\Delta H^\circ_{298.16} = -94.47 \pm 0.07 \text{ kcal.}$$

Because of the complex polymerization in sulfur vapor below 1,000°K [1, 53], the best value for the heat of formation of diatomic sulfur gas is obtained from measurements of dissociation of hydrogen sulfide at high temperatures, where sulfur exists primarily as S_2. Three series of such measurements are available [44, 45, 46]. All were carried out by determining the pressure of the hydrogen formed by the dissociation of hydrogen sulfide, using a platinum membrane. In addition, Preuner and Schupp [45] measured the increase in total pressure of a small sample of H_2S when heated in a sealed bulb; these results give a ΔH°_0 differing less than 0.02 kcal from the over-all average. Combination of the equilibrium constants calculated from these measurements with the appropriate free-energy functions [32] gives the values for the heat of dissociation

$$H_2S\ (g) = H_2\ (g) + 1/2\ S_2\ (g)$$

tabulated in table 5.

TABLE 5. *Heat of dissociation of* H_2S

Observer	Number of measurements	ΔH°_0 [a]
		kcal
Preuner [44]	5	19.506±0.040
Preuner and Schupp [45]	20	19.528±0.031
Randall and Bichowsky [46]	4	19.557±0.044

[a] The uncertainties given for ΔH°_0 represent the probable error of the mean of the measurements.

[3] The uncertainties in ΔH given in this section of the paper represent the present writers' best estimates of the overall uncertainties in the values.

The weighted average 19.53 ±0.02 kcal, the heat of formation of hydrogen sulfide selected previously, and the appropriate heat-content functions [32] give the heat of formation of diatomic sulfur gas:

$$2S\ (c,\ rhombic) = S_2\ (g)$$

$$\Delta H^\circ_{298.16} = 30.84 \pm 0.15\ kcal.$$

The best value for the heat of formation of monatomic sulfur gas appears to be that derived from spectroscopic studies. From a study of predissociation, Olsson [47] selected a value of 3.6 electron volts (ev) as an upper limit for the dissociation energy of diatomic sulfur gas into normal ^3P sulfur atoms.[4] Considering all such data and by comparison with molecules of similar structure Goldfinger, Jeunehomme and Rosen [48] selected 4.41 ev for the dissociation into one normal ^3P atom and one excited ^1D atom. Herzberg [5] favored a value of 3.6 ev or lower for the dissociation into normal atoms, and Gaydon [49], after summarizing the evidence, assumed that the value of 4.41 ev from predissociation measurements corresponds to the true dissociation energy. If the value 4.41 ev is selected as dissociation into one normal atom and one excited ^1D atom, as favored by Herzberg, then the dissociation energy is

$$S_2\ (g) = 2S\ (^3P)\ (g)$$

$$\Delta H^\circ_0 = 75.3 \pm 0.5\ kcal.^5$$

Partial confirmation of this lower value is furnished by high-temperature gas-density measurements. Nernst [50], using the Victor-Meyer method at 1,900 to 2,300 °K, obtained 71±8 kcal for ΔH°_0; von Wartenberg [51] in the same way obtained 75± 10 kcal. Using the spectroscopic value of ΔH°_0 and the value for diatomic sulfur gas,

$$S\ (c,\ rhombic) = S\ (g)$$

$$\Delta H^\circ_{298.16} = 53.54 \quad \pm 0.50 \quad kcal.$$

Additional confirmation is afforded by measurements of Bjerrum [52] on the heat of dissociation of hydrogen sulfide gas at 2,900 to 3,200 °K. For the dissociation to monatomic sulfur and diatomic hydrogen gases he found $\Delta H^\circ_0 = 51 \pm 15$ kcal, which leads to a value of $\Delta Hf^\circ_{298.16}$ for S (g) of 56 ±15 kcal.

The spectroscopic data on sulfur monoxide gas do not lead to a definite value for the dissociation of the molecule because of the uncertainty in the energy states of the dissociation products. Herzberg [5] favors dissociation into $S(^1D)+O(^3P)$, which leads to a dissociation energy of 4.001 ev. Gaydon [49] assumes dissociation to $S(^1P)+O(^1P)$, with a dissociation energy greater by the difference $S(^1D)-S(^3P)$, or 5.146 ev. (Dissociation into the third simple combination of products, $S(^3P)+O(^1D)$, appears unlikely because of the greater energy differences involved.) The lower value was selected because the dissociation is apparently of the same type as that of S_2 and O_2. Combining this value with the values for gaseous atomic sulfur and oxygen [25], the heat of formation of sulfur monoxide is calculated

$$S(c,\ rhombic) + 1/2O_2(g) = SO(g)$$

$$\Delta H^\circ_{298.16} = 19.30 \pm 0.50\ kcal.^6$$

In order to extend the useful range of the data on the reactions of formation, the values of ΔHf° selected above were converted to values based on $S_2(g)$ as the standard reference state for sulfur. The values of the heat of formation, ΔHf°; free energy of formation, ΔFf°; and logarithm of the equilibrium constant of formation, $\log_{10} Kf$, were then calculated at temperatures up to 1,500° K by the relations

$$\Delta Hf^\circ_T = \Delta Hf^\circ_0 + \Delta(H^\circ_T - H^\circ_0)$$

$$\Delta Ff^\circ_T = \Delta Hf^\circ_0 + T\Delta[(F^\circ - H^\circ_0)/T]$$

$$\log_{10} Kf = -(\Delta Ff^\circ_T / 4.57567\,T).$$

The values calculated in this manner, as well as the thermodynamic functions for the six gaseous molecules considered, are given in tables 6 to 12.

As examples of the applications of these tables, three industrially important reactions were considered. Figure 1 shows the equilibrium composition obtained when gaseous hydrogen sulfide decomposes

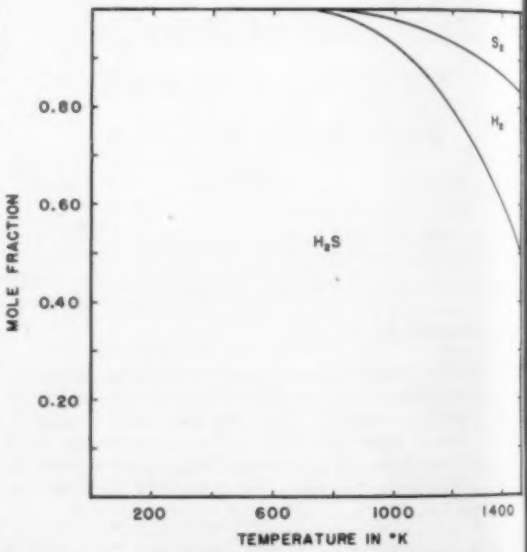

FIGURE 1. *Equilibrium composition for a $2H_2$:S_2 mixture at 1-atmosphere pressure as a function of temperature.*

The vertical width of a band represents the mole fraction of the component present.

[4] 1 ev/molecule = 23060.5 cal/mole.

[5] Since this report was written measurements of the heat of formation of HS (g) by Franklin and Lumpkin [55] and of the dissociation energy D_0 for HS by Porter [56] indicate that the higher value of 4.41 ev for D_0 of S_2 is probably the correct value. If this value is accepted, the values of ΔHf° and ΔFf° for S (g) will be increased by 13.2 kcal. with corresponding changes in $\log_{10} Kf$.

[6] As indicated in footnote 5, the best value of D_0 (S_2) appears to be 4.41 ev. By reasoning as above, the higher value of 5.146 ev appears more likely for D_0 of SO. If this value is accepted, as well as 4.41 ev for D_0 of S_2, the values of ΔHf° and ΔFf° for SO (g) will become more negative by 13.2 kcal, with corresponding changes in $\log_{10} Kf$.

der a tot l pressure of 1 atm. The ordinate gives e mole f ction of each component; the abscissa e absolu e temperature. The equilibrium com- sition wa obtained by first calculating the equili- ium cons ant for the reaction

$$H_2S\ (g)=H_2\ (g)+1/2S_2\ (g)$$

various temperatures, using the relation

$$-4.57567\ \log_{10} K=\Delta F^\circ_T/T$$

d the values of the free energies of formation given the present paper and in Rossini et al. [32]. The lues of K were then used to obtain the equilibrium mposition in the usual way. The side reactions

$$S_2\ (g)=2S\ (g)$$

$$H_2\ (g)=2H\ (g)$$

$$H_2S\ (g)=HS\ (g)+H\ (g)$$

$$2S_2\ (g)=S_4\ (g).$$[7]

ere also considered. After the values for H_2 and were obtained, they were used to calculate the ncentrations of the other possible products; in no se were the side reactions significant.

Figure 2 shows the equilibrium composition ob- ined in the gaseous decomposition of sulfur trioxide

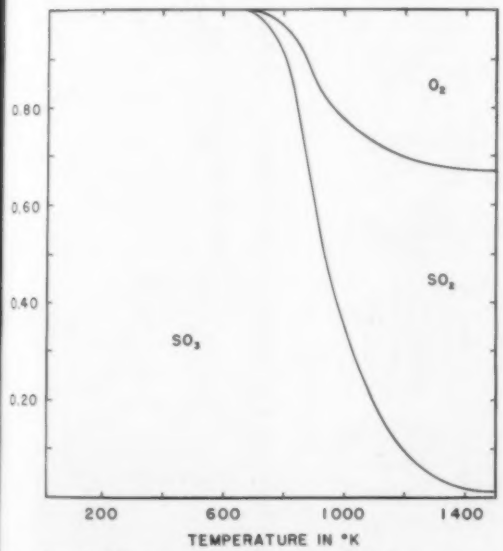

IGURE 2. *Equilibrium composition for a $3O_2$:S_2 mixture at 1-atmosphere pressure as a function of temperature.*

The vertical width of a band represents the mole fraction of the component esent.

[7] For the calculation of the equilibrium compositions of the various sulfur ecies the data of Braune, Peter, and Neveling [53] were used.

at a total pressure of 1 atm. Possible side reactions considered were

$$SO_2\ (g)=SO\ (g)+1/2O_2\ (g)$$

$$2SO_2\ (g)=S_2\ (g)+2O_2\ (g)$$

$$SO_3\ (g)=SO_2\ (g)+O\ (g);$$

all were unimportant.

Figure 3 shows the equilibrium composition of the vapor obtained from mixing two molecular volumes of hydrogen sulfide and one of sulfur dioxide at a total final pressure of 1 atm. At temperatures below about 500° K liquid sulfur separates [1] with a corresponding increase in the concentration of the water vapor. Side reactions considered, in addition to those listed above, were

$$3S_2\ (g)=S_6\ (g)$$

$$4S_2\ (g)=S_8\ (g)$$

$$H_2O\ (g)=OH\ (g)+H\ (g).$$

Of these, only the sulfur polymerization was significant; for this, the results of Braune, Peter, and Noveling [53] were used, although their data are not completely satisfactory. These results indicate that recovery of sulfur from hydrogen sulfide gas by partial oxidation should be feasible.

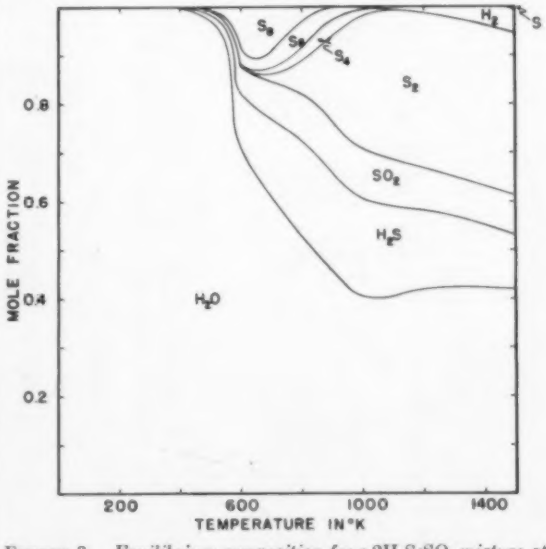

FIGURE 3. *Equilibrium composition for a $2H_2S$:SO_2 mixture at 1-atmosphere pressure as a function of temperature.*

The vertical width of a band represents the mole fraction of the component present.

TABLE 6. *Heat, free energy, and equilibrium constant of formation, free-energy function, heat-content function, entropy, heat content (or enthalpy), and heat capacity for* S (g)

Reference states for elements, used for calculating $\Delta Hf°$, $\Delta Ff°$, and log Kf: S_2 (g).

Property	Units	Temperature in °K														
		0	298.16	300	400	500	600	700	800	900	1,000	1,100	1,200	1,300	1,400	1,500
$\Delta Hf°$	kcal/mole	37.6	38.12	38.12	38.29	38.42	38.54	38.64	38.72	38.80	38.88	38.95	39.02	39.08	39.14	39.20
$\Delta Ff°$	kcal/mole	37.6	34.29	34.27	32.96	31.61	30.24	28.85	27.45	26.03	24.61	23.17	21.74	20.21	18.85	17.40
$\log_{10}Kf$			−25.134	−24.965	−18.008	−13.817	−11.015	−9.007	−7.499	−6.321	−5.378	−4.603	−3.959	−3.398	−2.943	−2.535
$(F°-H_0°)/T$	cal/deg mole	0	−34.7499	−34.7828	−36.3295	−37.5384	−38.5271	−39.3608	−40.0407	−40.7132	−41.2764	−41.7844	−42.2466	−42.6703	−43.0513	−43.4244
$(H°-H_0°)/T$	cal/deg mole	0	5.3364	5.3384	5.4033	5.4237	5.4177	5.4009	5.3803	5.3590	5.3383	5.3188	5.3007	5.2841	5.2691	5.2556
$S°$	cal/deg mole	0	40.0463	40.1212	41.7358	42.9621	43.9448	44.7617	45.4610	46.0722	46.6147	47.1032	47.5473	47.9544	48.3304	48.6800
$H°-H_0°$	cal/mole	0	1591.1	1601.5	2162.5	2711.8	3250.6	3780.6	4304.2	4823.1	5338.3	5850.7	6360.8	6869.3	7376.7	7883.4
$C_p°$	cal/deg mole	0	5.6585	5.6574	5.5534	5.4358	5.3398	5.2661	5.2107	5.1685	5.1363	5.1116	5.0928	5.0789	5.0393	5.0337

TABLE 7. *Free-energy function, heat-content function, entropy, heat content (or enthalpy), and heat capacity for* S (g)

Property	Units	Temperature in °K									
		1,600	1,700	1,800	1,900	2,000	2,100	2,200	2,300	2,400	2,500
$(F°-H_0°)/T$	cal/deg mole	−43.7631	−44.0806	−44.3795	−44.6617	−44.9290	−45.1830	−45.4249	−45.6560	−45.8770	−46.0889
$(H°-H_0°)/T$	cal/deg mole	5.2435	5.2328	5.2235	5.2155	5.2087	5.2031	5.1986	5.1951	5.1927	5.1911
$S°$	cal/deg mole	49.0066	49.3134	49.6030	49.8772	50.1377	50.3861	50.6235	50.8511	51.0697	51.2800
$H°-H_0°$	cal/mole	8389.6	8895.8	9402.3	9909.4	10417.4	10926.5	11436.9	11948.7	12462.5	12977.8
$C_p°$	cal/deg mole	5.0618	5.0632	5.0578	5.0752	5.0852	5.0974	5.1115	5.1272	5.1442	5.1623
Property	Units	2,750	3,000	3,250	3,500	3,750	4,000	4,250	4,500	4,750	5,000
$(F°-H_0°)/T$	cal/deg mole	−46.5837	−47.0354	−47.4514	−47.8371	−48.1970	−48.5343	−48.8518	−49.1518	−49.4363	−49.7058
$(H°-H_0°)/T$	cal/deg mole	5.1906	5.1943	5.2010	5.2099	5.2204	5.2318	5.2436	5.2555	5.2673	5.2787
$S°$	cal/deg mole	51.7743	52.2297	52.6524	53.0470	53.4174	53.7661	54.0954	54.4073	54.7036	54.9855
$H°-H_0°$	cal/mole	14274.2	15582.9	16903.2	18234.6	19576.5	20927.2	22285.3	23649.8	25019.7	26393.5
$C_p°$	cal/deg mole	5.2098	5.2581	5.3045	5.3472	5.3854	5.4185	5.4464	5.4694	5.4878	5.5021

TABLE 8. *Heat, free energy, and equilibrium constant of formation, free-energy function, heat-content function, entropy, heat content (or enthalpy), and heat capacity for* S_2 (g)

Reference states for elements, used for calculating $\Delta Hf°$, $\Delta Ff°$, and log Kf: S_2 (g).

Property	Units	Temperature in °K														
		0	298.16	300	400	500	600	700	800	900	1,000	1,100	1,200	1,300	1,400	1,500
$\Delta Hf°$	kcal/mole	0	0	0	0	0	0	0	0	0	0	0	0	0	0	0
$\Delta Ff°$	kcal/mole	0	0	0	0	0	0	0	0	0	0	0	0	0	0	0
$\log_{10}Kf$			0	0	0	0	0	0	0	0	0	0	0	0	0	0
$(F°-H_0°)/T$	cal/deg mole	0	−47.33	−47.37	−49.47	−51.13	−52.52	−53.72	−54.78	−55.72	−56.57	−57.34	−58.06	−58.72	−59.34	−59.92
$(H°-H_0°)/T$	cal/deg mole	0	7.18	7.18	7.38	7.56	7.71	7.84	7.95	8.04	8.11	8.18	8.24	8.29	8.34	8.38
$S°$	cal/deg mole	0	54.51	54.55	56.85	58.69	60.23	61.56	62.73	63.76	64.68	65.52	66.30	67.01	67.68	68.30
$H°-H_0°$	cal/mole	0	2141	2154	2952	3780	4626	5488	6360	7236	8110	8980	9848	10717	11676	12570
$C_p°$	cal/deg mole	0	7.76	7.77	8.14	8.39	8.54	8.63	8.68	8.71	8.73	8.75	8.76	8.77	8.78	8.79

Bind in

(10/13/52)

ERRATA TO ACCOMPANY RESEARCH PAPER 2350
(Sept. 1952 NBS Journal of Research)

In table 10 the values for 0 to 1,500°K should read:

T°K	ΔHf°	ΔFf°	$\log_{10}$ Kf
0		-85.746	---
298.16		-81.308	59.5974
300	-86.367	-81.276	59.2086
400		-79.56	43.469
500		-77.83	34.017
600		-76.08	27.710
700		-74.32	23.204
800		-72.57	19.824
900		-70.81	17.196
1,000		-69.06	15.094
1,100		-67.33	13.376
1,200		-65.58	11.943
1,300		-63.83	10.731
1,400		-62.08	9.691
1,500		-60.35	8.793

TABLE 9. *Thermochemical equilibrium constants for the reaction* $\frac{1}{2}H_2 + \frac{1}{2}F_2 = HF$

Reference states for elements, used for calculating ΔH°_f, S°, and the K_p functions

Temperature in °K

TABLE 9. *Heat, free energy, and equilibrium constant of formation, free-energy function, heat-content function, entropy, heat content (or enthalpy), and heat capacity for* [illegible]

Reference states for elements, used for calculating $\Delta Hf°$, $\Delta Ff°$, and log Kf: O₂ (g); S₂ (g).

Property	Units	Temperature in °K														
		0	298.16	300	400	500	600	700	800	900	1,000	1,100	1,200	1,300	1,400	1,500
$\Delta Hf°$	kcal/mole	3.9	3.88	3.88	3.87	3.86	3.86	3.86	3.87	3.87	3.87	3.87	3.87	3.87	3.87	3.86
$\Delta Ff°$	kcal/mole	3.9	3.49	3.49	3.36	3.24	3.11	2.99	2.87	2.74	2.61	2.48	2.35	2.23	2.11	1.99
$\log_{10} Kf$			−2.558	−2.542	−1.836	−1.416	−1.133	−0.934	−0.784	−0.665	−0.570	−0.493	−0.428	−0.375	−0.329	−0.290
$(F°-H°_0)/T$	cal/deg mole	0	−46.07	−46.10	−48.13	−49.73	−51.05	−52.20	−53.20	−54.10	−54.92	−55.67	−56.36	−56.99	−57.58	−58.14
$(H°-H°_0)/T$	cal/deg mole	0	7.01	7.01	7.11	7.23	7.36	7.48	7.59	7.69	7.77	7.85	7.92	7.98	8.04	8.09
$S°$	cal/deg mole	0	53.08	53.11	55.24	56.96	58.42	59.68	60.79	61.79	62.69	63.52	64.28	64.97	65.62	66.23
$H°-H°_0$	cal/mole	0	2040	2103	2844	3615	4416	5236	6072	6921	7770	8635	9504	10374	11256	12135
$C°_p$	cal/deg mole	0	7.23	7.24	7.57	7.87	8.11	8.29	8.42	8.52	8.60	8.66	8.71	8.75	8.79	8.82

TABLE 10. *Heat, free energy, and equilibrium constant of formation, free-energy function, heat-content function, entropy, heat content (or enthalpy), and heat capacity for* SO_2(g)

Reference states for elements, used for calculating $\Delta Hf°$, $\Delta Ff°$, and log Kf: O₂ (g); S₂ (g).

Property	Units	Temperature in °K														
		0	298.16	300	400	500	600	700	800	900	1,000	1,100	1,200	1,300	1,400	1,500
$\Delta Hf°$	kcal/mole	−85.746	−86.367	−86.387	−86.48	−86.55	−86.58	−86.59	−86.59	−86.57	−86.55	−86.51	−86.48	−86.43	−86.39	−86.35
$\Delta Ff°$	kcal/mole	−85.746	−87.578	−87.592	−88.38	−89.24	−90.17	−91.15	−92.18	−93.27	−94.41	−95.60	−96.82	−98.09	−99.37	−100.71
$\log_{10} Kf$			64.1935	63.8100	48.288	39.006	32.844	28.458	25.182	22.649	20.633	18.994	17.633	16.490	15.512	14.673
$(F°-H°_0)/T$	cal/deg mole	0	−50.84	−50.89	−53.38	−55.40	−57.11	−58.61	−59.96	−61.18	−62.30	−63.34	−64.30	−65.20	−66.04	−66.84
$(H°-H°_0)/T$	cal/deg mole	0	8.45	8.46	8.84	9.22	9.60	9.94	10.24	10.51	10.75	10.97	11.16	11.34	11.50	11.64
$S°$	cal/deg mole	0	59.29	59.35	62.22	64.62	66.71	68.55	70.20	71.69	73.05	74.31	75.46	76.54	77.54	78.48
$H°-H°_0$	cal/mole	0	2519	2538	3536	4610	5760	6958	8192	9459	10750	12067	13392	14742	16100	17460
$C°_p$	cal/deg mole	0	9.53	9.54	10.39	11.12	11.71	12.17	12.53	12.82	13.03	13.20	13.35	13.47	13.57	13.65

TABLE 11. *Heat, free energy, and equilibrium constant of formation, free-energy function, heat-content function, entropy, heat content (or enthalpy), and heat capacity for* SO_3(g)

Reference states for elements, used for calculating $\Delta Hf°$, $\Delta Ff°$, and log Kf: O₂ (g); S₂ (g).

Property	Units	Temperature in °K														
		0	298.16	300	400	500	600	700	800	900	1,000	1,100	1,200	1,300	1,400	1,500
$\Delta Hf°$	kcal/mole	−108.49	−109.89	−109.89	−110.05	−110.08	−110.00	−109.86	−109.67	−109.44	−109.16	−108.86	−108.54	−108.19	−107.82	−107.43
$\Delta Ff°$	kcal/mole	−108.49	−98.09	−98.02	−94.03	−90.02	−85.02	−82.04	−78.08	−74.15	−70.24	−66.37	−62.51	−58.68	−54.87	−51.08
$\log_{10} Kf$			71.899	71.407	51.375	39.347	31.332	25.614	21.330	18.006	15.351	13.186	11.384	9.865	8.565	7.442
$(F°-H°_0)/T$	cal/deg mole	0	−51.89	−51.95	−54.76	−57.14	−59.26	−61.18	−62.94	−64.57	−66.08	−67.50	−68.83	−70.09	−71.28	−72.40
$(H°-H°_0)/T$	cal/deg mole	0	9.30	9.32	10.25	11.18	12.04	12.80	13.48	14.08	14.63	15.12	15.56	15.96	16.33	16.67
$S°$	cal/deg mole	0	61.19	61.27	65.01	68.32	71.30	73.98	76.42	78.65	80.71	82.62	84.39	86.05	87.61	89.07
$H°-H°_0$	cal/mole	0	2773	2796	4100	5590	7224	8960	10784	12672	14630	16632	18672	20748	22862	25005
$C°_p$	cal/deg mole	0	12.10	12.13	14.06	15.66	16.90	17.86	18.61	19.23	19.76	20.21	20.61	20.96	21.28	21.58

TABLE 12. *Heat, free energy, and equilibrium constant of formation, free-energy function, heat-content function, entropy, heat content (or enthalpy), and heat capacity for* H_2S(g)

Reference states for elements, used for calculating $\Delta Hf°$, $\Delta Ff°$, and log Kf: H₂ (g); S₂ (g).

Property	Units	Temperature in °K														
		0	298.16	300	400	500	600	700	800	900	1,000	1,100	1,200	1,300	1,400	1,500
$\Delta Hf°$	kcal/mole	−19.53	−20.24	−20.24	−20.50	−20.74	−20.95	−21.13	−21.27	−21.38	−21.45	−21.50	−21.54	−21.55	−21.55	−21.54
$\Delta Ff°$	kcal/mole	−19.53	−17.47	−17.45	−16.48	−15.44	−14.36	−13.25	−12.11	−10.97	−9.80	−8.64	−7.47	−6.29	−5.11	−3.94
$\log_{10} Kf$			12.805	12.712	9.004	6.749	5.231	4.137	3.308	2.664	2.142	1.717	1.360	1.057	0.798	0.574
$(F°-H°_0)/T$	cal/deg mole	0	−41.17	−41.21	−43.52	−45.34	−46.85	−48.15	−49.31	−50.35	−51.29	−52.17	−52.99	−53.75	−54.47	−55.16
$(H°-H°_0)/T$	cal/deg mole	0	8.00	8.00	8.09	8.21	8.37	8.54	8.72	8.91	9.10	9.29	9.47	9.65	9.82	9.98
$S°$	cal/deg mole	0	49.17	49.21	51.61	53.55	55.22	56.69	58.03	59.26	60.39	61.46	62.46	63.40	64.29	65.14
$H°-H°_0$	cal/mole	0	2385	2400	3236	4105	5022	5978	6976	8019	9100	10219	11364	12545	13748	14970
$C°_p$	cal/deg mole	0	8.19	8.20	8.53	8.93	9.35	9.78	10.21	10.62	11.03	11.34	11.64	11.92	12.16	12.37

5. References

[1] K. K. Kelley, Contributions to the data on theoretical metallurgy. [VII] The thermodynamic properties of sulfur and its inorganic compounds, U. S. Bur. Mines Bul. **406** (1936).
[2] E. Wichers, J. Am. Chem. Soc. **72,** 1431 (1950).
[3] D. D. Wagman, J. E. Kilpatrick, W. J. Taylor, K. S. Pitzer, and F. D. Rossini, J. Research NBS **34,** 143 (1945) RP1634.
[4] C. E. Moore, Atomic energy levels, [I] NBS Circular 467 (U. S. Government Printing Office, Washington, D. C., 1949).
[5] G. Herzberg, Molecular spectra and molecular structure. [I] Spectra of diatomic molecules, 2d ed., 499–581 (D. Van Nostrand Co., New York, N. Y., 1950).
[6] See pages 141 to 144 of [5].
[7] H. L. Johnston, L. Savedoff, and J. Belzer, Contributions to the thermodynamic functions by a Planck-Einstein oscillator in one degree of freedom (Office of Naval Research, Washington, D. C., 1949).
[8] J. E. Mayer and M. G. Mayer, Statistical mechanics, p. 160–166 (John Wiley & Sons, New York, N. Y., 1940).
[9] B. P. Dailey, S. Golden, and E. B. Wilson, Jr., Phys. Rev. **72,** 871 (1951).
[10] M. H. Sirvetz, J. Chem. Phys. **19,** 938 (1951).
[11] G. F. Crable and W. V. Smith, J. Chem. Phys. **19,** 502 (1951).
[12] G. Herzberg, Molecular spectra and molecular structure. [II] Infrared and Raman spectra of polyatomic molecules (D. Van Nostrand Co., New York, N. Y., 1945).
[13] W. H. Stockmayer, G. M. Kavanagh, and H. S. Mickley, J. Chem. Phys. **12,** 408 (1944).
[14] K. K. Kelley, Contributions to the data on theoretical metallurgy. [XI] Entropies of inorganic substances. Revision (1948) of data and methods of calculation, U. S. Bur. Mines Bul. **477** (1950).
[15] W. F. Giauque and C. C. Stephenson, J. Am. Chem. Soc. **60,** 1389 (1938).
[16] H. C. Allen, Jr., P. C. Cross, and G. W. King, J. Chem. Phys. **18,** 1412 (1950).
[17] H. C. Allen, Jr., P. C. Cross, and M. K. Wilson, J. Chem. Phys. **18,** 691 (1950).
[18] H. S. Grady, P. C. Cross, and G. W. King, Phys. Rev. **75,** 1450 (1949).
[19] R. M. Hainer and G. W. King, J. Chem. Phys. **15,** 89 (1947).
[20] E. B. Wilson, Jr., J. Chem. Phys. **4,** 526 (1936).
[21] K. Clusius and A. Frank, Z. physik. Chem. **B34,** 420 (1936).
[22] W. F. Giauque and R. W. Blue, J. Am. Chem. Soc. **58,** 831 (1936).
[23] E. D. Eastman and W. C. McGavock, J. Am. Chem. Soc. **59,** 145 (1937).
[24] J. R. Eckman and F. D. Rossini, BS J. Research **3,** 597 (1929) RP111.
[25] F. D. Rossini, D. D. Wagman, W. H. Evans, S. Levine, and I. Jaffe, Selected values of chemical thermodynamic properties, NBS Circular 500 (U. S. Government Printing Office, Washington, D. C., 1952).
[26] J. Thomsen, Thermochemische Untersuchungen, I-IV (Barth, Leipzig, 1882–1886).
[27] M. Berthelot, Ann. chim. phys. [5] **13,** 1 (1878).
[28] M. Berthelot, Ann. chim. phys. [5] **22,** 422 (1881).
[29] H. Giran, Compt. rend. **139,** 1219 (1904).
[30] H. Zeumer and W. A. Roth, Z. Elektrochem. **40,** 7 (1934).
[31] F. Pollitzer, Z. anorg. Chem. **64,** 121 (1909).
[32] Thermodynamic functions for O_2 and H_2 were taken from Series III tables of the NBS tables of selected values of chemical thermodynamic properties.
[33] G. Bodländer and K. Koppen. Z. Elektrochem. **9,** 7 (1903).
[34] R. Knietsch, Ber. V Kong. angew. Chem. **I,** 614 (1903).
[35] G. Lunge and K. Reinhardt, Z. angew. Chem. **31,** 1 (1904).
[36] M. Bodenstein and W. Pohl, Z. Elektrochem. **11,** 3 (1905).
[37] R. Lucas, Z. Elektrochem. **11,** 457 (1905).
[38] A. F. Kapustinskiĭ and L. Shamovskiĭ, Acta Physicochim. U. R. S. S. **4,** 791 (1936).
[39] A. F. Kapustinskiĭ and L. Shamovskiĭ, Trudy Vsesoyuz. Nauch. Issledvatel'. Inst. Mineral'. Syr'ya. No. 1 55 (1936).
[40] G. B. Taylor and S. Lenher, Z. physik. Chem. **Bodenstein-Festband,** 30 (1931).
[41] W. A. Roth, R. Grau, and A. Meichsner, Z. anorg. Chem. **193,** 161 (1930).
[42] R. Grau and W. A. Roth, Z. anorg. Chem. **186,** 173 (1930).
[43] R. Grau and W. A. Roth, Z. anorg. Chem. **186,** 1 (1930).
[44] G. Preuner, Z. anorg. Chem. **55,** 279 (1907).
[45] G. Preuner and W. Schupp, Z. physik. Chem. **68,** 1 (1910).
[46] M. Randall and F. R. Bichowsky, J. Am. Chem. Soc. **40,** 368 (1918).
[47] E. Olsson, Z. Physik **100,** 656 (1936).
[48] P. Goldfinger, W. Jeunehomme, and B. Rosen, Nature **138,** 205 (1936).
[49] A. G. Gaydon, Dissociation energies and spectra of diatomic molecules, p. 194–196 (Chapman and Hall, London, 1947).
[50] W. Nernst, Z. Elektrochem. **9,** 622 (1903).
[51] H. von Wartenberg, Z. anorg. Chem. **56,** 320 (1908).
[52] N. Bjerrum, Z. physik. Chem. **81,** 281 (1912).
[53] H. Braune, S. Peter, and V. Neveling, Z. Naturforsch. **6a,** 32 (1951).
[54] Private communication from Dr. George Guthrie, Jr.
[55] J. L. Franklin and H. E. Lumpkin, J. Am. Chem. Soc. **74,** 1023 (1952).
[56] G. Porter, Discussions Faraday Soc. No. **9,** 60 (1950).

WASHINGTON, May 14, 1952.

Journal of Research of the National Bureau of Standards Vol. 49, No. 3, September 1952 Research Paper 2351

A Correlation of Polarized Light Extinctions With Crystal Orientation in 70 Nickel–30 Copper Alloy

H. C. Vacher

After etching 70 nickel-30 copper alloy to produce an optically anisotropic surface, the orientations of 12 crystals were determined by the twin-boundary method, and the positions of polarized light extinctions (obtained at normal incidence with crossed nicols) were measured. A comparison of the orientations with the positions of the extinctions showed that one was near the cubic pole farthest from the surface normal. Little or no extinction was obtained when a (100) or (111) plane was nearly parallel to the surface. Study of the results indicated that the optical anisotropy probably was caused by parallel furrows formed by the tendency of the etching reagent to develop etch pits whose facets were parallel to cubic planes.

1. Introduction

Previous work by D. H. Woodard [1][1] at the National Bureau of Standards showed that the surface of isotropic Monel, the 70 nickel-30 copper alloy, was optically anisotropic after the surface had been polished electrolytically and etched with "Monel contrast solution" [2]. It was noted that extinctions obtained at normal incidence, with crossed nicols, were not uniform over a grain in a specimen that had been deformed plastically as it was for a grain in an annealed specimen. This nonuniform extinction of individual grains was interpreted as indicating differences in orientation resulting from inhomogeneous strain.

The brilliant contrast of the grains and sharpness of the extinctions suggested that polarized light might be useful in determining the orientation of individual crystals. Accordingly, a study was undertaken in order to obtain quantitative data on the relation of extinctions to crystalline orientation.

2. Procedures and Results

Coarse-grained Monel was required so that individual crystals could be identified easily after several polishing and etching treatments. Suitable specimens were obtained by subjecting ½- by 8-in. strips of commercial Monel sheet, 0.1-in. thickness, to several strain-anneal cycles. A cycle consisted of straining in tension, 0.6 to 0.8 percent, followed by annealing at 1,150° C for 16 hrs.

In order to determine whether or not the optical anisotropy was reproducible, a specimen was photographed before and after repolishing and reetching, taking care to replace the specimen at the same angular setting with respect to the plane of vibration. The repolishing treatment consisted of removing the etched surface with fine alumina. Inspection of the photographs, figure 1, shows that the degrees of contrast between crystals were in general reproduced. This was confirmed by measurements of the four extinction positions with respect to a line on another specimen which had been adjusted so that the line coincided with the direction of vibration of the incident light. The amount of rotation required to obtain an extinction is designated as ϕ and will be referred to as such in the remainder of the paper. Results obtained after two polishing and etching treatments are listed in table 1. It can be seen that values for ϕ could be reproduced to $\pm 4°$. The degree of reproducibility was found to produce differences in shading equivalent to that shown in figure 1.

TABLE 1. *Reproducibility of extinction positions after successive polishing and etching treatments*

Crystal	Etching treatment	Extinction positions			
		1	2	3	4
A	1	26	118	207	298
	2	27	115	205	294
B	1	85	171	263	352
	2	81	173	258	352
C	1	44	135	221	316
	2	44	132	221	313
D	1	2	95	182	272
	2	6	95	186	273

The Monel crystals were too small for their orientations to be determined conveniently by X-ray diffraction. Inspection of etched surfaces had shown many areas in which four first-order twins were present. Therefore, it was possible to determine the orientations of a cluster of crystals from the angles between their twin boundaries. By choosing crystal 1, figure 2, as the zero order, it followed that crystals 2, 3, 4, and 5 were first-order twins, crystals 6, 7, 11, and 12 were second-order twins and crystals 8, 9, and 10 were third-order twins. The angles between the reference boundary 1–3 and the twin boundaries of crystals 1 to 12 are given in table 2.

TABLE 2. *Azimuth angles between twin boundaries of numbered crystals in figure 2*

Twin boundary	Azimuth *	Twin boundary	Azimuth *
	Degrees		*Degrees*
1-3	0	4-6	161
1-2	110	4-7	54
1-4	66	7-8	119
1-5	48	7-9	174
3-11	71	7-10	16
3-12	115		

[1] Figures in brackets indicate the literature references at the end of this paper.

* Angles are measured clockwise from twin boundary 1-3, see figure 2.

FIGURE 1. *Reproducibility of intensity of reflections after repolishing and reetching.*

Monel contrast solution, ×50. 1, Initial polishing and etching; 2, after repolishing and reetching.

Taking advantage of the well known fact that in face-centered cubic metals, such as Monel, the twin boundaries are traces of (111) planes and using the procedure described by Barrett [3], the orientation of crystal 1 was determined, figure 3. This procedure gave two solutions either of which would correspond to one of two orientations that would be obtained by plotting opposite poles on the same projection plane; however, the twin-trace method could be used because opposite extinctions differed by 180°.

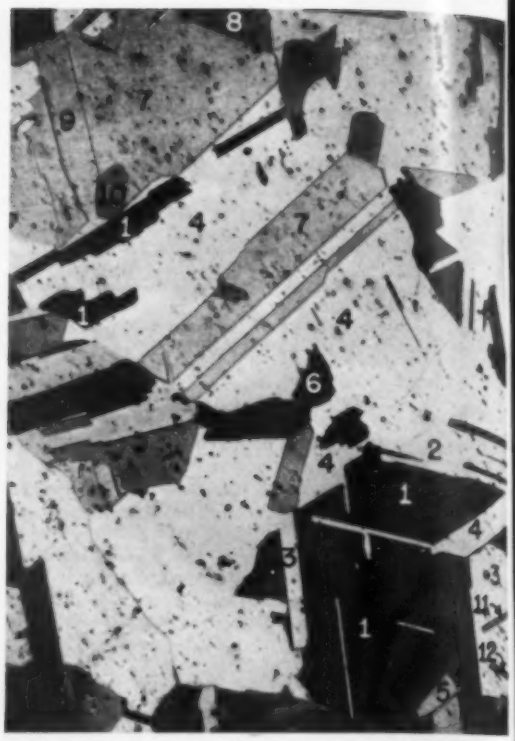

FIGURE 2. *Crystals whose orientations were determined.*

Monel contrast solution, ×50.

In order to verify the orientation of crystal 1, the coincidence of the 111-poles of the first- and second-order twins with the corresponding loci of normals of the observed twin boundaries was determined as indicated in figure 3. The 111-poles of the first- and second-order twins were located with the aid of a standard stereographic projection, figure 4. This projection gives the angular relationships for the 100- and 111-poles of a zero order crystal and its four first-order twins. A 100-pole of the zero order crystal coincides with the center of the projection. With this projection and a Wulff net, it was possible to locate the 100- and 111-poles of the first-order twins for any orientation of a zero-order crystal. By considering a first-order twin as a zero-order crystal, the 100- and 111-poles of four second-order twins could be located. In this way 100- and 111-poles of high-order twinning could be located. The coincidence of the 111-poles with corresponding loci of normals to the observed twin boundaries was good, thereby checking the orientation assigned to crystal 1.

After determination of the orientations of crystals 1 to 12, their four extinction positions were measured. Average ϕ values differed by 90° within the experimental error; therefore, they were adjusted so that the difference would be 90°. Crystals 1, 2, 3, and

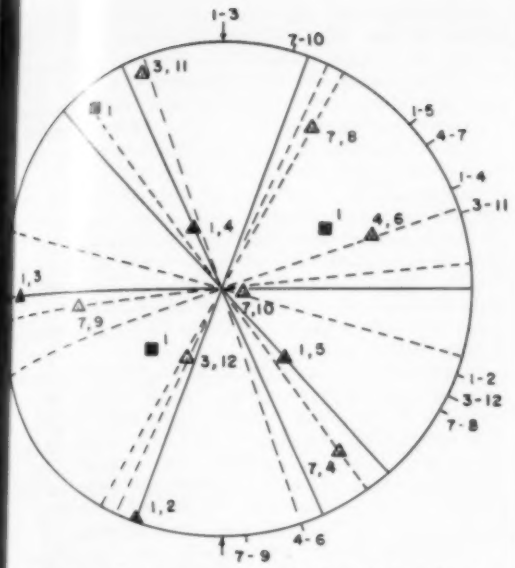

FIGURE 3. *Determination of orientation by twin-boundary method.*

(1) Angles between twin-boundaries are indicated at the periphery; (2), the solid meridians are loci of normals corresponding to the twin boundaries of crystal 1; (3), the solid triangles and squares indicate 111- and 100-poles, respectively, of crystal 1 as determined by its twin boundaries; (4), dashed meridians are loci of normals corresponding to the twin-boundaries of the first- and second-order twins; (5), the open triangles are the 111-poles of the first- and second-order twins of crystal 1, as determined by its orientation.

FIGURE 4. *Standard stereographic chart of zero- and first-order twins.*

Open triangles and squares are 111- and 100-poles, respectively. A, B, C, and D identify first-order twins of crystal 0.

11 gave sharp extinctions, therefore ϕ values were easier to obtain than for crystals 4, 5, 6, 7, 8, and 12, whose extinctions were less sharp. The values of ϕ for each crystal are listed in table 3, together with the spherical coordinates of the cubic poles. The latitude, δ, is referred to the polished surface and the azimuth, ψ, to the 1–3 twin boundary. The small differences in brightness during a 360° rotation for crystals 9 and 10, made it impossible to obtain reproducible ϕ values. Therefore, no values are listed in table 3.

FIGURE 5. *Correlation of crystal orientation and extinctions for numbered crystals in figure 2.*

100-poles are indicated by squares, 110-poles by ellipses.

TABLE 3.—*Extinctions and orientations of numbered crystals in figure 2*

Crystal	Angles	Extinction positions			
		1	2	3	4
1	ϕ	53	143	233	323
	ψ	60	.....	227	325
	δ	40	.....	50	6
2	ϕ	74	164	254	344
	ψ	.....	157	253	351
	δ	.....	41	7	48
3	ϕ	36	126	216	306
	ψ	.....	122	215	310
	δ	.....	38	4	51
4	ϕ	30	120	210	300
	ψ	14	132	.....	278
	δ	13	64	.....	22
5	ϕ	84	174	264	354
	ψ	98	189	.....	343
	δ	6	13	.....	76
6	ϕ	20	110	200	290
	ψ	7	129	225	.....
	δ	62	16	22	.....
7	ϕ	80	170	260	350
	ψ	87	197	.....	331
	δ	25	37	.....	43
8	ϕ	58	148	238	328
	ψ	54	160	250	.....
	δ	71	7	18	.....
9	ϕ	(*)	(*)	(*)	(*)
	ψ	40	130	223	.....
	δ	6	1	84	.....
10	ϕ	(*)	(*)	(*)	(*)
	ψ	32	141	262	.....
	δ	33	27	45	.....
11	ϕ	13	103	193	283
	ψ	23	.....	186	286
	δ	43	.....	45	9
12	ϕ	63	153	243	333
	ψ	50	168	262	.....
	δ	66	12	21	.....

* Poor extinction.

In order to determine if there was a correlation between extinctions and crystal orientation, the data for extinctions and orientations were plotted as shown in figure 5. For convenience in comparing differences between ϕ and ψ, the four extinctions were represented as mutually perpendicular meridians. Then for each crystal, the 100-pole making the smallest angle with the polished surface was plotted, using the nearest extinction as the fiducial line. The 110-pole nearest the surface normal also was plotted. Inspection of figure 5 shows that the 100- and 110-poles of crystals 1, 2, 3, and 11, which have the sharpest extinctions, were near an extinction meridian and the surface normal, respectively. The results also show that if the 110-pole is displaced from the surface normal, then the reference extinction will be displaced to the opposite side of the 100-pole nearest the plane of the surface. These data are not sufficient to justify the statement of quantitative relationships, but it appears that there is a definite correlation between the orientation of a crystal and the location of the extinctions.

The surface normal of crystal 9, which gave poor extinctions, was nearly parallel to a cubic plane. The crystallographic orientations of the surface normal for crystals 7 and 10 were nearly the same and near a 111-pole. However, the extinctions of crystal 10 were less sharp than those of crystal 7. There was no apparent explanation for this inconsistency in the results. In general, the following could be stated: Sharp extinctions indicated that the surface was nearly parallel to a (110) plane. Very poor extinctions indicated that the polished surface was nearly parallel to either a (100) or a (111) plane.

3. Discussion

Recent reviews by Mott and Haines [4] and by Perryman [5] show that polarized light has been used in many investigations to reveal the polycrystalline nature of metals. In only a few cases [6, 7] was it demonstrated that polarized light could be used to obtain quantitative information on the orientation of crystals. The results in this paper show a correlation between extinctions and crystal orientation. Knowing the orientation, it is possible to locate the extinctions with a fair degree of accuracy and conversely a cubic pole can be located near one of the four extinctions. It is believed that further investigation will show that an empirical relationship can be worked out that will permit orientation of individual crystals in a polycrystalline metal to be determined more readily than is now possible, particularly by combining polarized light data with twin-boundary relationships or incomplete X-ray diffraction data.

In the earlier work [1] it was suggested that the optical anisotropy of the etched Monel surfaces was caused by an anisotropic film. Considering the work of Jones [8], Perryman and Lack [9], and the results described in this paper, it appears that the optical anisotropy can be explained equally well on the basis of the "ridged, or furrowed, structure" observed by Jones.

Jones observed striations on etched surfaces of certain metals that extinguished in polarized light at normal incidence when the striations were parallel or perpendicular to the vibration direction of the polarizer, the anlyzer being in the crossed position. In additional experiments with ordinary light at oblique incidence, Jones observed two bright reflections in a plane normal to the surface and to the striations. The normals to the reflecting planes differed by approximately 90°. Models were made from metal plates to simulate right-angle furrows. The models gave similar extinctions with crossed nicols. These observations led to the conclusion that the optical anisotropy was caused by a furrowed structure that was formed by the action of the etching reagents.

Perryman and Lack deposited a silver film, 800-Å thickness, on a surface on Monel that had been prepared in a manner similar to that used in this work and found that the optical anisotropy was not destroyed. This experiment was repeated on an aluminum specimen, the surface of which had been anodized by a procedure developed by Hone and Pearson [10]. The same result was obtained. Similar films, deposited on suitably prepared surfaces on anisotropic cadmium and zinc specimens obliterated the optical anisotropy. They concluded from these results that the optical anisotropy of the etched Monel and anodized aluminum surfaces was caused by the shape of the surface contours and not by the anisotropy of a surface film. Hone and Pearson had shown that the anodized aluminum surface was striated but had concluded that the film was anisotropic.

The results summarized in figure 5 show close agreement between extinctions and meridians that can be passed through the surface normal and cubic poles for orientations approximating the "110-surface".[2] This also indicates that the anisotropy was caused by a "ridged or furrowed structure", as described by Jones [9], the sides of the furrows being parallel to cubic planes whose intersections were parallel to the surface. This structure satisfies the geometry necessary for a reflection from two surfaces to be coincident with the incident beam. However, if etch pits whose facets were parallel to cubic planes were perfect, the structure described by Jones could give a coincident double reflection only for orientations in which the surface normal was in a cubic plane. Figure 5 shows that this condition need not be satisfied in order to obtain sharp extinctions. In the absence of data to the contrary, the optical anisotropy of crystals 4, 5, 6, 7, and 12 could be explained as being due in part to imperfection of the etch pits and in part to the fact that the incident beam was convergent. There is also the possibility of a striated film, such as the anodized aluminum surface, the directions of the striations being controlled by the general shape of the etch pits. As yet no direct evidence has been obtained to verify the presence of parallel furrows on etched Monel surfaces.

[2] The crystallographic orientation of the surface normal is denoted by giving the indices of the plane that is parallel to the surface, immediately before the word "surface."

When the etched surface is parallel to a (100) plane, only coincident single reflection is possible, and if plane polarized light is used, the reflected beam would be extinguished by the analyzer. This fact was used by Dunsmuir [7] to estimate the number of crystals in silicon iron sheet that approximated the 100-surface, assuming that all other orientations would give extinctions. This assumption apparently is not true, as the foregoing results showed that orientations approximating the 111-surface also do not always show extinctions. The result of the following experiment also supports this conclusion. Impressions of a cube corner were made in a polished surface on a stainless steel specimen, keeping the cube diagonal normal to the surface during the compression. These impressions simulate etch pits having facets parallel to cubic planes in crystals having a 111-surface. The impressions did not show extinctions.

It appears probable then that the optical anisotropy of the Monel crystals was caused by imperfect etch pits that combined in such a way that parallel furrows were formed. On this basis, extinctions should be obtained when the furrows were parallel or perpendicular to the vibration direction of the polarizer, as is the case with parallel scratches.

4. Conclusions

The twin-boundary method provides a useful method for determining the orientation of crystals in annealed Monel.

The results indicate a qualitative relationship between crystal orientation and the extinctions of polarized light reflected from the crystals.

The optical anisotropy of etched Monel metal surfaces probably was caused by parallel furrows formed by the tendency of the etching reagent to develop etch pits whose facets were parallel to cubic planes.

D. H. Woodard, now a member of the staff of the Metallurgical Project, Massachusetts Institute of Technology, Cambridge, Mass., cooperated in some of the preliminary stages of this work.

5. References

[1] D. H. Woodard, Stages in the deformation of Monel metal as shown by polarized light, Am. Inst. Min. Met. Engrs., Metals Trans. **185,** 722 (1949).
[2] David I. Sinizer, The metallography of nickel and nickel alloys, Metals Handbook, 1948 Ed., p. 1048 (Am. Soc. Metals, Cleveland, Ohio).
[3] C. S. Barrett, The structure of metals, p. 40 (McGraw-Hill Book Co., New York, N. Y., 1943).
[4] B. W. Mott and R. H. Haines, Examination of metals under polarized light. I. Theory and apparatus, Research **4,** 24 (Jan. 1951); II. Applications, Research **4,** 63 (Feb. 1951).
[5] E. C. W. Perryman, Recent development in metallography, Metal Ind. **79,** 71 (July 27, 1951).
[6] P. F. George, Some special metallographic techniques for magnesium alloys, Trans. Am. Soc. Metals **38,** 687 (1947).
[7] P. G. Dunsmuir, A summary of the proceedings of the conference on the examination of metals by optical methods, British Iron and Steel Research Association Report, p. 51 (May 1949).
[8] Olwen Jones, Reflection of plane polarized light by etched metals, Phil. Mag. **48,** 207 (1924).
[9] E. C. W. Perryman and J. M. Lack, Examination of metals by polarized light, Nature **167,** 479 (March 24, 1951).
[10] A. Hone and E. C. Pearson, Grain orientation in aluminum revealed by anodic film, Metal Progress **53,** 363 (March 1948).

Washington, July 1, 1952.

Journal of Research of the National Bureau of Standards Vol. 49, No. 3, September 1952 Research Paper 2352

Magnesium-Rich Side of the Magnesium-Zirconium Constitution Diagram

J. H. Schaum and H. C. Burnett

The magnesium-rich side of the magnesium-zirconium constitution diagram has been studied for the purpose of improving the previous work on this subject. A diagram has been developed that is similar in form to that found by previous investigators, but the phase boundaries differ as to temperatures and alloy compositions. The peritectic reaction was found to take place at 654° C, beginning at 0.58 percent of zirconium.

1. Introduction

The rapid expansion of the aircraft industry during World War II set the pace for the production and the development of magnesium alloys. Zirconium proved one of the most beneficial of the alloying elements used with magnesium. Additions of 0.4 to 0.8 percent of zirconium to magnesium impart a very fine grain size (0.02 mm diam.), relative insensitivity to notches, superior corrosion resistance, high strength, and ease of working.

The industrial utilization of zirconium in magnesium has proceeded more rapidly than the accumulation of basic data on the magnesium-zirconium system. Siebel [1] found a peritectic reaction at a temperature close to the melting point of magnesium. The liquidus and the peritectic temperatures coincided at 0.26 percent of zirconium, and then the liquidus rose very steeply with increase of zirconium until temperatures in the neighborhood of 1,000° C were reached, at which point the liquidus curved away toward the horizontal.

Nowotny [2] and his associates showed an alpha phase region with a maximum solubility of 0.87 percent of zirconium at 700° C. Adjacent to this zone was a two-phase region containing magnesium-rich alpha solid solution plus zirconium-rich beta solid solution. The structure became entirely beta when zirconium exceeded 30.3 weight percent. Volume curves for the beta phase showed a minimum in the region of 34.5 weight percent, possibly arising from a chemical affinity that forms Mg_2Zr, a valence bond type of compound analogous to Mg_2Si. The tendency for valence compound formation grew weaker with the increasing solubility of magnesium in zirconium. The results of this work are open to question because raw materials containing over 12 percent of impurities were used.

Sauerwald [3] melted magnesium and powdered zirconium in a steel crucible under an atmosphere of argon and determined the diagram shown in figure 1. Solution of iron by the melt affected the results adversely. By use of solid diffusion techniques, more zirconium was dissolved in the solid magnesium than in the liquid.

Recently, G. A. Mellor [4] of the National Physical Laboratory published a magnesium-zirconium diagram, figure 2, based on the addition of a "chloride-master-alloy" to melts made in iron and magnesia crucibles. Determining solid solubility by electrical resistivity measurements was hindered by contamination from atmospheric elements.

In all of these previous efforts, the inherent difficulties of obtaining accurate and reproducible results were apparent in the limited data obtained and the wide spread of compositions used in determining the points on the resulting diagrams. Nevertheless, figures 1 and 2 show that Sauerwald and Mellor are in fair agreement as to the general form of the magnesium-rich end of the diagram and differ only in degree.

A comparison of the fundamental characteristics of significance in studying the magnesium-zirconium system are summarized in table 1. Since the atomic diameter of magnesium is 3.20 and of zirconium 3.19 (crystal angstroms), the latter may be said to have an almost perfect "favorable-size factor" for alloying with magnesium. Solid solubility of zirconium in magnesium is also favored by the fact that both elements have a hexagonal-close-packed crystal structure. However, magnesium is in group II with a valence of 2, whereas zirconium is a transition element in group IV with zero alloying valency. As the valency between solvent, magnesium, and solute metals becomes more unequal, solid solutions become more restricted. Zirconium, therefore, has an unfavorable valence for solid solution in mag-

TABLE 1. *Comparison of physical constants of magnesium and zirconium*

	Mg	Zr
Atomic number	12	40
Group	IIA	IVA
Period	3	5
Crystal structure	HCP	α-HCP
Do	HCP	β-BCC
Atomic diameter (crystal angstroms)	3.20	3.19
Atomic weight	24.32	91.22
Density (g/cm³)	1.74	6.4
Melting point (° C)	650 ±2	1,750 ±700
Boiling point (° C)	1,110	----------
Latent heat of fusion (cal/g)	70.0	----------
Alloying valence	2	0
Electrical potential (referred to H^+)	+2.34	+1.53
Electrical resistivity (microhm/cm)	4.33 (18° C)	41.0 (0° C)
Modulus of elasticity (psi×10⁶)	6.5	10.7

[1] G. Siebel, Unpublished work, referred to in The Technology of Magnesium and Its Alloys, by Adolph Beck p. 77 (F. A. Hughes & Co., Ltd., London, England 1941).

[2] H. Nowotny, E. Wormnes, and A. Mo rnheim, Investigations of Al-Ca, Mg-Ca, and Mg-Zr; Z. Metallkunde **32**, Heft 2, 39-42 (February 1940).

[3] Von F. Sauerwald, Das Zustandsdiagramm Magnesium-Zirkonium, Z. Anorg. Chem., **255**, Heft 1-3, 212-220 (December 1950).

[4] G. A. Mellor, The constitution of magnesium-rich alloys of magnesium and zirconium. J. Inst. Metals **77**, part 2 (1950).

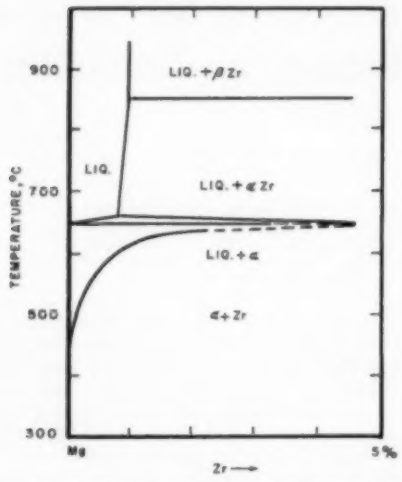

FIGURE 1. *Magnesium-zirconium constitution diagram.*

By Sauerwald [3]

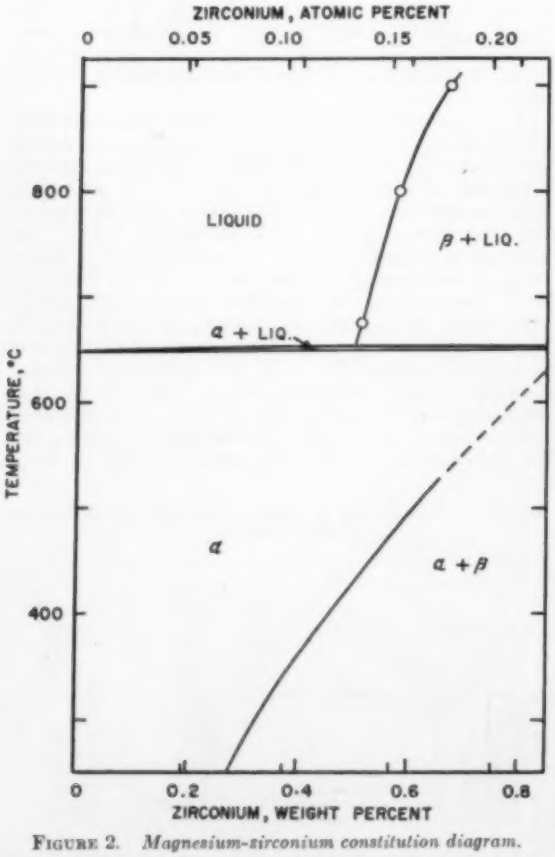

FIGURE 2. *Magnesium-zirconium constitution diagram.*

By Mellor [4]

nesium. Also, the more unequal the respective valency factors, the steeper is the slope of the liquidus and solidus curves, the latter being affected the most. A metal of lower valency tends to dissolve a metal of higher valency more readily than vice versa. This explains the low solubility of zirconium in magnesium and the high solubility of magnesium in zirconium. Zirconium is unique in that it is the only commercially significant transition element in groups III, IV, V, and VI used in magnesium-base alloys.

The more electropositive the solvent metal and the more electronegative the solute metal, the greater is the tendency to restrict solid solubility and form stable intermetallic compounds. If the solute atom, zirconium, has a choice of entering solid solution or forming a stable compound, it will form the latter.

Since the solubility of zirconium in magnesium is low and increases with temperature, it would be expected to manifest age-hardening properties.

Transition elements, such as zirconium, tend to form electron compounds, which are actually phases with wide ranges of homogeneity (like brass), in contrast to the restricted ranges of general intermetallic compounds. For zero valence type elements, such as zirconium, the valency electron concentration will vary from 2.0 to 1.5 when the atomic percent of solute varies from 0 to 25 percent.

Some doubt appears to exist as to the exact melting point of pure magnesium. The accepted figure is 651° C, but competent workers have obtained values from 647 to 652° C. This spread is quite small compared to the values of 1,750° ± 700° C reported for the melting point of zirconium.

2. Experimental Procedures

2.1. Survey of Raw Materials

As a preliminary step to actual study of the phase diagram, a survey of the purity and alloying characteristics of the available raw materials was made. Table 2 lists the spectrochemical analyses of the raw materials used. Because of the technical difficulties of removing hafnium from its "Siamese twin" zirconium, practically all commercial zirconium contains two to four percent of hafnium. Hafnium-free zirconium has only recently become available in quantity. The hardeners, such as 60 percent Zr-40 percent Mg and 40 percent Zr-60 percent Mg alloys, and the proprietary compound, TAM flux,[5] contained the most impurities. Spectrochemical analyses of the magnesium-zirconium alloys made from these raw materials showed no discernible increase in impurities beyond those already present in the commercially pure magnesium. The highest contents of zirconium in the alloys resulted when the hardeners and the flux were used. In subsequent heats it was discovered that the hardeners were very heterogenous in composition because they were mechanical mixtures of magnesium and zirconium. It was difficult

[5] Contains 50 percent of $ZrCl_4$, 25 percent of NaCl, and 25 percent of KCl.

TABLE 2. *Spectrochemical analyses of raw materials*

VS=10 to 100%; S=1 to 10%; M=0.1 to 1.0%; W=0.01 to 0.1%; VW=0.001 to 0.01%; T=0.0001 to 0.001%; FT=0.00001 to 0.0001%

Raw material	Chemical elements																			
	Ag	Al	B	Ba	Ca	Cr	Cu	Fe	Hf	K	Mg	Mn	Mo	Na	Ni	Pb	Si	Sr	Sn	Ti	Zr
Dow commercially pure magnesium	.....	T	.....	T	T	.....	VW	W	.....	.....	VS	W	.....	.....	.....	.....	VW	.....	.....	.....	.....
Zr metal	FT	T	W	.....	W	.....	W	M	S	.....	VW	.....	.....	.....	M	.....	T	.....	T	T	VS
TAM flux[1]	T	W	.....	M	M	T	VW	W	M	VS	VW	T	T	VS	W	T	W	M	.....	T	VS

[1] Contains 50% of $ZrCl_4$, 25% of NaCl, and 25% of KCl.

avoid inclusions in alloys made with the flux because of the formation of a large amount of slag and dross. Zirconium tetrachloride was unsatisfactory because it reacted too readily with the atmosphere and was ineffective in introducing zirconium into the molten magnesium because of the violence of its dissociation. Zirconium hydride floated on the surface of the melt, was pyrophoric, and formed considerable slag. Powdered zirconium also oxidized rapidly. Despite its slow rate of solution, the high purity and low reactivity of zirconium sheet made it the preferable material for most of the subsequent work.

2.2. Melting Techniques

In the course of this investigation various melting procedures were evaluated and modifications were adapted to fit the special requirements unique to phase-diagram studies. In screening the raw materials, described in the preceding section, approximately 350 g of magnesium were placed in an ingot-iron crucible, covered with a graphite lid, and melted by means of a 35-kva high-frequency induction furnace. One percent of zirconium, in the various raw material forms tested, was added to the molten magnesium at 760° C, superheated to 960° C, cooled to 800° C, and poured into a graphite-ingot mold.

Because zirconium is so much heavier than magnesium, some heats were stirred with a graphite rod attached to the shaft of an electric motor. This procedure proved undesirable because it stirred many inclusions into the alloy and tended to emulsify the zirconium in the magnesium, making a mechanical mixture with a highly insoluble zirconium constituent.

Induction melting was not used extensively in the project because it was difficult to hold melts at constant temperature for long periods of time with this type of melting.

In order to have accurately controlled heating, cooling, melting, and holding cycles, an electric resistance furnace was built. Nichrome wire was wound around a 3-in.-diameter Alundum tube, coated with Alundum cement, placed within another larger Alundum tube, and then packed in diatomaceous earth for thermal insulation. Partial on and off controls were incorporated into the electrical system by the use of a variable transformer, slide wire resistances, and an electronic high-speed controller-recorder. A Chromel-Alumel thermocouple was located between the two Alundum tubes, adjacent to the Nichrome coil, and connected to the controller. Graphite and ingot-iron crucibles, measuring 2½ in. in diameter by 8 in. high, were used for melting without protective atmosphere. A brick of diatomaceous earth on top of the furnace tube reduced heat loss by radiation.

In order to melt the alloys under a protective atmosphere, a steel bomb-type container was designed, as shown in figure 3. A 2-in.-diameter graphite crucible held the melt in the bomb. Water-cooling of the lid and flange protected the rubber gasket between them. A steel tube sheathed the Chromel-Alumel thermocouple used in measuring melt temperatures and taking cooling curves. An inlet pipe was connected to a system of valves and gages that permitted the bomb to be evacuated with a vacuum pump and filled with helium. Another opening in the lid was provided for removing molten alloy samples.

Limited stirring of melts was effected by attaching a mechanical vibrator to the steel thermocouple protection tube.

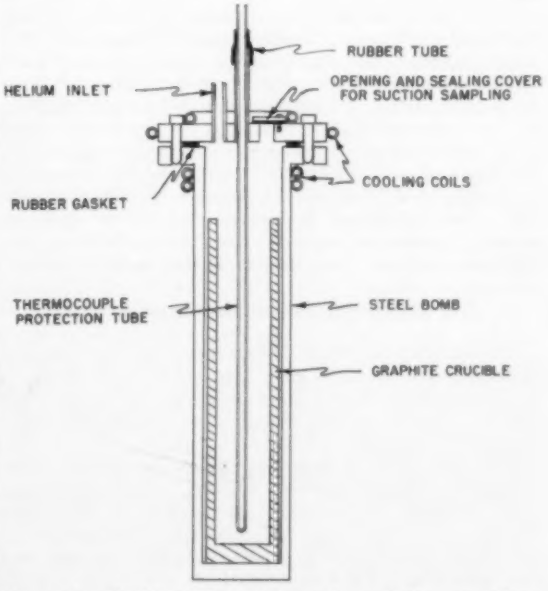

FIGURE 3. *Steel bomb for melting under protective atmosphere.*

2.3. Chemical Analysis

One of the difficulties encountered in studies of the magnesium-zirconium system is the tendency for zirconium, elemental or combined, to become mechanically entrapped as an extremely fine colloidal suspension. It is necessary, then, to distinguish between zirconium in solution in the magnesium and zirconium mechanically suspended as inclusions. Some of the disagreement in the results of previous investigations may be attributed to variation in the effectiveness of analytical procedures in distinguishing between the dissolved and the undissolved constituents of the alloys. The insoluble zirconium can be observed in the microstructure but its quantitative evaluation has required analytical techniques involving differential solubility in acid. Hydrochloric acid, nitric acid, and sulfuric acid of various concentrations have been used for this purpose with varying results and degrees of success.

The Analytical Chemistry Section of the Bureau cooperated by developing the analytical procedure used and compared the results with those of other investigators. Because the chemical-analysis technique is an important factor in the development of the diagram, it is given in detail in the Appendix, section 5. In brief, the magnesium-zirconium alloy sample was dissolved in 15-percent hydrochloric acid and filtered. As only the soluble zirconium constituent of the alloy dissolved in the acid, the amount was determined by precipitating it from the filtrate with ammonium phosphate. The insoluble zirconium constituent of the alloy remaining on the filter paper was put in solution by fusion with potassium bisulfate and sulfuric acid and the zirconium determined by precipitation as the diammonium phosphate.

Because of the conflict of opinion concerning the best acid and concentration to use for dissolving the alloy samples, tests were made in which duplicate magnesium-zirconium specimens were treated with 10-percent HCl, 15-percent HCl, 4.8-percent H_2SO_4, and 11-percent HNO_3 solutions. The latter three acids were all the same normality, that is, 1.7 *N*. Soluble and insoluble zirconium were then determined according to steps II and III described in the Appendix. No significant difference in soluble and insoluble zirconium contents were obtained from the different acids or concentrations used in the tests.

2.4. Electrical Resistance Measurements

Because the electrical resistance of an alloy changes abruptly as melting occurs, this method was used to determine both the solidus and liquidus of some of the alloys. Electrical resistance test specimens were made by pouring magnesium, or its alloys with zirconium, into a graphite mold containing four Nichrome wires inserted at the corner positions. Two of these wires carried the current to and from the specimen; the other two were used to measure the potential drop across it. The specimen was cast as a slab measuring 1 3/4 in. long, 1 in. wide, and 3/16 in. thick, and was sawed as shown in figure 4. Figure 5

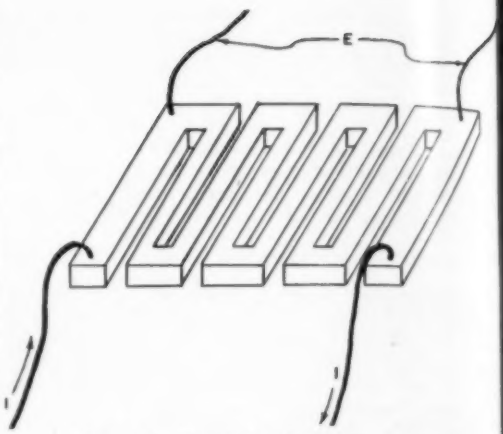

FIGURE 4. *Electrical resistance test specimen.*

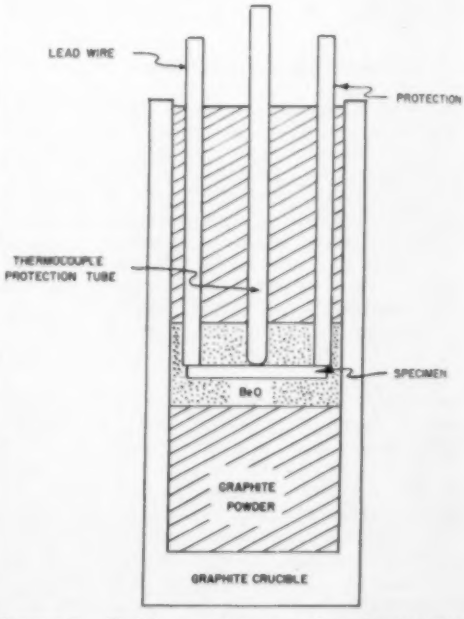

FIGURE 5. *Packing arrangement of resistance specimen in crucible.*

illustrates the manner in which the resistance grid was packed in a graphite crucible, and figure 6 is a schematic drawing of the electric circuits required. The crucible and contents were placed in the electric resistance furnace and heated at a rate of 0.5 deg C per minute. A steady current from a 6-volt battery was sent through the specimen, using the wires marked I, figure 4, during the period of the test, and the IR drop across the specimen was continuously recorded with an electric recorder, using the

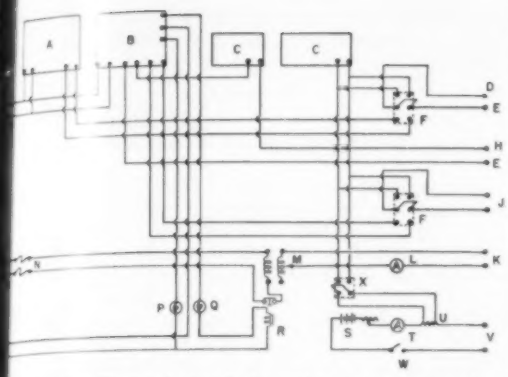

FIGURE 6. *Electrical circuits for resistance measurements.*

A, Recorder; B, controller recorder; C, potentiometers; DE, specimen thermocouple; F, DPDT switch; G, 110-v a-c current; HE, furnace thermocouple; J, Nichrom grid; K, furnace coil; L, 0 to 20-amp ammeter; M, variable transformer; N, 15-amp current; O, 220-v a-c current; P, green light; Q, red light; R, relay; S, 6-v battery; T, 0 to 1.5-amp ammeter; U, known 0.001 standard ohm; V, emf to E.M.F.; W, SPST switch; X, DPST switch.

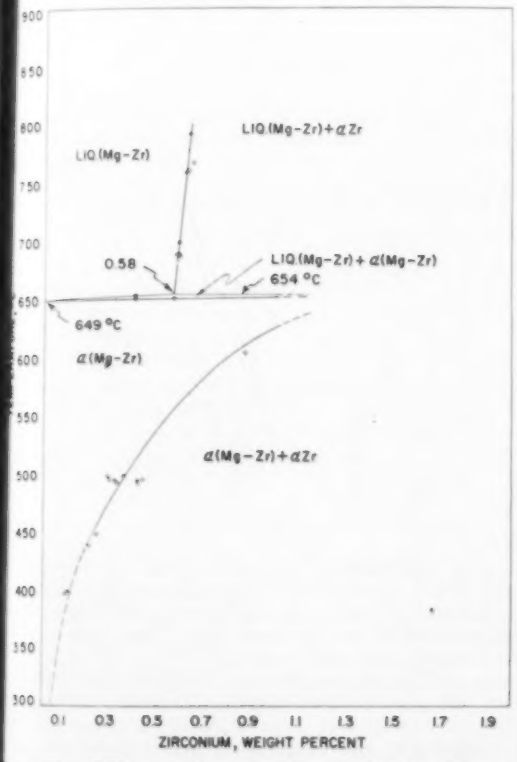

FIGURE 7. *NBS magnesium-zirconium constitution diagram.*

wires marked E. The temperature was simultaneously recorded with a second electronic recorder. A standard resistance was incorporated into the circuit to standardize the current during the course of an experiment and to permit conversion of millivolts to ohms when necessary. As the temperature of the specimen approached a critical point, temperature was measured with a semi-precision potentiometer. As the temperature increased, the resistance of the specimen gradually increased until a sharp increase in resistance indicated the beginning of melting. Careful packing in beryllia held the grid in shape and prevented short circuits even when the specimen was molten.

2.5. Suction Sampling

Previous investigators found that the liquidus above the peritectic line had an almost vertical slope and consequently precluded the use of cooling curves for locating its position. As an alternative, dip samples of the molten alloys were analyzed to find the solubility limits.

In this project, points on the liquidus were determined in the following manner. One hundred grams of commercially pure magnesium were charged into a graphite crucible with 2 percent of zirconium as narrow strips of pure zirconium sheet. After the crucible was placed in the steel bomb and sealed, it was evacuated and flushed with helium several times as the temperature rose and finally held under helium pressure of about 5 lb/in^2. When the alloy melted, the protection tube was lowered to the bottom of the crucible so that the thermocouple bead was located 1½ in. from the bottom of the melt. This thermocouple was connected to a semiprecision potentiometer. Experimental data obtained but not included in this paper showed that 3 hr, the period for which the alloys were held molten, was adequate for the attainment of equilibrium between the liquid and the excess zirconium. The access lid on the top of the bomb was then slid open and a Pyrex glass tube (4-mm inside diam) was immersed in the melt to a point opposite the thermocouple bead. An alloy sample was quickly sucked out of the melt by the action of a rubber suction bulb on the other end of the tube. At the moment of sampling a temperature reading was made with the adjacent thermocouple. The samples obtained in this manner were analyzed for total zirconium because it was presumed that all the zirconium in the melt at the time of sampling would have to be in solution. The excess zirconium, not in solution, settles to the bottom of the melt because its density is 6.4 compared with 1.74 for magnesium.

An alternative procedure for obtaining suction samples proved quite successful and was used for locating six of the points shown on the diagram (fig. 7). In these heats 300 g of commercially pure magnesium were melted in a graphite crucible with Dow 310 flux for protection. At 760° C, 6 percent of zirconium in the form of the chloride flux was stirred into the melt and the alloy held at constant temperature for 3 hr. Suction samples were taken, as described in the previous technique, at a point opposite the thermocouple bead indicating the melt temperature.

2.6. Heat Treatment

Determination of points on the solvus are unusually difficult because the magnesium-zirconium alloys comprise a sluggish metastable system in the solid state. During heating or cooling there is no measurable heat of reaction when crossing the solvus line and apparently no change in soluble zirconium. Most of these alloys exist at room temperature with from 0.4 to 0.8 percent of zirconium in solid solution when theoretically zirconium is practically insoluble in magnesium at room temperature. Such pseudo-stability indicated the need for lengthy heat treatments in order to approach true stable equilibrium. The heat-treatment time required to reach equilibrium probably becomes longer as the temperature is lowered.

The stability of the alpha solid solution was demonstrated by heating alloys, in about one-half hour, to within 2 deg of the melting point, followed by water quenching. Chemical analysis showed no change in zirconium in solid solution. Microscopic examination revealed grain growth, as would be expected.

It was planned originally to follow the progress of zirconium solution into, or rejection from, the alpha solid solution by observing the change in electrical resistance of alloy grids held at constant temperature for extended periods of time. The extensive equipment required for this work (described in a previous section) and the long periods of time needed for the heat treatments led to the substitution of the following procedure for location of points on the solvus. Ingots of different analyses were sectioned and cold rolled to a reduction of 25 percent, the purpose of the cold-rolling being to reduce the stability of the zirconium in solid solution. Four small duplicate samples were cut from a rolled specimen with high soluble and low insoluble zirconium content and another four obtained from a specimen with low soluble and high insoluble zirconium. Nichrome wires were tied to each specimen to facilitate their removal at various stages of heat treatment. The samples were then packed with graphite dust in a graphite crucible and placed in an electric resistance furnace. Various sets of samples were subjected to isothermal heat treatments at temperatures ranging from 190° to 635° C for periods of 100 to 500 hr.

At the end of 50- or 100-hr intervals one specimen of each analysis was removed from the furnace by means of the Nichrome wire and water-quenched. These samples were analyzed for the amount of solid soluble and insoluble zirconium (as described in Appendix) to observe their progress toward reaching equilibrium.

Because of the low vaporization point of magnesium, the alloys were prone to evaporate, even below their melting point, given sufficient time. Also, a steady conversion of soluble zirconium to the insoluble form, with time and temperature, seemed to indicate the formation of an inert compound such as the carbide, nitride, or oxide. Both of these effects were reduced by covering the specimens with several coats of a wash made from a cristobalite investment material.

3. Results

3.1. Melting Point of Magnesium

The melting point of the basic raw material—Do commercially pure magnesium—was determined b means of inverse-rate cooling curves taken on 450 melts contained in a graphite crucible. Heating an cooling was controlled in the resistance furnace t give a rate of 2° C per minute. Three heating an cooling cycles indicated the melting point to be 648.7 ±0.2° C. The 22 gage Chromel-Alumel thermo couples used were standardized against the melting point of NBS Standard Temperature Sample 44 (pure aluminum, 659.7° C).

The melting point also was determined by usin the electrical resistance technique described pre viously. Although less accurate than the cooling curve results, the observed melting point of 648. ±0.5° C was in good agreement.

3.2. The Liquidus

Points on the liquidus were determined by analyz ing the total zirconium content of samples remove from saturated melts by the suction technique de scribed in section 2.5.

The data obtained in these tests are shown i table 3 and plotted in figure 7.

TABLE 3. *Points on the liquidus as determined by suction te*

Temperature	Zirconium	Raw material
° C	*Percent*	*
791	0.65	TAM flux.
767	.66	Zr sheet.
760	.64	TAM flux.
758	.63	Zr sheet.
698	.60	Do.
688	.59	TAM flux.
688	.59	Do.
688	.60	Do.
687	.60	Do.

The proximity of the solidus and the liquidus t the left of the peritectic line makes it difficult to dis tinguish between them. Although past investigator have claimed the location of the liquidus by arrest on the cooling and heating curves, examination o this portion of the diagram in figure 7 reveals tha the change in heat evolution when crossing th liquidus is almost imperceptible, whereas the hea evolution at the solidus, as indicated by the lever arm principle, is quite marked.

Electrical resistance measurements proved to b sufficiently sensitive to differentiate between th liquidus and solidus. Figure 8 is a plot of the tem perature versus millivolt drop across an electrica resistance grid made from an alloy containing 0.4 percent of zirconium in solution. By slowly heatin

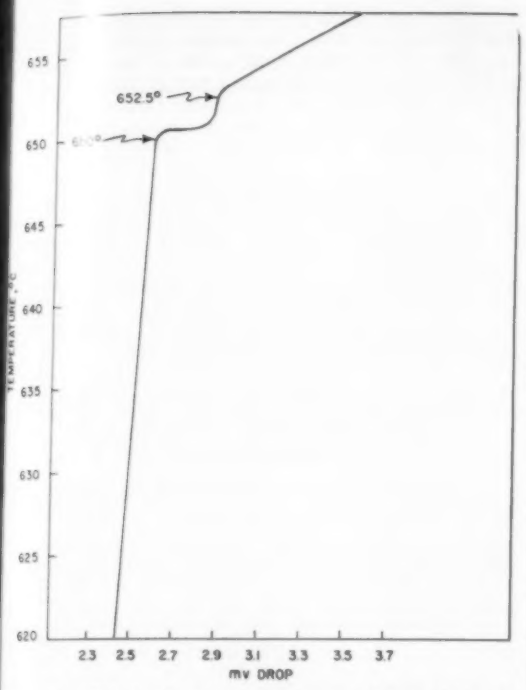

FIGURE 8. *Relation between temperature and electrical resistance on heating a magnesium-zirconium alloy containing 0.42 percent of zirconium in solution*

the alloy grid up to and beyond the melting point it was possible to observe both the solidus, at 650° C, and the liquidus, at 652.5° C.

By extrapolating a line from the melting point of magnesium through this one point on the liquidus to the intersection with a similar extension of the liquidus line above the peritectic, the beginning of the peritectic line was located at 0.58 percent of zirconium and 654° C.

3.3. The Solidus

Since the heat evolution at the solidus is quite marked, thermal analysis was utilized for locating its position. Three inverse-rate cooling curves and one heating curve of melts saturated with zirconium (from zirconium sheet) revealed the solidus thermal arrest at 650.5 ±0.5° C. This point is shown on figure 7, directly below the left end of the peritectic line.

An electrical resistance experiment, described in section 3.2, located the solidus of a sample containing 0.42 percent of soluble zirconium at 650° C. The complete solidus line is located in figure 7 by drawing a straight line from the melting point of magnesium through the two points noted above and extending it to the point of intersection with the horizontal peritectic line, determined as noted in section 3.2.

3.4. The Solvus

Points on the solvus were determined by lengthy isothermal heat treatments described in section 2.6. Table 4 contains data obtained in these experiments, and figure 7 shows the solvus line plotted from them.

Below 400° C the alloys were so stable that no change in soluble zirconium took place during the entire heat treatment and above 500° C results were erratic because of the strong tendency for the alloys to react with environmental elements. It is of interest to note that there was always some insoluble zirconium present in the alloys regardless of the temperature or time of heat treatment.

TABLE 4. *Composition of alloys after isothermal heat treatment*

Temperature of heat treatment	Time held at temperature	Zirconium		
		Soluble	Insoluble	Total
°C	*Hours*	*Percent*	*Percent*	*Percent*
604	113	0.89	0.88	1.77
498	172	.37	.15	0.52
498	172	.32	.18	.50
495	387	.45	.11	.56
495	387	.31	.19	.50
494	292	.43	.11	.54
494	292	.33	.20	.53
492	196	.43	.11	.54
492	196	.34	.17	.51
449	363	.25	.31	.56
438	242	.22	.31	.53
398	156	(a)	(a)	(a)
305	503	(a)	(a)	(a)

a No change from original composition

3.5. Other Observations

The similarity of the lattice constants of magnesium and zirconium precluded the use of X-ray diffraction techniques. However, the two metals do differ sufficiently in their X-ray absorption characteristics to distinguish between them in microradiographs. A number of microradiographs were made but were of no value as an accurate quantitative measure of zirconium content. They were of interest, however, from a qualitative viewpoint to indicate distribution of insoluble zirconium and its compounds, as may be seen in figure 9A. The specimen shown in this microradiograph contained 0.09 percent of soluble zirconium plus 0.26 percent of insoluble zirconium. The dark background is the magnesium-zirconium solid solution containing 0.09 percent of zirconium and the light particles and clusters are the 0.26 percent of undissolved or insoluble zirconium.

Brinell-hardness measurements on a series of magnesium-zirconium alloys showed no correlation with total or soluble zirconium content.

Although photomicrographs were of no value in indicating the amount of zirconium in solid solution, the grain-refining influence of zirconium can be observed by comparing the grain size of unalloyed magnesium, figure 9, B, with that of an alloy containing 0.54 percent of zirconium in solution, figure 9, C.

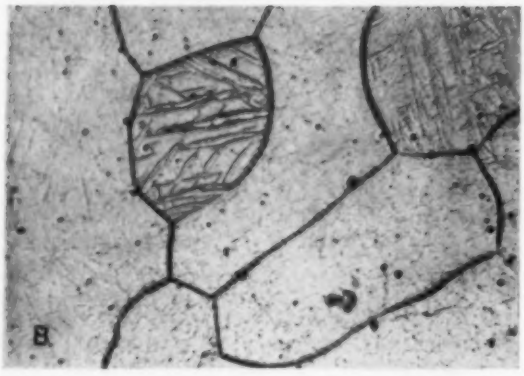

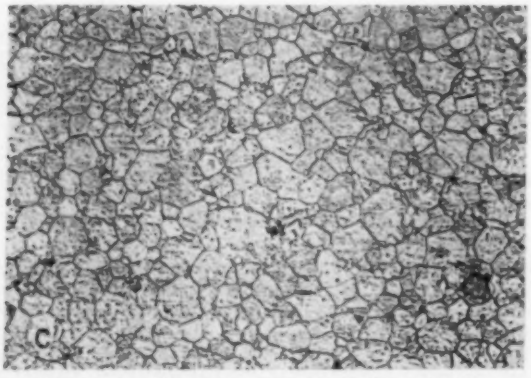

FIGURE 9. *Magnesium-zirconium alloys at ×100.*

A, Photomicroradiograph of an "as cast" magnesium-zirconium alloy containing 0.09 percent of soluble zirconium and 0.26 percent of insoluble; B, photomicrograph of "as cast" commercially pure magnesium; C, photomicrograph of "as cast" magnesium-zirconium alloy containing 0.54 percent of soluble and 0.06 percent of insoluble zirconium (B and C, etched with ethylene glycol).

4. Summary

As a result of the work described it was found that the magnesium-rich side of the magnesium-zirconium diagram, shown in figure 7, was similar in form to those developed by Sauerwald and Mellor. The intersection of the liquidus and peritectic lines was located between the values reported by these two previous investigators. The peritectic reaction and the solidus were observed at higher temperatures than in the other two diagrams. Location of the solvus at high temperatures was handicapped by the vapor pressure of magnesium and the reactivity of zirconium. Heat treatments below 400° C apparently had no effect on the soluble zirconium constituent of the alloys. In order to distinguish accurately between the soluble and insoluble zirconium, an improved chemical-analysis technique was developed. All the alloys analyzed contained an insoluble zirconium constituent at room temperature. Microradiography proved useful for observing the distribution of insoluble zirconium and its compounds.

5. Appendix. Determination of "Soluble" and "Insoluble" Zirconium in Magnesium

R. K. Bell, B. B. Bendigo, and E. E. Maczkowskie

1. Reagents

(a) Ammonium phosphate solution, 15 percent: Dissolve 150 g of $(NH_4)_2HPO_4$ in about 800 ml of water and dilute to 1 liter.

(b) Hydrogen perioxide, 30 percent.

(c) Ammonium nitrate wash solution (50 g/liter).

2. Procedure

I. Decomposition of Sample.

(a) Transfer a 1–g sample (approximately ¼-in. cubes) to a 600-ml beaker and add 300 ml of hydrochloric acid (15+85). (All the acid should be added at one stroke.) When the sample is decomposed, *immediately* filter through a tight paper, using paper pulp, and wash with hot water.

(b) Reserve the filtrate, (a), which contains the "soluble" zirconium. Place the paper, (B), which contains the insoluble zirconium, in a platinum crucible and reserve.

II. Determination of "soluble" zirconium.

(a) Add 60 ml of sulfuric acid (1+1) to the reserve filtrate (A), section 2 I(b), and heat to fumes of sulfuric acid. Fume for 5 to 10 min., cool, and dilute to 275 ml.

(b) Add 1 ml of H_2O_2 (30 percent) and 25 ml of the ammonium phosphate solution. Digest at 40° to 50° C for 2 hr or overnight if only a small amount of precipitate is visible.

(c) Cool and add a little paper pulp. Stir and allow the precipitate to settle. Filter through a tight paper containing a little paper pulp and wash about 10 times with the NH_4NO_3 wash solution. Discard the filtrate.

(d) Place the paper and contents in a weighed platinum crucible and ignite carefully under good oxidizing conditions until the carbon has been removed. Finally, ignite at 1,050° C for 20 min. Weigh as ZrP_2O_7.

$$\% \text{ Zr} = \frac{0.344 \times \text{wt of } ZrP_2O_7 \text{ in grams}}{\text{wt of sample in grams}} \times 100.$$

III. Determination of "insoluble" zirconium.

(a) Ignite the reserved paper and contents (B), section 2 I(b), at 500° C until the carbon is destroyed. Cool, and add 2 drops of sulfuric acid (1+1) and 5 ml of hydrofluoric acid (48 percent). Heat cautiously until fuming has ceased. Cool, and add just enough fused $KHSO_4$ to cover the residue and heat until the melt is clear. Cool, transfer the crucible and its lid to a 250-ml beaker, and add 40 ml of sulfuric acid (1+1). When the melt has dissolved, wash and remove the crucible and lid. Dilute to 175 ml.

(b) Continue as directed in section 2, II(b) to (d).

WASHINGTON, June 5, 1952.

Journal of Research of the National Bureau of Standards Vol. 49, No. 3, September 1952 Research Paper 2353

A Study of the Diphenylamine Test for Aliphatic Nitrocompounds

Kivi Grebber and J. V. Karabinos*

A study has been made of the diphenylamine test for aliphatic nitrocompounds. It is not given by all nitroparaffins. However, the test is at least a thousand times more sensitive than previously supposed. Structural factors are discussed.

Spectroscopic measurements indicate that the blue color in the diphenylamine test with nitrosating agents is similar to that produced by oxidizing agents. It is probably caused by colored phenazine and benzidine derivatives. A possible free radical mechanism for the reactions involved is presented.

1. Introduction

The blue color that has been obtained by the action of nitrosamines, nitrates, nitrites, and aliphatic nitrocompounds on diphenylamine in sulfuric acid has been regarded [1][1] as a specific test for these substances in the absence of various oxidizing agents that also produce a blue color. In view of the fact that certain nitrocompounds did not give this test, a reinvestigation with pure aliphatic mono- and polynitrocompounds seemed in order.

The nature of the blue color itself has been the subject of investigations by Wieland [2, 3] and Kehrmann [4, 5] and their coworkers, but evidence about the structure of the colored products has been incomplete. It therefore seemed desirable to obtain spectroscopic evidence as to the nature of the colored products.

2. Experimental Details

2.1. Reagents and Materials

a. *Sulfuric acid solution* (approximately 29 *N*) was prepared by adding 4 volumes of sulfuric acid (approximately 36 *N*) to 1 volume of distilled water.

b. *Diphenylamine reagent* was prepared daily by dissolving 20 mg of recrystallized diphenylamine in 100 ml of warm 29 *N* sulfuric acid solution.

c. *Aliphatic nitro compounds*, some of which were laboratory preparations and others commercial products, are listed in table 1.

d. *N-Nitrosodiphenylamine*, mp 67° *C*, was obtained by nitrosation of diphenylamine [6].

e. *Tetraphenylhydrazine* was prepared by oxidizing diphenylamine with lead dioxide [7].

f. *N,N'-Diphenylbenzidine*, mp 238° *C*, was prepared by rearrangement of tetraphenylhydrazine with sulfuric acid [7].

g. *N,N'-Diphenyldihydrophenazine*, mp 170° *C*, was obtained by refluxing tetraphenylhydrazine with toluene [2].

*Present address, Blockson Chemical Co., Joliet, Ill.

[1] Figures in brackets refer to references at the end of this paper.

TABLE 1. *Results of the diphenylamine test for aliphatic nitrocompounds*

Compound	Time in minutes before appearance of blue color [a]	
	Direct method	Indirect method
Nitromethane	[b] Negative	Negative.
Tetranitromethane	do	Do.
Nitroethane	do	Do.
1-Chloro-1-nitroethane	1½	1.
1,1-Dinitroethane	6 to 20	5.
1-Bromo-1,1-dinitroethane	Negative	Negative.
1,1,1-Trinitroethane	do	Do.
1-Nitropropane	do [b]	Do.
1-Chloro-1-nitropropane	4 to 6	5.
1,1-Dichloro-1-nitropropane	0.5	0.5.
1,1-Dinitropropane	22	9.
2-Nitropropane	5 to 6	1.
2-Bromo-2-nitropropane	0.2	Immediate.
2-Chloro-2-nitropropane	Immediate	0.2.
2,2-Dinitropropane	Negative	Negative.
2-Nitro-2-methyl-1-propanol	3	3.
1,3-Dinitro-2,2-dimethylpropane	Negative	Negative.
2,3-Dimethyl-2,3-dinitrobutane	Immediate	3.
β-Nitrostyrene	Negative	Negative.

[a] A test was regarded as negative after 1 hr. It is evident that the time required for the formation of the blue color would be dependent upon various factors, including purity and structure of the substance.

[b] The unpurified sample gave a positive test with 1 mg of nitrocompound.

2.2. Performance of the Diphenylamine Test with Pure Aliphatic Nitrocompounds

a. Direct Method

Ten microliters of liquid or 10 mg of solid nitrocompound was dissolved in 10 ml of the sulfuric acid solution, and 10 μliters of the resultant solution was added to 1 ml of diphenylamine reagent. The test tube containing the mixture was maintained in a boiling water bath (approximately 98° *C*) for 1 hr. The time required for the appearance of a blue color is recorded in table 1. Although a test was regarded as negative if no blue color was observed within 1 hr, actually in such cases no blue color appeared even after 8 hr. With nitrocompounds which give a positive test the lower limit of sensitivity seemed to be in the neighborhood of 1 μg.

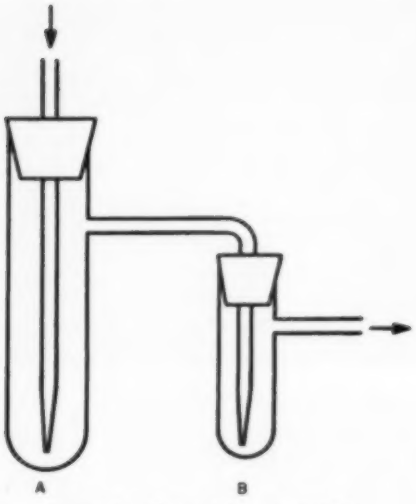

FIGURE 1. *Gas evolution apparatus.*

b. Indirect Method

In tube A of the apparatus, figure 1, was placed 10 mg of solid or 10 μliters of liquid nitrocompound and 2 ml of the sulfuric acid solution. Tube B contained 2 ml of diphenylamine reagent. The apparatus was maintained at 98° C for 1 hr while a slow but continuous stream of air was allowed to flow through the system. In a blank determination, the air did not show oxidizing effects. As before, a test was again regarded as negative if no blue color was observed in tube B within 1 hr. The results are recorded in table 1. The test performed in this manner required more than 1 mg of nitrocompound.

2.3. Isolation of *N*-Nitrosodiphenylamine formed in the Diphenylamine Reaction

In tube A of the gas-evolution apparatus (fig. 1), maintained at 98° C, was placed 500 mg of 2,3-dimethyl-2,3-dinitrobutane and 5 ml of the sulfuric acid solution. Fifty milligrams of purified diphenylamine, dissolved in 5 ml of ethanol, was placed in tube B, which was surrounded by an ice bath. Air was passed through the apparatus at a moderate rate for 1 hr. The solution in tube B was diluted with water to turbidity and refrigerated overnight. The yellow crystals, after recrystallization from pentane, melted at 66° to 67° C and did not depress the melting point of an authentic sample of *N*-nitrosodiphenylamine (mp 67° C).

2.4. Spectroscopic Study of the Blue Color

Solutions containing 8 mg of the following substances were prepared with 100 ml of diphenylamine reagent and allowed to stand overnight at room temperature; A, sodium nitrite; B, potassium nitrate; C, 2,3-dimethyl-2,3-dinitrobutane; D, *N*-nitrosodiphenylamine; E, hydrogen peroxide; F, 1,1-dichloro-1-nitropropane; G, sodium chlorate; H, 2-nitropropane; I, tetraphenylhydrazine; J, *N,N'*-diphenyldihydrophenazine+sodium nitrite; K, *N,N'*-diphenylbenzidine+sodium nitrite; L, J+K (1:1). Substances D, I, J, K, and L, however, were dissolved in 29 *N* sulfuric acid solution containing no diphenylamine. The deep-blue solutions that resulted were then diluted with the sulfuric acid solution to approximately the same relative intensity, and absorption spectra were determined for each solution from 320 μ to 1,000 μ with a Beckman spectrophotometer. The absorption curves are presented in figure 2.

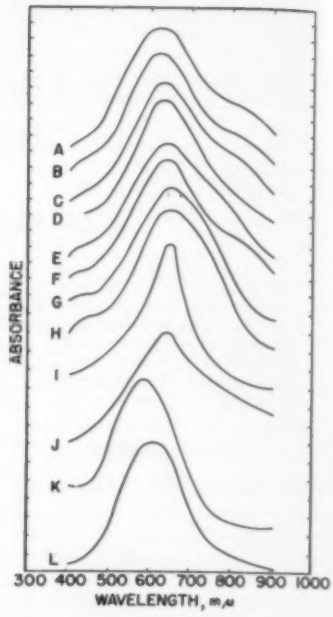

FIGURE 2. *Some absorption curves related to the oxidation and nitrosation of diphenylamine.*

3. Discussion of the Diphenylamine Test

3.1. Effect of Structure of the Aliphatic Nitrocompounds

From the results presented in table 1, it is apparent that the aliphatic nitrocompounds may be divided into two general groups (table 2). (1) Nitrocompounds that have either a single hydrogen atom or three alkyl groups attached to the carbon bearing the nitrogroup give a positive reaction. (2) On the other hand, primary nitroparaffins, 2,2-dinitro- and 1,1,1-trinitrocompounds do not give the test. It is interesting to note that halogen apparently behaves in this test in the same manner as an alkyl group.

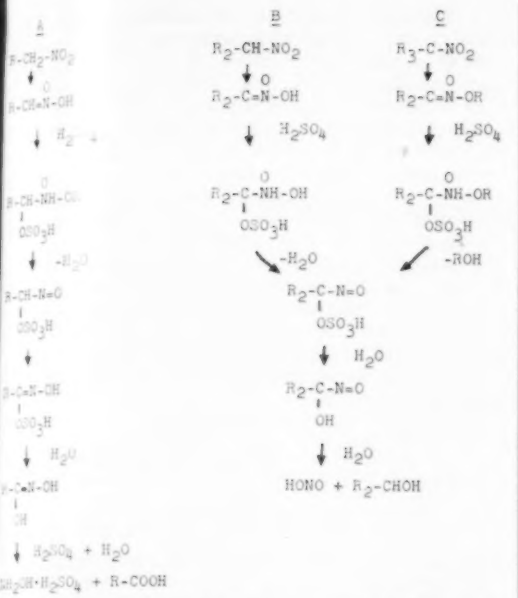

FIGURE 3. *Proposed mechanism for reactions of primary, secondary, and tertiary nitroparaffins in sulfuric acid.*

A possible explanation for this behavior can be arrived at by considering the reaction of nitroparaffins in relatively concentrated sulfuric acid. It is believed [8] that sulfuric acid adds to the double bond of the aci-form of nitroparaffins (fig. 3) and the product loses water to form a nitroso derivative, which in the case of primary nitroparaffins (A), would enolize to a sulfated hydroxamic acid derivative. This, in turn, could hydrolyze through the hydroxamic acid to the carboxylic acid and hydroxylamine sulfate. Hydroxylamine not only does not give a positive diphenylamine test, but actually tends to inhibit the formation of the blue color. By an analogous series of reactions (fig. 3) one may consider that secondary (B) and tertiary (C) nitroparaffins could yield nitrous acid under similar conditions. Actual experimental support for the formation of nitrous acid or oxides of nitrogen was indicated by the fact that those nitrocompounds that gave a test by the direct method also gave it by the indirect method. Further substantiation was afforded by isolation of *N*-nitrosodiphenylamine from the reaction of a tertiary nitroparaffin with sulfuric acid, as described in section 2.3.

TABLE 2. *Results of the diphenylamine test for aliphatic nitro compounds*

Positive	Negative
$R-\underset{\displaystyle NO_2}{\underset{\vert}{CH}}-R'$	$R-CH_2-NO_2$
$R-\underset{\displaystyle NO_2}{\underset{\vert}{\overset{\displaystyle R''}{\overset{\vert}{C}}}}-R''$	$R-\underset{\displaystyle NO_2}{\underset{\vert}{\overset{\displaystyle NO_2}{\overset{\vert}{C}}}}-R$
	$R'''-C(NO_2)_3$

R, Alkyl; R′, alkyl, nitro, or halogen; R″, alkyl or halogen; R‴, alkyl or nitro.

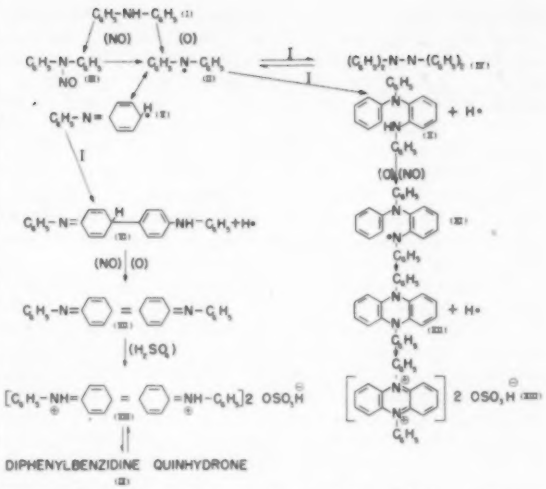

FIGURE 4. *Electronic interpretation of the oxidation and nitrosation of diphenylamine.*

3.2. Nature of Blue Products Formed

In order to ascertain the nature of the blue color derived from diphenylamine, sulfuric acid solutions containing various oxidizing and nitrosating agents were prepared with this reagent, and spectroscopic curves were determined (fig. 2). The absorption curves obtained after either oxidation (B, E, and G) or nitrosation (A, C, D, F, and H) of diphenylamine are quite similar. According to Kehrmann and his coworkers [4, 5], the blue color obtained by oxidation of diphenylamine in sulfuric acid is caused by a quinoidal immonium salt of diphenylbenzidine (VIII, fig. 4), in equilibrium with a hypothetical substance termed "diphenylbenzidine quinhydrone." In support of this hypothesis, they succeeded in isolating diphenylbenzidine in good yields by the zinc-dust reduction of their blue-colored products. Furthermore, Wieland and Gambarjan [7] were able to show that diphenylamine can be oxidized to tetraphenylhydrazine, which in turn could be rearranged in sulfuric acid to *N*,*N*′-diphenylbenzidine. In his earlier work, Wieland [1] had reported the isolation of *N*,*N*′-diphenyldihydrophenazine (XII, fig. 4) from tetraphenylhydrazine in toluene and postulated that some such phenazine sulfate derivative as represented by formula XIII (fig. 4) may be responsible for the blue color in the diphenylamine test. Therefore, both *N*,*N*′-diphenyldihydrophena-

zine and *N,N'*-diphenylbenzidine were synthesized. After treatment in sulfuric acid solution with sodium nitrite, they gave spectral curves J and K, respectively. A mixture of both substances upon treatment with nitrite gave a curve, L, quite similar to curves A through H. Thus, it would seem that both phenazine sulfate and benzidine sulfate derivatives may be responsible for the blue color obtained from diphenylamine with either nitrosating or oxidizing agents. In addition, curve I, obtained for tetraphenylhydrazine, indicates that this substance also may be an intermediate in the reaction.

A possible explanation for the formation of the blue color is outlined in figure 4. Diphenylamine (I) on treatment with oxidizing agents, such as potassium nitrate, hydrogen peroxide, and sodium chlorate, could give the free radical diphenylnitrogen (II), which could also be obtained from (I) by way of *N*-nitrosodiphenylamine (III). The latter compound, which has been isolated previously by the action of sodium nitrite and hydrochloric acid on I, was also obtained from an aliphatic nitrocompound in this study (section 2.3). The free radical II, which is probably in equilibrium with tetraphenylhydrazine (IV), may be written as the paraquinoid form (V). This latter free radical may displace a parahydrogen atom of another molecule of diphenylamine (I), giving *N,N'*-diphenylbenzidine (written as a monoquinoid structure VI), which, on further oxidation or nitrosation, may be converted by way of a diquinoid structure VII to a sulfate such as VIII.

The formation of a phenazine derivative may be explained as follows: The free radical diphenylnitrogen (II) may displace an orthohydrogen atom from another molecule of diphenylamine, giving a derivative of *o*-phenylenediamine (X), which, by way of another free radical (XI), may be converted into *N,N'*-diphenyldihydrophenazine (XII).

The results obtained by Kehrmann and Wieland in conjunction with the spectral curves presented herein, seem to indicate that blue-colored derivatives of both phenazine and benzidine are probably involved in the diphenylamine test. The free radical interpretation is also supported by the fact that nitrosodiphenylamine dissolved in sulfuric acid gives a curve similar to those obtained from diphenylamine upon treatment with oxidizing or nitrosating agents; hence, nitrosodiphenylamine may be an intermediate when diphenylamine in sulfuric acid is treated with either sodium nitrite or aliphatic nitro compounds.

4. References

[1] S. P. Mulliken, A method for the identification of pure organic compounds, p. 27 (John Wiley & Sons, Inc., New York, N. Y., 1916).

[2] H. Wieland, Ann. **381,** 210 (1911).

[3] H. Wieland, Ber. deut. chem. Ges. **46,** 3296 (1913); **52,** 886 (1919).

[4] F. Kehrmann and St. Micewicz, Ber. deut. chem. Ges. **45,** 2641 (1912).

[5] F. Kehrmann and G. Roy, Ber. deut. chem. Ges. **55,** 15 (1922).

[6] S. Wexman, Farm. Chilena **20,** 299 (1946).

[7] H. Wieland and S. Gambarjan, Ber. deut. chem. Ges. **39,** 1499 (1906).

[8] H. B. Hass and E. F. Riley, Chem. Rev. **32,** 397 (1943).

WASHINGTON, June 13, 1952.

Journal of Research of the National Bureau of Standards Vol. 49, No. 3, September 1952 Research Paper 2354

Influence of Prior Strain History on the Tensile Properties and Structures of High-Purity Copper

William D. Jenkins and Thomas G. Digges

Tensile tests were made at room temperature on oxygen-free high-conductivity (OFHC) copper initially as annealed, as cold-drawn different amounts, and as prestrained in creep at 110°, 250°, and 300° F.

The shape of the true stress-strain curves obtained on copper cold-drawn 34-, 40-, and 70-percent reduction in area indicate a strain aging effect in the specimens when subjected to stresses in the vicinity of the maximum load. This phenomenon of strain aging is usually more closely associated with alloys of the ferrous type than with a high-purity nonferrous metal. The present results show that the strength, ductility, and hardness of the copper is markedly affected by its prior strain history. The test conditions are correlated with the tensile properties, hardness, necking characteristics, formation of microcracks, and substructures.

1. Introduction

The tensile and other properties at room temperature of both annealed and cold-drawn high-purity copper were determined as a part of the Bureau's research investigations of the mechanism of creep and of the effects of subzero temperatures on the mechanical properties of metals and alloys. The creep behavior of this same lot of copper as annealed and as cold-drawn 40-percent reduction in area and the influence of low temperatures on the true stress-strain relation in tension of the annealed copper have been discussed in previous publications [1, 2, 3.[1]] The resistance to creep and to fracture at moderately elevated temperatures was materially increased by cold-drawing the copper, but this superiority was accomplished by a decrease in ductility. The strain history of the copper also affected the degree of dissociation of the parent grains into subsize grains during creep and the type of fracture. However, the strength in tension of the annealed copper increased continuously with a decrease in temperature to −320° F without any impairment of its ductility.

The present tests were made to evaluate the effects of prestraining different amounts in creep under tension at 110°, 250°, and 300° F and of cold-drawing on the tensile properties at room temperature and on the hardness and structures produced in the fractured specimens. The straining treatments used prior to testing the specimens in tension at room temperature are summarized in table 1.

2. Material and Procedures

All the specimens were prepared from 13/16- or 7/8-in. diameter bars processed from one lot of oxygen-free high-conductivity (OFHC) copper containing 99.99+ percent of copper. The four bars

TABLE 1. *Strain history of specimens prior to testing in tension at room temperature and reference to the figures used in the text for summarizing the test data*

Initial condition	Creep test			Figure reference	
	Temperature	Rate	Plastic extension	Tensile properties and hardness	Structures
	°F	%/1000hr	%		
A1; annealed 800° F	None	None	None	1, 2, 3, 5, 7, 18, 19	6A
Do	110	2.75	39.7	3, 5, 19	9B, 11A, 12A, 14A, 17C
Do	110	1.08	19.0	19	9C
Do	250	10.1	49.0	18, 19	12D, 14D
Do	250	1.04	23.1	3, 5, 18, 19	9D, 10B, 11B, 12C, 14C, 16A, 17D.
A1; annealed 800° F; strained 9% in tension at room temperature	250	1.1	7.0		12B, 14B
A2; cold-drawn 34% reduction in area	None	None	None	1, 2, 18, 19	6B, 13C
A3; cold-drawn 40% reduction in area	Do	do	do	1, 2, 4, 5, 18, 19	11C, 15A, 17E
Do	250	0.20	0.73	4, 5, 18, 19	9E, 11D, 13A, 15B, 16B
Do	300	.36	.98	4, 5, 18, 19	9F, 10C, 11E, 15C, 17F
Do	{110 {300	.63 200+	.73} 2.8}	4, 5, 18, 19	9G, 11F, 13B, 15D
B1; cold-drawn 70% reduction in area	None	None	None	1, 2, 18, 19	6C, 13D
B1; cold-drawn 70% reduction in area; then annealed 1300° F	do	do	do	7, 8, 18, 19	6D, 9A, 10A, 16C, 16D, 17A, 17B

Figures in brackets indicate the literature references at the end of this paper.

used were procured in conditions as follows:

A. Bright annealed at 800° F for 1 hr:

1. As annealed ..... 0.025-mm average grain diameter.
2. Cold-drawn ..... 34-percent reduction in area.
3. Cold-drawn ..... 40-percent reduction in area.

B. Bright annealed at 1150° F for 50 min (0.045-mm average grain diameter):

1. Cold-drawn ..... 70-percent reduction in area.

Tensile specimens, 0.505 in. in diameter with 2-in. gage length, were prepared from the above bars. In addition, a portion of the bar cold-drawn 70 percent (condition B1) was reannealed in the laboratory at 1,300° F in air for 1 hr, thereby producing an average grain diameter of 0.120 mm, before preparing the tensile specimen. Some tensile specimens prepared from the bars as annealed at 800° F and as cold-drawn 40 percent (conditions A1 and 3, respectively) were strained in creep at various temperatures before fracturing them in tension at room temperature.

The tensile tests were made at room temperature at a rate of approximately 1-percent reduction of area per minute. A micrometer was used to follow the change in diameter of the tensile specimen during the testing. Simultaneous observations were made of the minimum diameters and loads.

Two flats were prepared approximately 0.2 in. apart, diametrically opposite, symmetrical to and parallel to the longitudinal axis of the fractured specimen. Rockwell hardness (F scale, 60-kg load, 1/16-in.-diameter ball) readings were made at various points along the center line of each flat. Specimens were also cut from the bar cold-drawn 70 percent for use in determinirg the effect of annealing temperature on its grain size and hardness.

3. Results and Discussion

3.1. Effect of prestraining on tensile properties

a. Cold-drawing at room temperature

The relations between true stress and the total true strain [2] (due to cold-drawing and tension) for specimens of copper as annealed and as cold-drawn different amounts are shown in figure 1. The true stress at the beginning of plastic deformation in tension, and the true stress and true strain at maximum load increased with an increase in the amount of cold-drawing. The values for true stress at the beginning of fracture in each specimen as annealed, or as cold-drawn 40 or 70 percent, were nearly alike but cracking started at a somewhat lower value of stress in the specimen cold-drawn only 34 percent. However, the total true strain at the beginning of fracture of this specimen was about the same as that of the specimen as annealed or as cold-drawn 40 percent. In this series of tests the total strain at the beginning of fracture attained a maximum in the specimen cold-drawn 70 percent.

The observed differences in the relative positions and slopes of the true stress-strain curves can be partly ascribed to variations in the stress system during plastic deformation in tension in addition to variations in the degree of strain hardening induced by cold-drawing. For the annealed specimen the deformation was essentially by unidirectional tension for stresses up to the maximum load. As the specimen began to neck at this point, further deformation was under a triaxial stress system. This triaxiality results in modifying the position of the curve to higher values of stresses for similar strains than would have been the case had deformation to complete fracture been under a unidirectional system. Similarly, necking began at maximum load in each of the cold-drawn specimens and thereafter deformation was by triaxiality. The effect of triaxiality, however, varied with the amount of cold-working and thereby affected the stress-strain relationship. Furthermore, some triaxiality also existed during cold-drawing, and this is a factor that would be expected to decrease the value of the stress at the maximum load. Obviously, some strain hardening occurred during cold-drawing, and the capacity of the copper to further strain harden was thereby reduced.

The effect of cold-drawing on the hardness and tensile properties of the copper is shown by the results given in figure 2. The yield strength, tensile strength and hardness increased at a decreasing rate with an increase in the amount of cold-drawing. The plastic extension in tension, however, was materially decreased by cold-drawing, but the magnitudes of the decrease in plastic extension and of the increase in hardness were not significantly affected by varying the degree of cold-working from 34 to 70 percent. For example, the plastic extension at maximum load did not exceed 1 percent in any of the cold-drawn specimens but was about 30 percent in the annealed specimen. Thus the improvements in strengths and in hardness by cold-drawing the copper were accompanied by an impairment in its plastic extension in tension at room temperature.

b. Cold-working in creep at different temperatures

(1) Initially as annealed. The influence of straining specimens of the annealed copper in creep at 110° and 250° F on the true stress–true strain relation at room temperature is shown by the curves in figure 3. The curves for the specimens prestrained in creep fall somewhat below that of the annealed specimen. However, the true stress at maximum load (point M) of the annealed copper was increased slightly by prestraining 23.1 percent in creep at 250° F and further increased in another specimen strained 39.7 percent in creep at 110° F before fracturing in tension at room temperature. The curves for stresses from the maximum load to the beginning of fracture for the two specimens prestrained in creep were nearly alike, but the specimen prestrained at 250° F began to fracture at considerably lower stress and strain than

[2] "True strain" is defined as the natural logarithm of the ratio of the initial cross-sectional area (A_0) of the specimen to its current minimum cross-sectional area (A).

the specimen prestrained in creep at 110° F. stress required to initiate fracture in the latter imen was only slightly less than that of the ealed specimen and the corresponding total ins at this point were nearly alike for the two imens. Although the specimen prestrained at ° F was strained into the third stage of creep, the e indicates that its mode of deformation in ten- at room temperature was similar to that of the ealed specimen; however, straining the specimen the second stage of creep at 250° F was believed be sufficient to initiate cracks of submicroscopic ensions, and these possibly are partly responsible its restricted ductility at room temperature. se assumptions are supported by the evidence ained from a metallographic examination of the ctured specimens. In the specimen prestrained percent at 250° F, numerous cracks were ob- ed in the region adjacent to and at some distance necked portion of the specimen) from complete ture (fig. 12C), whereas in the specimens pre- ined 39.7 percent at 110° F, the microcracking confined to the region of complete fracture 12A); the mode of fracture of the latter specimen similar to that previously described for an an- led specimen [1].

Straining the specimen 23.1 percent in creep at ° F also lowered appreciably both the true stress the strain at complete fracture in relation to se of the specimens as annealed or as prestrained percent at 110° F.

2) Initially as annealed and then cold-drawn 40 ent. The effect of prestraining the cold-drawn per in creep at different temperatures on some sile properties at room temperature is shown in re 4. The strain in creep at moderately elevated peratures resulted in some modification of the itions of the true stress-strain curves at room perature for values of true stresses below 65,000 In this range of stresses, the curves for the imens prestrained in creep fall somewhat below t of the specimen as cold-drawn. At true stresses 65,000 psi, or higher, the true stress-strain curve the specimen strained 0.73 percent at 110° F, and n 2.8 percent at 300° F nearly coincided with that the specimen as cold-drawn. The values for true ss at maximum load, and true stress and strain the beginning of fracture were also similar for se two specimens, but the values for stress and in at complete fracture were lower in the specimen ained in creep.

Prestraining a specimen 0.73 percent at 250° F and ther specimen 0.98 percent at 300° F lowered ewhat the true stresses at maximum load and preciably decreased the true stresses and strains the beginning and at complete fracture. The rease in stresses and strains at fracture was con- erably more pronounced in the specimen pre- ained at 300° F than in the specimen prestrained 250° F. The values of stress and strain at com- te fracture of the former specimen were lower than e corresponding values at the beginning of fracture the latter specimen. This deterioration, as shown in the tensile properties at room temperature, is believed to be due partly to the initiation of cracks of submicroscopic or possibly microscopic dimension (fig. 15, C) by the presence of tensile stresses induced in creep. Moreover, the tendency towards brittle fracture was increased by increasing the temperature of the creep test from 250° to 300° F and adjusting the stresses to produced strain rates of 0.2 to 0.4 percent/1,000 hr. (figs. 11, D and E).

The true stress-strain curves at small strains of the annealed and cold-drawn copper specimens are reproduced on an enlarged scale in figure 5. The reversal of curvature of the curve for the cold-drawn specimen not prestrained in creep indicates that an aging effect took place subsequent to the cold-drawing operation (fig. 5, A). This initial effect is in contrast to the recovery behavior usually associated with nonferrous metals such as aluminum [4] after cold-extending and appears to be more closely associated with the strain-aging behavior of alloys of the ferrous type [5]. The residual stresses due to cold-drawing and aging of the copper are partly relieved after the specimen has been deformed slightly past its maximum load. This caused a lowering of the true stress values over a limited range of increasing strains. This effect of aging is less pronounced but still present, as is shown by the positions of the true stress-strain curves for the two cold-drawn specimens prestrained in creep at 250° and 300° F to true strains of less than 0.01. The relief of the causes of the aging phenomenon appears to be more pronounced for the specimen prestrained at the higher temperature even though the creep strain was slightly less. The true stress-strain values for the specimen prestrained in creep at 110° and at 300° F to a higher strain value show a pronounced recovery characteristic, as evidenced by a decrease in true stress values at small strains. This effect, however, was followed by rapid strain-hardening in contrast to the other two specimens whose rate of strain-hardening was approximately equal to that of the cold-drawn specimen in the region from the inflection range up to a true strain value of about 0.15. A relief of internal stress followed by rapid strain-hardening is also shown by the position of the true stress-strain curve for the annealed specimen that was prestrained in creep at 250° F, whereas aging appeared to predominate for the specimen prestrained in creep at the lower temperature (fig. 5, B). The recovery phenomenon associated with straining in creep above the temperature that was used in the tensile tests is further illustrated by the values labeled e_1, e_2, etc. in figure 5. The broken lines intersecting the true stress-strain curves at e_1, e_2, e_5, . . . are in each case the extrapolation of the linear portion of the corresponding true stress-strain curve for a specimen prestrained in creep. The points e_2, e_4, e_8 represent the strains actually obtained at the corresponding stress. In spite of the fact that the true stress-strain curve was lowered considerably for the specimens prestrained at 110° and 300° F to about 0.09 strain (fig. 5, A), the attainment of the stress at e_{10}, corresponding to the stress of the

cold-drawn copper at e_9, took place at a much smaller change in strain than similar attainments for the other two specimens (e_8 and e_7, and e_8 and e_3). However, prestraining in creep to different strains at different temperatures had no appreciable effect on the initial recovery characteristics of the annealed specimens when the relationships are evaluated by this means. A comparison of the properties at small strains with the true stress-strain relationships, shown by figures 3 and 4, indicates that the instantaneous strain state of the material does not necessarily predict the subsequent flow properties.

Burghoff and Blank [6] extended cold-drawn specimens of oxygen-free copper in creep at 300° and 400° F prior to testing in tension at room temperature. The tensile strength was materially decreased and the elongation was increased in specimens initially cold-drawn 84 percent after exposure of 6,500 hr at 300° or 400° F, with zero or small stresses. Partial or complete recrystallization occurred in the specimens exposed at 300° or 400° F.

Some strain-aging effects, associated with OFHC copper have recently been discussed by Lubahn [7]. From results of room-temperature tensile tests, interrupted by various heat treatments, he suggests that the aging process may be associated with (a) yield-point phenomenon, (b) increase in flow stress, (c) discontinuous yielding, and (d) abnormally low rate sensitivity.

3.2. Effect of grain size

A change from 0.025 to 0.120 mm in the average diameter of the grains in the annealed copper (fig. 6, A and D) caused a decrease in the yield strength (0.2% offset) from about 11,000 to 6,000 psi, a slight lowering of the true stress-strain curve for stresses in the region of strain below 0.15, and a decrease in the stess and the strain at the beginning of fracture (fig. 7). However, the tensile strength and the strain at this stress were not affected by the increase in grain size.

The effect of annealing temperature (1 hr at temperature) on the grain size and hardness of the copper cold-drawn 70 percent from an average grain diameter of 0.045 mm (condition B1), is shown in figure 8. Increasing the annealing temperature from 800° to 1,100° F resulted in a slight increase in grain size. The size of the grains continued to increase gradually as the temperature was further increased to 1,200° F and then increased markedly at an annealing temperature of 1,300° F. This grain growth and recovery was accompanied by a corresponding decrease in hardness of the recrystallized specimens.

The features observed in necking and fracturing the specimens in tension at room temperature can be conveniently classified into three groups, as illustrated in figure 10, A, B, and C. All the specimens fractured at room temperature were of the ductile, or fibrous, type, but the values for strain and reduction of area varied appreciably with the prior-strain history. Roughing of the surface, necking down to nearly a point and then fracturing at approximately right angles to the longitudinal axis of the specimen (fig. 10, A) were characteristics of all specimens strained prior to testing in tension at room temperature. Possibly the relatively large grains contributed to the excessive roughing of the surface in the region of the fracture of this particular specimen. The appearance of the surface at and near the fracture of the specimens prestrained by cold-drawing and in creep is represented by the specimen shown in figure 10, C. Some roughening of the surface is evident in this specimen, but it is considerably less pronounced than that of the specimen not prestrained in creep (fig. 10, A). The fractures of the prestrained specimens were usually in a plane about 45° to the longitudinal axis. No macrocracks were observed in the surfaces near complete fracture of the specimens shown in fig. 10, A and C, but there was some evidence of their presence in B. Moreover, macrocracks were prominent in an initially annealed specimen after being strained to complete fracture in creep at 300° F (figure 10, D).

An end view of some of the fractured specimens is given in figure 11. The cavities located in the central regions and their relative absence near the outer surface support the belief that cracking was initiated near the axis and the outer surface was the position of final rupture.

3.3. Effect of prestraining on structures

a. Necking and fracturing characteristics

Figures 9, 10, and 11 are photographs of some of the specimens selected as representative of the necking and fracture characteristics as affected by prior strain history. As all of the specimens showed some necking (fig. 9), it is believed that cracking eventually leading to failure started at the axis of each specimen and progressed outward, and the final fracture was that of the "rim" at the surface. However, the degree of necking and the magnitude of the rim effect of the specimens were influenced by the amount, rate, and temperature of prestraining. For example, an initially annealed specimen prestrained 39.7 percent extension in creep at 110° F developed both a relatively pronounced neck (fig. 9, B) and rim (fig. 11, A), whereas the specimen cold-drawn 40-percent reduction of area and then strained in creep only 0.9 percent at 300° F developed a relatively small neck (fig. 9, F), a small rim (fig. 10, C and fig. 11, E), and fractured in a relatively brittle manner. As these two specimens were processed from the same lot of copper and tested in tension at room temperature at the same strain rate, the defference in ductility at fracture must be attributed to changes brought about by the different methods of prestraining.

b. Rim formation and microcracks

The influence of prestraining on the formation of microcracks and the flow characteristics at the rim in the region of complete fracture in tension at room temperature is shown by the photomicrographs of figures 12 and 13. (No microcracks were evident near the surface or axis of the annealed specimen not prestrained in creep.) Furthermore, it was

sible to strain a specimen at 110°F into the third stage of creep without the development of numerous microcracks except in the vicinity of complete fracture, in subsequent fracturing at room temperature (fig. 12, A). Microcracks were not observed in another specimen (fig. 12, B) prestrained only into second stage of creep at a somewhat higher temperature (250° F). However, a general disintegration is shown in two other specimens that were strained at 250° F into either the second or third stage of creep (fig. 12, C and D). As previously pointed out [2], the presence or absence of microcracks in specimens fractured solely in creep depended on the initial condition of the copper, the creep temperature, and amount of extension in creep; relatively slow creep rates, high temperatures, and increase in amount of extension into the third stage of creep favored a general disintegration.

Relatively few microcracks are evident near the surface of the copper that was cold-drawn before testing in tension (fig. 13) even when the specimens were prestrained into third stage of creep (fig. 13, A and B). The effect of prestraining at the higher temperature (fig. 13, B) seems to promote a grain recovery effect causing a healing of the broken bonds to take place and thus a restoration of ductility and strength (fig. 4). Limited grain fragmentation and realinement of the grains in a wavy manner results in cold-drawing the copper 34-percent reduction in area prior to testing in tension (fig. 13, C), whereas further cold-drawing to 70-percent reduction in area (fig. 13, D) appeared to result in considerable grain fragmentation and an increase in tensile strength and total ductility at fracture (fig. 1).

c. Microcracks and structures at axis

Structures at the surface do not necessarily reflect the flow characteristics in the interior of these specimens as the stress systems in these regions are different. However, as shown in figures 14 and 15, microcracks are evident near the axis of all the specimens that showed the tendency toward crack formation near the surface (figs. 12 and 13). Relatively few cracks are visible in the annealed specimen prestrained at 110° F to a large strain (fig. 14, A) or at 110° F to a small strain (fig. 14, B). A number of cracks are evident at the axis of the specimen prestrained in creep into the second stage at 250° F with a slow creep rate (fig. 14, C) and of another specimen prestrained into the third stage of creep at the same temperature with a faster creep rate (fig. 14, D). However, the contour of the cracks is different, probably due to the different mechanisms of crack nucleation in creep and subsequent growth in the tensile test.

The effect of prior straining on the formation of microcracks at the axis of the cold-drawn copper is shown in figure 15. Some microcracks of elliptical shape are evident in specimens not strained in creep (fig. 15, A), but these are much smaller than the cracks in a specimen prestrained in creep at 250° F to a small strain (fig. 15, B). The type of fracture and the shape of the microcracks appear to be affected significantly by raising the creep test temperature (fig. 15, C) without appreciable change in creep rate or in plastic strain. Straining in creep at a higher temperature (300° F) and at a faster rate after prestraining at 110° F to a small strain value seems to cause an effect that is reflected in the absence of microcracks even in the region of complete fracture at room temperature (fig. 15, D).

A further indication of the effects of prior history on the internal structure and the initiation and growth of microcracks is shown in figure 16. The presence of microcracks in the regions representative of structure at the limit of uniform strain (fig. 16, A and B, several cracks are enclosed in circles) indicates that a partial disintegration was evident throughout these specimens. As no microcracks have been found in any of the copper specimens previously strained into the second stage of creep [1, 2], it is believed that the conditions for crack formation are initiated during the second stage of creep, and with a continued straining in tension at room temperature the cracks grow to such a size that the flow properties of the copper are affected. Representative structure in the unnecked portion of the specimens not tested in creep is shown in figure 16, C and D. No microcracks were evident in this region of either this specimen or of any of the specimens not prestrained under creep conditions. The relative straightness of portions of the twins and the difference in orientation between the twins and the surrounding material (fig. 16, D) indicate that these are annealing twins that were nucleated at a grain boundary (lower arrow) and grew toward another boundary (upper arrow) of the grains. During deformation portions of the annealing twins were bent, thus indicating that they are ductile (fig. 16, C).

d. Substructures

The effect of prestraining on the formation of substructures is shown in figure 17. Etch patterns representative of the initially annealed structure are shown in figure 17, A. It has been previously pointed out [8] that the size of these substructures is influenced by the temperature of annealing and that the tendency toward formation of substructures of smaller size during deformation increased with decrease in test temperature and with increase in creep rate [1, 2]. However, the latter observations were based on tests carried to completion in creep tests only. The present tests show that the sizes of the substructures in the copper were materially reduced by testing in tension at room temperature only (fig. 17, A and B). It is also evident that both the size and distribution of the substructures are affected by the temperature, creep rate, or strain in creep prior to the tensile test (figs. 17, C, D, E, and F). Both high temperatures and slow strain rates appear to increase the tendency toward the formation of a large number of these substructures.

3.4. Effect of prestraining on specimen contour and on hardness at room temperature

The relation of reduction of area to distance from the fractured surface and to hardness at room temperature, of specimens tested in tension at room temperature, as affected by prestraining, is shown in figures 18 and 19. The distribution of ductility as measured by the reduction of area values along the specimen was materially affected by cold-drawing the copper prior to testing in tension (fig. 18, A) but increasing the amount of cold-drawing from 34- to 70-percent reduction of area had no appreciable effects on the final contour of the surface of the specimen. Annealing at 1,300° F appeared to restore the original necking characteristics so that the curve nearly coincided with the curve obtained with the specimen annealed at 800° F (fig. 18, B). However, when specimens cut from the latter bar were strained in creep before the room-temperature tensile test, a more brittle type of fracture, as shown by decrease in sharpness of the neck (fig. 18, C), was obtained. This tendency toward brittle fracture was also evident in the cold-drawn specimens after straining in creep (fig. 18, D), and was promoted by an increase in creep temperature or by a decrease in creep rate.

The effect of prestraining on the relation between hardness at room temperature and reduction of area is shown in figure 19. The trend was for the hardness to increase with increase in reduction of area up to values of about 35 percent for the initially cold-drawn and 50 percent for the initially annealed specimens. Thereafter, the hardness either remained constant or decreased with an increase in reduction of area. The specimen initially cold-drawn 40 percent (fig. 19, A) had numerous cracks in the region corresponding to 50-percent reduction of area (fig. 15, A). Reannealing at 1,300 °F after cold-drawing 70 percent caused a lowering of the hardness, at all strains, to values approximately the same as those of the specimen initially annealed at 800° F (fig. 19, B). The average grain diameter of the specimen annealed at 1,300° F was about five times that of the specimen annealed at 800° F (0.120 and .025 mm, respectively). Straining in creep at 110° F to an extension of 19 percent had no appreciable effect in lowering the hardness-reduction of area curve of the initially annealed specimens (fig. 19, C). However, the relative positions of the hardness-reduction of area curves and the peak-hardness values were altered by straining in creep at higher temperatures or to higher strain values (fig. 19, C and D). Several factors, such as differences in the stress systems, size and distribution of the microcracks and substructures, appear to influence the hardness values of the copper.

4. Summary

Tensile tests were made at room temperature on OFHC copper initially as annealed, as cold-drawn, and as prestrained under creep conditions. Microscopic examinations and hardness tests were m at room temperature to ascertain the effects of prior thermal-strain history on the structure hardness.

Yield strength, tensile strength, initial hardn true stress at maximum load, increased with incre in prestraining by cold-drawing; this superiority the strength and hardness properties was acc panied by a decrease in ductility at maximum l and at fracture.

The general trend was for a decrease in the stress, fracture stress, and ductility as the straining temperature in creep increased and creep rate decreased.

Aging, due to prestraining, and recovery w evidenced by the shape of the true stress-st curves.

The degree of necking and the tendency for formation of a rim at fracture increased with decrease in prestraining temperature or with increase in prestraining rate. However, the tend cy for recovery, disintegration by microcracking, the size of substructure were increased as the straining temperature was increased. Microcrack also was increased by decreasing the prestrain rate in creep.

An increase in grain size tended to lower both hardness and yield strength. The temperature rate of prestraining also materially affected hardness.

The authors gratefully acknowledge their inde edness to C. R. Johnson for his assistance in test program.

5. References

[1] W. D. Jenkins and T. G. Digges, Creep of high-pu copper, J. Research NBS **45,** 153 (1950) RP2121.

[2] W. D. Jenkins and T. G. Digges, Creep of annealed cold-drawn high-purity copper, J. Research NBS 272 (1951) RP2254.

[3] G. W. Geil and N. L. Carwile, Tensile properties copper, nickel, and some copper-nickel alloys at temperatures, NBS Circular 520 (1952).

[4] W. D. Jenkins, Creep of high-purity aluminum, Research, NBS **46,** 310 (1951) RP2201.

[5] D. J. McAdam, Jr., G. W. Geil, D. H. Woodard W. D. Jenkins, Influence of strain aging on the fract stress of low carbon steel, Trans. AIME **176,** 436 (19

[6] H. L. Burghoff and A. I. Blank, The creep characteris of copper and some copper alloys at 300, 400, 500° F, Proc. Am. Soc. Testing Materials **47,** (1947).

[7] J. D. Lubahn, Strain aging effects, Trans. Am. Metals **44,** 643 (1952).

[8] P. Lacombe and L. Beaujard, The application of figures on pure aluminum to the study of some mi graphic problems, J. Inst. Metals LXXIV, 1 (19

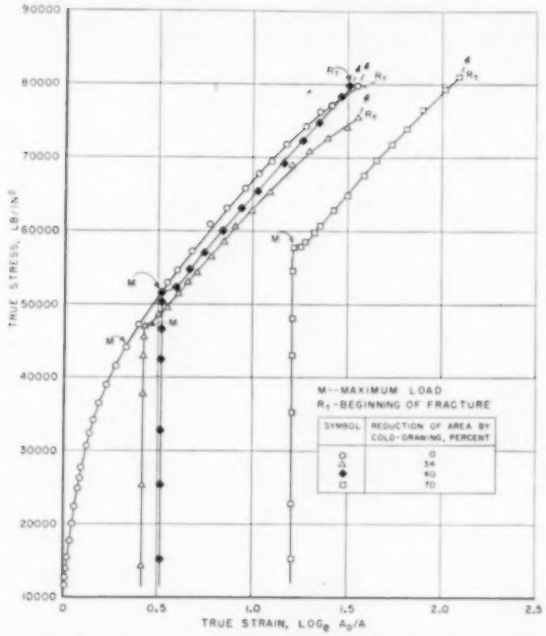

FIGURE 1. *Effect of cold-drawing on the true stress-strain relation at room temperature of copper.*

The strains corresponding to cold-drawing are included in the plotted values.

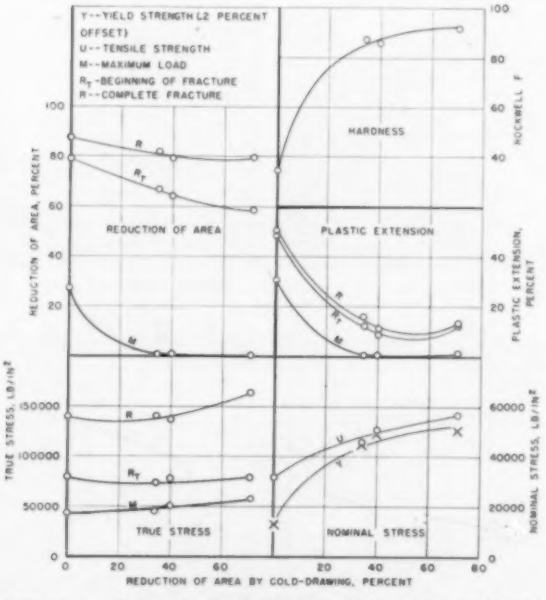

FIGURE 2. *Effect of cold-drawing on the hardness and tensile properties at room temperature of copper.*

The hardness tests were made on cross sections of the bars initially as annealed and as cold-drawn.

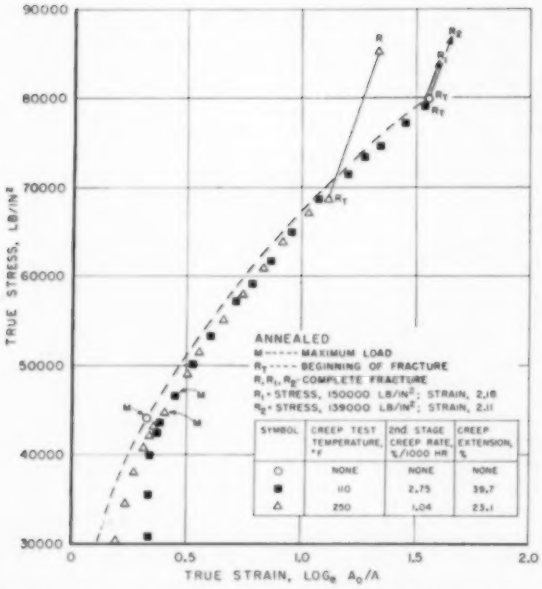
ANNEALED
M----- MAXIMUM LOAD
R_T ---- BEGINNING OF FRACTURE
R, R_1, R_2 COMPLETE FRACTURE
R_1 = STRESS, 150000 LB/IN²; STRAIN, 2.18
R_2 = STRESS, 139000 LB/IN²; STRAIN, 2.11
SYMBOL | CREEP TEST TEMPERATURE, °F | 2nd STAGE CREEP RATE, %/1000 HR | CREEP EXTENSION, %
○ | NONE | NONE | NONE
■ | 110 | 2.75 | 39.7
△ | 250 | 1.04 | 23.1
TRUE STRESS, LB/IN²
TRUE STRAIN, LOG$_e$ A_o/A

FIGURE 3. *Effect of prestraining in creep on the true stress-strain relation at room temperature of annealed copper.*

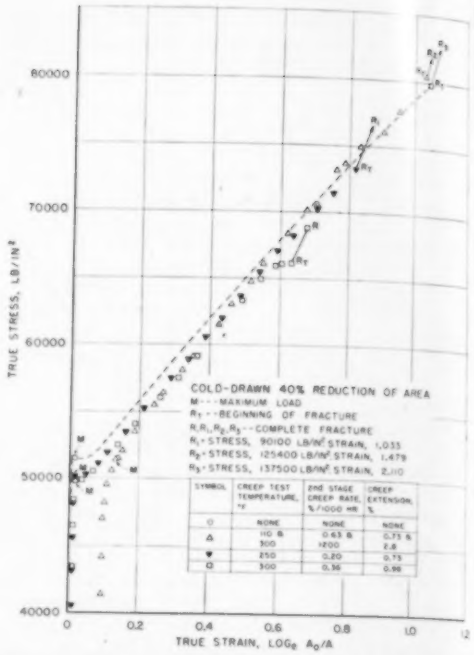
COLD-DRAWN 40% REDUCTION OF AREA
M---MAXIMUM LOAD
R_T--BEGINNING OF FRACTURE
R,R_1,R_2,R_3--COMPLETE FRACTURE
R_1=STRESS, 90100 LB/IN² STRAIN, 1.033
R_2=STRESS, 125400 LB/IN² STRAIN, 1.479
R_3=STRESS, 137500 LB/IN² STRAIN, 2.110
SYMBOL | CREEP TEST TEMPERATURE, °F | 2nd STAGE CREEP RATE, %/1000 HR | CREEP EXTENSION, %
○ | NONE | NONE | NONE
△ | 110 & 300 | 0.63 & >200 | 0.75 & 2.8
▼ | 250 | 0.20 | 0.75
□ | 300 | 0.36 | 0.96
TRUE STRESS, LB/IN²
TRUE STRAIN, LOG$_e$ A_o/A

FIGURE 4. *Effect of prestraining in creep on the true stress-strain relation at room temperature of cold-drawn copper.*

* The strain corresponding to cold-drawing 40-percent reduction in area is not included in the plotted value.

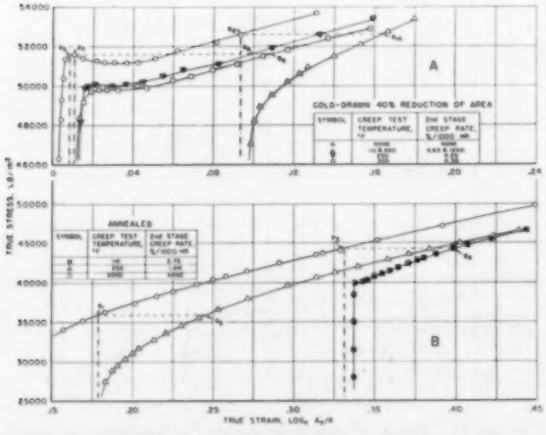

FIGURE 5. *Effect of prestraining in creep on the true stress-strain relation, at small strains, at room temperature, of both cold-drawn and annealed copper.*

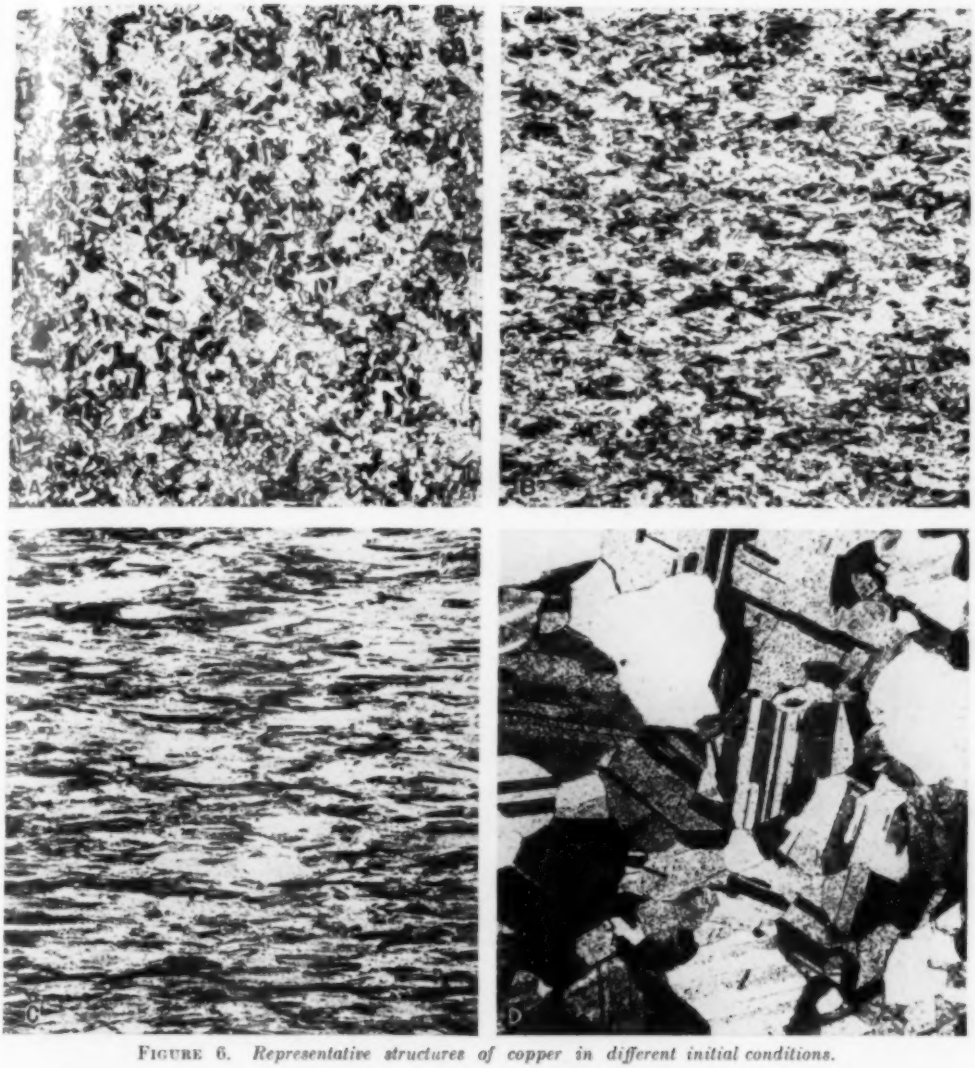

FIGURE 6. *Representative structures of copper in different initial conditions.*

Longitudinal sections etched in equal parts NH_4OH and H_2O_2 (3%). ×75.
A, Annealed at 800° F; 0.025 mm average grain diameter; B, annealed at 800° F, then cold-drawn 34-percent reduction in area; C, annealed at 1,150° F, then cold-drawn 70-percent reduction in area; D, cold-drawn 70-percent reduction in area and then annealed at 1,300° F; 0.120-mm average grain diameter.

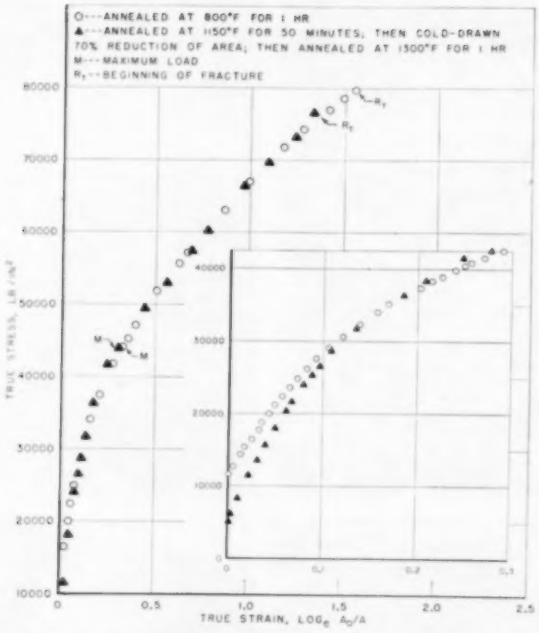
O---ANNEALED AT 800°F FOR 1 HR
▲---ANNEALED AT 1150°F FOR 50 MINUTES, THEN COLD-DRAWN 70% REDUCTION OF AREA; THEN ANNEALED AT 1300°F FOR 1 HR
M---MAXIMUM LOAD
R---BEGINNING OF FRACTURE
TRUE STRESS, LB/IN²
TRUE STRAIN, LOGe A0/A

FIGURE 7. *Effect of grain size on the true stress-strain relation at room temperature of annealed copper.*

Annealed at 800° F, 0.025 mm average grain diameter. Annealed at 1,300° F, 0.120-mm average grain diameter.

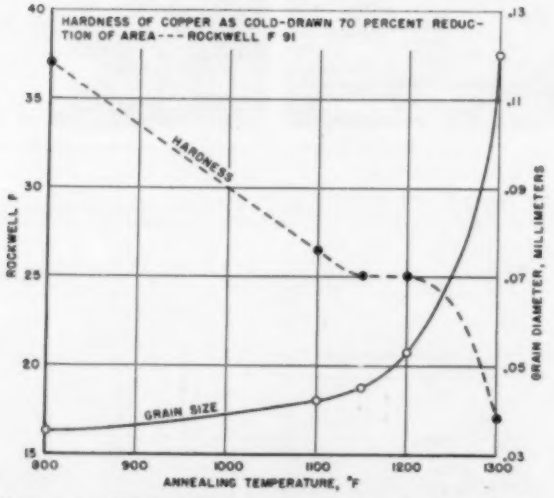

FIGURE 8. *Effect of annealing temperature on the grain size and hardness of cold-drawn copper.*

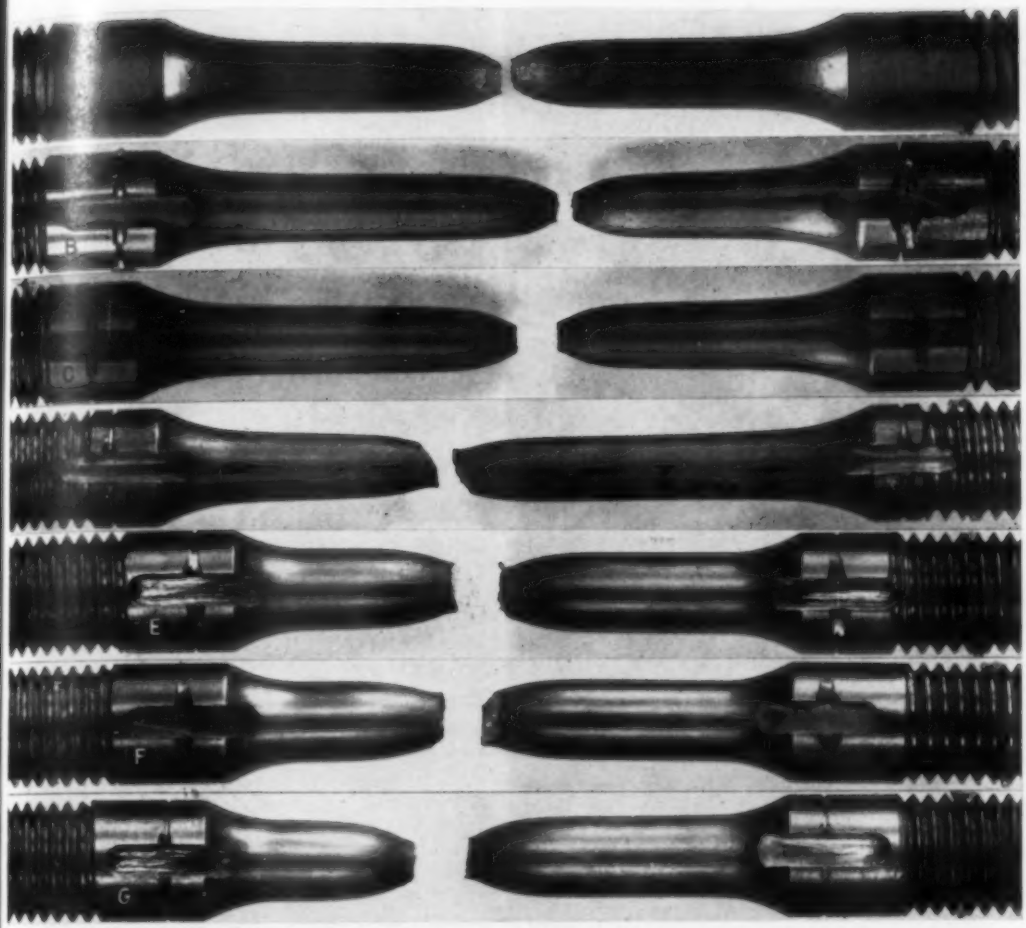

FIGURE 9. *Some of the copper specimens after fracturing at room temperature.*

Unetched, ×1.

	Initial condition	Creep test			True strain at complete fracture
		Temperature	Rate	Plastic extension	
		°F	%/1,000 hr	%	
A	Cold-drawn 70%; annealed 1,300° F.	None	None	None	1.96
B	Annealed, 800° F.	110	2.75	39.7	2.18
C	do	110	1.08	19.0	1.94
D	do	250	1.04	23.1	1.35
E	Cold-drawn, 40%	250	0.20	0.73	1.03
F	do	300	.36	.98	0.68
G	do	110	.63	.73	1.48
		300	200+	2.8	

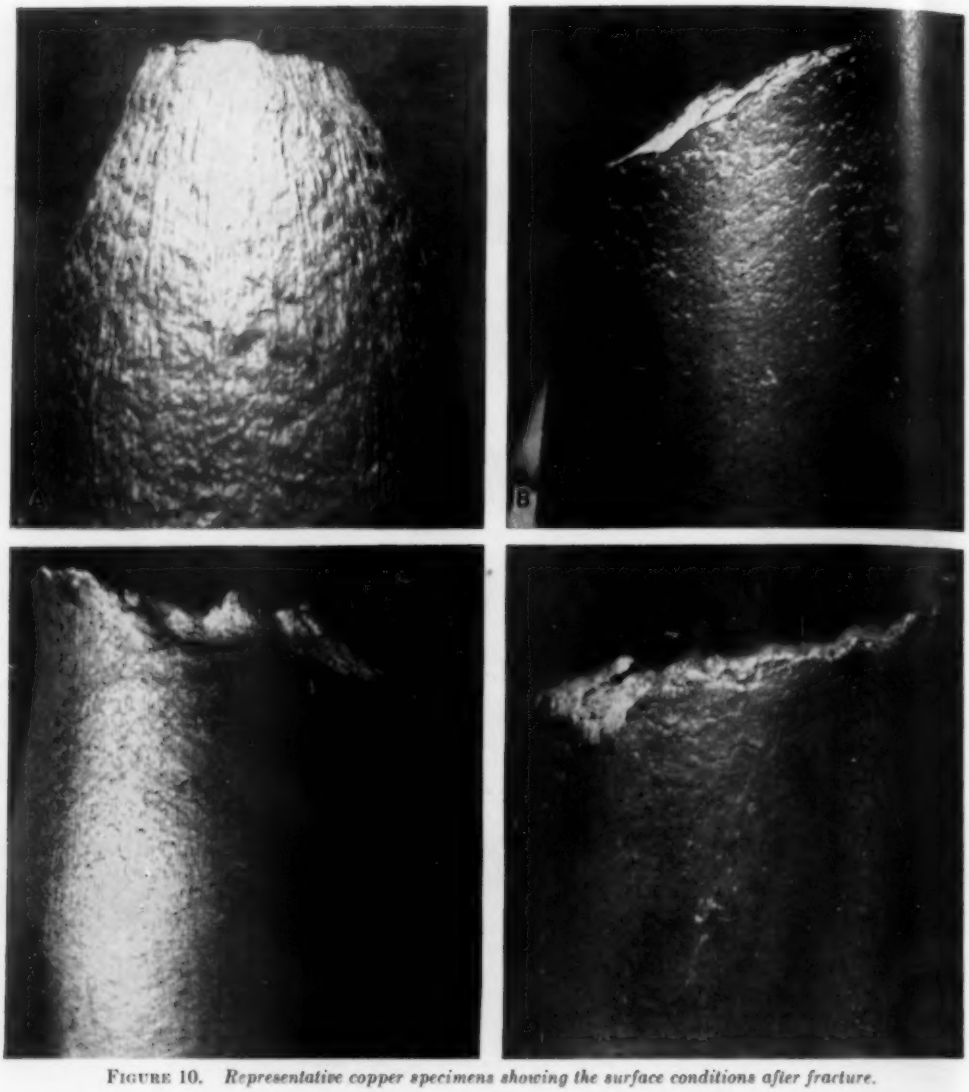

FIGURE 10. *Representative copper specimens showing the surface conditions after fracture.*

Unetched, ×7.

	Initial condition	Creep test			Remarks
		Temperature	Rate	Plastic extension	
		°F	%/1,000 hr	%	
A	Cold-drawn 70% an-Annealed 1,300° F.	None	None	None	Fractured at room temperature.
B	Annealed 800° F	250	1.04	23.1	Do.
C	Cold-drawn 40%	300	0.36	0.98	Do.
D	Annealed 800° F	300	8.3	36.5	Fractured in creep at 300° F.

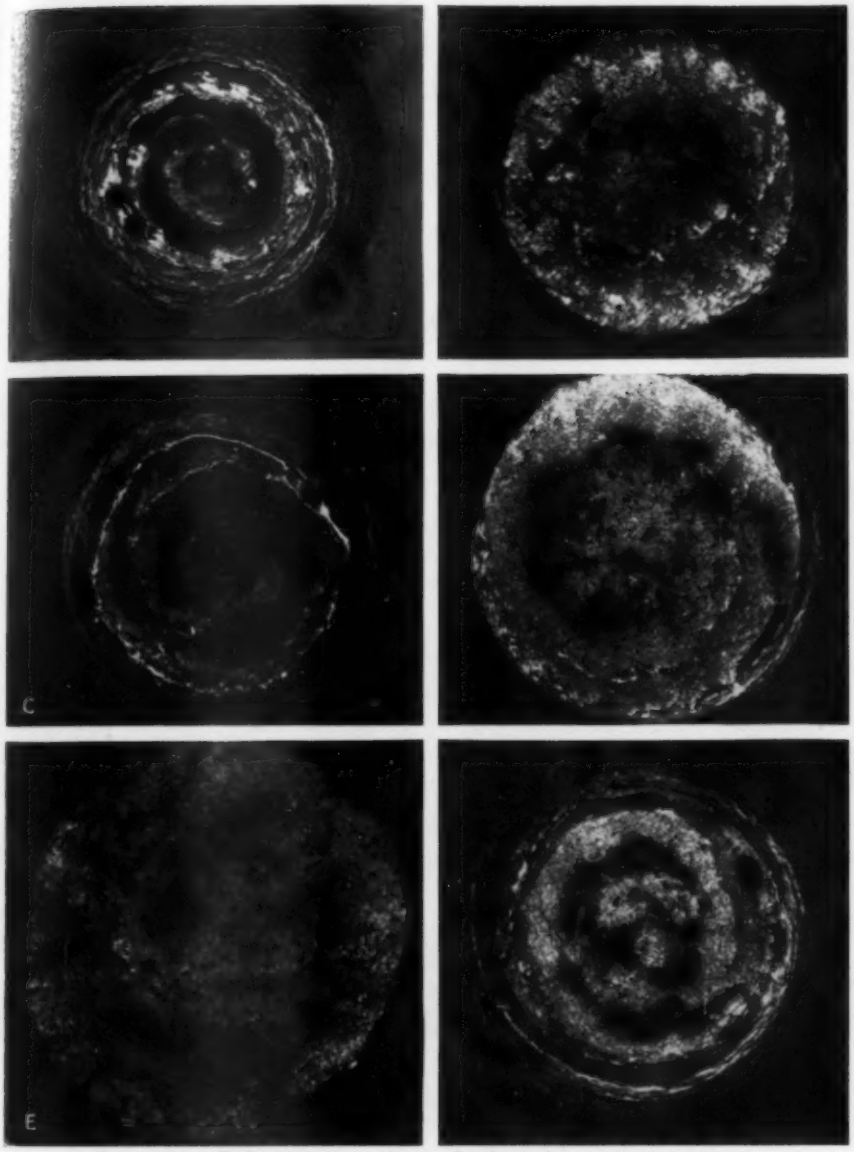

FIGURE 11. *Ends of copper specimens after fracturing at room temperature.*
Unetched, ×7.

	Initial condition	Creep test		
		Temperature	Rate	Plastic extension
		°F	%/1,000 hr	%
A	Annealed 800° F	110	2.75	39.7
B	do	250	1.04	23.1
C	Cold-drawn 40%	None	None	None
D	do	250	0.20	0.73
E	do	300	.36	.98
F	do	110	.63	.73
		300	200+	2.8

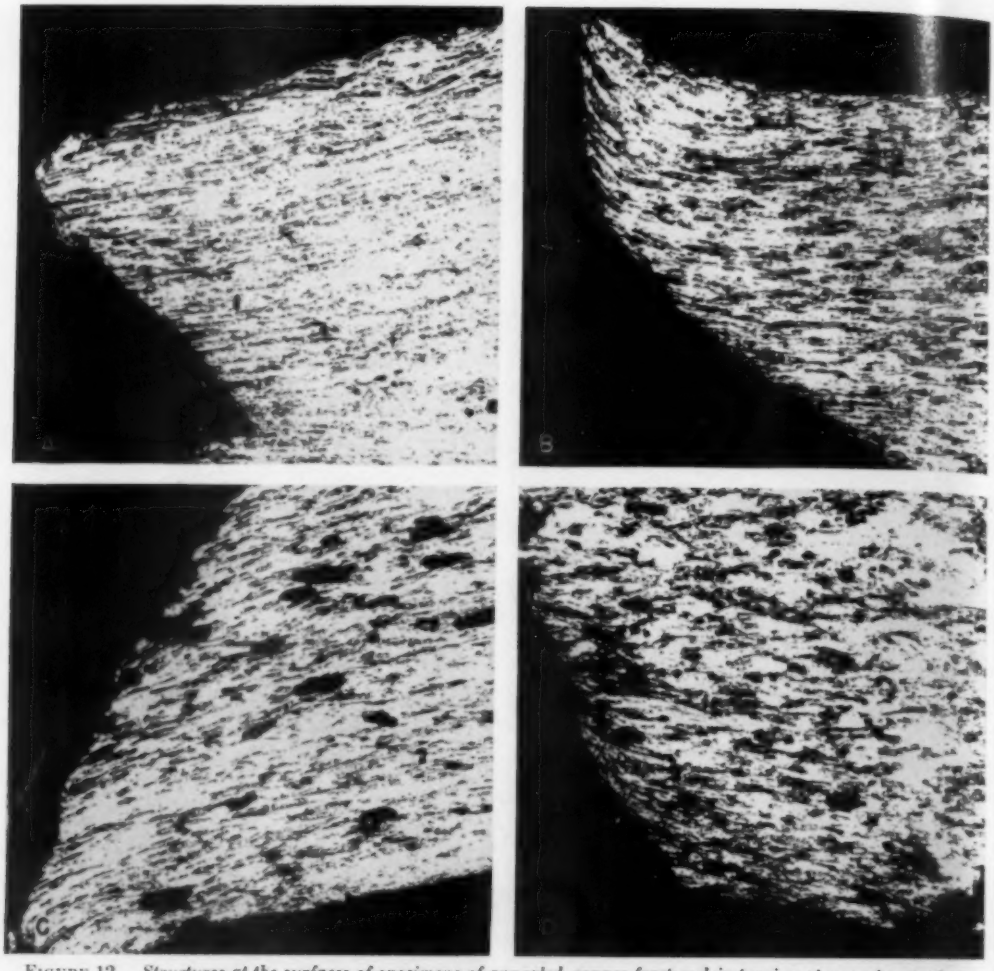

FIGURE 12. *Structures at the surfaces of specimens of annealed copper fractured in tension at room temperature.*

Longitudinal sections at the intersection of the outer (original) and fracture surfaces. Etched in equal parts NH_4OH and H_2O_2 (3%). ×100.

	Initial condition	Creep test		
		Temperature	Rate	Plastic extension
		°F	%/1,000 hr	%
A	Annealed 800° F	110	2.75	39.7
B	Annealed 800° F; extended 9% in tension at room temperature	250	1.1	7.0
C	Annealed 800° F	250	1.04	23.1
D	do	250	10.1	49.0

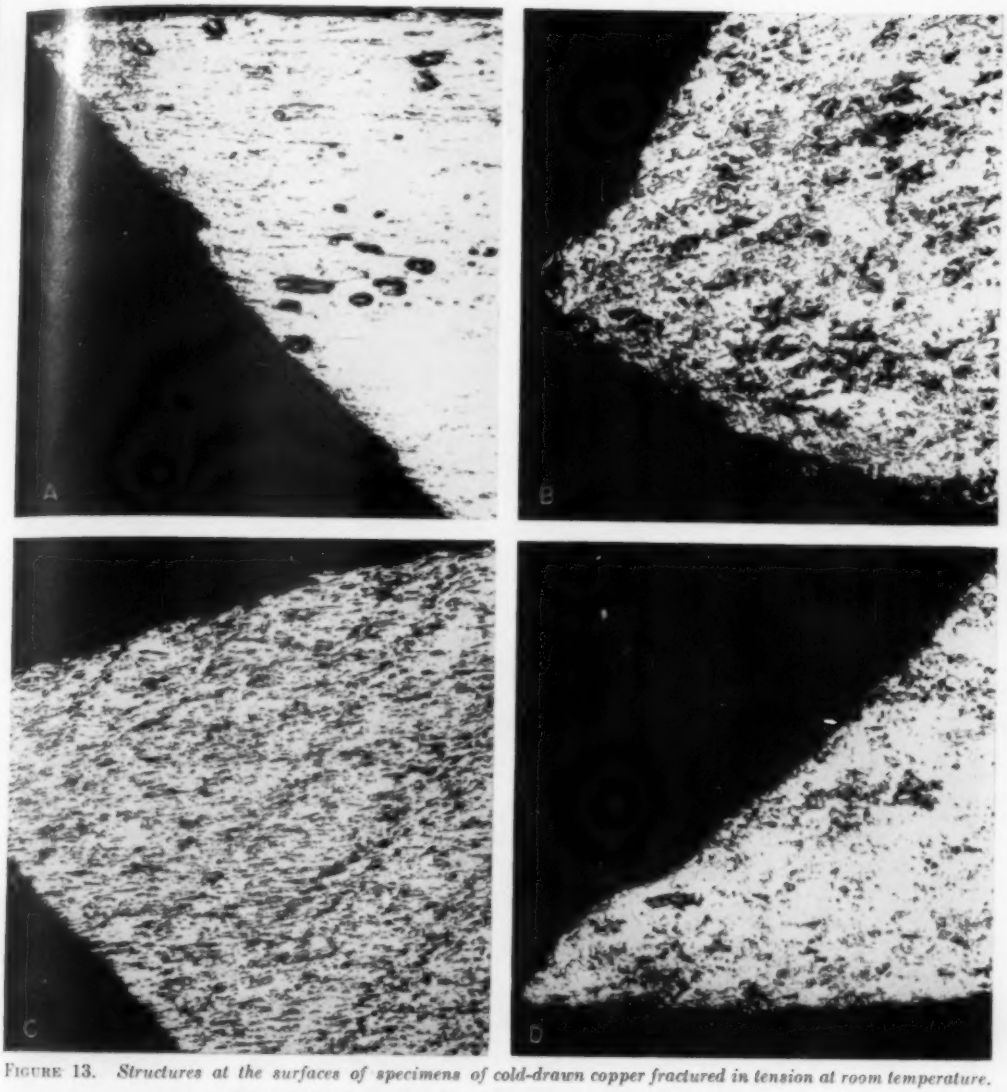

FIGURE 13. *Structures at the surfaces of specimens of cold-drawn copper fractured in tension at room temperature.*

Longitudinal sections at the intersection of the outer (original) and fracture surfaces. Etched in equal parts of NH_4OH and H_2O_2 (3%). ×100.

	Initial condition	Creep test		
		Temperature	Rate	Plastic extension
		°F	%/1,000 hr	%
A	Cold-drawn 40% reduction in area	250	0.20	0.73.
B	do	110	.63	.73.
		300	200+	2.8.
C	Cold-drawn 34% reduction in area	None	None	None.
D	Cold-drawn 70% reduction in area	do	do	Do.

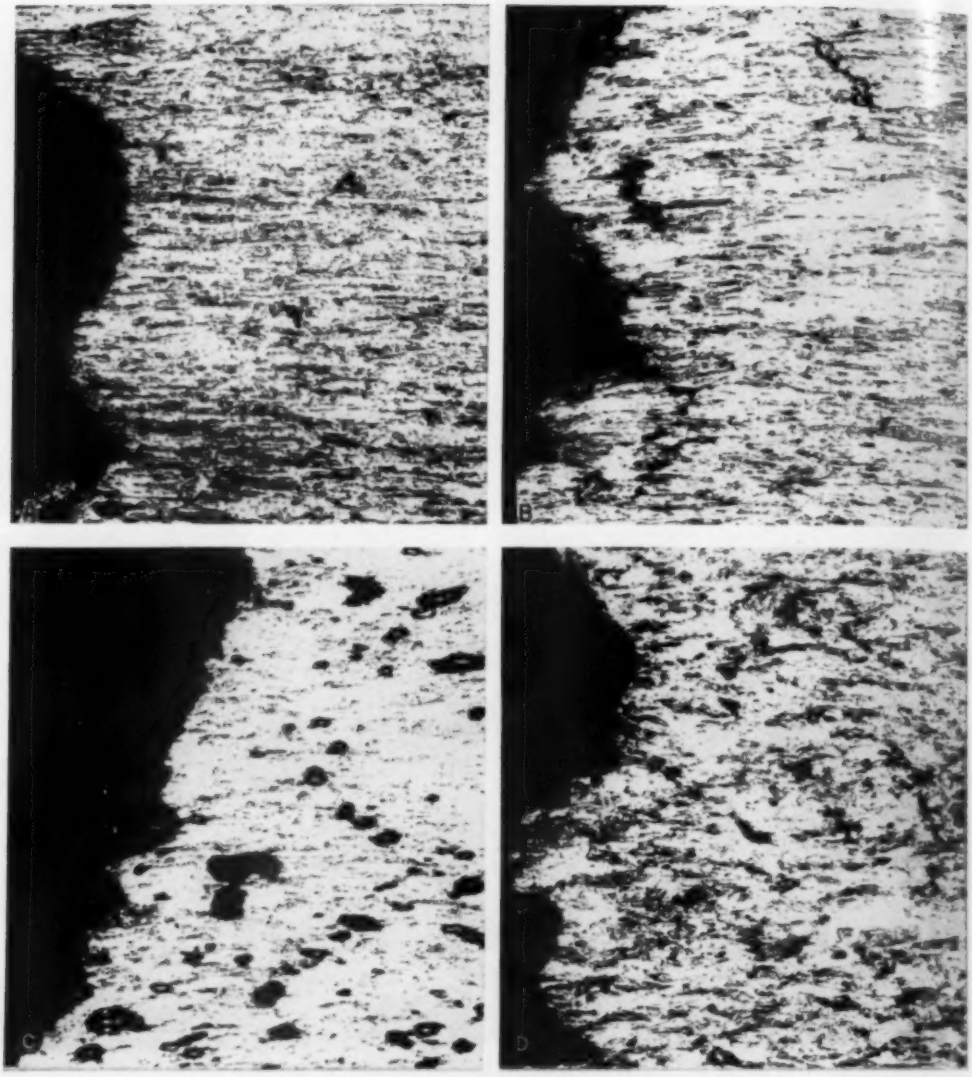

FIGURE 14. *Structures at the axis of specimens of annealed copper fractured in tension at room temperature.*

Longitudinal sections at the intersection of the axis and fracture surface. Etched in equal parts of NH_4OH and H_2O_2 (3%). ×100.

	Initial condition	Creep test		
		Temperature	Rate	Plastic extension
		°F	%/1,000 hr	%
A	Annealed 800° F	110	2.75	39.7
B	Annealed 800° F extended 9% in tension at room temperature.	230	1.1	7.0
C	Annealed 800° F	230	1.04	23.1
D	do	230	10.1	49.0

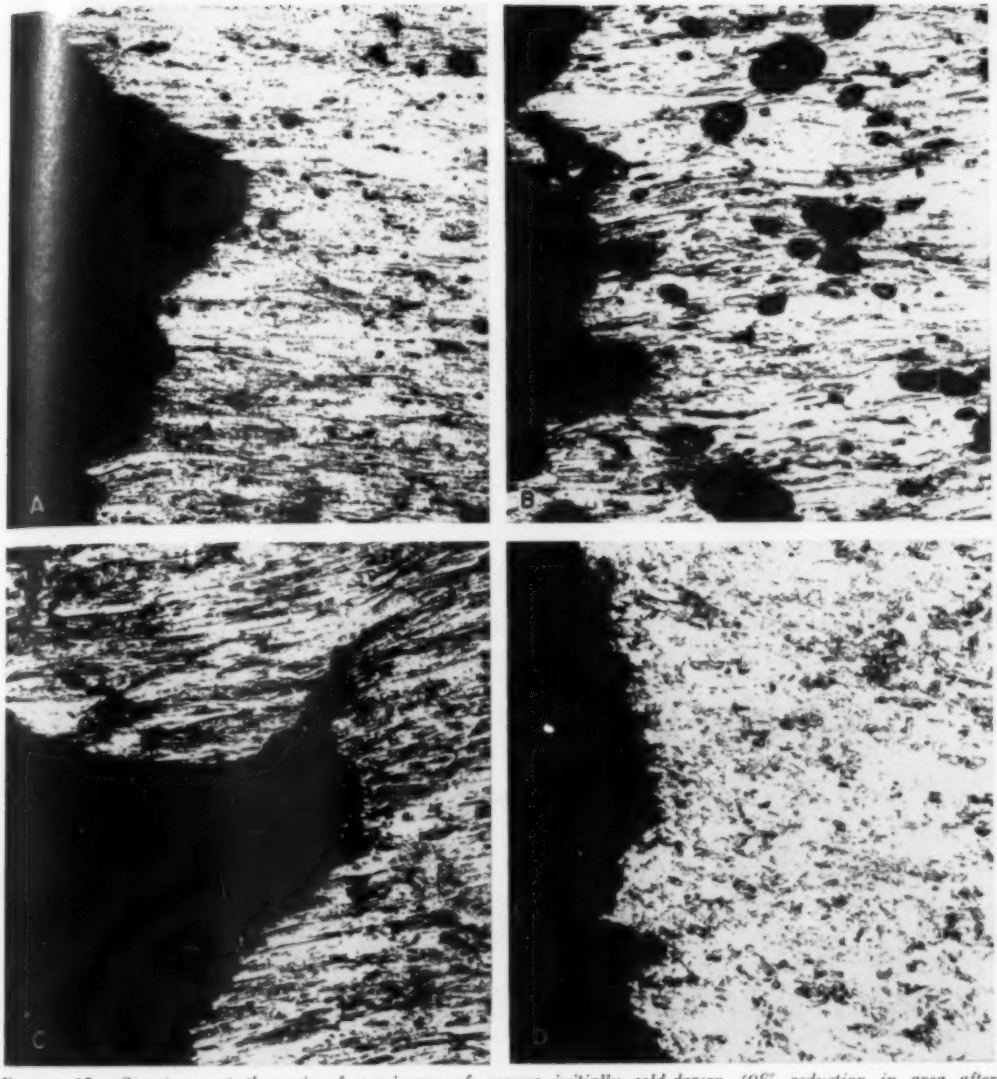

FIGURE 15. *Structures at the axis of specimens of copper initially cold-drawn 40% reduction in area after fracturing in tension at room temperature.*

Longitudinal sections at the intersection of the axis and fracture surface. Etched in equal parts of NH_4OH and H_2O_2 (3%). ×100.

	Creep test		
	Temperature	Rate	Plastic extension
	°F	%/1,000 hr.	%
A	None	None	None
B	250	0.20	0.730
C	300	.36	.98
D	{110	.63	.73
	{300	200+	2.8

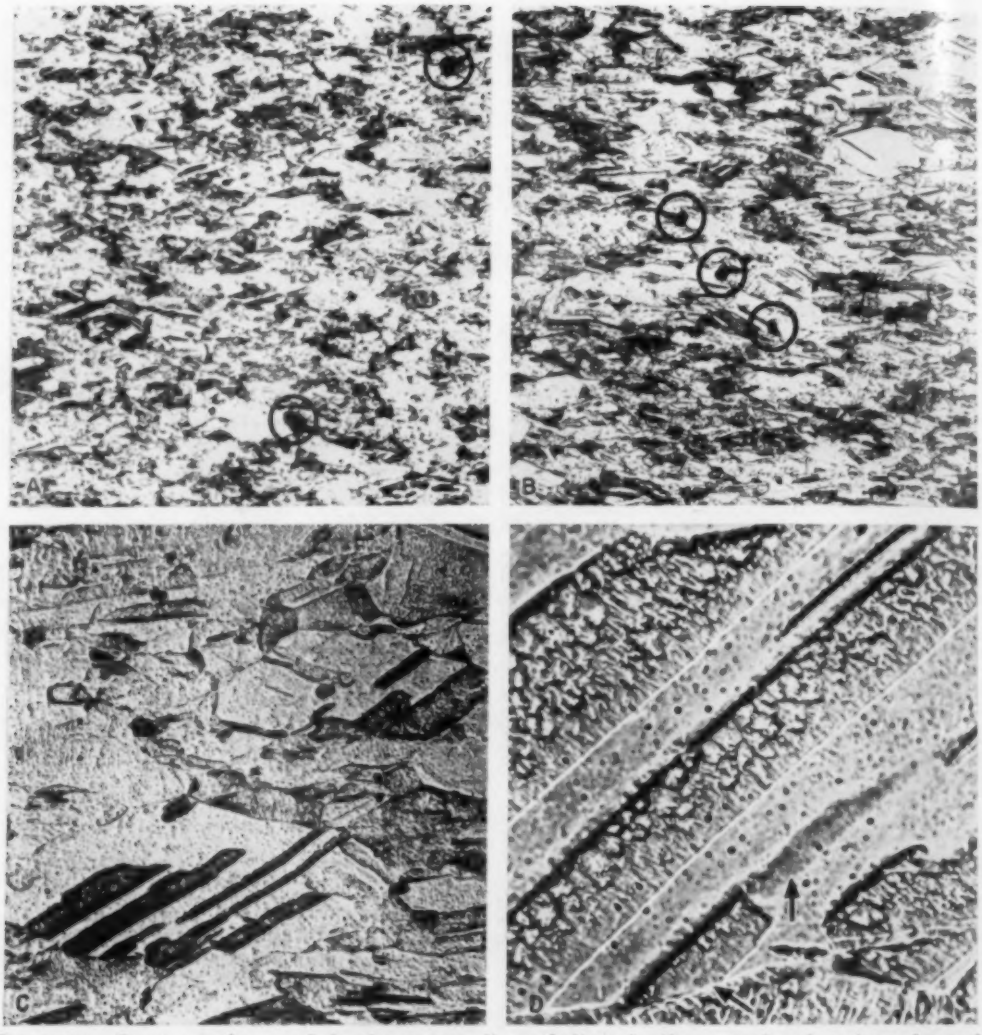

FIGURE 16. *Structure in the un-necked region corresponding to the limit of uniform extension of specimens fractured in tension at room temperature.*

Longitudinal sections near axis, etched in equal parts of NH_4OH and H_2O_2 (3%).

	Initial condition	Creep test			Magnification
		Temperature	Rate	Plastic extension	
		°F.	%/1,000 hr.	%	
A	Annealed 800° F.	250	1.04	23.1	×100.
B	Cold-drawn 40% reduction in area.	230	0.20	0.73	×100.
C	Cold-drawn 70% reduction in area; annealed 1300° F.	None	None	None	×100.
D	do	do	do	do	×500.

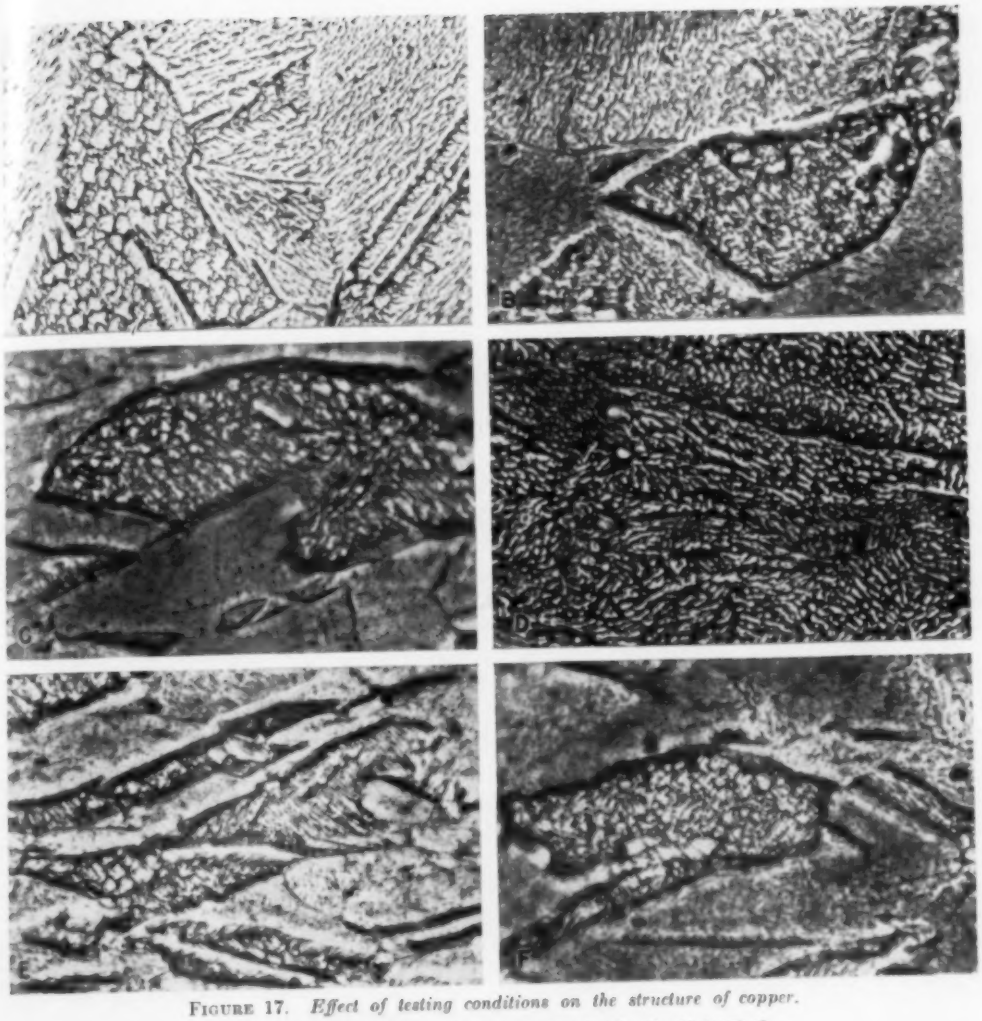

FIGURE 17. *Effect of testing conditions on the structure of copper.*

Longitudinal sections near axis, etched in 3 parts of glacial acetic acid, 6 parts of nitric acid (conc.) and 1 part of ethylene glycol. ×750.

	Initial condition	Creep test			Remarks
		Temperature	Rate	Plastic extension	
		°F.	%/1,000 hr.	%	
A	Cold-drawn 70% reduction in area; annealed 1,300° F.	None	None	None	As annealed.
B	do	do	do	do	Structure 0.10 inch from complete fracture.
C	Annealed 800° F	110	2.75	39.7	Do.
D	do	250	1.04	23.1	Do.
E	Cold-drawn 40% reduction in area.	None	None	None	Do.
F	do	300	0.36	0.98	Do.

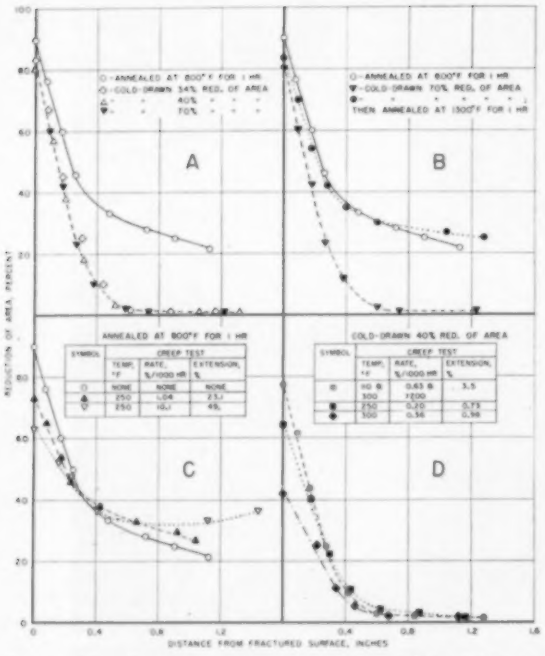

FIGURE 18. *Effect of prestraining on the necking characteristics of specimens fractured in tension at room temperature.*

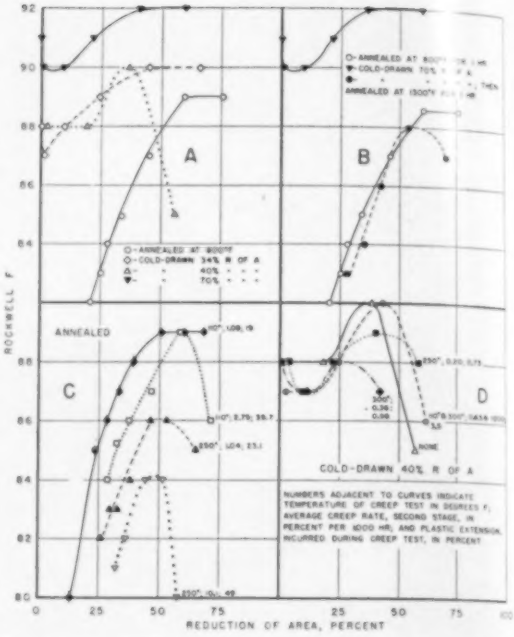
ROCKWELL F
REDUCTION OF AREA, PERCENT
A
B
C
D
ANNEALED
COLD-DRAWN 40% R OF A
NUMBERS ADJACENT TO CURVES INDICATE TEMPERATURE OF CREEP TEST IN DEGREES F, AVERAGE CREEP RATE, SECOND STAGE, IN PERCENT PER 1000 HR, AND PLASTIC EXTENSION INCURRED DURING CREEP TEST, IN PERCENT

FIGURE 19. *Effect of prestraining on the hardness-reduction of area relation of specimens fractured in tension at room temperature.*

WASHINGTON, March 31, 1952.

Journal of Research of the National Bureau of Standards Vol. 49, No. 3, September 1952 Research Paper 2355

A Description of the Arc and Spark Spectra of Rhenium

William F. Meggers

For purposes of chemical identification and of structural analysis, a more complete and accurate description of the atomic emission spectra of rhenium was required. Such a description was obtained by using solid metal electrodes of rhenium in conventional arcs or sparks, photographing the spectra with the aid of large spectrographs containing concave gratings, and measuring the wavelengths of spectral lines relative to secondary standards in the spectrum of iron. Relative intensities were carefully estimated for all lines, and the total widths of many broad lines were measured. Results are presented for approximately 6,000 lines ranging in wavelength from 2000.47 A in the ultraviolet to 11788.9 A in the infrared. A comparison of the estimated intensities in arc and spark spectrograms provides a separation of the spectral lines arising from neutral rhenium atoms from those originating in ionized atoms. In this description the Re I spectrum is represented by about 4,200 lines and the Re II spectrum by nearly 1,800 lines.

1. Introduction

Rhenium is the last stable element to be discovered in the earth's crust. Since its discovery in 1925, rhenium has been found to possess many remarkable properties. For example, its high melting point (3,170° C) is exceeded only by those of carbon and tungsten; its density (20.5) is next to those of osmium, iridium, and platinum. The metal is very hard and can be rolled or drawn only at red heat. Combined with various other metals rhenium forms alloys that are extremely resistant to acids and stable at high temperatures in air. Alloyed with platinum or rhodium and paired with pure platinum, rhodium or palladium, thermocouples are formed that give four times greater thermoelectric forces than the common couples of noble metals, and are stable and useful to nearly 1,900° C. In high vacuum, even at high temperatures, rhenium shows no inclination to sputter and is therefore ideal for filaments of incandescent lamps and vacuum tubes. By depositing rhenium upon metals or glass, optical mirrors of high permanance and reflectance are produced.

The terrestrial abundance of rhenium (0.001 g/ton) is about the same as that of rhodium or iridium, and the current price ($2.00/g) is less than that of platinum and only a third that of iridium. The total annual production of rhenium metal is now only some hundreds of pounds, but its remarkable properties insure increased concentration and extensive future application in science and industry. When this wonder metal becomes common in metallurgy, it will be desirable to have for spectrochemical determination, a satisfactory description of its optical spectra. Furthermore, the spectra of rhenium atoms and ions exhibit some unusual features that lead to interesting information concerning atomic structure, electronic binding forces, and properties of atomic nuclei. To supply descriptions of the arc and spark spectra of rhenium that will be adequate for spectrochemical analysis and for structural analyses of the first two spectra is the purpose of the present paper.

The principal proof of discovery of rhenium by Noddack, Tacke, and Berg [1][1] was the observation of five Röntgen radiations with wavelengths ranging from 1.216 to 1.430 A. The first reference to the optical spectra of rhenium was made in 1928 by Noddack [2], who reported "we know at present several hundred lines which certainly belong to rhenium . . . . The optical last lines of rhenium, especially the triplet at 3640 A permit its identification in concentrations down to 10^{-7}". This first numerical value contains two transposed figures; it should read 3460 A.

In 1931, preliminary data for the arc spectrum of rhenium were published by Meidinger [3], by Schober and Birke [4], and by Meggers [5]. Meidinger [3] observed the spectrum of rhenium powder in a d-c arc between carbon electrodes. The interval between 2600 and 3500 A was photographed with a quartz prism spectrograph and the interval 4040 to 5300 A with a glass prism spectrograph, the reciprocal dispersions for the longer waves being 25 and 30 A/mm, respectively. The wavelengths of 229 lines were given to five figures "for spectrochemical purposes", and intensities of weak, medium, or strong were assigned to the lines.

Schober and Birke [4] reported the wavelengths (3108.94 to 6441.28 A) of 31 strong lines of rhenium on the Rowland scale and stated that 3452.02 (5), 3460.61 (5), and 3464.87 (5) were the last lines to disappear when salt solutions of rhenium were diluted. Schober [6] then published a description of "the arc spectrum of rhenium in the photographic range", giving wavelengths (2391.60 to 6494.15 A) of about 400 lines, and estimated relative intensities (1 to 100). These data were obtained from concave grating spectrograms with reciprocal dispersion of 4 A/mm, the source being a carbon arc with rhenium solution added to the anode. This work was repeated with copper instead of carbon electrodes and reported in three papers [7], which give for more than 2,000 rhenium lines wavelengths ranging from 2405.14 to 7641.20 A, intensities from 1 to 1000, and line

[1] Numbers in brackets refer to literature references at the end of this paper.

widths from 0.1 to 1.0 A. In the region of short waves Schober's lists are a mixture of Re I and Re II spectra without any means of distinguishing them.

A preliminary report on the optical spectra of rhenium by Meggers [5] announced observations of arc and spark spectra, hyperfine structure, and the first atomic energy levels and spectral terms for Re I. More details were given in a paper on the arc spectrum of rhenium [8], which presented 2,200 wavelengths (2500.59 to 8797.6 A), 115 atomic energy levels, and approximately 500 classified lines. Because the data on rhenium spark spectra were less complete, they were withheld. That list of rhenium arc lines, obtained with crystals of pure potassium perrhenate on silver electrodes in a d-c arc, was extended [9] to longer waves (10639.44 A) in 1933, when new infrared sensitive emulsions became available.

A statement in 1931 by Schober [10] that among 60 strong rhenium lines, 24, including the 3 strong ultraviolet lines and 2 green ones, coincide with the Fraunhofer spectrum was contradicted by Moore and Meggers [11], who found that the accordance of solar and laboratory wavelengths of strong rhenium lines does not appear to be exact or real when the hyperfine components of these lines are taken into account. These hyperfine-structure measurements were the first to be reported for rhenium. Almost identical measurements for 3 rhenium lines were independently made by King [12], who observed 19 low-level lines of Re I in a carbon-tube furnace containing metallic rhenium at a temperature near 2,800° C. The striking hyperfine structure of certain rhenium spectral lines was investigated and interpreted by Meggers, King, and Bacher [13], by Gremmer and Ritschl [14], by Sommer and Karlson [15], by Zeeman, Gisolf, and deBruin [16], and finally by Schüler and Korsching [17]; all agreed that the two isotopes of rhenium, with masses 185 and 187, possess nuclear moments of 5/2 ($h/2\pi$). The last [17] also measured the magnetic moments, electric-quadrupole moment, and isotope shifts characteristic of rhenium isotopes.

Additional measurements of wavelengths in arc and spark spectra of rhenium appear in the MIT Wavelength Tables [18] where data for 2256 lines are given, partly new and the rest quoted from other published tables. Employing the MIT data, Klinkenberg [19] extended the analysis of the Re I spectrum to include approximately 1600 lines as combinations of 221 atomic energy levels. An extension of the Re I analysis was independently made by Velasco [20], but further progress in this direction is greatly handicapped by the inadequacy of the published data for rhenium spectra. The paucity and poor quality of published data for spark lines have frustrated earlier attempts to establish and analyze Re II spectrum of singly ionized rhenium atoms. Except for the paper by Zeeman, Gisolf and deBruin [16], which describes the partially resolved Zeeman patterns of three Re I lines (3452, 3460, 3464 A), no further details of the Zeeman Effect in rhenium have been published. All these deficiencies have recently been removed, and a preliminary announcement of rhenium magnetic splitting factors and of the structure of the Re II spectrum has been made by Meggers, Catalán, and Velasco [21].

In concluding this review of contributions to information regarding the spectra of rhenium, attention is called to the beautiful photographic charts of arc and spark spectra of rhenium prepared by Gatterer [22]. Six 40 cm prints show prismatic spectra of the rhenium arc from 2156.71 to 6250.75 A, and six similar prints reproduce the prismatic spectra of the rhenium spark from 2091.50 to 6250.75 A. A table accompanying this Atlas gives the wavelengths of 232 of the stronger arc and spark lines of rhenium, with intensities ranging from 1 to 10.

All previous observations of rhenium spectra were made with electric arcs or sparks between either carbon, silver, or copper electrodes to which samples of rhenium were added either in the form of solutions, salts, or metal powder. Under these conditions it is practically impossible to produce complete descriptions of the spectra because bands due to carbon compounds or lines characteristic of silver or copper will mask a certain number of rhenium lines and falsify the wavelengths and intensities of others blended with electrode lines. The present observations of rhenium spectra are justified by the following facts: They were made mainly with solid metallic electrodes of pure rhenium, thus avoiding confusion on account of coincidence with other spectral lines; they were extended to shorter and to longer waves by using new types of photographic emulsions; they were made with generally higher spectrographic dispersion and resolving power than the first observations; and they are based on juxtaposed arc and spark spectra that provide the first useful identifications of Re I and Re II spectra. In short, the present observations have more than doubled the previous number of real rhenium lines and have provided homogenous material of increased accuracy in wavelengths and relative intensities to meet the future needs of spectrochemistry and the search for atomic energy levels as derived from analyses of optical spectra.

2. Experimental Details

Most of the new data for rhenium spectra presented in this paper were obtained from arcs or sparks between electrodes of commercial rhenium metal. The electrodes were made by pressing rhenium metal powder in a Dietert hydraulic press developed especially for compacting metal powders, filings, borings, turnings, etc. into cylindrical rods for spectroscopic electrodes. The cylindrical electrodes were approximately 6 mm in diameter and 10 mm long. These solid cylinders of rhenium were pinched in slotted copper or brass rods, which served as arc or spark electrode holders.

The arc spectra were excited in a d-c arc with an applied potential of 220 v and a current of 6 to 10 amp. The spark spectra were obtained with a high-voltage condensed discharge from mica condensers of 0.006—μf capacity connected to the secondary coil of

transformer rated at 30,000 v when the primary was connected to the 120-v a-c power line.

All the spectrograms were made with concave diffraction gratings of about 22 ft radius of curvature, mounted to perform stigmatically as described by Meggers and Burns [23]. Three mountings of this Wadsworth type were available, containing respectively 6 in. gratings with 30,000, 15,000, or 7,500 lines/in. The first is used primarily to photograph spectra in the ultraviolet and visible, the second mainly for visible and near infrared, and the third for infrared spectra only. Further information concerning these spectrographs and the photographic plates used with each is given in table 1.

TABLE 1. *Data on spectrographs and photographic plates for recording* Re *spectra*

Spectral region	Grating	Spectral order	Reciprocal dispersion	Photographic plate
A	*Lines/inch*		*A/mm*	
2000 to 2550	30,000	I	2.4	Eastman SWR
2500 to 3500	30,000	II	1.1	Eastman 33
3500 to 4500	30,000	II	0.9	Eastman 33
4400 to 6800	30,000	I	2.2	Eastman II F
6600 to 8800	30,000	I	1.8	Eastman I N
7200 to 9000	20,000	I	3.7	Eastman I R, I P
8000 to 11000	15,000	I	4.8	Eastman I Q
10000 to 12500	7,500	I	10.2	Eastman I Z

In the 1933 observation [9] of the infrared arc spectrum of Re, Eastman plates I R and I P were used with a Rowland grating having 20,000 lines/in., and "Xenocyanine" plates were used with the Anderson grating, 7,500 lines/in. These combinations, it was found, were hard to surpass, and although these spectral ranges were reobserved with other plates and gratings, very little was added to the existing data in those ranges. However, some additional lines of longer wavelength were recorded on I Z plates, which were not available in 1933. The Q and Z plates were hypersensitized immediately before use by bathing them in a 2- to 5-percent solution of ammonia in water. They were then rinsed in alcohol and dried with moving warm air.

The durations of exposure required for recording arc or spark spectra under different conditions were determined by estimation and trial, so that the background continuum imposed the limit. The exposure times for the Re arc ranged from a few seconds in the ultraviolet to 5 hr in the infrared. Likewise, the spark spectra were recorded in times ranging from a few minutes to 2 hr. Between the limits 2000 and 6800 A, the arc and spark spectra of Re were photographed either side by side with iron comparison spectra flanking each or the arc and spark spectra were recorded respectively above and below a center strip showing the iron spectrum with its standard wavelengths.

An effort was made to match the arc and spark spectra, especially in the ultraviolet, so that most of the lines appearing in the arc spectrogram were recorded with almost equal intensity in the spark spectrogram. Under these conditions all lines appearing only, or with greater intensity, in the spark spectrograms may safely be assumed to originate in ionized rhenium atoms, whereas the others belong to neutral atoms. Although some spark lines are enhanced more than others, the stronger ones are generally found also on the arc spectrograms, and there is no good reason to believe that any rhenium lines reported here belong to doubly ionized rhenium atoms.

Because the spark spectra above about 6000 A contained no new or enhanced lines relative to the arc spectra, spark excitation was omitted for waves longer than 6500 A. In photographing the red and infrared spectrum (6500 to 12000 A) the arc was imaged on the spectrograph slits through deep-red glass filters, which transmit only waves longer than 6500 A, and one or two narrow strips of the iron arc spectrum were superimposed to furnish standard wavelengths. These standards were always taken from the same spectral order as the rhenium waves to be measured, except beyond 8800 A to 12000 A, where iron standards were taken from the second or third spectral orders and multiplied respectively by two or three.

The rhenium spectrograms were measured with a large comparator made by the Gaertner Scientific Corporation. The screw has a length of 50 cm and the scales permit direct reading of linear distances to 1μ. Every rhenium spectral line retained in the final list was observed and measured at least twice, and many of them were measured on four or five spectrograms. In all, approximately 20,000 readings of linear distances between images of rhenium and of standard iron lines were recorded and each observation of a rhenium line was accompanied by an estimated intensity. The final values of rhenium wavelengths and relative intensities are averages of the individual observations. When the average deviation of individual values of wavelength from their mean is 0.005 A or less, the final value is given to three decimals, and if the average deviation is greater than 0.005 A, the final value is rounded off to the nearest second decimal.

In reviewing the earlier work on rhenium spectra, reference was made to the hyperfine complexity of some of its lines. When these spectra are observed with high dispersion and resolving power, it is at once obvious that a majority of Re I and Re II lines are more or less wide and complex. Even with the average gratings used in this investigation several dozen rhenium lines were completely resolved, usually into six components, and many hundreds of lines were either partially resolved or shaded to indicate intensity degradation either to shorter (*s*) or to longer (*l*) waves. In most cases, the observed wavelengths of rhenium represent values obtained by bisecting their slit images, except that when the complex line appeared to be more than 0.1 A wide the edges were measured and thus both width and mean wavelength were recorded. In the observed infrared some rhenium lines have widths exceeding 2 angstroms, or 2 wave numbers. The details of rhenium hyperfine structure are omitted here because they are not accurate enough for nuclear physics and are not of vital importance either in industrial

spectrochemistry or in structural analysis of these spectra.

It may be remarked, however, that because of the relatively coarse hyperfine structure in the strongest spectral lines of rhenium, the sensitivity of spectral detection is low compared with that of otherwise comparable metals having narrower lines. A complication for spectrum analysis arises from the fact that many rhenium lines appear to have hyperfine structures deviating from the usual "flag pattern" of regular decrement of spacing and intensity. It is often difficult to decide if close pairs or irregular groups of rhenium lines are in fact separate lines or components of complex lines. Some of these doubts may be resolved in establishing further atomic energy levels of rhenium from analyses of optical spectra without regard to hyperfine structure.

The conspicuous hyperfine structures in rhenium spectra not only complicate the determination of wavelengths but also affect the estimation of relative intensities of the lines. Usually such estimated relative intensities depend on the widths as well as the densities of the photographic images, and when the widths are greatly increased by hyperfine structure, there is a tendency to overestimate intensities. In the present work a conscious effort was made to discount the contribution of hyperfine width to intensity, but it may not be entirely eliminated.

A final difficulty in describing the arc and spark spectra of rhenium arises from a strong background that is continuous throughout the spectrum on fully exposed spectrograms, and in the visible and infrared regions has superimposed on it the coarse rotation structure of molecular spectra, presumably of rhenium oxide. This background imposes a limit on the detection of faint lines, and the molecular lines are often blended with the atomic lines. The molecular lines were not intentionally measured, but band heads were included when they were obvious or unmistakable; these are marked B in the list of lines.

3. Results

The results of this investigation are presented in table 2, where the measured wavelengths (in angstroms) of rhenium spectral lines (column 1) are followed by estimated relative intensities in arc and spark spectra. The intensity numbers range from 1 to 10000; they are accompanied in many cases by letters and other numbers. The letters accompanying intensities impart additional information concerning the lines; they have the meaning adopted by the International Astronomical Union [24] in a proposed notation for the description of spectral lines as follows: B, band head; c, complex (narrow fine structure, isotopic or nuclear-spin hyperfine structure); d, unresolved double (approximate coincidence of two lines); h, hazy, diffuse, nebulous; H, very hazy, diffuse, nebulous; l, shaded or displaced to longer waves; s, shaded or displaced to shorter waves; r, narrow self-reversal; R, wide self-reversal; w, wide; W, very wide.

Table 2 represents a careful selection of data from the much more extensive observational material that included spectral lines due to impurities, components of resolved hyperfine structure, lines doubtfully belonging to molecular spectra, lines observed only once, and lines arising from overlapping spectral orders.

Because the rhenium metal used in this investigation was extremely pure, the identification and removal of spectral lines due to impurities was not difficult; the total number of such lines was about 30. Only the stronger lines of common contaminants appeared, as follows: B (2497.72 A), Si (2506.89 A), Ca (3933.66, 3968.47 A), Mg (2795.53, 2802.70, 2852.12 A), Al (3944.03, 3961.53 A), Cu (3247.74, 3273.96 A), Ag (3280.68, 3382.89 A), Pb (3683.47, 4057.81, 10290.6, 10499.1 A), Cr (4254.34, 4274.80, 4289.72 A), and Na (5889.95, 5895.92, 8183.29, 8194.82, 11403.9 A). In the visible spectrum a few lines of Cu (5105.54, 5153.22, 5782.13 A) and Zn (4680.15, 4722.17, 4810.53 A) were observed, but these are believed to arise from accidental flashes of the arc to the brass holders of rhenium electrodes rather than from the rhenium. The only other impurity deserving mention is potassium (7664.91, 7698.98, 11690.3, 11769.6, 11772.9 A), which indicates that the rhenium metal was probably prepared from potassium perrhenate. The presence of the above-mentioned impurity lines provided reliable check on the scale of wavelengths for the rhenium lines. In nearly every case the measured wavelength of the impurity line agreed with its accepted value [18] within ± 0.01 A.

As stated before, the hyperfine structure of several dozen rhenium lines was resolved into two to six components, but the wavelengths of the individual components are omitted from table 2, where only the mean wavelength and over-all width of flag patterns is shown. There is some evidence of irregular hyperfine structures and mutilated multiplets in rhenium spectra, and such cases as appear in table 2 may be revealed in future analyses of these spectra.

Several hundred lines of low intensity were measured but not included in table 2 because some were recorded only once, and the remainder, mainly in the visible and infrared, were suspected of belonging to molecular compounds. A few lines published in earlier papers were not confirmed as atomic rhenium lines, and most of those now appear to be parts of molecular bands.

Despite the abandonment of many hundreds of lines observed in the arc and spark spectra of rhenium, table 2 contains more than twice as many lines as have heretofore been published. It should meet all present requirements for spectrochemistry and structural analysis of Re I and Re II spectra between the wavelength limits 2000 and 12000 A.

4. References

[1] W. Noddack, I. Tacke and V. Berg, Naturwissenschaften **13,** 567, 571 (1925).
[2] I. Noddack, Z. Electrochem. **34,** 629 (1928).
[3] W. Meidinger, Z. Physik **68,** 331 (1931).
[4] H. Schober and J. Birke, Naturwissenschaften **19,** 211 (1931).

[5] W. F. Meggers, Phys. Rev. **37,** 219 (1931).
[6] H. Schüler, Sitzungsber, Akad. Wiss. Wien **140,** 79 (1931).
[7] H. Schüler, Sitzungsber, Akad. Wiss. Wien **140,** 629 (1931); **141,** 601 (1932); **142,** 35 (1933).
[8] W. F. Meggers, BSJ. Research **6,** 1027 (1931) RP322.
[9] W. F. Meggers, BSJ. Research **10,** 757 (1933) RP564.
[10] H. Schüler, Naturwissenschaften **19,** 310 (1931).
[11] C. E. Moore and W. F. Meggers, Pub. Astron. Soc. Pacific **43,** 345 (1931).
[12] A. S. King, Astrophys. J. **75,** 379 (1932).
[13] W. F. Meggers, A. S. King, and R. F. Bacher, Phys. Rev. **38,** 1258 (1931).
[14] W. Grotrian and R. Ritschl, Z. Instrumentenk. **51,** 170 (1931).
[15] L. A. Sommer and P. Karlson, Naturwissenschaften **19,** 1021 (1931).
[16] P. Zeeman, J. H. Gisolf, and T. L. deBruin, Kon. Akad. Amsterdam **35,** 2 (1932).
[17] H. Schüler and H. Korsching, Z. Physik, **105,** 168 (1937).
[18] G. R. Harrison, M. I. T. Wavelength Tables (John Wiley & Sons, New York, N. Y., (1939).
[19] P. F. A. Klinkenberg, Physica **13,** 581 (1947); **14,** 269 (1948).
[20] R. Velasco, Ann. Real Soc. Esp. Fis. Quim. **45,** 215 (1949).
[21] W. F. Meggers, M. A. Catalán, and R. Velasco, J. Opt. Soc. Am. **42,**
[22] A. Gatterer, Atlas der Restlinien III, Specola Vaticana (1949).
[23] W. F. Meggers and K. Burns, BS Sci. Pap. **18,** 185 (1922) S441.
[24] Trans. Int. Astron. Union **6,** 100 (1938).

TABLE 2. *Arc and spark spectra of rhenium*

MEANING OF LETTERS

P=band head, *c*=complex (narrow fine structure, isotopic or nuclear-spin hyperfine structure),
d=unresolved double, *h*=hazy, diffuse, nebulous, *H*=very hazy, diffuse, nebulous,
l=shaded or displaced to longer waves, *s*=shaded or displaced to shorter waves,
r=narrow self-reversal, *P*=wide self-reversal, *w*=wide, *W*=very wide.

INTERPRETATION OF MIXED LETTERS AND NUMBERS

c .18*W*=complex, 0.18 A range of wavelength, very wide.
c .15*Ws*=complex, 0.15 A range of wavelength, very wide, shaded to shorter waves.
c 3, .21*Wl*=complex, 3 components, 0.21 A range of wavelengths, very wide, shaded to longer waves.
c 6, .222*Wl*=complex, 6 components, 0.222 A range of wavelengths, very wide, shaded to longer waves.
c 6, 1.25*Wl*=complex, 6 components, 1.25 A range of wavelengths, very wide, shaded to longer waves.

Wavelength	Intensity and other characteristics	
	Arc	Spark
A		
2000.47	.....	6
2001.02	.....	5
2001.16	.....	30
2001.47	2	2
2002.32	.....	3
2002.62	.....	4
2003.532	50*R*	30*c*
2003.665	.....	30*c*
2004.14	.....	6
2004.39	2	1
2004.68	2	200
2005.40	.....	4
2006.00	.....	10
2006.28	.....	15
2006.53	.....	15
2006.87	.....	7
2007.06	8*c*	.....
2007.12	.....	10*c*
2007.88	.....	8
2008.06	20*r*	15*c*
2008.67	.....	2
2009.19	.....	5
2009.92	2	100
2010.32	.....	20*c*
2010.66	.....	5
2010.98	.....	10
2011.09	.....	20
2011.82	.....	10
2012.01	2	2
2012.44	.....	4
2012.74	2	2
2013.02	.....	4
2013.13	.....	2
2013.47	3	1
2013.65	5*cw*	2*c*
2013.88	.....	4
2014.66	7*c*	2*c*
2015.02	.....	2
2015.43	1	50
2015.49	2	.....
2015.61	.....	10
2015.91	.....	9
2016.17	3*c*	2*h*
2016.56	20*r*	3*c*
2016.59	.....	10*c*
2017.08	.....	6
2017.56	.....	5*c*
2017.866	200*R*	10*cw*
2017.98	.....	30*cw*
2018.54	1	40
2018.95	.....	2
2019.28	2*H*	30*c*
2019.63	4	1
2019.82	.....	2
2019.97	.....	10
2020.12	9*c*	1*c*
2020.34	.....	4*c*
2020.475	.....	10*c*
2020.82	.....	3
2021.07	2	1
2021.31	.....	10*c*
2022.54	.....	6
2022.74	.....	3
2022.88	.....	2
2023.07	.....	5
2023.11	5*c*	.....
2023.644	2	2*C*
2023.787	2	.....
2024.05	.....	4
2025.43	4*c*	.....
2025.51	.....	30*c*
2026.23	4	1
2026.40	.....	10
2026.86	.....	6*c*
2027.29	.....	10
2027.41	6	.....
2027.45	.....	3
2027.69	.....	9
2027.93	6	3
2028.27	2	2
2029.375	.....	3
2029.70	5*cw*	.....
2029.84	.....	7*d*
2030.26	4	2
2030.495	.....	20
2030.68	.....	2
2030.903	40*r*	10*cw*
2031.521	.....	20
2031.655	4	.....
2031.96	8*cl*	.....
2032.02	.....	30
2032.29	.....	5
2032.59	.....	20
2032.944	10*c*	1*c*
2033.335	1	7
2033.78	20*r*	15*c*
2034.020	.....	20
2034.44	.....	3
2034.824	.....	2
2035.00	6*c*	5*h*
2035.49	3	.....
2035.51	.....	10
2035.96	10*ch*	.....
2036.20	3	15
2036.885	.....	3
2037.14	5	20
2037.86	.....	30
2037.96	4	15
2038.23	.....	20
2038.99	30*r*	20*c*
2039.204	50*r*	30*c*
2039.57	.....	60*c*
2039.88	3	70
2040.36	.....	15
2040.64	.....	2
2040.81	3	10
2041.00	7*h*	1*h*
2041.27	.....	15
2041.82	.....	2
2042.346	1	.....
2042.470	3	.....
2042.64	2	40
2043.06	.....	3*h*
2044.36	.....	4*h*
2044.825	.....	4
2044.903	2	.....
2045.75	10	5
2046.244	5	.....
2046.318	.....	6*h*
2046.774	.....	10
2046.922	1*h*	2
2047.67	.....	7
2047.857	2	.....
2047.955	.....	6
2048.170	.....	5

TABLE 2. *Arc and spark spectra of rhenium*—Continued

Wavelength	Intensity and other characteristics	
	Arc	Spark
A		
2048.380		3
2048.754	4	
2049.079	400*R*	200*c*
2050.120		5
2050.458		6
2050.64		15
2050.73		10
2051.34		3
2052.32	10	10*c*
2052.546		10
2052.772		2
2053.10		10
2053.597	1	50
2053.730	3	
2054.98		9
2055.25	2	20
2056.01	2	2
2056.29	15*c*	7*c*
2056.59		15*c*
2056.70	2	
2057.11	3	
2057.43		6
2057.743	20*c*	10
2058.10		5
2058.33		2
2058.520	1	15
2058.92		7
2059.33		5
2059.75	2	80
2060.16	3*c*	4*c*
2060.392		3
2060.55	8	5
2060.76		9*cl*
2061.042	4	3
2061.19	3	2*h*
2062.02		10*c*
2062.26	2	
2062.46		40*c*
2062.74	3*H*	
2062.86		3
2063.13		5
2063.792	40*cwn*	10*cw*
2064.16		20
2064.762	30	5
2064.87		30
2065.17		20
2065.64		3
2065.83		15
2066.53		8
2066.89	20	
2066.91		30*c*
2067.64	10	40*c*
2067.89	20*r*	8*c*
2069.15		3
2069.42	6	60*c*
2069.86		9
2070.13		5
2070.42		6
2070.82	3	
2071.11	3	
2071.175		10
2071.423		20
2071.65	3	
2072.09		20
2072.19	6	1
2072.59	5	
2072.62		30
2072.88		15*c*
2073.273	20*c*	10*c*
2073.898	10	6
2073.97	3	1
2074.70	20*r*	15
2074.82	5	2
2075.11		20
2075.20	5	2
2075.65	10*c*	
2075.70		50*c*
2076.30		20*c*
2076.55		9*c*
2077.08		4
2077.280	50*r*	20*c*
2077.78		20
2077.92	8*h*	1*h*
2078.21		7
2078.33		7
2078.65	5*h*	1*h*
2079.05		
2079.33		8
2079.92		20
2081.26	1	40
2081.35	7	
2081.98		60
2082.234	5*c*	100*c*
2083.342	4	20
2083.67	4	80
2083.925	40*r*	8*c*
2084.11	15*c*	5*c*
2084.53	15	5
2085.14		40*c*
2085.594	200*R*	30*c*
2085.76	7	80
2086.25	30*H*	10*H*
2086.96	20*H*	5*H*
2087.16	4	1
2087.30		10
2087.67	5	30*c*
2087.855	8	3
2088.23	3*h*	
2088.40		4
2088.56		8*c*
2088.61	3*c*	
2089.15		7
2089.68		3
2090.20	3	60*c*
2090.34	7	3
2091.48	3	
2091.535		30
2091.725	7	
2091.920		7
2092.24	50*r*	10*c*
2092.41	5	100*cw*
2092.50	2	50*c*
2092.835	15*c*	2*c*
2092.96		5*c*
2093.431		7*c*
2093.792		15
2094.00		2
2094.50	5	1
2094.622	8	2
2094.90		10*c*
2095.26	5	3
2095.33	2	
2095.52	4	
2095.57		6*c*
2096.22		3
2097.122	100*R*	20
2097.693	4	6
2097.703	4	
2097.77		10
2098.41	4	2
2098.53		3
2098.62	7*cl*	2
2099.28		10
2099.59		3*c*
2099.85		7
2100.10	3	3
2100.58		7
2100.63	5	
2100.753	5	
2100.85		8
2101.12	2	3
2101.51		8
2101.72	10*c*	5*c*
2102.28		4
2102.67	3	
2102.99		6*c*
2103.29		4*c*
2103.575	1*c*	40*c*
2103.864		6
2104.102	10*c*	6
2104.422		10
2104.59	3	
2105.573	1	30
2106.062		15*c*
2106.13	4	
2106.51	3*c*	60
2106.90	10*c*	4*c*
2107.452	60*r*	10*cw*
2108.447	10	5
2108.83		3
2109.22	100*R*	30*cw*
2109.46		3
2109.65		2
2109.86	3	
2109.953		40
2110.24	20*H*	3*h*
2110.868	3	2
2111.854	10	60
2112.245	4	150
2113.03		4
2113.87	30*r*	10*c*
2114.25	10	100
2115.51	1*c*	20*c*
2115.76	5	
2116.13	10	
2116.23		7
2117.64		10
2118.54		5
2118.671	1	15
2119.015		2
2119.52	4	
2119.67		1
2121.15	4	
2121.27		10
2122.081	2	20
2122.24	3	
2123.213		5
2123.84		2*c*
2123.89	5	
2124.445		9
2125.183		9
2125.576		3
2126.42	5*c*	
2126.73	3	4
2126.85	4	5
2126.96		3
2127.28		2
2127.85	2*c*	
2128.09		3*c*
2128.392		8
2128.53		4
2128.773	4*c*	6
2129.40		1
2129.579	2	10
2129.91		1
2130.16	2*c*	
2130.513	4*c*	10
2131.01	2	
2131.285		2
2131.44	2	2*h*
2131.59	2	
2132.53	4*c*	
2133.122	2	9
2133.41	5	2
2133.776		20
2134.34	4	
2134.594		6
2134.773		10*c*
2135.07	5	2
2136.10	3	
2136.22		5
2136.36	2*c*	
2136.701		4
2137.07		2
2137.50	20*Hc*	10*Hc*
2138.10	4*H*	1*h*
2138.44	5*h*	2*h*
2138.56		4
2138.63	4	
2139.04	3	100

TABLE 2. *Arc and spark spectra of rhenium*—Continued

Wavelength	Intensity and other characteristics	
	Arc	Spark
A		
2138.20	4	
2138.45		3
2138.59	2	
2138.780		3
2140.190		4
2140.66		6c
2140.924	6	2
2141.329		2
2141.545		2
2141.745	6	
2142.736	10c	20c
2142.97	20r	5
2143.443	4	2
2143.89	3	
2143.96		8h
2144.085	2	30
2144.45	10c	5c
2145.01	2	
2145.41		10
2145.69	1	5
2145.90	1	30
2146.20	3cw	
2146.72		2
2147.03		2
2147.483	8	4
2147.97	6	4
2148.13		3
2148.261	1	20
2148.92	3	
2149.23		3
2149.43	5cw	4
2149.59	1	4
2149.818		20cw
2150.118		2
2150.44	2	20
2150.82		10c
2151.40	4	3
2151.74	6	2
2152.04		2
2152.79		5
2152.98		2
2153.30	8	4
2153.53		1
2153.79		3c
2154.01	2	1
2154.20	10c	2c
2154.45		6
2155.056		5c
2155.24	2	2
2155.53		2
2155.73	7	1
2155.86	10	4
2156.103		2
2156.23		2
2156.673	100R	50
2157.89	4	1
2158.05		4cs
2158.292	2	20
2158.73	15cw	8cw
2159.14	7c	4c
2160.04		1
2160.42	10c	8c
2160.934		20
2161.15	15cw	7cw
2161.914		10
2162.326		1
2162.81	15cw	10cw
2163.07		7
2163.10	10	
2163.56	6	3
2163.704		20
2163.72	3	
2164.29		6
2164.56	20cw	10cw
2164.773		4
2164.91	6cw	
2165.409	2	30
2165.65	3	
2165.901		15c
2166.52		2

Wavelength	Intensity and other characteristics	
	Arc	Spark
A		
2166.726		4
2166.880	2	40
2167.29		4c
2167.39	10H	1h
2167.44		4
2167.938	200R	50
2168.42	15	10
2168.77	5	1
2169.240		5
2169.49	5	3c
2169.62		5c
2169.77		2
2170.340	5	10
2170.806	2	50
2170.970		10
2171.145		4
2171.267		3
2172.094		2
2172.618	1	30
2173.233		20
2173.39		10H
2174.05	8	4
2174.24	10	5
2174.692		4
2175.346	20c	6c
2175.806	20c	10c
2176.016		5
2176.206	200R	50
2176.35		3
2176.56		1
2177.28	50Hw	20Hw
2177.382		4
2177.579	1	20
2177.851	2	100
2178.04	6	
2178.59	10	5
2178.778	1	20
2178.87	3	
2179.03	4	
2179.09		5
2179.18	8c	
2180.136	5	3
2180.405	30c	10c
2180.54		5
2180.78	15	
2180.804		10
2181.02	20	10
2181.430		4
2181.65	3	
2181.77		100cw
2181.81	4	
2182.374		2
2183.158		5
2183.443		15c
2183.72	100cwR	10cw
2184.19		1
2184.540	10	10
2184.73		3
2185.16	20	3
2185.215		3
2185.915		8
2186.358	2	50
2187.02	3	
2187.556		4
2187.77	50c	10h
2188.01	10	2
2188.221		10
2188.38	3	1
2188.50	6	2
2188.755		2
2189.60	8	
2189.870	6	5
2190.260	4	50
2190.518	10c	10
2191.03	20H	3H
2191.471	40c	10c
2192.23	8	
2192.44	10	
2192.567		20c
1292.84	3c	

Wavelength	Intensity and other characteristics	
	Arc	Spark
A		
2193.14	6	4
2193.507	10c	8c
2193.85	5	
2193.933		15c
2194.433		10
2194.561		10
2194.68	1	
2195.284	1	40
2195.84	8	1
2195.97	10	3
2196.284		2
2196.72	50cw	10cw
2196.834		8
2197.130		30c
2197.373		10
2197.44	10c	
2197.610		4
2197.928		15
2198.213		6
2198.401	15	3
2198.617	5	1
2198.914	200R	40
2199.113		3
2199.50	10c	
2199.69	7	2
2199.82	4	
2199.96	4	3
2200.219		4
2201.075	8	2
2201.32		1
2201.640		8
2201.68	7	
2201.911		20
2202.00	10cw	
2202.15	7	
2202.19		10
2202.49	5	3
2202.695		2
2202.815	10c	5
2203.010	40	20
2203.46		2
2203.579	1	20
2203.71		2
2204.55	20c	7
2205.15	50cw	20c
2205.344		15c
2205.41	4c	
2206.154	2	40
2206.707		4
2206.76	4	
2206.870	2	100
2207.376		3
2207.680	20	5
2208.188		2
2208.28	2	
2208.394	2	
2208.58	6	1
2209.045		2
2209.320		7
2209.800	30	
2209.87		20c
2210.02	40H	
2210.655	6	2
2210.81	4	2
2211.197	10	7
2211.33	10c	
2211.52		2
2211.933	10	4
2212.088	10	1
2212.211		7
2212.495		3
2212.809	10	4
2212.900		4
2213.23	6	1
2213.50	2	
2213.68		20
2213.98	5	
2214.261	500R	1000cw
2214.58	300r	50cw
2215.353	4	

TABLE 2. *Arc and spark spectra of rhenium*—Continued

Wavelength	Intensity and other characteristics	
	Arc	Spark
A		
2215.535	2	2
2215.80	6c	1c
2216.161	1	50
2216.52		5c
2217.03		3
2217.158	10c	2
2218.36	8c 3, .21 *WI*	
2218.648		5
2218.715	15	5
2218.940		7
2218.97	10	
2219.260	15c	8c
2219.75		1
2220.438		2
2220.577	10	5
2220.69		2
2220.920	2	5
2221.845		7c
2222.32		2
2222.465	10	3
2222.76	15	6
2222.932		5
2223.08	2	
2223.16	5	
2223.20		5
2223.407	1	20
2223.77	3	
2223.93		6cw
2224.31		15b
2224.41	5	
2224.851		7
2226.048		20
2226.418	300*R*	50
2226.87	50cw	5c
2227.021		20
2228.05	30c	10c
2228.389		8c
2229.104	1	20
2229.61	2	
2230.43	2	
2230.47		10c
2230.61	5	
2230.68		1
2230.83	10c	
2231.127		8c
2231.561	4	
2231.92	2	
2232.08	3	1
2232.292	4	50
2232.48	3	
2232.62	5	
2232.964		3
2233.404		1
2233.84	20	
2233.91	3	10
2234.07	30c	5c
2234.50	20c	3c
2234.865		10
2235.110	7	3
2235.440	50r	20
2235.803	2c	100c
2236.03		5c
2236.577		6
2236.77	6	1
2237.47	2	
2237.63	8	2
2237.85	2	
2238.169		10
2238.211	5	
2238.348		10
2238.603	40r	10
2238.830		3
2238.944	8	4
2239.16	6c	1c
2240.00		5
2240.05	30	10
2240.29	2	
2240.63	30	2
2240.977	30	1
2241.34		2

Wavelength	Intensity and other characteristics	
	Arc	Spark
A		
2242.40	30	10
2242.66	50	?
2243.19		20
2243.261	10	4
2243.476	8	1
2243.79	8	1
2244.112	15	7
2244.500		4
2244.63		3
2244.72	5	1
2245.120	8	3
2245.37	50*H*	5*Ir*
2245.43		9c
2245.884		3c
2246.18	2	
2246.444	20c	7c
2247.326		10
2247.49	3	
2247.544		9
2247.948		10
2247.97	3	
2248.55	5	
2248.63	2	50
2248.90	2	
2249.04	2	
2249.24	2	
2249.51	50cw	5cw
2249.753		1
2250.273		15
2250.33	3	
2250.632		3
2251.148		15
2251.273	15	1
2251.41	2	
2251.593	2	40
2251.76	7c	
2251.94	6	2
2252.154		10
2252.53	4	
2252.61		2
2253.28		8
2253.48		7cl
2253.848		9
2253.94	50cw	5cw
2254.196		15
2254.790	30	10
2255.729	100r	30
2255.937		10
2256.193	150*R*	50
2256.74		2
2256.935	5	2
2257.25	15	5
2258.406	3	
2258.55		8
2258.62	2	
2258.933		7
2258.98	10	
2259.310	20	10
2259.796		6
2260.00		2
2260.20	5	
2260.500	5	30
2260.83	10c	2c
2261.38	4	2
2261.595	2	
2261.846	1	50c
2262.276	15c	5c
2262.424	10	4
2262.773	15c	3c
2263.13	5h	2
2263.617	8	1
2263.748		9c
2263.96	10cw	2
2264.393	200*R*	100
2264.98		1A
2265.10		3h
2265.416	40c	10c
2266.072	30c	10
2266.18	2	10
2266.387		2

Wavelength	Intensity and other characteristics	
	Arc	Spark
A		
2266.582		4
2266.733		2
2266.889		4
2267.256		40
2267.358	3	
2267.652	20	10
2268.08	1	
2268.41	4	
2268.46		40c
2268.803	10	2
2269.061		10c
2269.228		2
2269.613		2
2269.793	2	10
2270.018	10c	10c
2270.170	8	2
2270.574	4	1
2270.928		5
2271.04	50cw	3c
2271.300	40r	10
2271.611	15	10
2271.97	2	
2272.15		1
2272.644	2	50
2272.931	5	1
2273.14	2	
2273.98		10
2274.016	4	
2274.20		1
2274.618	300*R*	100c
2275.25	200cw	500 c .22*W*
2275.724		1
2276.41		1
2276.632	20	5
2277.012		10
2277.340	30c	5c
2277.926		5
2278.431	2	
2278.550	5	3
2278.635		1
2278.73	10	10
2278.948		2
2279.15		1
2279.563	2	15
2279.87		1
2280.00	2	2
2280.540	10	3
2281.07		1
2281.29	10cs	3c
2281.406		10
2281.620	200*R*	40
2282.51		5h
2282.980	2	20
2283.191	6	2
2283.568	15	2
2283.69		1
2283.818	5	1
2284.78		1
2285.30	50	30
2286.608	2	60
2287.003		1
2287.17		3
2287.506	400*R*	100c
2289.178		1
2289.688		7
2290.196		10
2290.715	50cw	20cw
2291.299	10	5
2291.66	8c	1
2291.884		50cw
2292.327	2	
2292.50	1	
2292.520		2
2292.71	2	1
2293.641	5	2
2293.678		10
2294.486	400*R*	100c
2295.060		15
2295.217		3
2295.661	4	1

TABLE 2. *Arc and spark spectra of rhenium*—Continued

Wavelength	Intensity and other characteristics	
	Arc	Spark
A		
2296.09		1
2296.211	15	
2296.24		15*cl*
2296.926	40*r*	10
2297.43	1	
2297.497		6
2297.81	7	
2298.094	8*cw*	100*cw*
2298.35	15*c*	3
2298.586		10
2299.413	7	1
2299.680		2
2299.769	20*c*	20*c*
2299.880		2
2300.109	6	1
2300.613	6*c*	
2300.736		15*c*
2301.318	8	2
2301.612		7
2301.815	1	40*c*
2301.884	4	
2302.25	1	
2302.345		6
2302.643	8	4
2302.992	150*R*	30*c*
2303.370	3	
2303.517	10	5
2303.660	10	5
2303.993		30*cw*
2304.443	8	1
2304.587	8	4
2304.714	10	5
2305.021		8
2305.22	4*c*	
2305.545	20*cw*	2*c*
2305.726	10	3
2305.934		2
2306.14		2
2306.24	2	
2306.268	2	4
2306.540	60*r*	20
2307.03		1
2307.215		5
2307.39	10*cw*	2*c*
2308.060		10
2308.167		10
2308.354	20	2
2308.45		20*c*
2308.592	30*c*	4
2308.658		15
2308.972		3
2309.619		30
2310.00	3	1
2310.134	10	3
2310.703		3*c*
2310.938		
2311.189	20	5
2311.576	8	3
2312.011	7	
2312.109		30*c*
2312.200	5	
2312.814	9	5
2312.971	10*r*	8
2313.12	5	1
2313.267		10
2313.340	20	8
2313.638		2*c*
2313.922		4
2313.98	6	
2314.209		2
2315.186		2
2315.238	10	4
2315.956	30*r*	10
2316.04		2
2316.49		10*c*
2316.523	30*c*	10
2317.24	6*cs*	2*cs*
2317.722		5
2317.889	2	20
2318.242		30

Wavelength	Intensity and other characteristics	
	Arc	Spark
A		
2318.46	3*c*	2
2319.091		1
2319.19	30*r*	10
2319.288		2
2320.162	50*r*	20
2320.78		4
2320.89		4
2321.11	4	2
2321.272	8	4
2321.41	10	6
2321.57	6	4
2321.70	10	4
2321.75		10
2321.91		2
2322.490	50*R*	20
2322.700	4	2
2322.89		10*c*
2322.945	10*c*	5
2323.409	2	60
2324.108		3
2324.45		10*c*
2325.045	20	5
2325.424		2*c*
2325.64		1
2326.16	2	
2326.82	4	
2326.88	10	10
2327.095	3	
2327.265	7	
2327.306		100*c*
2328.189		5
2328.664	30*r*	10
2329.28	4*H*	3*H*
2329.89		8*cw*
2330.18	6	2
2330.424	8	3
2330.544	5	2
2330.706	4	1
2330.878		10
2331.135	20*c*	10*c*
2331.19		3
2331.374	8	4
2331.599		10
2331.73	20*c*	2
2331.81		10
2332.51		2
2332.77		2
2333.019	15	5
2333.32	20*c*	5
2333.75		1
2333.91		5
2334.33	20*r*	10
2334.45	10	2
2335.00	10*c*	3*c*
2335.61	5	2
2335.730	20*r*	10
2336.04		2
2336.10	20*r*	10
2336.47	1	15
2336.718	10	4
2336.923	2	50
2337.092	10	4
2337.43	3*c*	1
2337.953	40*R*	20*c*
2338.451	20	5
2339.04		4
2339.26	3	
2339.48		1
2339.71		2
2339.86		3
2340.29	3*h*	
2340.344		20
2340.938		7
2341.23	2	
2341.31		10
2341.38	8	7
2342.06	2	
2342.18		10
2342.731	30	5
2343.320	2	7

Wavelength	Intensity and other characteristics	
	Arc	Spark
A		
2343.46		4
2343.78	3*c*	
2344.006	4	
2344.19	10	
2344.544		1
2344.776	100*R*	40
2345.282	20*r*	6
2345.51		10*c*
2345.653	30*c*	10*c*
2345.985	3	
2346.139		1
2346.37	4*h*	
2346.43		2
2346.614	8	4
2346.774	6	2
2346.987		20
2347.064	10	2
2347.288		5
2347.611	3	10
2347.84	3*c*	
2348.22	3*cw*	20*cw*
2348.557	4	1
2348.792	8	2
2349.391	30*r*	10
2349.55	20*c*	
2349.61		10*cl*
2349.86		1
2349.94		3
2350.31	2	
2350.46	20	10
2350.60	20*r*	5
2350.653		3
2351.14	4	1
2351.41		3
2351.925		2
2352.069	100*R*	30
2352.24		3*H*
2352.481		4
2352.59		2
2352.790	4	1
2352.900	10	4
2353.115		30
2353.18	5	
2353.55		4
2353.95	30*r*	5
2354.08	30*r*	10
2354.372		4*c*
2354.66	4	1
2354.773	15	3
2355.02	10*c*	
2355.423	1	40*c*
2355.868	10	2
2356.125		10
2356.496	30*r*	10*c*
2356.62		1
2357.035	15*c*	5
2357.26	5	1
2357.60	3	
2357.66		3
2357.72		1
2357.91		10*cw*
2358.022		3
2358.570	10	5
2358.940		2
2359.157		5
2359.323		1
2359.47	5*H*	
2359.760		1
2359.98	4	4
2360.287	10	5
2360.897	10*c*	2
2360.94		5*c*
2361.47		10*c*
2362.078	2	5
2362.415		10
2362.54	2	10
2362.64	20*c*	
2362.85	20*c*	
2362.89		10*c*
2363.805	20	5

TABLE 2. *Arc and spark spectra of rhenium*—Continued

Wavelength	Intensity and other characteristics	
	Arc	Spark
A		
2364.125		5
2364.23	3c	
2364.44	3	
2364.91		1
2365.316	50r	20
2365.666	20r	5
2365.90	150*R*	30
2366.078		40
2366.68	3	6cw
2366.997	10	5
2367.16		4c
2367.55	7	
2367.683	50r	20
2367.75		1
2367.88	10	2
2368.062		2c
2368.12	4c	
2368.20		4
2368.527	5c	50c
2368.88	15c	5
2368.93		4
2369.152		10
2369.27	50r	15
2369.475	10	4
2369.97		20c
2370.762	10	100
2371.500	30r	10
2371.69		1
2371.842		4
2372.610	40c	10c
2372.880		7
2373.274	7	4
2373.476	10	50
2373.56	3	
2373.747	15	4
2373.962	1	15
2374.57		3
2375.073	100r	20c
2375.33	2	
2375.815	15r	10
2375.93	10	2
2376.334	4	1
2376.629	10	3
2377.104	10c	3
2377.333	20c*H*	10c
2377.620		10
2378.40	3	
2378.526	5	20
2378.98		4
2379.101	3	20
2379.587		3
2379.774	40r	15
2379.950	5	
2379.992		5c
2380.225	20c	10c
2380.63		2
2380.890	15	5
2381.136	40cw	20c
2381.81	6	4
2382.07		10
2382.40	5*H*	2*H*
2383.04	8	4
2383.12		7
2383.46	50r	20
2383.97	10h	3h
2384.382		7
2384.50	10h	3h
2385.02		8
2385.362		15c
2385.48	15	4
2385.68	10	2
2385.834	6	
2386.176		
2386.536	10	5
2386.895	5c	100cw
2387.458	10	5
2387.745	20c	5c
2387.92		2
2388.319		5c
2388.569	100r	20c

Wavelength	Intensity and other characteristics	
	Arc	Spark
A		
2388.918		2
2389.110	20r	10
2389.270	5	
2389.379		2
2389.62	1	30
2389.75		3
2390.430	50r	10
2390.593	15	3
2391.278	30r	10
2391.845	10c	3c
2391.94		3
2392.36	15	5
2392.67	6	3
2393.645	50r	10
2393.81		40cw
2393.883	5	
2394.252	4	
2394.37	30r	
2394.72		10
2395.09	10c	5
2395.33	7*H*	2c
2395.41		3
2395.96		3
2396.03	7	1
2396.06		4
2396.13	3	1
2396.22		1
2396.60		10
2396.791	40r	15
2397.31	50c	20c
2397.605	4c	
2398.25	10	2
2398.420	2	60
2398.58		10cw
2398.71	15	3
2398.888	15	4
2399.02		4
2399.533	10	3
2399.648	6	4
2400.72	20c	20cw
2400.893	30	10
2401.680	30	20c
2402.115	15	5
2402.604	40c	20c
2403.036	10	50c
2403.87		7
2404.340	100r	20c
2405.056	300*R*	70
2405.602	200r	30
2405.91		3
2406.11		2
2406.33		7c
2406.695	60r	20c
2407.39		3
2408.23		5
2408.405	4	1
2408.578	3	1
2408.989	1	20
2409.777		7
2410.000	1	20
2410.28		5
2410.37	30r	20c
2410.80	6	2
2410.99	40r	20c
2411.220	4	
2411.245		2
2411.947		20c
2412.626		2c
2412.974		3c
2413.216	30	10
2413.629		7cw
2413.741	10	
2413.81		15
2414.198		7
2414.48		7
2414.587	30r	10
2414.99		2h
2415.261	4	4
2415.84	10c	10c
2415.93	4h	4h

Wavelength	Intensity and other characteristics	
	Arc	Spark
A		
2416.265	5	40
2416.30	10	2
2416.441	10	7
2417.026		6
2417.661	15	10
2417.815		2
2417.89	2	
2418.03		3
2418.201	2	30
2418.392	4	15
2418.96		6
2419.404	60r	10
2419.807	100r	20
2419.955	3h	5c
2420.214		10c
2420.28	2	
2420.35	5	1
2420.72	5	1
2421.38	30	
2421.41		60
2421.66	3	
2421.730	40r	10c
2421.883	30r	10
2422.11	2	
2422.34		2
2422.60		9
2423.112		20
2423.50	30c	4h
2423.78	10*H*	
2423.842	10c	100cw
2424.652	10	10
2424.95	2	2
2425.18		1
2425.38	30c	10c
2425.45		3c
2425.700	7	3
2426.195	10	3
2426.456		2
2426.635	30	10
2427.148		15
2427.21	7	
2427.73	8*H*	3*H*
2428.145	3	5
2428.576	300*R*	60
2428.84		3
2429.097		4
2429.204	10	6
2429.648	10	7
2429.78	8c	2
2430.515		40
2430.750		2
2431.068		5
2431.338	50r	20
2431.744	8	4
2432.18	80c .18*W*	4cw
2432.617	5	1
2432.70	20	5
2432.87		10c
2433.07		2
2433.28	20	10
2433.365		5
2433.608	5	2
2433.741		40
2433.803	10	3
2434.536	5c	
2434.62		20cw
2435.31		15
2435.82		4d
2436.046	10	5
2436.48		3c
2436.51	3	2
2436.71	5	
2436.74		10
2436.95		4
2437.23	10	2
2437.43	1	10
2437.710		10
2438.145	5	1
2438.20	1	8
2438.462	30	10

TABLE 2. *Arc and spark spectra of rhenium*—Continued

Wavelength	Intensity and other characteristics	
	Arc	Spark
A		
2459.06	50c	10c
2459.62	4	3
2459.84		5h
2459.89	3	
2460.41	30	20
2460.58	10	3
2460.91		1
2461.05		1
2461.35	3	10
2461.47	100*R*	30
2462.08		1
2462.310	40r	10
2462.64		1
2462.88	2	
2463.10		10
2463.353	20	4
2464.09	100c*w*	
2464.14		7h
2464.54		20
2464.943	70r	15
2465.085		10c*l*
2467.144	8c	1
2467.283	8	3
2467.404	3	1
2467.575		10
2467.881	10	5
2467.978	30c	10c
2467.656	5	2
2467.852	2	
2468.051	5	3
2468.20	20	4
2468.26	1	6
2469.033	5c	100c
2469.723	20c	20c
2469.710	60r	20
2470.329		7
2470.413	2	
2470.895	30	3
2471.24		50*H*
2471.32	2	
2471.683	6	1
2471.910	8	2
2472.067		2
2472.22		2
2472.93		2c
2472.760	2	
2472.949	3	1
2473.14	40r	20c
2473.493	10	3
2473.936		4c
2474.082	3	
2474.334		1
2474.55		2
2475.051	4	
2475.097		10
2475.63		2
2475.827	10c	100c
2475.987	20c	4c
2476.154		1
2476.435		2
2476.797		8
2476.961	10c*s*	2c*s*
2477.36	1c	100c*l*
2477.396	4c	
2478.200		1
2478.377	2	
2478.833		8
2479.105	5	2
2479.62	1	4
2479.672	2	
2479.81	4	1
2479.89		1
2480.24	20	5
2480.99		3c
2481.196	200*R*	40
2481.84	40c*w*	200c*w*
2482.181		2
2482.539	10	3
2482.658		2
2482.915	8c*w*	6c*w*

Wavelength	Intensity and other characteristics	
	Arc	Spark
A		
2463.141		1
2463.307	15	5
2463.84	5	1
2463.964	8	2
2464.29		1c
2464.63	3	1
2465.13	30	8
2465.29		10
2465.80	2c	20c
2465.97		3ch
2466.042	5	
2466.546	3	
2466.810	2	20c
2467.308	15	2
2467.574	15c	100c
2467.706	2	
2467.80		4
2467.85	20c	20c*l*
2468.195		10c
2468.480		7
2468.608		4
2468.695	5	
2469.03	15	15
2469.356	5c	100c*wl*
2470.052	8c	2
2470.164	4	1
2470.275	3	
2470.610	5	50
2470.92	3c	
2471.049	2	20
2471.205		4
2471.426		2h
2471.486	2	
2471.93	2	1
2472.006	3	1
2472.14	2	
2472.55		3
2472.78		1
2473.72	5c	100c
2474.208	15	2
2474.725	15	7
2475.172	10	30
2475.470		5h
2476.197	7	2
2476.275	5	
2476.332		10c
2477.43		100c
2477.50	10	?
2478.07	5h	1
2478.545		10c*l*
2478.58	2h	
2478.99		80
2479.02	20c	
2479.17		2h
2479.289	1	
2479.541		4
2480.631		6
2480.820	20c	
2481.12	1	1h
2481.226	4	2
2481.357	2	
2481.534	2	2h
2481.668	4	1
2481.98	1c	8c*w*
2483.109	6	2
2483.38	5	1
2483.920	200*R*	80
2484.12		2h
2484.406		2
2484.51	2c	
2484.60		3
2485.159	10c	2c
2485.48		5*Hw*
2485.50	3c	
2485.805	20c	10
2486.102		2
2486.329		2
2486.46		4c*wl*
2486.779	30c*w*	6c
2486.970	10c	3

Wavelength	Intensity and other characteristics	
	Arc	Spark
A		
2487.21	5	2
2487.331	200*R*	100
2487.362		70c*l*
2488.104		6c
2489.04		30*l*
2489.335		2
2489.482		4
2490.161	3	50
2490.26	2	30
2490.40		3h
2490.50	4	
2490.769	8	3
2490.91		1
2491.07	9c	1c
2491.234	2	10
2491.497	2	
2491.881	1	30
2492.13	27	3
2492.537	1	5
2492.55	9	8
2492.751	8	3
2492.838	3c	3
2493.17		1h
2493.25		2h
2493.461		1
2493.597		2
2494.01	1	
2494.217		3h
2494.250	3	
2494.517		1
2494.609	1	1
2494.709	2	1
2495.141		7
2495.263	8c	4
2495.386		3h
2495.620	2	1
2495.93	5*H*	
2496.039	30	20
2496.692	10	3
2497.168	3h	
2497.320		4c
2498.03	4c	
2498.080		6
2498.215	20	10
2498.566		1
2498.861	20	5
2499.19	1	
2499.475	7	3
2499.608	2	1
2499.968		2
2500.012	6	2
2500.312	10	4
2500.568	10	10
2501.05		2
2501.35	2h	
2501.721	50r	20
2502.09	1	
2502.348	30c*s*	200c*w*
2503.775		3
2504.08		2h
2504.36		2
2504.493		10h
2504.595	20c	30c
2504.861	1	
2505.11		1
2505.210		4
2505.39		4
2505.43	30h	
2505.945	30c	20c
2506.585		1
2506.999		10
2507.403	30c	10
2507.854		5c
2508.08	2h	
2508.482		2h
2508.861	2	20
2508.991	200*R*	100c
2509.50		2h
2509.562	5c	2h
2510.11		20c*w*

TABLE 2. *Arc and spark spectra of rhenium*—Continued

Wavelength	Intensity and other characteristics	
	Arc	Spark
A		
2510.771	.....	5
2511.250	.....	10
2511.285	.....	10h
2511.616	5	2
2511.720	2	.....
2511.944	.....	5
2512.317	4	1
2512.414	.....	2
2512.550	15	4
2513.87	2h	1h
2514.35	2h	2h
2514.510	20	8
2514.651	5	2
2514.805	3c	1c
2515.190	.....	2h
2515.351	2	2
2515.470	6	5
2516.120	150r	100
2516.381	3	2
2516.52	.....	3c
2516.765	2	1
2517.083	7	4
2517.350	7h	4h
2517.99	.....	2h
2518.54	3h	.....
2518.720	.....	10hw
2518.87	5c	.....
2519.139	6	2
2520.009	50r	20
2520.658	.....	2h
2521.50	10c	10c
2521.59	5	5
2521.691	.....	10h
2522.004	5c	2h
2522.719	5	2
2523.190	4	1
2523.308	.....	2
2523.415	3	1
2523.519	3	1
2523.798	.....	7
2524.155	5	2
2524.30	.....	8h
2524.546	6	2
2525.049	2h	.....
2525.548	20c	5
2525.653	.....	4
2525.755	.....	10
2526.32	.....	10
2526.37	.....	6
2526.536	.....	3
2526.66	.....	1
2526.809	10	4
2526.905	.....	2h
2527.311	5	2
2528.186	.....	2h
2528.30	3c	.....
2528.486	1	20c
2528.62	1	10cw
2528.87	4c	1
2529.26	.....	2
2529.50	15c	10
2529.57	.....	3h
2529.898	.....	4
2530.237	.....	4h
2530.260	2	.....
2530.457	3	1
2530.93	2h	.....
2531.404	5c	1h
2531.672	2	1
2532.33	.....	7cw
2532.48	5c	2c
2532.536	.....	5h
2532.848	5	3
2532.963	4	2
2533.119	4	3
2533.310	15r	10
2533.74	1	.....
2534.099	5	80
2534.805	30cw	20c
2535.725	1h	.....

Wavelength	Intensity and other characteristics	
	Arc	Spark
A		
2535.774	.....	10h
2536.398	.....	3
2536.510	.....	2
2536.913	4	1
2537.015	6	3
2537.49	.....	5c
2537.517	4	2
2537.65	5c	2c
2537.877	4	2
2539.326	20c	10
2539.727	.....	7
2539.86	1	.....
2540.057	7	5
2540.45	3	.....
2540.513	40r	20
2540.706	5h	7h
2541.070	20h	3h
2541.27	20h	3h
2541.514	.....	6
2541.651	.....	4h
2542.09	3	4h
2542.920	4	2
2543.022	2	1
2543.210	.....	3h
2543.671	10	15
2543.835	8	5
2544.215	10	8
2544.739	100r	40
2544.878	20cw	20cw
2544.952	8	5
2545.485	30r	30c
2545.258	.....	15h
2546.098	2	1
2546.456	.....	2
2546.74	1	.....
2546.02	.....	2h
2547.398	5	2
2547.521	1	2h
2548.020	.....	7
2548.136	10	6
2548.386	.....	3h
2548.885	20	10
2549.372	6	3
2549.847	5hc	.....
2550.091	4c	100cw
2550.338	4h	.....
2550.444	.....	5
2550.613	5h	2
2550.827	1	30cw
2551.463	2c	2c
2552.021	40r	20
2552.73	10c	20c
2553.588	3c	100cw
2554.18	15	10
2554.630	4	200
2554.929	6	3
2555.116	2	1
2555.24	.....	2h
2555.32	3	1
2555.531	4	3
2555.666	5	3
2556.512	80R	40
2556.784	.....	2h
2556.918	2	2
2557.414	.....	20
2557.694	.....	15
2558.062	10c	7c
2559.076	20R	10
2559.478	.....	5h
2559.707	6	3
2559.882	6	4
2560.366	.....	1
2560.602	.....	1
2560.754	.....	1
2561.184	.....	8h
2561.27	2	.....
2561.462	8	5
2561.712	.....	2h
2561.920	.....	4
2562.051	2h	.....

Wavelength	Intensity and other characteristics	
	Arc	Spark
A		
2563.006	20c	10c
2563.971	2	1
2564.186	50R	20
2564.347	10c	8hl
2564.650	.....	2
2565.297	.....	1h
2565.582	.....	10
2565.839	6	4
2565.967	3	1
2566.366	.....	60
2566.569	8	3
2566.735	4	1
2566.92	.....	4hl
2568.329	5	3
2568.638	10c	300
2568.817	2	.....
2569.02	4h	.....
2569.192	.....	3h
2569.327	4c	2
2569.828	.....	
2570.046	4	3
2570.186	.....	3h
2571.255	10	10
2571.605	1	.....
2571.810	10cw	300cw
2572.117	.....	5h
2572.476	2h	1h
2573.760	20c	15c
2573.988	3h	1h
2574.211	6	5
2574.686	3	1
2575.317	.....	30
2575.664	.....	1h
2575.95	6cw	3c
2576.238	.....	20
2576.316	6	3
2576.408	4	1
2576.68	1	.....
2576.818	.....	3cw
2577.030	3	1
2577.614	6	3
2578.120	10cW	8cW
2578.862	.....	10
2579.005	10c	6c
2579.343	2	1
2579.590	.....	1
2579.778	2h	1h
2580.102	.....	4h
2580.203	4	2
2580.311	7	15hl
2581.166	.....	4h
2581.421	.....	6
2581.438	9hl	.....
2581.649	2h	1h
2582.111	.....	10cWs
2582.240	2	1
2582.767	10	10
2582.870	.....	7cw
2583.146	.....	4
2583.406	3	2h
2583.873	4	2
2584.523	6	4
2584.798	10	7
2585.061	6	3
2585.580	8c	2c
2586.425	.....	1
2586.788	50R	30c
2586.998	7	5
2587.160	15cw	4c
2588.034	.....	50h
2588.297	.....	2
2588.579	.....	60cd
2588.786	2	1
2589.218	3	2
2589.310	4	2
2589.594	6	3
2590.489	4	2
2590.629	3c	1c
2591.100	5	2
2591.133	6	6

TABLE 2. *Arc and spark spectra of rhenium*—Continued

Wavelength	Intensity and other characteristics	
	Arc	Spark
A		
2591.430	6	3
2591.582	30*r*	15
2591.889	10*c*	5*c*
2592.843	10*cws*	5*cw*
2593.048	----------	8*h*
2594.267	----------	2
2594.854	30*R*	15*cw*
2594.982	5	1
2595.234	60*R*	30*cw*
2596.016	----------	5
2596.404	10*c*	7
2596.780	10*r*	8
2596.950	15*c*	10*c*
2597.283	----------	1*h*
2597.961	9	5
2598.108	----------	3*h*
2598.631	10*R*	5*cw*
2599.528	7*cw*	2*c*
2599.856	50*R*	20
2600.215	----------	1*h*
2600.518	5*c*	2*c*
2600.866	10*c*	5*c*
2601.874	15*c*	8*c*
2602.350	10*c*	7*c*
2602.681	----------	2
2602.926	10	7
2603.462	15	9
2603.82	47	60*bl*
2603.89	40*cw*	20*c*
2604.832	----------	2*h*
2606.480	----------	10
2607.316	8	3
2607.612	----------	200*cwl*
2607.936	10*c*	2*c*
2608.043	3	1
2608.501	10	400
2608.746	3	1
2609.085	5	2
2609.204	5	2
2609.404	9	4
2609.705	----------	2
2609.839	----------	5
2609.86	2*h*	----------
2610.120	----------	2*h*
2610.545	----------	20*h*
2610.690	4	1
2610.874	----------	8*c*
2611.536	50*R*	10
2611.603	40*R*	15
2611.702	5	2
2612.463	----------	7*Hw*
2612.730	10*c*	3*c*
2612.788	----------	8
2612.858	6	2
2612.929	5	2
2613.235	10	3
2613.903	----------	2*h*
2613.744	15	6
2614.168	2	1
2614.558	50*R*	20*c*
2614.856	3	1
2615.274	----------	2*h*
2615.59	----------	5*h*
2615.676	6	5?
2615.76	----------	5*h*
2616.042	1	----------
2616.130	----------	2
2616.215	3*h*	1*h*
2616.720	4*cw*	150*cwl*
2617.112	15	6
2617.442	10	5
2618.374	4*h*	4*h*
2618.71	----------	4*h*
2618.742	4*h*	?
2618.80	----------	5*h*
2619.082	----------	4*h*
2619.502	----------	1*h*
2619.658	1	----------
2619.805	----------	10*hs*
2620.036	40*R*	20

Wavelength	Intensity and other characteristics	
	Arc	Spark
A		
2620.344	30*R*	20
2620.528	3*c*	1
2620.937	----------	2*h*
2621.144	10	5
2621.208	----------	10
2621.310	5	2
2621.779	----------	2
2621.870	----------	3
2621.975	15	6
2622.276	----------	3
2622.752	40*R*	20
2622.882	3*H*	1*H*
2623.285	20*cw*	10*cw*
2623.772	2	1
2624.591	----------	10*h*
2624.906	----------	2
2625.041	8	3
2625.128	3	1
2625.154	----------	2*h*
2625.438	----------	2*h*
2625.806	7	2
2625.898	----------	2*h*
2626.200	1	----------
2626.636	5	2
2626.870	----------	2
2627.450	1	----------
2627.868	----------	4*h*
2627.880	3	1
2628.258	----------	100*h*
2629.144	1	----------
2629.603	----------	2*h*
2630.150	8	3
2630.436	----------	8
2630.652	3*h*	----------
2630.754	7	3
2630.861	1	30?
2630.957	2	----------
2631.569	20*cs*	8*c*
2631.836	----------	6*h*
2632.16	----------	20*c* .16*WT*
2633.006	10	3
2633.084	----------	8
2633.614	20	15
2633.775	----------	2*h*
2633.892	2	----------
2634.352	10	4
2634.798	----------	2*h*
2634.908	2	1
2635.115	----------	2*H*
2635.831	3*c*	200*cwl*
2636.019	2	----------
2636.637	100*R*	20
2637.006	10*c*	150*c*
2638.147	----------	7*h*
2638.656	2*h*	1*h*
2638.919	3	2
2639.346	----------	3
2640.140	----------	5*cw*
2640.282	8*c*	2*c*
2641.021	2	30
2641.173	10	1
2641.300	----------	3
2642.131	1	10
2642.25	----------	30*cw*
2642.752	60*R*	50*c*
2643.092	3	1
2643.672	----------	2*H*
2644.266	1	5
2644.563	----------	4*h*
2644.701	3	1
2644.768	5	2
2645.212	----------	2*H*
2645.804	10	4
2646.100	----------	1*h*
2646.379	9	3
2646.513	----------	1*h*
2647.128	30*R*	20*c*
2647.240	2	1
2647.578	1	20
2647.798	3*h*	----------

Wavelength	Intensity and other characteristics	
	Arc	Spark
A		
2648.100	7	2
2648.462	----------	50*h*
2648.508	6	----------
2649.050	50*R*	40*c*
2649.584	10	5
2650.197	----------	10*h*
2650.339	----------	8*c*
2650.593	----------	4*cw*
2650.977	----------	2
2651.349	----------	2*H*
2651.662	----------	5
2651.903	100*R*	30
2652.288	----------	2
2652.392	6	1
2652.506	----------	6*h*
2652.911	20	10
2653.186	----------	1*h*
2653.485	----------	5*h*
2653.740	7	4
2654.120	40*R*	15
2654.390	----------	2*h*
2654.773	10	2
2654.908	----------	10*cw*
2655.048	----------	3*c*
2655.178	10	5
2655.292	----------	1*h*
2655.844	15*c*	8*c*
2656.392	----------	2*h*
2656.486	2*h*	----------
2656.846	----------	3
2656.950	5	1
2657.449	10*c*	5*c*
2657.50	----------	1
2658.235	----------	7*c*
2658.688	7	4
2659.024	20	8
2659.236	----------	1
2659.510	15*cw*	2*cw*
2659.552	----------	4
2659.792	10	7
2660.040	2*c*	----------
2660.214	----------	20*c*
2660.342	5	2
2660.538	7	4
2660.628	8	4
2660.928	----------	7
2661.034	9	3
2661.223	2	1
2661.506	1	1
2661.760	5	2
2662.196	4	2
2662.464	----------	4
2663.159	1	1
2663.633	50*cw*	30*cw*
2664.215	10	5
2664.556	----------	1
2664.807	15	6
2664.908	2*h*	1*h*
2665.688	----------	1
2665.90	5*Hc*	2*Hw*
2666.224	----------	1
2666.421	1	----------
2666.632	----------	2*h*
2667.130	20*c*	9*c*
2667.54	----------	4*H*
2667.793	10	4
2667.893	----------	4*h*
2668.011	----------	2*h*
2668.194	2	----------
2668.887	5*H*	4*H*
2669.354	----------	3*h*
2669.536	----------	1
2669.740	----------	1
2669.868	5*cw*	1*cw*
2670.236	20	9
2670.790	30*c*	20*c*
2671.329	3*c*	1*c*
2671.842	40*cw*	20*c*
2672.054	7	4
2672.285	2	----------

TABLE 2. *Arc and spark spectra of rhenium*—Continued

Wavelength	Intensity and other characteristics	
	Arc	Spark
A		
2672.420	5	2
2672.770	20c	6c
2674.339	200*R*	100
2674.44	----------	1h
2674.594	----------	4h
2674.917	5	2
2675.525	2	1
2675.990	10	4
2676.088	9	2
2676.253	10	3
2676.866	6*H*	3*H*
2677.032	30c	20
2677.231	----------	2h
2677.416	----------	6h
2677.764	15c	8
2678.054	3c	1
2678.530	----------	4
2678.857	2	1
2679.086	20c	10c
2679.626	7	3
2679.914	30c	20c
2681.010	9	4
2681.838	----------	5*H*
2682.067	----------	2
2682.368	3	2
2682.502	7c	3c
2682.888	----------	6h
2683.030	3c	1c
2683.558	40c*w*	30c
2683.688	----------	3h
2684.382	3	1
2684.438	1	----------
2684.697	6c	1
2684.748	----------	80h
2684.905	3	1
2684.980	----------	10c*wd*
2685.214	5	2
2685.311	10	5
2686.160	2	1
2686.344	2	1
2687.199	6c	2c
2687.592	----------	3h
2688.319	----------	3h
2688.528	100c*w*	60c
2689.340	7*Hwd*	3*Hw*
2689.828	----------	2c*w*
2690.17	1	----------
2690.247	20*Hw*	20*H*
2690.785	30*Hw*	10*H*
2691.262	----------	3c*W*
2691.694	----------	30c*w*
2692.596	----------	2h
2693.104	----------	30
2693.224	4	2
2693.719	8	3
2693.822	8	3
2694.034	3	1
2694.394	20c	10c
2695.248	----------	8c
2695.41	----------	1h
2695.562	15c	7h
2695.698	----------	4h
2695.91	----------	1
2696.150	2	1
2695.298	----------	3h
2696.376	7c*ws*	4c*w*
2696.640	7	2
2696.988	3h	1
2697.265	30c*w*	10c
2697.368	3	1
2697.804	30c*w*	10c*w*
2698.794	15h	6h
2699.462	----------	5
2699.580	15c	4c
2699.978	3	1
2700.027	----------	5
2700.211	----------	8c
2700.475	2	----------
2700.891	8	2
2700.977	2	----------

Wavelength	Intensity and other characteristics	
	Arc	Spark
A		
2701.206	3h	2h
2701.556	----------	1h
2701.726	----------	1h
2702.329	----------	20h
2702.668	20	8
2703.245	10	6
2703.510	2*H*	1*H*
2703.743	----------	3h
2704.099	----------	3
2704.179	3	1
2704.369	20c	10
2704.769	6	2
2705.076	6c	2c
2706.056	15	7
2706.39	----------	2h
2706.480	5	2
2706.996	----------	2h
2707.074	2h	1
2707.401	15c	3c
2707.852	10	5
2708.322	----------	4h
2708.442	7	3
2709.500	2	1
2709.91	----------	10c*w*
2710.224	20c*w*	8c*w*
2710.36	----------	2h
2710.403	15c*ws*	6c
2710.562	----------	5c
2710.667	1	----------
2711.008	----------	10h
2711.298	----------	6h
2711.382	2	----------
2711.835	----------	1
2712.249	2	----------
2712.476	20c	9c
2712.646	----------	8h
2712.700	5	1
2713.024	15c	7c
2713.160	10c	7c
2713.375	----------	15c
2713.664	8	3
2713.828	----------	2h
2713.99	3*H*	----------
2714.130	----------	2
2715.052	----------	2h
2715.474	300*R*	150
2715.770	30r	15
2716.054	2	----------
2716.144	----------	3
2716.246	20c*w*	7c*w*
2716.419	5	2
2716.63	----------	2c
2716.754	15	7
2717.080	3c*w*	1c*w*
2717.219	7c	3c
2717.670	----------	10c*w*
2718.01	3*H*	2*H*
2718.659	----------	3
2718.780	10c	4c
2719.324	----------	2
2719.536	15	6
2719.836	----------	6h
2719.848	9	----------
2720.098	9	7h
2720.304	2	1
2720.059	10c	3
2721.093	1c	----------
2721.211	----------	5h
2721.316	----------	4h
2721.55	----------	8h
2721.675	7	3
2722.206	60c	50ch
2722.702	80c	50ch
2723.356	10	3
2723.836	30c	20c
2724.046	2	1
2724.253	----------	3h
2224.361	----------	2h
2724.437	5h	2h
2724.686	9	3

Wavelength	Intensity and other characteristics	
	Arc	Spark
A		
2724.934	3c	1
2725.520	----------	3c*w*
2725.890	1	15
2726.323	2	1
2726.57	----------	3c*l*
2726.870	----------	15h
2727.34	----------	10c .19W1
2727.548	20c	9c
2727.998	----------	2h
2728.286	3h	2h
2728.628	10	4
2729.040	----------	3c
2729.209	2	1h
2729.427	4c	1c
2729.635	10	5
2729.712	----------	4h
2729.803	----------	2h
2730.027	----------	10
2730.247	4c	1c
2730.658	----------	10h
2730.826	10	2
2730.911	----------	2
2731.228	3h	1h
2731.416	2c	----------
2731.562	5c*l*	150c*wl*
2732.206	50*R*	10
2732.398	----------	6c*w*
2733.04	10c*l*	300c*l*
2733.41	15c*w*	5c*w*
2733.96	5h	2h
2734.31	10	4
2734.43	----------	2h
2734.886	10	5
2735.350	----------	2h
2735.74	1c	4c*w*
2736.270	----------	1h
2736.522	6	5h
2736.767	10c	4c
2737.556	----------	5h
2738.323	15	8
2738.625	4	2
2738.752	10c	4h
2739.945	20c	10c
2740.074	4	2
2740.468	----------	2h
2741.506	----------	1h
2741.967	15c	30c
2742.744	7	3
2742.856	10	6
2743.122	2	1
2743.258	4c	1c
2743.650	3	2
2743.735	2	1
2743.874	15	10
2744.207	20c	6c
2745.014	2	1
2745.264	----------	2*H*
2745.564	5*H*	2*H*
2745.867	15	6
2747.438	20r	10
2747.627	1	----------
2748.55	----------	20d
2750.322	6	1
2750.564	----------	80c
2751.38	2h	1h
2751.51	3	1
2751.620	----------	6h
2752.494	----------	6c*w*
2752.852	15	7
2753.046	30c	20h
2753.289	----------	2
2753.638	2c	100c*ws*
2754.014	----------	3
2754.510	5h	3h
2755.212	20c	4c
2755.330	----------	6h
2755.854	----------	10h
2756.71	3h	1h
2756.806	----------	2
7752.486	15	6

TABLE 2. *Arc and spark spectra of rhenium*—Continued

Wavelength	Intensity and other characteristics	
	Arc	Spark
A		
2757.700		4h
2757.996	40r	15
2758.05	10h	7h
2758.418		3h
2758.706	10	4
2758.767	3	2
2759.140		1*H*
2760.004	2*H*	2*H*
2760.212	1h	
2760.404	3h	2h
2760.494		1h
2761.008	3h	2h
2761.502	2h	1h
2761.926	20c	8
2762.786	4	2
2763.295	40cwl	15cl
2763.792	40c	20c
2764.704	5h	3h
2765.065		2*d*
2765.282	2	
2765.30		7h
2765.69		30h
2766.051	9	3
2766.102		7
2766.390	30c .13*W*	20cw
2766.548	7	4
2767.576	5	2
2767.744	20	10
2768.177		2h
2768.282	6*H*	3*H*
2768.851	15	8
2768.954	3	1
2769.313	30cw	20cw
2769.735	4cw	2c
2770.030		2
2770.130		2cw
2770.417	70*R*	30
2770.51		2h
2770.84		1h
2771.009	15c	8c
2771.994		2
2772.423	8	4
2772.667	3	1
2773.109	20c	10
2773.214	2	1
2773.602	3	2
2774.042		3h
2774.383	10c	4c
2774.599	5	2
2775.126	10cw	5cw
2775.457	2	i
2775.639	15c	4
2775.948	10cw	6c
2776.296		3h
2776.560	1	
2776.960	9	5
2777.223	8	4
2777.438	1	1
2777.71	15cw	6cw
2777.797		50c
2778.092	15	9
2778.418	3c	1c
2778.698	10	5
2779.062	10c	5
2779.250	15c	5c
2780.094		3
2780.850	15cw	8c
2781.094		4h
2781.434	30r	15c
2781.714		3h
2782.101		10h
2783.141	7	3
2783.570	60cw	40cw
2784.042		3h
2784.389	2c	1c
2784.618		1
2785.206	50r	30
2785.424	10	5
2785.714	9	4
2785.990	2	1
2786.138	15	9
2786.450	3	1
2786.558	20r	8
2786.652		5h
2787.386	7	4
2787.540	1	1
2788.207		3h
2789.026	1	5h
2789.173	7c	2c
2789.268	15	6
2789.58		5cwl
2789.65	2*H*	2*H*
2790.415		2h
2790.939	30c	15c
2791.04		1h
2791.290	50r	30c
2791.39		1h
2791.626	10	5
2792.010	3	1
2792.382	3cw	3cw
2792.940	2	1
2793.654	15c	10c
2793.896	10c	7c
2794.036	2	1
2794.171	9h	3h
2794.472	3	1
2794.632		20h
2795.028		3h
2795.426		10h
2796.078	10l	3l
2796.467	2	1
2796.616	9	3
2796.958		1h
2797.208		1h
2797.444	7c	3c
2797.992		5h
2798.104	10	5
2798.640	3	1
2798.870		5h
2798.918		3c
2799.245	3	2h
2800.112	8c	4c
2800.296	3	1
2800.621	5	3
2800.746	4	1
2801.184	3c	2h
2801.562		2h
2801.993	1	1
2802.24	15*Hw*	5*Hw*
2802.408	3	2
2802.829	10cw	3cw
2802.97		1
2803.053		1
2803.28	3cl	20c .10wl
2803.925		10*hl*
2804.506	5c	2c
2805.105	4c	1c
2805.398	3c	1c
2805.977	7	3
2807.510	3h	2h
2807.618		2h
2807.895	20cwv	10cw
2808.456	4h	2h
2809.109	3	2
2809.370	3c	1
2809.435		10h
2809.98	2c	1c
2810.330		10h
2810.518	2	1
2811.495		2h
2812.073	15	7
2812.356	20	9
2813.112	15	7
2813.53		20h
2813.64	5	2
2813.964	20h	10
2814.676	40*R*	30
2815.278	2c	
2815.31		3c
2815.640	10	5
2816.319	30c	20c
2816.954	30c	15
2818.444	9c	3c
2818.474		3h
2818.783	2cw	20cwl
2819.528	4	2
2819.779	4cw	60cwl
2819.951	50cw	40cw
2820.01	10r	57
2820.280	4	2
2820.976	4	2
2821.110		8
2822.123	15	7
2822.341		3h
2822.407	9	1
2822.494		3h
2823.193	15	8
2823.310	2c	1c
2823.592	2	1
2823.641	2	1
2823.750	2cw	
2823.882	2cw	150cw
2824.245	20	7
2824.365	4c	4
2824.596		5h
2824.939		5*H*
2825.458	20	10
2825.50		4h
2825.846	2	1
2825.952		1cw
2826.670	1h	1h
2826.759	3	1
2826.812	4	2
2826.904		1h
2827.284	7	5
2827.523	30c	15c
2827.834	7	3
2828.226	10cwl	10c
2829.164	4	2
2829.887	10c	4c
2830.096	6c	2h
2830.352	15h	10h
2830.833	9	3
2831.162		2h
2831.560		1
2831.752		3h
2831.854	2h	2h
2832.245		5h
2832.540	2h	2h
2832.857		1h
2833.02	2	1
2833.05		4c
2834.077	40cw	20d
2834.608	15c	6c
2834.782		4cw
2835.034	5	2
2835.844	3	1
2836.005	6	2
2836.361		5h
2836.696	7hs	3h
2836.991	15cw	8cw
2837.547	30c	20c
2837.972	3h	
2838.109	7	3
2838.238		10
2838.566	3	2
2839.06		5c .20*Wl*
2839.193	8	3
2839.657		3h
2840.024		4h
2840.348	50r	40c
2840.44		2h
2840.979	3	3
2841.275		1
2841.669		2*H*
2841.798		2h
2842.588		2
2843.000	60r	50
2843.10		3h
2843.562		3h

217025—52——6

TABLE 2. *Arc and spark spectra of rhenium*—Continued

Wavelength	Intensity and other characteristics	
	Arc	Spark
A		
2843.665	3	1
2843.762	----------	5h
2844.162	20	10
2844.854	----------	1h
2845.040	----------	1h
2845.176	6	5
2846.478	8	3
2846.970	20c	10c
2847.185	----------	5c
2847.568	----------	7h
2847.744	6	3
2848.112	2h	2h
2848.280	3	1
2848.360	3	1
2848.400	3	1
2848.966	----------	10h
2849.22	----------	6c .12*Wl*
2849.602	3*H*	2*H*
2850.275	8c	3c
2850.590	----------	3
2850.975	60r	40
2851.188	----------	3h
2851.720	----------	8h
2851.744	2	----------
2852.054	10c	3
2852.181	6c	2c
2852.394	9	5
2852.841	20cw	7cw
2852.966	----------	6hl
2853.740	----------	4h
2853.776	3*Hs*	----------
2854.122	----------	3h
2854.304	----------	1
2854.434	----------	2
2854.740	----------	3cw
2855.334	3*H*	1*H*
2855.528	10	5
2855.772	3c	1c
2856.447	----------	1
2856.720	3*H*	6h
2856.908	----------	2h
2857.075	2cw	1*H*
2857.435	10	6
2857.575	----------	8h
2857.662	----------	2h
2857.808	4cw	2cw
2857.985	----------	4
2858.250	3	1
2859.445	8c .14*Wl*	4cw
2859.839	10c	----------
2859.87	----------	15cw
2859.92	----------	2
2860.074	20	6
2860.254	15	5
2860.550	----------	20h
2860.933	3h	1h
2861.260	----------	10c
2861.682	----------	10c
2862.009	2	1
2862.187	8	3
2862.56	3	1
2862.85	----------	6cw
2862.890	15cw	5cw
2863.00	----------	2c
2864.280	----------	10h
2864.563	15c	10c
2864.831	10c	5c
2864.526	3	----------
2865.554	----------	3h
2865.612	2	1
2866.294	----------	2*H*
2866.582	3h	1h
2866.926	3h	2h
2867.193	30c	20c
2867.276	3	2
2867.770	3*H*	2*H*
2869.143	10c	3c
2869.200	----------	4c
2869.764	3c	2h
2869.864	3c	2h
2870.000	----------	7h
2870.397	----------	2h
2870.784	----------	3
2871.102	----------	2
2871.432	----------	2
2871.82	30cw	20c
2872.008	----------	3h
2872.304	10	5
2872.668	10c	4c
2872.73	----------	4c
2873.104	3cw	2cw
2873.840	6	2
2875.282	30cw	20d
2875.698	----------	30
2876.024	5	3
2876.860	15	5
2877.528	----------	3h
2878.226	----------	5cw
2878.538	1	----------
2879.271	20	10
2879.391	3	1
2880.212	1	----------
2880.630	----------	8h
2880.840	6	----------
2880.856	----------	10h
2881.546	10	5
2881.874	----------	60h
2882.226	9	3
2882.367	----------	2h
2883.083	3cw	1cw
2883.444	30c	20c
2883.045	15c	10c
2884.244	----------	20h
2884.452	7c	2c
2884.636	15	10
2885.120	4	3
2885.220	4	5
2885.54	2c	2h
2885.710	----------	2h
2885.930	10	3
2886.312	4	1
2886.435	----------	2h
2886.544	7	3
2886.774	----------	10h
2886.935	15c	6
2887.307	15c	6
2887.676	300*R*	200
2888.06	3cl	40c .10*wl*
2888.113	1	4
2888.456	4	1
2889.448	20c	10c
2889.832	----------	10cw
2891.481	20	10
2891.878	30c	15c
2892.093	----------	10c
2892.634	20c	10c
2892.724	----------	3h
2893.475	----------	3c
2893.636	----------	3cw
2894.123	1h	1h
2894.322	10	6
2894.422	2	1
2894.960	4*H*	1*H*
2895.176	----------	2h
2895.328	2	1
2895.650	15c	8c
2896.012	60*R*	30c .15*Wl*
2896.446	8	4
2896.668	1h	----------
2897.022	5	2
2897.242	----------	10c
2897.401	3c	1c
2897.456	3	2
2897.585	10c	6
2898.785	10	6
2899.621	3	2
2900.012	----------	6
2900.386	----------	7c
2900.959	3c	1c
2901.352	2c	1h
2901.54	----------	2c
2902.112	3c	1c
2902.48	100*cl*	?
2902.55	?	60cw
2902.886	----------	6
2903.293	1	1
2903.760	5	2
2904.043	3c	2*H*
2904.55	3cl	30c 3, .12*Wl*
2904.982	----------	6h
2905.393	10c	6c
2905.584	30c	20c
2905.854	----------	2cw
2906.016	15c	10c
2906.11	----------	2h
2906.775	----------	1h
2907.100	10	5
2907.231	1	2
2907.434	2h	1h
2908.132	3cw	2cw
2908.344	20	15
2908.676	----------	4h
2908.704	2	----------
2909.127	----------	4hc
2909.166	2	1
2909.820	60r	50
2909.93	----------	3h
2910.084	9	6
2910.308	----------	1h
2910.818	----------	7hc
2911.094	2	1
2911.232	8	6
2912.025	3h	3h
2912.580	5	4
2912.915	3	2
2913.154	10	8
2913.639	----------	5
2913.805	4	2
2914.298	----------	1h
2914.570	----------	2
2915.246	3	2
2915.286	2	1
2915.643	----------	2wl
2916.256	3	2
2916.348	2cw	2c
2916.731	----------	20
2916.850	5c	3c
2917.173	----------	1h
2917.468	----------	8h
2917.484	5	----------
2917.834	3cw	2cw
2918.052	2	1
2918.760	1	1
2918.877	7	5
2919.407	20	15
2920.608	----------	3h
2921.076	1	1h
2921.332	----------	1h
2921.676	3	2
2921.804	2h	3h
2922.694	----------	6h
2923.220	2	1h
2923.344	1	1
2923.686	----------	6h
2924.388	----------	1h
2924.60	20c .15*Wa*	15cwa
2924.784	----------	9h
2925.195	20	15
2925.606	2d	----------
2925.703	----------	10h
2926.124	1	----------
2926.134	----------	10h
2926.661	----------	20h
2926.934	9c	6c
2927.42	40c .14*Wl*	40cw
2927.714	5	4
2927.852	2	5h
2927.90	----------	2h
2928.576	?	5
2929.044	1h	1h

TABLE 2. *Arc and spark spectra of rhenium*—Continued

Wavelength	Intensity and other characteristics	
	Arc	Spark
Å		
2925.18	10c	5c
2926.530	10	8c
2928.411	4	4h
2930.610	20c	20
2931.429	1	1
2931.660	4	4
2932.223	4	3
2932.317	7	5
2932.457		6h
2932.434	4	3
2933.342		7h
2934.010	5	3
2934.329		40
2935.32	6c .15W	5cW
2935.752		1h
2936.500	15	15
2937.431		1h
2937.810	8	6
2938.442		1h
2938.570	1	1
2938.644	1	1
2938.772	5	3
2938.841	2	1
2939.083		5h
2939.357		3
2939.572	3	2
2940.049	5	4
2940.554	3	2
2940.674		50cl
2941.141		3h
2941.337	9	7
2942.878		4cw
2943.145	50r	40
2943.282	10c	6c
2943.798		8h
2944.220	8	6
2945.106	3c	2c
2945.163		3h
2945.708	5h	3h
2945.886	5	3
2946.572	9	7
2946.802	1c	1c
2947.49		2H
2947.54	2H	
2948.104		1h
2948.184	2h	2h
2948.640	2cw	2cw
2949.088	15c	10c
2949.201	7cw	5c
2949.880	10	9
2950.220		2h
2950.731		3h
2950.828	10	7
2950.920	7	4
2951.090	2h	2h
2951.961	2c	
2952.982		3h
2953.852	1	2
2954.335	15c	15c
2954.454	1	2h
2954.980	6	5
2954.988	5	3
2954.998	2	
2954.99		10c .14Wl
2955.730		8c
2956.086	2h	1h
2956.254		5
2956.466	3	2
2957.413	3c	2c
2957.762	2cul	1
2957.907		80cw
2958.904	7	6
2959.33	2h	3h
2959.718	2	2
2959.808	2	1
2960.296	4cw	3cw
2961.163	3c	4c
2961.144		3c .18Wl
2961.744	20cw	15cw
2961.880	2c	2c

Wavelength	Intensity and other characteristics	
	Arc	Spark
Å		
2962.266	30r	20
2962.870	15	10
2964.01	2cw	1c
2964.458	2	1
2965.112	80R	80c
2965.502	2	1
2965.756	150R	150c .15W
2966.416	2	1
2966.746	2c	1
2967.018		2h
2967.246	10	8
2967.415	8cs	10c .17Ws
2968.044	20c	20c
2968.330	3	2
2968.452		3cws
2968.975	8	9
2969.374	3	2
2969.74	4Hw	
2969.778		5h
2970.778		2h
2971.596		1h
2971.734		2h
2971.802	2h	2h
2972.102	5c .15Ws	4cs
2974.44		4c
2974.563	1c	10cw
2974.844		5h
2975.023	8	5
2975.250	10	10
2975.658	3c	2c
2976.294	40cw	30cw
2977.102	1	
2977.148		2cw
2977.300	9c	7c
2977.844		3
2977.956	2	1
2978.152	20c	20c
2978.509	1h	
2978.622	1	
2979.345	2c	1c
2980.244	2	1
2980.306	4	3
2980.820	20cw	20c
2980.90		50c
2981.010	7	4
2981.350	2	1
2981.495	3c	2c
2981.702	2h	2h
2982.188	50cw	40cw
2982.948	2c	1c
2983.074	1	1
2983.996	3	3
2984.504	4c	4
2984.750	7	6
2985.207		3
2985.552	4	4
2985.822		3cw
2986.050	7d	5d
2988.19		1h
2988.302	1	1
2988.471	20c	20c
2988.602	3c	2c
2988.918	4	3
2990.007	2cw	1cw
2990.326	3	2
2990.433		3
2990.604		5
2990.713	1	
2990.926		5h
2991.448	2	1
2991.828	6	5
2992.363	150R	100c
2992.746		10h
2992.815	10cwl	6cw
2993.176	8	7
2993.769		1
2994.98		1h
2995.118		3cw
2995.395	20	20
2995.69		6c .18Wl

Wavelength	Intensity and other characteristics	
	Arc	Spark
Å		
2995.786	4	2
2995.946	2	1
2996.074	2	4
2996.182		2
2996.533	3	1
2996.842		6
2997.124	2	1
2997.420	4	3
2997.686	9c	6c
2997.902	4	3
2997.980	5	4
2998.550	5	4
2998.700		5h
2999.599	200R	150c
2999.947		4h
3000.327	2h	1h
3000.581	4	2
3000.828		3h
3001.137	20r	20
3001.44		2h
3002.250	1	1
3002.490	1	1
3002.633	3c	3c
3003.626	1	1
3004.136	20c	15c
3004.342	9	8
3005.232	4c	2c
3005.69	2H	2H
3005.975	10cw	8cw
3006.425	20	20
3007.04	7	5
3007.19	4	3
3007.62		7h
3008.826		8c
3008.984		2cw
3009.362		8c
3009.902	2cw	2cw
3010.322		3
3010.611		2c
3010.648	2cw	
3010.825	1	1
3010.977		2h
3011.48	4	3
3011.92	20c .17Ws	15Ws
3012.36		7
3013.141	15	15
3013.857		2
3014.419		7cw
3014.939	6c	4c
3015.362		3h
3015.866	4c	3c
3016.015	40c .15W	40cw
3016.480	20cw	20cw
3016.972	6	5
3017.294	3c	2c
3017.592	4	3
3017.891	5c	4c
3018.150	2c	1c
3018.345		1H
3018.981		5h
3019.776	2h	1h
3021.881	15	15
3022.194		2c
3022.989	15c	15c
3023.573	5	5
3023.858		9cw
3024.111	1h	1h
3024.490	3	2
3025.058	9	7
3025.36		3c .19Wl
3026.203	4	3
3026.288	5	4
3026.555		15cws
3027.128	1	
3027.958	2c	1c
3028.099	2	1
3030.446	30c	30c
3031.266	6	5
3031.458	2	1
3032.486		1h

TABLE 2. *Arc and spark spectra of rhenium*—Continued

Wavelength	Intensity and other characteristics	
	Arc	Spark
A		
3032.792	9	7
3033.374	----------	2h
3034.552	20h	15hl
3035.622	8cwl	7cwl
3035.776	----------	3h
3036.100	1	1
3036.552	9	8
3037.222	1	----------
3037.463	4	3
3037.960	15c	15
3038.368	----------	10
3038.684	----------	1
3038.812	----------	2
3039.804	1h	1h
3040.033	20cwr	20cwr
3040.592	----------	5
3041.000	10	9
3041.272	4h	4h
3041.760	7c	4c
3041.993	6	5
3042.101	2	1
3042.292	8c	8c
3043.608	2cw	1
3044.084	10	9
3044.969	----------	7
3045.286	3c	2c
3045.732	1	----------
3045.780	----------	2h
3046.000	5	4
3046.352	2h	1h
3046.644	----------	3h
3047.252	30cw	30cs
3048.036	----------	5cw
3048.586	4	4
3049.802	8cw	6cw
3050.430	----------	5cwr
3050.814	1	1
3051.590	4	3
3052.232	5	5
3052.799	3	2
3052.884	3	2
3053.629	10	9
3053.766	3	2
3053.88	----------	1
3054.486	----------	2h
3054.899	9	8
3055.004	1	5h
3055.172	----------	3h
3055.980	10c .16Ws	10cs
3056.136	2	1
3056.454	4	4
3056.733	----------	1h
3057.538	----------	2h
3057.660	10	8
3057.852	6	5
3058.149	----------	15
3058.780	20	20
3060.319	9	9
3061.218	4c	3c
3061.998	9	9
3061.844	----------	3
3061.930	----------	4
3062.040	----------	8
3062.500	3cw	2cw
3062.636	----------	2
3062.954	1	1
3063.383	3c	3c
3063.762	----------	15
3063.984	1	1
3064.499	1	1
3064.597	7	5
3065.279	5	4
3065.576	5	4
3066.020	----------	15
3067.398	20dr	100
3068.762	5	4
3069.022	1cw	1cw
3069.714	1	1
3069.942	60r	40c
3070.679	2cw	1cw
3071.164	20c	20c
3072.452	3	2
3072.708	1	1
3072.965	20	20
3073.722	3cw	2cw
3073.922	2cw	1cw
3074.102	3	2
3074.657	----------	3cw
3074.99	----------	3Hw
3075.02	8Hw	----------
3075.909	1	3
3076.142	10cWl	8cW
3076.304	5	4
3076.716	3	4
3077.44	1	1
3077.740	3	2
3077.908	5cw	4cw
3078.864	15c	15c
3079.263	1	----------
3080.048	----------	4
3080.660	----------	10
3080.922	7cwl	5cwl
3081.656	2c	2c
3082.050	----------	2h
3082.426	50c .13W	40cW
3082.772	3	2
3083.552	1h	1h
3084.210	15c	15c
3084.772	5	5
3085.344	4	4
3085.528	3	3
3086.03	3	2
3087.154	10	8
3087.36	----------	7c
3087.854	----------	6
3088.257	----------	1
3088.702	30r	20
3089.341	2	1
3089.932	10c	10c
3091.356	----------	1
3092.288	----------	10
3092.304	4	----------
3092.607	----------	3c
3093.636	20c	20c
3093.994	4	3
3094.784	3	2
3094.998	2	1
3095.060	10	10
3095.314	----------	4cw
3095.788	20cwr	20cwr
3096.312	----------	15
3096.414	7	6
3097.922	4	4
3098.262	3	2
3098.674	2cw	1c
3099.064	----------	2cw
3099.61	3c .19Wl	2cw
3099.765	3c	2c
3100.672	40R	30
3100.998	7cw	5cw
3101.555	1	1
3101.700	3	2
3101.909	2	2
3103.655	1	20
3103.260	2cW	20c .15W
3103.709	2cw	1
3104.038	2cw	1cw
3104.647	10	10
3105.082	----------	7h
3105.660	2	2
3106.180	----------	1h
3106.490	2c	1c
3106.948	----------	2h
3107.208	----------	3c
3107.436	2	1
3107.864	5c	4c
3108.808	100R	60
3109.156	----------	2h
3109.478	4c	3c
3109.576	----------	6
3109.756	8	5
3109.983	----------	2
3110.326	----------	2h
3110.860	40r	40c
3111.236	2	2
3111.564	9	8
3112.404	2	2
3112.594	1	----------
3113.205	7	5
3113.350	----------	2h
3113.740	----------	1
3114.004	----------	3cw
3114.136	----------	2
3114.370	2	1
3114.631	4	4
3114.914	3cw	2cw
3116.720	----------	2
3116.924	----------	2
3117.414	4	4
3117.561	----------	2
3117.652	----------	3 | c?
3117.776	----------	5 |
3118.002	----------	2
3118.192	40c .15Ws	40cW
3119.192	4	3
3119.288	2	2
3119.744	2	2
3119.854	3	2
3120.244	3	2
3121.360	30c	30c
3121.733	4	3
3122.206	3	3
3122.411	1h	----------
3123.161	9	9
3123.413	3	3
3123.622	2h	2h
3124.134	----------	3h
3124.313	----------	3H
3124.956	1c	1
3125.288	2	2
3125.384	1	1
3125.518	10c	10c
3126.069	2H	1H
3126.420	1	1
3127.521	----------	2
3128.023	----------	1
3128.353	3	2
3128.944	40cw	40cw
3130.203	----------	7h
3130.432	2h	1h
3130.608	1	----------
3130.921	----------	2h
3131.270	3c	2c
3131.952	----------	20
3132.013	2	----------
3132.560	2	----------
3132.926	----------	2cw
3134.022	10	10
3134.344	2c	1
3134.438	----------	2cw
3135.068	10cw	8cw
3136.178	----------	4cw
3137.640	----------	4
3138.026	3	2
3138.663	----------	1h
3138.786	----------	6
3139.263	5	4
3139.792	10c	9c
3139.945	9	7
3140.31	1h	----------
3141.254	4c	2
3141.381	10	15
3141.718	3	2
3141.857	1	1
3142.018	2	2
3142.525	3cw	2cw
3142.646	10cw	9cw
3142.847	----------	2
3142.909	2c	1c
3143.628	2cw	1c

TABLE 2. *Arc and spark spectra of rhenium*— Continued

Wavelength	Intensity and other characteristics	
	Arc	Spark
A		
3143.974		1*h*
3144.86	1	
3145.354		1*h*
3145.616	4*c*	3*c*
3146.536	10*c*	8*c*
3147.660	10*cw*	10*cw*
3147.911	3	2
3148.200	6	5
3148.699	2	1
3150.047	4	4
3150.529	6	5
3151.162	10	9
3151.402		1
3151.498		1
3151.636	40*cw*	40*cw*
3152.456	1	1
3152.822	2*h*	1*h*
3153.640		1
3153.79	40*r*	20*c*
3154.530	3	2
3155.209		1*H*
3156.372		1*h*
3156.532	2*c*	1*c*
3156.827	4	3
3157.348	1*h*	1*h*
3157.712	4	3
3158.206	50*c* .15*W*	50*cW*
3158.852		2*h*
3158.992		2*h*
3159.312	6	5
3159.617	4*cw*	4*cw*
3160.121	1	1
3160.213	5*h*	4*h*
3161.692		1*h*
3162.208	2	1
3162.485	10*cw*	10*cw*
3163.243	4	3
3163.323		2*h*
3164.106	5*c*	4*c*
3164.412		3*h*
3164.520	10	10
3164.864	7	7
3165.802	7*c*	6*c*
3166.476	7	6
3166.609		8*h*
3166.904	7	6
3167.155	10*c*	10*c*
3167.594	5	4
3168.374	50*cw*	50*cw*
3169.097	2*c*	1*c*
3169.356	1	
3170.074		7*h*
3170.346	2	1
3170.992	10*cwl*	9*cwl*
3171.533		1*h*
3173.094	9	9
3173.242	2*h*	2*h*
3173.604		2*h*
3174.610	20*c*	20
3174.776	20*cw*	20*cw*
3175.094		2*h*
3175.265		1
3175.367		2
3176.084	2	1
3177.714	30*r*	30
3177.934	2*cw*	1*cw*
3178.176	2*cw*	1*c*
3178.488	6	5
3178.612	15	15
3179.344		2*h*
3179.864	2	2*h*
3181.258	3*h*	2*h*
3181.407		1*h*
3181.792	1*c*	1
3182.064	7	6
3182.869	100*R*	100*c*
3183.910		2
3184.760	200*R*	150*c*
3185.574	250*R*	200*c*
3186.198	1	1

Wavelength	Intensity and other characteristics	
	Arc	Spark
A		
3186.292	10	10
3186.856	1	1
3187.800	6*cw*	5*cw*
3187.956	3	3
3189.750	2*c*	2*c*
3189.916	2*c*	1*c*
3190.170	20	20
3190.782	20	20
3191.112	1	
3192.164	1	1*h*
3192.362	20*c*	20*c*
3192.608		3
3192.682	4*c*	3*c*
3192.852		1
3192.982		2*h*
3193.199	10	10
3193.979	1	1
3194.097	1	2
3194.497	30*cw*	30*cw*
3195.206		15
3195.666	3	2
3196.354	1*c*	1*c*
3196.682		1
3197.248	3	3
3197.334	2*c*	1*c*
3197.59		2*h*
3198.06		3*h*
3198.330		3
3198.470	4*cw*	3*c*
3198.578	15	15
3199.257		10*cw*
3199.486	8*c*	6*c*
3199.604	2*h*	1*h*
3200.035	20*cw*	20*cw*
3200.725	10	10
3202.224	6	4*H*
3203.560		1*h*
3204.245	100*c* .22*WI*	100*cWI*
3204.682	6	6
3205.420	15*c*	15*c*
3206.470	7*cw*	5*cw*
3207.708	10*cw*	10*cw*
3208.222	9	9
3208.582	1	1
3208.662	1	
3208.822	2	1
3209.323		3*h*
3210.564	2*c*	1*c*
3210.905		5*h*
3211.752	20*c*	20*c*
3212.379	5	5
3212.938	15*cw*	15*cw*
3213.152	2	
3213.168		6*h*
3213.486	10*c*	10*c*
3213.646	3	2
3213.890	3	3
3214.110	9	10
3214.646	2*c*	1*c*
3214.818	4	4
3214.967		2
3215.078		3*c*
3216.316		6*cw*
3217.13		10*c* .21*WI*
3218.458		3*h*
3218.653		5*h*
3218.264	2	1
3219.538	1*c*	1*c*
3219.712	2	1
3219.906		50*c*
3220.258		3
3220.466	2	1
3220.550		6
3221.194	2*cw*	1*cw*
3221.836		15
3221.860	2	
3222.180		1
3222.549	1	1
3223.512	1	2
3224.260	2	1

Wavelength	Intensity and other characteristics	
	Arc	Spark
A		
3226.37		10*bl*
3227.45	8	7
3227.48	8	7
3227.618		3
3227.700	1	1
3227.76		2
3227.82		1
3227.918		2
3228.329	6*c*	6*c*
3228.428	3	2
3228.734	15	15
3229.804	1*H*	2*H*
3230.954	2	2
3231.454	1	1
3231.983	1	1
3233.988	1*h*	1*h*
3235.312		2*cw*
3235.944	30	30
3236.990	5*cw*	5*cw*
3237.513	10	10
3237.825	2*cw*	1*cw*
3238.363	4*c*	3*c*
3238.470		1
3238.804	2	1
3238.938	2	2
3239.156	4	3
3239.807	1	1
3240.331	4*cw*	4*cw*
3241.023	1	1
3241.112	1	1
3241.466	10	10
3241.910		10*cw*
3242.174	2	2
3242.701	1	1
3244.464		15*l*
3245.472		1*h*
3246.311	2	80
3247.801	2	1
3248.547	10	9
3249.021		1*h*
3249.105	2	1
3250.142		1*h*
3251.548	2	2
3252.259	20	20
3252.482		1
3252.736	2	1
3253.186	10*cw*	8*cw*
3253.951	15*cw*	15*cw*
3254.488		5*cw*
3254.886	2	
3254.936		9*h*
3255.292	3	2*h*
3255.801	5	5
3256.286	8	7
3256.666	2*cw*	1*cw*
3256.802		1
3256.868	1	1
3257.435		1
3257.89		2*cw*
3258.055	7*cw*	5*cw*
3258.848	40*r*	40
3259.550	50*r*	50
3260.052	1	1
3261.424		5*h*
3261.559	20*c*	15*c*
3262.410	1	1
3262.768	10	10
3263.297		3*h*
3263.361	4	3
3263.877	1	1
3264.090	2*cw*	2*cw*
3264.534	1*h*	1*h*
3265.598	2	1
3265.760	2	1
3266.340	2*h*	1*h*
3266.851	15*c*	15*c*
3267.596		2
3268.077	15*c*	15*c*
3268.278		7*h*
3268.480	10	15

UNIVERSITY OF MICHIGAN LIBRARIES

TABLE 2. *Arc and spark spectra of rhenium*—Continued

Wavelength	Intensity and other characteristics	
	Arc	Spark
A		
3268.782	1	1
3268.894	15c	15c
3269.033	15c	15c
3270.050	7c	7c
3271.087	5c	4c
3272.780	2	1
3273.282	4	3
3274.354	1	1
3274.658	3	3
3275.478	1	1
3276.060	8cw	7cw
3276.544	4cw	3c
3277.18	4	1
3277.710	20cws	20cw
3278.902	3c	2c
3279.43	1	1
3279.82	1	1
3279.97	2	1
3281.248	5	5
3281.457	2	1
3281.850	5c	4c
3282.042	----	1
3282.318	3	15
3282.863	4	3
3283.124	4cw	3cw
3283.907	5	4
3284.454	3	2
3285.638	8	5
3285.706	5	4
3285.954	1	1
3286.636	----	3
3287.127	10c	10c
3287.92	3c	2c
3288.402	1	1
3289.396	----	1h
3289.900	----	1h
3290.093	6c	3c
3290.580	1h	2h
3291.139	1	1
3292.088	3	3
3292.65	2c	1c
3294.834	10	10
3295.168	2c	2c
3295.76	2hs	2hs
3296.099	2c	2c
3296.696	15c	15c
3296.992	10	8
3298.184	----	5cw
3298.535	----	2h
3298.662	1	1
3299.143	2	3h
3299.780	----	10c
3300.972	10c	7
3301.274	----	1
3301.595	15	15
3302.230	10	10
3302.578	2	10
3302.708	1	1
3302.935	2	2
3303.208	5cw	50cw
3303.595	6cw	3cw
3303.754	15	15
3304.394	1	----
3304.542	----	5cw
3304.833	5c	3c
3305.156	----	1h
3306.484	3	2
3307.007	10c	10c
3307.454	1	1
3307.972	2	2
3308.246	9	8
3308.38	1	20
3308.468	----	5
3308.54	1	20
3308.872	8c	6c
3309.164	1	1
3309.324	7	6
3309.585	3	3
3309.795	1	1
3310.276	2h	2h
3310.953	2cw	----
3311.080	----	9h
3312.288	9	8
3312.749	----	1
3313.105	2c	2c
3313.948	15	15
3314.52	2h	2h
3315.143	----	4h
3316.062	6cw	6cw
3316.612	1	1
3317.613	5	4
3317.152	2	1
3317.282	----	2h
3317.754	----	15c
3318.155	1	1
3318.316	1	1
3318.671	10	8
3318.780	----	30cw
3319.146	1h	1h
3319.622	1	----
3320.647	2	1
3321.124	1	----
3321.450	6c	4c
3322.196	9c	8c
3322.478	50cws	40cw
3324.20	----	1h
3324.510	2cw	2cw
3324.930	10	9
3325.191	1	1
3326.086	----	1h
3326.482	1	1
3326.896	5cw	3cw
3327.204	5	4
3327.712	9c	8c
3328.172	4c	3c
3328.418	----	1h
3328.874	3cw	2cw
3329.319	2	2
3329.412	----	4cw
3330.116	2	1
3331.336	----	4
3331.520	15	10
3332.849	2cw	2c
3334.130	3c	2c
3335.364	20cws	20cw
3335.664	1c	1c
3336.160	----	1h
3337.250	2	1
3337.312	2	1
3338.178	300*R*	300
3338.574	----	20c
3339.35	5c .21*Wl*	4c*Wl*
3339.685	15c	15c
3340.304	3	3
3340.976	1	1
3342.245	250*R*	250
3342.652	1	1
3343.092	1	1
3344.322	100c	100h
3345.010	4	50
3345.564	1	5
3346.199	40	30
3346.606	4	4
3347.572	8c	7c
3348.292	2cw	2cw
3348.508	1	1
3348.640	2	2
3349.150	2c	2c
3349.569	----	3h
3349.828	4cw	3cw
3349.916	8	7
3350.094	4c	3c
3351.136	2	2
3351.948	4	4
3352.521	1	1
3353.208	20c	15c
3353.648	1	1
3353.84	----	1h
3354.36	----	2h
3355.288	30cl	20cl
3355.626	4	3
3355.983	10cl	9cl
3356.328	10	10
3356.462	9	8
3356.821	4	3
3358.021	10	10
3358.56	6	5
3359.22	10h	10h
3359.818	10cw	9cw
3360.177	4	3
3360.755	1	1
3360.879	----	2h
3361.145	10	9
3361.828	3	3
3362.284	2cws	1cw
3362.745	15	15
3363.025	6	5
3363.412	----	4cw
3364.58	3cw	3cw
3365.168	----	2
3365.732	9	8
3365.838	8	7
3366.180	8cw	8cw
3366.418	2cw	1cw
3366.892	3	2
3367.298	1	----
3367.384	1	----
3367.482	6	4
3367.677	5c	4
3367.924	----	10h
3368.132	2h	----
3368.172	----	2
3368.605	8cw	7cw
3370.328	1	1
3370.764	2	2
3370.902	8c	7c
3371.142	2cw	2cw
3372.435	----	2h
3372.98	----	2h
3374.150	2c	1h
3375.040	1h	1h
3375.992	----	2h
3376.448	4	3
3377.619	8cw	6cw
3377.743	10	10
3379.063	6cws	100cw
3379.700	20c	20c
3380.308	5cw	5cw
3380.544	2	2
3381.424	9c	8c
3381.576	2cw	3cw
3381.794	5	4
3382.646	3	2
3383.259	2c	1c
3383.814	1c	----
3384.452	30cw	20cw
3385.166	----	2h
3385.757	40cws	30cw
3386.264	2c	2c
3387.053	2	1
3387.575	2*H*	----
3387.706	----	2h
3389.428	20	20
3389.767	8	7
3390.032	4c	3c
3390.254	30cw	20cw
3390.970	1	2
3391.052	1	1
3391.256	5hw	3hw
3392.376	8c	8c
3392.988	1	1
3394.122	8	7
3394.430	1	1
3395.650	2	2
3397.210	9	9
3397.686	5	5
3398.404	3	2
3398.793	8c	7c
3399.302	400*R*	300c .16c*W*
3399.963	2c	2c

TABLE 2. *Arc and spark spectra of rhenium*—Continued

Wavelength	Intensity and other characteristics	
	Arc	Spark
A		
3400.843	3*c*	3*h*
3401.168	10*cwr*	10*cw*
3402.71		2*cw*
3402.97	1	
3403.20	1	1
3403.59	3*c* .22*wl*	1*cw*
3403.718		20
3404.438	1	1
3404.724	80*R*	60
3405.12	1*h*	2*h*
3405.888	60*c*	50*c*
3406.388	3	2
3407.79		10*c* .21*Ws*
3408.673	30*c*	20*c*
3409.831	15	20
3409.960	2	2?
3410.282	1	1
3410.44	1*h*	1*h*
3411.507	3	3
3411.703		3
3412.701	5*cwl*	3*cwl*
3413.150	2	1
3413.744	10	10
3414.380	2	2
3414.605	2*c*	2*c*
3414.760	3*c*	3*c*
3415.900		4*cw*
3417.274		5
3417.767	40*c*	30*c*
3418.330	1	
3418.933	2	2
3419.242	5	4
3419.410	60*r*	50
3420.754	20*c*	15*c*
3421.218	1	
3421.582	5	4
3422.923	1*h*	1*h*
3423.17	1	1
3423.737	1*d*	1*d*
3424.620	600*R*	500*c* .22*W*
3425.412	3*c*	2*c*
3426.189	40*r*	50
3426.527	2	1
3426.67	1*c*	1*c*
3426.884	3*c*	2*h*
3427.61	50*cw*	40*cw*
3427.964		2*h*
3428.513	7	6
3428.826	6	4
3429.611		6*h*
3429.780	2	1
3430.44	1	
3430.80	1	1*h*
3431.818	4	3
3432.382	2*c*	2*c*
3432.668	5	3
3433.198	4	3
3433.557	1	1
3433.828	1*cw*	30*cwr*
3434.834		15*h*
3436.193	3	1
3436.39	1*c*	
3437.714	50*c*	30*c*
3438.589	4	4
3439.027	2*c*	1
3439.168	1	1
3439.67	2*h*	1*h*
3439.776	3	2
3440.173	2*h*	1*h*
3440.52		2*cw*
3440.843	5	3
3441.247	15*cw*	10*c*
3441.692		20*cwl*
3442.13	4*c* .16*Wl*	2*cW*
3442.407	2*h*	2*h*
3442.722	5*h*	3*h*
3442.967	10	8
3444.964	3*cw*	2*c*
3446.256	1	
3446.43		30*c* .33*Ws*
3446.743	1	1
3447.359	2	1
3447.801	1*h*	1
3447.915	2	2
3449.333	15	10
3449.407	15	10
3451.880	4000*R*	3000*c* 6, .142*Wl*
3452.649		4*h*
3453.280	15	10
3453.495	50*c*	50*c*
3454.006	2*h*	
3454.041		4*h*
3454.23		3*h*
3455.327		2*cw*
3455.680		3*h*
3455.988		3*h*
3457.077		2*h*
3457.246		1
3457.360		2*h*
3457.956	1	1
3458.458	2	2
3458.881	15	15
3460.465	10000*R*	7000*c* 6, .222*Wl*
3461.24		3*H*
3461.654	1	2
3461.965		4*h*
3463.053	2*c*	2*c*
3464.726	7000*R*	5000*c* 6, .189*Wl*
3465.988	10	10
3467.093	1*c*	1*c*
3467.284		2*h*
3467.656	1*h*	1*h*
3467.960	80*cw*	80*cw*
3468.645	4	4
3470.75	2	2
3470.976	1*h*	1*h*
3471.657	2*c*	1*c*
3471.923	6*c*	4*c*
3472.071	8*cw*	6*cw*
3472.723	30	20
3472.875	7	4
3473.000	2	1
3473.467	6	4
3473.688		6
3474.183	10*c* .20*Wl*	6*cW*
3474.700	5*c*	4*c*
3475.201	5	5
3476.031	4*cw*	3*c*
3476.442	30	20
3477.143	8	7
3477.920		1
3478.322		1
3478.491	3*cw*	3*c*
3478.629	4*cw*	4*cw*
3478.991		2*h*
3479.529	2	1
3480.381	30	30
3480.852	40	40
3481.398	1*h*	1*h*
3482.233	40*c*	40*c*
3482.853	2*cw*	2*cw*
3484.365	5	4
3484.728	5	3
3485.35		4*cwr*
3486.183	1	40*h*
3487.521	4*cwl*	3*cw*
3488.013	1*cw*	1*cw*
3488.77	4*cwl*	3*cw*
3488.87	4*cw*	3*cw*
3489.850	5*c* .20*Ws*	4*cW*
3490.860	10*c*	8*c*
3491.433	4	3
3491.772	2*c*	1*c*
3492.372	2	1
3492.545	2*c*	1*c*
3492.953	2	2
3493.863		3*Hw*
3494.06	2*cw*	2*cw*
3494.725	10	8
3495.415	1	1
3495.904	10*c* .21*Wl*	8*cWl*
3496.13	3*cwr*	3*cw*
3497.696		7*h*
3498.630		3*h*
3500.24		2*h*
3500.32		1*h*
3502.021	2*h*	1*h*
3502.25		3*h*
3502.727	9*c*	7*c*
3503.056	40*c*	40
3503.305	4	2
3503.522	4*c* .21*Wl*	3*cW*
3503.748	5*cw*	4*cw*
3505.375	2	1
3505.68		2*h*
3506.177	3	2
3506.360	10*c*	7*c*
3507.334	3*c*	2*c*
3508.626	1	1
3509.288	2*cw*	1*H*
3509.432		5
3510.333	1	1
3510.61		2*h*
3510.889	10*c*	6*c*
3511.343	4*cwl*	4*cw*
3512.280	20*c* .23*Wl*	15*cW*
3512.65	2	1
3515.01	5*c*	4*c*
3515.756	5	4
3516.146	5*c*	3*c*
3516.646	40*c*	40*c*
3517.326	60*c*	50*c*
3518.245		2*h*
3520.723	15*c* .19*Wl*	10*cW*
3521.041	1	
3521.507	3	2
3521.740	4	3
3522.171	6	4
3522.321	8*c*	6*c*
3522.528	4*c*	3*c*
3523.170		6
3523.779	2*h*	1*h*
3524.539	4	3
3524.736	3*cw*	2*cw*
3525.259	3	2
3525.64		1*h*
3526.21	2*h*	1*h*
3526.368	3	1
3526.734	20	10
3527.118		5*h*
3527.229	2	1
3528.214	4*c*	2*c*
3528.516	1	
3529.213	15	10
3529.545	2	1
3529.74	4	2
3529.81	5	3
3530.41		3*h*
3530.893	4*cw*	3*cw*
3531.795	2*cw*	1*cw*
3532.69	2*H*	3*H*
3533.412	2	
3533.503		2
3534.245	4*c*	2*c*
3534.822	20	15
3535.30	1	
3536.157	5	3
3536.88	1*cw*	1*cw*
3537.462	50*cwl*	40*cw*
3537.69		3*h*
3538.36		4*h*
3538.784	2	2
3539.022	1	1
3539.329	20	15
3539.813		80*h*
3539.944	10*c*	6*c*
3540.223	1	1
3541.340	3*c*	2*c*
3542.735		30*h*
3543.688	5	3

UNIVERSITY OF MICHIGAN LIBRARIES

TABLE 2. *Arc and spark spectra of rhenium*—Continued

Wavelength	Intensity and other characteristics	
	Arc	Spark
A		
3544.277	.....	3
3544.370	4	3
3544.656	2*cwn*	1*cw*
3545.41	.....	2*h*
3546.33	.....	3*cw*
3546.466	4	2
3547.024	3	2
3548.106	8	4
3549.319	5	3
3549.891	50	30
3550.644	2	3
3551.294	4*Ccwn*	20*cw*
3551.58	10c 3, .14*W*	5c*W*
3553.078	2c	1
3553.50	3*cw*	2*cw*
3553.650	2*bc*	10c
3556.935	.....	7*h*
3557.93	.....	5*H*
3558.15	.....	4*H*
3558.935	30*cw*	20*cw*
3559.239	1	1
3559.407	6	3
3561.078	2	1
3561.140	3	2
3561.83	.....	2*h*
3562.454	10c	6c
3562.634	.....	2*h*
3563.233	3	2
3563.653	3*cwl*	1*cw*
3564.280	.....	2*h*
3564.732	20	10
3565.195	5	3
3565.706	1	.....
3566.213	3*c*	2*c*
3566.373	2	1
3566.816	4	2
3566.964	4*cwl*	2*cw*
3567.600	1	.....
3568.234	30*cwl*	15*cw*
3568.780	2*c*	1*c*
3569.27	.....	2*H*
3570.255	30	20
3570.485	1	.....
3571.052	2*c*	.....
3571.694	8*c*	6*c*
3571.857	1	.....
3572.213	2	1
3572.804	8	4
3572.961	2*cw*	1*c*
3573.263	.....	3*h*
3573.730	3*cl*	2*c*
3574.75	.....	2*H*
3575.10	.....	4*Hw*
3575.197	2*c*	1*c*
3576.93	.....	2*Hw*
3577.09	1	.....
3577.325	6	2
3577.923	1	1
3578.054	2	1
3578.690	2	1
3578.977	2*c*	1*c*
3579.125	60*c*	30*c*
3580.15	10*c* .16*Wl*	300*cW*
3580.970	50*c*	30*c*
3581.434	.....	6*h*
3583.02	80*cwn*	50*cw*
3583.146	7	3
3585.030	15*cwl*	10*cw*
3585.329	10*d*	4*d*
3586.538	2*h*	1*h*
3586.842	1	1
3588.628	1*c*	.....
3589.264	2*c*	1*c*
3590.878	10	5
3591.86	1	.....
3593.388	10*cn*	4*c*
3593.91	.....	10*cwl*
3595.164	15*c*	8
3595.32	2*h*	1*h*
3595.600	1	1

Wavelength	Intensity and other characteristics	
	Arc	Spark
A		
3595.887	2*c*	1*c*
3596.230	10*c*	5*c*
3596.392	20	10
3597.039	3	2
3598.767	15	8
3600.803	2*c*	1*c*
3601.161	1	1
3601.600	.....	3*h*
3603.795	1	.....
3604.394	15*cwl*	8*cl*
3605.25	.....	3*Hw*
3605.332	2	1
3605.971	2*c*	1*c*
3606.558	4	3
3607.232	10	4
3607.833	2	1
3608.661	10*cw*	4*cw*
3609.330	.....	2*c*
3610.492	30*cwl*	15*cwl*
3610.65	.....	2*h*
3611.01	.....	1*h*
3611.10	.....	2*h*
3611.437	2*c*	1
3611.80	.....	1*h*
3611.996	.....	3*h*
3612.774	5*c* .24*Wl*	3*cW*
3613.41	.....	2*Hw*
3613.62	.....	2*Hw*
3615.372	8*cw*	4*cw*
3615.426	4	2
3616.427	3	2
3617.085	80*c*	40*c*
3617.252	20	10
3617.859	20*cwn*	10*cw*
3618.192	1*c*	.....
3619.203	1	1
3619.390	3	2
3619.83	3*Hw*	1*Hw*
3620.145	2	1
3620.230	2	1
3621.460	30*cwl*	15*cwl*
3622.183	10*c*	5*c*
3622.265	2*c*	2*h*
3623.980	6*h*	5*h*
3624.11	.....	4*h*
3625.908	20	10
3626.053	8	4
3626.80	.....	3*H*
3628.116	3*h*	2*h*
3629.200	20	7
3629.694	3*h*	1*h*
3630.69	2*h*	1*h*
3632.154	2	1
3632.615	1	1
3633.352	.....	3*h*
3636.772	4	2
3637.064	40	20
3637.228	10	5
3637.732	15	5
3637.848	60	40
3639.12	10*Hw*	5*Hw*
3640.75	.....	7*h*
3641.202	2	1
3642.986	15	5
3643.712	4	3
3644.924	3	2
3645.33	5*c* .18*Ws*	2*cWs*
3645.590	8	3
3646.636	5	2
3646.69	1	1
3647.544	.....	10*hc*
3649.210	2*c*	1
3649.47	6*c*	3*c*
3651.656	20*c* .16*Wl*	10*cW*
3651.972	80*c*	40*c*
3652.29	2*c*	1
3652.563	2	1
3653.17	3*H*	.....
3653.621	15*c*	5
3654.366	4*c*	2*c*

Wavelength	Intensity and other characteristics	
	Arc	Spark
A		
3654.935	8*c*	4*c*
3656.230	2*c*	1*c*
3656.834	.....	7*h*
3658.084	.....	10*hcw*
3658.735	7*cw*	3*c*
3660.162	2	1
3660.17	.....	3*h*
3660.515	20*c*	10*c*
3662.126	10	5
3663.034	5	3
3665.251	2	1
3665.522	2	1
3667.33	.....	2*h*
3668.496	.....	7*h*
3669.159	3	2
3669.436	8	4
3669.778	40*c*	20*c*
3669.993	7*cwn*	2*cw*
3670.358	10*c*	6*c*
3670.528	50	30
3672.407	20	10
3673.54	.....	2*h*
3673.868	2*c*	1*c*
3674.182	2	1
3674.87	.....	15*cw*
3675.093	3	1
3676.000	15	8
3676.570	4	2
3677.722	2	1
3678.392	6	3
3679.050	3*c*	2*c*
3680.206	10	6
3681.284	8	4
3681.407	2*c*	1*c*
3681.834	4*c*	2*c*
3682.155	5*c*	2*c*
3682.714	8*cwl*	3*cw*
3685.303	1*c*	.....
3685.444	2*c*	1
3685.803	.....	8*h*
3686.452	3	2
3688.646	6*c*	3*c*
3688.897	10	4
3689.26	.....	8*h*
3689.504	150*cwn*	80*cwn*
3689.824	1	1
3690.394	15	7
3690.547	1	1
3690.614	1	1
3691.385	20	10
3691.48	200*c*	100*c*
3692.115	10*cw*	4*cw*
3692.783	.....	10*h*
3692.808	2	.....
3693.636	.....	4*h*
3693.664	2	.....
3695.313	2	1
3695.424	.....	5*hc*
3695.600	3*c*	1*c*
3696.800	1	.....
3697.124	2	1
3697.710	20*cwl*	10*cwl*
3697.932	.....	20*h*
3698.565	.....	30*h*
3699.780	2*c*	1*c*
3700.374	10*cwl*	5*cwl*
3700.579	2*c*	1*h*
3700.684	2*d*	1*h*
3701.184	4*c*	2*c*
3702.098	5	3
3702.74	.....	2*hw*
3703.243	100	60
3703.53	1	.....
3704.450	20*c*	10
3704.842	10*cwn*	5*cw*
3705.02	20*c*	10*c*
3705.686	8*c*	4*c*
3706.268	2*h*	1*h*
3707.192	.....	8*h*
3708.774	6*h*	2*h*

TABLE 2. *Arc and spark spectra of rhenium*—Continued

Wavelength	Intensity and other characteristics	
	Arc	Spark
Å		
3708.47	10c 6, .26*WI*	5c*WI*
3709.930	60c	30c
3710.22	----------	5h
3710.64	2	1
3710.70	2	1
3711.46	5c*w*	2c*w*
3711.844	4c*w*	2c*w*
3712.10	----------	1h
3712.920	5h	2h
3713.160	10c*w*	5c*w*
3714.02	2c*w*	1c*w*
3714.51	----------	10h
3714.530	1c	----------
3714.712	1c	----------
3714.995	5	2
3715.042	5	2
3715.702	2c	1
3717.285	100c .16*WI*	50c*W*
3717.44	20c	8c
3720.860	2h	1
3721.146	4c*wl*	2c*w*
3725.760	2000*R*	1000
3726.502	8	4
3726.68	4	2
3726.752	4	2
3727.498	7	4
3728.498	2*Hw*	1*Hw*
3728.684	1h	----------
3728.820	2	1
3730.08	----------	2h
3730.306	2*H*	1*H*
3730.89	----------	5*He*
3731.662	----------	10*Hcw*
3731.870	20	10
3732.058	----------	5*Hcw*
3732.278	40c	20c
3735.01	20c*ws*	10c*w*
3735.314	1000c	500c
3736.193	4h	2
3736.808	10c	5c
3737.697	2h	1h
3737.806	1	1
3738.538	1	----------
3738.575	4c	2c
3739.82	----------	3*H*
3740.10	200c	100c
3740.414	30	10
3742.257	2	200h
3742.334	1	60h
3743.072	2	1
3743.194	1	1
3743.572	2	1
3744.53	----------	2*H*
3745.436	80c*w*	40c*w*
3746.441	1h	1h
3746.923	9h	5h
3749.010	5h	3h
3750.19	----------	1h
3750.666	5	2
3751.088	2	1
3751.555	1h	----------
3752.15	----------	4h
3752.718	2	1
3752.864	4c*w*	2c*w*
3753.052	2c*w*	1c*w*
3753.316	1	----------
3753.770	2c	1
3755.624	15	7
3756.356	2	1
3757.00	----------	1h
3757.622	15c*ws*	7c*ws*
3758.51	----------	1h
3759.749	2	1
3761.046	6c*w*	5c*w*
3765.08	2h	1h
3765.878	2	1
3766.480	15	5
3768.260	5h	2h
3768.846	2c*w*	1c*w*
3769.297	5*d*	2*d*

Wavelength	Intensity and other characteristics	
	Arc	Spark
Å		
3770.738	8c	4c
3771.252	2h	1h
3773.018	----------	15c*w*
3774.83	2c	1
3775.460	3	1
3776.300	----------	20c .24*WI*
3776.70	----------	2h
3777.05	----------	5h
3777.63	20	10
3777.69	30	15
3778.084	3	2
3778.535	2	1
3779.82	----------	3h
3780.357	15	7
3780.54	2	1
3781.864	4c	2c
3782.21	----------	3h
3782.95	----------	3h
3784.179	15	6
3784.496	3h	2h
3785.535	2c	1c
3786.182	2	1
3787.192	10	6
3787.520	15c*w*	80c*wl*
3788.009	2	1
3788.144	3*s*	1
3789.212	4c	2c
3789.771	4c	2c
3790.33	5*Hw*	3*Hw*
3791.57	----------	2
3792.165	3	1
3794.35	----------	2*Hw*
3795.505	3	1
3795.800	10c 6, .21*Ws*	5c*Ws*
3796.590	50c*w*	30c*w*
3797.586	50	30
3798.252	3	1
3799.86	----------	2h
3800.561	4c*w*	2c*w*
3803.95	2c*w*	100c*w*
3801.53	----------	1
3801.742	3	2
3802.113	----------	4
3802.21	2	1
3802.33	----------	2
3804.527	2c	1
3805.41	5c*w*	3c*w*
3807.193	1c	----------
3807.433	1	----------
3807.742	40	20
3808.200	10*dl*	3*dl*
3808.640	2c*w*	1c*w*
3809.752	3	2
3810.098	20c	10c
3811.38	----------	2h
3812.259	20c	10c
3812.812	7c	4c
3814.24	----------	1*Hw*
3815.655	40c	20c
3816.294	2	1
3816.73	----------	1*Hw*
3816.95	2h	1h
3817.539	30c .19*Ws*	15c*W*
3818.655	5c .20*WI*	2c*W*
3819.327	1	----------
3819.627	1	----------
3819.940	3c	2c
3820.21	1	----------
3821.43	----------	2
3821.598	3c*wl*	1c*w*
3821.962	2h	1h
3823.478	3c	2c
3823.772	10c .18*WI*	5c*W*
3825.30	----------	2*Hw*
3826.55	----------	2h
3827.04	15c 6, .24*WI*	6c*WI*
3827.625	9*dl*	4*dl*
3828.325	50	30
3829.80	20	10
3829.83	10	5

Wavelength	Intensity and other characteristics	
	Arc	Spark
Å		
3830.098	2	1
3830.525	----------	8h
3830.621	----------	10h
3831.028	3c	1
3832.402	8c*wl*	3c*w*
3832.92	----------	2h
3833.702	70c	40c
3834.235	100	50
3836.305	70c	40c
3836.786	----------	20c*w*
3837.088	1h	----------
3837.696	2h	1h
3837.894	2h	1h
3838.654	3c	1c
3839.540	----------	10h
3840.08	1h	----------
3841.498	10	5
3843.415	60c .19*Ws*	20c*W*
3845.891	2c*w*	1c*w*
3846.857	7	3
3847.27	----------	2
3847.38	----------	1h
3847.72	----------	10*Hw*
3848.95	3c*wl*	2c*wl*
3851.988	15	8
3852.689	5c	2c
3855.936	30c	15c
3856.72	----------	2h
3858.301	1	1
3858.528	----------	5h
3858.584	1	----------
3859.328	2	1
3859.450	2	1
3860.862	9	4
3861.647	6	2
3862.103	6c	3c
3863.153	5	2
3863.708	15	7
3863.932	4c*w*	2c*w*
3864.108	4	2
3864.766	4	2
3865.126	1	----------
3865.875	2h	1h
3867.21	2c*w*	1c*w*
3868.213	2	1
3869.14	----------	1h
3869.944	100c*w*	50c*wl*
3873.037	3	2
3873.501	----------	6*Hw*
3873.870	4	2
3875.26	100c*ws*	50c*ws*
3876.861	150c .16*Ws*	70c*Ws*
3878.868	20	10
3879.016	10c	4c
3880.336	2	1
3881.89	40	15
3881.97	7	3
3883.958	5c	3c
3884.888	2h	1h
3886.21	----------	5h
3887.29	----------	2
3887.488	40c	20c
3887.950	40c	15c
3888.09	4h	2h
3888.92	----------	7c*ws*
3889.36	2c*w*	1c*w*
3889.962	40c*l*	15c*l*
3890.309	2c	1c
3890.54	1	----------
3891.399	10	5
3893.48	5c .23*WI*	2c*W*
3893.59	----------	2h
3893.914	5c*l*	3c*l*
3895.41	4c	2c
3896.110	30c	10c
3896.40	1	----------
3898.41	2c	1
3898.50	----------	5h
3898.55	1	----------
3898.65	1	----------

UNIVERSITY OF MICHIGAN LIBRARIES

TABLE 2. *Arc and spark spectra of rhenium*—Continued

Wavelength	Intensity and other characteristics	
	Arc	Spark
A		
3900.24		2*cnl*
3900.34	2*el*	1*h*
3900.50	3	1
3900.85	6	3
3900.907	30	10
3901.092	20	8
3902.580	5	3
3902.82	3	2
3905.12	10*el*	5*el*
3907.20	3*cw*	1*c*
3907.74	3	1
3908.210	40	20
3909.84	1	
3910.157	2	1
3910.272	2	1
3910.59		3*h*
3911.76	2*c*	1*c*
3913.49		3*hc*
3913.924	60	30
3915.234	2*c*	1*c*
3915.382		10*h*
3917.270	200*cw*	100*cw*
3919.076	10*cw*	4*cw*
3920.85	20*c* ,20*Ws*	10*cW*
3921.759	10*c*	5*c*
3922.274	10	5
3923.58	5*cws*	2*cw*
3924.090	10*c*	4*c*
3924.67	4*c* ,25*Wl*	2*cW*
3925.038	2*c*	1*c*
3925.63	2	1
3926.14		2
3926.28		4*Hw*
3926.522	10*c*	4*c*
3926.85	4*cwl*	2*cwl*
3927.31		1*h*
3927.59	30*c* ,20*Ws*	15*cWs*
3928.364	2	1
3928.704	15	7
3929.198	6	3
3929.847	200	100
3930.48	10*c* ,23*Wl*	5*cW*
3930.53	6*c* ,19*Wl*	3*cW*
3931.201	20	10
3932.538	2*c*	1*c*
3932.934	4*cs*	2*cs*
3934.28	1	
3936.70	2	1
3936.899	100*c*	50*c*
3937.628	2*h*	1*h*
3939.381		5*h*
3941.468	6	3
3941.540	8	4
3942.42		2*h*
3942.562	10	5
3943.52		1*h*
3944.344	15	7
3944.718	50*cw*	30*cw*
3945.906	150*c*	80*c*
3946.75	2	1
3947.428		10*h*
3950.570	15	6
3950.64	10*cw*	4*c*
3951.45	2*cw*	1*cw*
3951.836	2*c*	1*c*
3952.10		3*h*
3953.23	3*h*	1*h*
3954.428	15*c*	7*c*
3956.60	2*c*	1*c*
3957.173	3	1
3957.363	10	4
3958.357	7	3
3959.39	10*c* 6, .35*Wl*	4*cWl*
3960.552	15*c*	7*c*
3961.036	150	80
3962.484	300*cw*	150*cw*
3963.267	40	20
3963.53		3*c* .22*Wl*
3963.707	7	3
3964.11		2*Hw*

Wavelength	Intensity and other characteristics	
	Arc	Spark
A		
3964.279	5*c*	3*c*
3964.53	2*c*	1*c*
3964.810	15	7
3965.27	1*c*	
3965.59		2*Hw*
3967.39	30*cw*	15*cw*
3967.707	2*c*	1*c*
3970.93		1*h*
3971.47		1*h*
3971.63		3*Hw*
3975.374	3	1
3975.648	20*c*	8*c*
3976.759	4*cwl*	2*cwl*
3978.620	10*Hw*	5*Hw*
3979.66		2*Hw*
3981.14		2*Hw*
3981.455	7	3
3982.286	7*cws*	3*cw*
3983.41	10*c* 6, .27*Ws*	4*cWs*
3983.91	15*cw*	5*cw*
3984.200		50*h*
3984.254	10*H*	20*h*
3984.28		10*h*
3984.74	2*cw*	1*cw*
3985.31	1	
3985.42	1	
3987.086	5*h*	2*h*
3987.83		2*Hw*
3987.915	4	2
3988.63		3*Hw*
3990.660	15	6
3990.83		2
3991.033	30*cws*	10*cw*
3991.571	10*cw*	5*cw*
3992.72	10*cws*	4*cw*
3993.20		2*Hw*
3994.154	4*d*	2*c*
3995.690	10*Hw*	4*Hw*
3996.987	3*c*	1*c*
4000.122	3*cws*	1*cw*
4001.19	3	1
4004.38		3*h*
4004.930	70	30
4007.22	2	1
4007.34		2*h*
4008.97	1	
4008.99		2*h*
4009.54		3*h*
4009.94		10*h*
4010.322	3*cw*	1*cw*
4012.26	15	5
4014.855	4*h*	2*h*
4016.60		1*h*
4016.95	1	1
4018.016		4*h*
4018.40	20*c*	10*c*
4019.124	6*c*	3*c*
4020.860		10*h*
4022.86	10*c*	4*c*
4022.965	60	20
4023.313	40*cws*	15*cw*
4024.040		6*h*
4025.07	3*d*	1*d*
4025.56		2*h*
4025.614	9*c*	4*c*
4026.707	3*c*	1*c*
4027.124	4*c*	2*c*
4028.53	30*c*	15*c*
4029.63	60*c* ,23*Wl*	30*cW*
4031.42		20*c* 6, .46*Ws*
4032.143	8*c*	4*c*
4032.35		5*h*
4033.31	100*c* ,18*Wl*	40*cW*
4033.63	10*c* ,22*Wl*	4*cW*
4034.74	1*h*	
4037.49	50*c*	20*c*
4038.63	2*c*	1*c*
4039.52	2*h*	
4040.178	10	4
4041.11		1*h*

Wavelength	Intensity and other characteristics	
	Arc	Spark
A		
4041.305	3	1
4042.78		3
4043.10		3
4044.798	3*c*	1*c*
4045.237	4*c*	2*c*
4045.94	2	1
4047.106	2	1
4048.99	80*c*	40*cs*
4050.926	10	4
4051.200	2	1
4051.45		2*h*
4052.852	3	1
4053.36	3*c*	2*c*
4054.265	15*c*	7*c*
4054.59	1	
4055.330	20*Hw*	10*Hw*
4056.91		10*h*
4057.001	10	4
4058.68	2	1
4058.81		2*h*
4059.753	2*c*	1*c*
4061.643	3*cw*	2*cw*
4061.856	30	15
4062.40		4*h*
4064.328	15*h*	5*h*
4064.920	5*cwl*	3*cw*
4066.94	2*c*	1*c*
4067.246	2	1
4067.44	1	1
4069.12		30*c* ,26*Wl*
4069.16	10*c* ,15*Wl*	?
4072.36	1	
4073.069	4*c*	2*c*
4074.01	2*c*	1
4075.09	1*h*	
4078.120	8	4
4079.364	10*c*	5*c*
4081.432	80	40
4082.65	2	1
4083.365	20*cws*	8*cws*
4083.584	20*cws*	8*cws*
4084.77		3
4085.01		4
4085.14		2
4085.67		2*h*
4086.31		2*h*
4087.89	4*cw*	1
4088.10	4*c* ,16*Ws*	2*cW*
4088.69	1	2*h*
4089.01	5*cwl*	3*c*
4089.407	4*cws*	2*c*
4089.919	30*cw*	15*cw*
4090.59	2	1
4091.12	4*cw*	2*cw*
4091.96		20*h*
4094.60		1*h*
4095.30		2*h*
4096.44	3*h*	1*h*
4096.94		4*h*
4097.42		1*h*
4099.31	2*h*	1
4102.16	8*Hw*	4*Hw*
4103.763	3*h*	1
4104.422	70	30
4106.440	10*c* ,23*Wl*	4*cW*
4106.829	5*h*	2*h*
4107.431	2*h*	1
4107.832	1	
4107.973	3	1
4108.618	10	4
4109.451	1	
4110.894	100*c* ,16*Ws*	40*cW*
4111.672	2	1
4111.598	5	2
4112.275	3*c*	1*c*
4113.402	30*cws*	10*cw*
4114.676	3	1
4116.30		3*c* ,34*Wl*
4120.23		3*Hw*
4121.548	10	3

TABLE 2. *Arc and spark spectra of rhenium*—Continued

Wavelength	Intensity and other characteristics		Wavelength	Intensity and other characteristics		Wavelength	Intensity and other characteristics	
	Arc	Spark		Arc	Spark		Arc	Spark
A			*A*			*A*		
4121.635	30	10	4230.55	1c	.....	4318.585	10	6
4122.738	8c	3c	4231.53	.....	20c .28*W1*	4319.531	15	7
4122.896	2c	1	4232.956	2)	10	4324.33	3c	1c
4123.507	2	1	4233.275	10c	4c	4328.716	3	1
4123.82	2c*w*	1	4234.43	6c .24*W*	2c*W*	4329.076	3	1
4124.893	10c 6, .30*W1*	4c*W1*	4234.95	10c .25*Ws*	3c*W*	4330.69	.....	9
4128.092	2	1	4235.38	2c	1c	4331.14	2h	.....
4128.136	2	1	4236.237	20	10	4331.365	3	1
4130.136	8	4	4238.016	7c	3c	4332.25	80c*ws*	30c*w*
4130.458	10	5	4238.586	15	6	4335.23	.....	2h
4133.425	100c 6, .39*W1*	40c*W1*	4239.956	2	1	4335.860	9	5
4135.43	.....	2h	4240.18	.....	4c*w*	4339.68	8c	2c
4136.45	200c .22*Ws*	100c*Ws*	4241.16	40c	15c	4340.65	.....	5h
4137.603	20	8	4241.35	50	20	4342.145	4	3
4138.532	3	1	4241.42	50	20	4344.65	4c .30*Ws*	1c*W*
4142.767	4	2	4241.806	2	1	4345.32	1	.....
4144.363	200c*w*	100c*w*	4243.85	2	1	4345.505	2	1
4146.233	10c	4c	4244.12	20c .21*Ws*	4c*W*	4351.72	2h	1h
4146.70	.....	5c .21*W1*	4246.820	40*bl*	10*bl*	4352.46	4c .26*W1*	1c*W*
4148.276	5h	2h	4247.679	4h	1h	4356.29	.....	6
4149.46	.....	5*Hw*	4248.27	.....	4h	4357.06	10c*wl*	6c*w*
4149.96	50c .17*W*	20c*W*	4248.357	2	1	4357.96	10	?
4150.527	10	4	4255.10	2c	1c	4357.98	.....	20
4150.790	2	1	4255.33	2c	1c	4358.69	100c*wl*	60c*wl*
4151.076	3c	1c	4255.749	20	7	4359.310	7	4
4152.29	10h	4h	4257.60	200c .24*Ws*	100c*W*	4360.375	10c	3c
4152.632	30c*wl*	15c*w*	4258.68	2h	1h	4361.26	4c*wl*	1c
4157.252	3c	1c	4259.51	.....	2	4363.37	6c*wl*	4c*w*
4159.925	20	10	4259.880	3	1	4364.13	10c*wl*	9c
4160.773	5c*wl*	3c*w*	4260.91	6	3	4364.851	9	3
4161.79	3h	1h	4261.37	6c 6, .29*W1*	3c*W*	4367.58	100c .21*W1*	60c*W*
4162.36	.....	1h	4261.86	3c	1c	4368.67	.....	1h
4164.10	2c	1c	4263.35	3	1	4369.64	2	1
4164.32	1	.....	4263.76	3c	1c	4369.77	4	2
4165.29	.....	1h	4264.26	2h	2h	4372.18	.....	10c*wl*
4165.31	1h	.....	4264.73	2h	1h	4373.202	5	2
4165.94	.....	4h	4267.97	3c .26*Ws*	2c*W*	4377.056	2	1
4165.976	5c	2c	4268.71	5c*w*	3c*w*	4377.44	3c	1
4166.408	10c*wl*	4c*w*	4269.79	3c	1c	4378.48	2c	.....
4168.588	15	5	4269.94	.....	20c .39*W1*	4380.45	1	.....
4170.395	100*d*	30*d*	4272.95	2	1	4380.89	2c	.....
4172.047	2	1	4274.34	10c .21*W1*	6c*W*	4381.00	.....	10c*wl*
4173.678	2	1	4279.185	3	1	4384.44	.....	2
4173.978	10c	4c	4280.59	6	3	4385.443	10c	4c
4175.186	10c	4c	4281.664	2c	1c	4386.14	2c*w*	.....
4176.540	10c .18*W1*	4c*W*	4282.734	10	4	4387.404	10c*ws*	5c
4176.867	6c	3c	4282.99	4	3	4389.60	.....	10c*wl*
4177.419	2c	1c	4285.55	1h	.....	4391.342	100c*ws*	40c*w*
4178.599	3	2	4286.084	5	4	4392.122	3	1
4179.73	3c*w*	2c*w*	4286.463	10c	5c	4392.45	40c .28*Ws*	20c*W*
4181.29	2c*w*	1c*w*	4288.08	.....	4h	4394.30	80c	30c
4182.902	100	50	4289.09	.....	4h	4394.46	50c	20c
4183.056	100	50	4291.17	100c 6, .29*W1*	40c*W1*	4396.089	10c*w*	5c*w*
4184.48	2h	1h	4291.654	30c	10c	4396.802	30	10
4185.72	2h	1h	4291.80	8	3	4399.80	8c*w*	5c
4186.26	.....	2h	4294.62	2c	1c	4400.92	.....	2h
4187.909	5	2	4295.97	.....	2h	4402.600	40c	20c
4188.441	2	1	4298.14	4c*w*	2c*w*	4403.683	5	3
4189.52	.....	2h	4298.20	3h	2h	4404.27	1	.....
4190.782	2c*w*	1c*w*	4299.917	20	20	4406.30	20c	6c
4191.92	3*Hl*	2*Hl*	4301.052	4	2	4406.47	30c*ws*	10c*w*
4194.668	50c*wl*	20c*w*	4301.774	4c*w*	2c*w*	4406.89	.....	2h
4195.741	10c	4c	4302.11	3*bl*	1	4408.64	3c*w*	.....
4198.60	.....	2c*w*	4302.28	2	1	4409.56	.....	3c*wl*
4203.308	7c*w*	3c*w*	4304.404	100c*Wl*	50c*Wl*	4410.39	2h	.....
4204.525	30c*ws*	10c*w*	4304.78	2	1	4413.500	1	2
4204.95	.....	2h	4305.334	15c	5c	4415.822	80	80
4204.964	2c	1	4308.802	4c	2c	4417.22	8	2
4208.53	.....	2h	4309.474	9c	4c	4417.33	10	3
4210.69	.....	4h	4310.41	2c	1	4418.808	6	5
4212.56	3h	2h	4311.68	.....	20h	4419.86	2h	1h
4213.266	30c*wl*	10c*w*	4312.75	.....	3h	4423.C2	.....	20
4214.974	2	1	4313.31	2h	.....	4423.810	2	1
4215.500	15	7	4314.578	15	7	4425.762	2	1
4221.079	200c	100c	4315.71	20c 6, .38*Ws*	6c*Ws*	4426.47	2c	5h
4222.500	2c	1h	4316.18	4	2	4427.67	2	.....
4223.178	15c*wl*	7c*w*	4316.52	.....	4h	4427.951	7c*wl*	2c
4224.163	15c	5c	4317.11	5c*w*	5h	4428.864	2h	.....
4227.46	2000c .32*W1*	1000c*W*	4317.68	2h	1h	4429.76	.....	4h
4228.748	3c*w*	1c*w*	4317.93	2h	1h	4432.846	1h	.....

UNIVERSITY OF MICHIGAN LIBRARIES

TABLE 2. *Arc and spark spectra of rhenium*—Continued

Wavelength	Intensity and other characteristics	
	Arc	Spark
A		
4433.72		5h
4434.24	2	
4434.43		5h
4436.614	3	1
4440.44	20*cw*	10
4445.97	2h*w*	
4448.115	2	
4448.259	2	1
4452.68		10
4453.26	2*cw*	
4453.92	20*c*	5*c*
4454.62	50*c* .36 *W's*	20*c W's*
4456.370	3	2
4456.668	6*c*	4*c*
4457.47	2	3h
4458.122	2*c*	2h
4459.405	3	2
4463.53	20	10
4464.627	2	1
4465.834	5	2
4467.544	15	7
4467.924	40	20
4468.38		2h
4472.06	2	1
4473.23	4	
4473.31		20
4473.60		2h
4475.082	80	80
4475.73		5h
4476.78	6*cl*	5*cl*
4477.642	3	2
4477.986	30*c*	20*c*
4478.386	60	40
4480.75		3h
4481.32		100*c* .50 *W's*
4481.443	10	?
4483.16		7*l*
4486.44		5h*cw*
4486.58	3h	1h
4486.991	5	4
4489.99		8*c*
4493.460	1	5*c*
4494.12	3	4
4495.01	2*cw*	
4496.432	15	10
4498.378	10	5
4499.04	3	2
4502.52	4	3
4502.98		6
4504.41	4	3
4505.49		5
4507.035	100*c*	100*c*
4508.007	60	50
4508.39	1	
4511.25		3h
4513.31	500*c* .32 *W's*	500*c W*
4514.26	20*c*	10*c*
4515.142	7	5
4516.638	200	200
4517.774	1	
4518.570	3	2
4519.09		5
4519.762	80*c*	80*c*
4520.97		20
4522.73	400	400
4523.878	100	100
4526.009	80*c*	70*c*
4526.98	10*cw*	8*c*
4528.966	60	50
4529.950	150	150
4530.889	30	15
4531.36	1	
4536.014	40	30
4537.48		6
4537.54	3*c*	
4539.16	5*c* .37 *W's*	?
4539.23	?	10*Hw*
4541.80	50	40
4542.89		4*cw*
4543.98	1	2

Wavelength	Intensity and other characteristics	
	Arc	Spark
A		
4545.174	100	70
4545.53	10	5
4549.82		3h
4551.502	4	3
4556.025	3	2
4556.820	1	2
4557.33	4*cw*	3*c*
4557.80		3
4559.268	50	15
4559.682	50	50
4562.325	3	3h
4562.92		7h
4563.63	7*cs*	6*c*
4564.633	4	2
4565.30	50*c*	30*c*
4565.51	60*c*	40*c*
4568.748	2h	2h
4569.75		5h
4572.195	4	3
4575.935	2*cw*	1*c*
4577.27		2
4577.550	3	2
4578.251	4	3
4578.93	3h	2
4580.68	100	50
4583.796	2*c*	
4584.49		30*c* .51 *W's*
4586.06	3*c* .18 *W*	2*cw*
4587.141	8	4
4588.821	2	1
4590.540	3	1
4591.682	20	10
4592.53	4*cl*	3*cl*
4595.263	4	4
4595.64	1	
4596.56		100h
4597.32	5*c* .19 *W*	2*c W*
4598.143	6	4
4599.764	1	
4601.13	1h	
4605.73	200	100
4607.80	3*cw*	
4608.802	4	2
4609.81	1h	
4613.95	5	?
4614.66	50*c* .24 *W*	40*c W*
4616.57	30*c*	20*c*
4621.38	80	70
4623.34	5*c*	4*c*
4625.96	30*c*	10*c*
4626.50		5h
4628.76	1	
4630.24	7*cwl*	?
4630.82	80*cw*	?
4634.41	10*c* .22 *W*	5*c W*
4635.78	3	1
4640.63	1h	
4640.94	1h	
4641.412	1h	
4642.68	2	?
4642.78	1	
4644.95	20*cwl*	10*cw*
4646.27	1h	
4647.46	10*c*	6*c*
4648.56	4	?
4649.19	1h	
4649.70	3	2
4650.083	3	2
4650.825	3h	2h
4651.20	1h	
4651.82	4	2
4652.33	100	70
4652.77	2*cw*	
4654.53	10*c*	
4654.63		20*hl*
4656.29	2h	
4656.47	10*c*	7*c*
4660.51	10	5
4661.483	9	10
4662.493	60	10

Wavelength	Intensity and other characteristics	
	Arc	Spark
A		
4662.99	8*cw*	5*c*
4664.01	1	8
4665.217	5	4
4666.713	6	4
4668.56		3h
4669.81	2*c* .31 *W's*	
4673.15		100*c*
4674.304	9	6
4675.38	2	1
4679.476	15	6
4681.89	2h	1h
4682.319	60*c*	30
4684.02		5h
4685.05	1h	
4685.20	1h	
4685.853	20	10
4688.87	1h	
4690.90		10h
4691.45	4h	5h
4692.80	1	1h
4693.38	8	7
4694.99	30*c* .27 *W's*	10*c W*
4698.08	2h	
4698.38	1h	
4699.69	4	3
4700.440	50	20
4703.70		10*cw*
4703.78	4*c*	
4703.91	1	
4705.04	60*c*	40
4708.570	2	1
4709.45	2	
4711.22	2	
4712.14	2	
4712.76	20	10
4714.78		10
4719.57		5h
4724.62		4
4725.02	4*c* .36 *Wl*	3*c W*
4725.93	20	15
4727.60	80	60
4730.43	2h	2
4733.87	4	5
4739.24		5h
4739.95		5
4740.80		8
4742.19		9h
4742.84	2	
4743.46	4	3
4745.67	2	2
4746.24	5	5
4748.66	8	8
4748.38	80*c* .20 *W's*	60*c W*
4749.03	40	30
4750.21		3h
4750.99	5	5
4751.23	1	
4751.345	10*c*	10*c*
4752.10	4	2
4755.64		10h
4758.833	40	20
4763.672	20*cw*	10*c*
4765.81		8h
4766.89	2	2
4771.807	4	4
4772.04	1h	
4778.99	4h	?
4781.83	2h	?
4789.206	10	2
4789.60	3*cw*	
4791.418	200*cw*	50*c*
4796.895	4	1
4799.127	15	2
4799.49	9	2
4800.778	4*cw*	1*cw*
4802.28	1	
4805.56	2h	
4813.139	3	1
4814.92	2*c* .36 *Wl*	
4816.03	2*c*	1

TABLE 2. *Arc and spark spectra of rhenium*— Continued

Wavelength	Intensity and other characteristics	
	Arc	Spark
A		
4820.37	20c .26*Wl*	5c*W*
4822.63	2	2
4825.11	2	
4829.87	6c .33*Wl*	1c*W*
4833.98	3c .35*Wl*	
4834.79	9*cn*	2
4835.23	1*h*	
4845.67	3	1
4846.26	3c	1c
4848.45	20c .27*Wl*	5c*W*
4849.23	1	
4852.57	7*cw*	2c
4853.73	3*cw*	10c .67*Ws*
4856.70	1*h*	
4862.539	5	1
4868.43	2	
4870.03	3*cw*	1c
4872.032	3c	1c
4872.43	2	
4874.237	2	1
4874.85	10	2
4876.929	2	
4881.278	3c	1c
4882.45	3	1
4884.10	3	1
4885.80	2	
4889.14	2000c 6, .548*Wl*	500c*Wl*
4892.222	4*cw*	1c
4896.167	10	3
4897.529	4c	2c
4899.634	6	2
4901.445	3	2
4903.73	15*cw*	2*cw*
4904.33		10*cw*
4904.75	2	
4905.93	1	
4906.208	30	4
4908.562	20	3
4909.066	4*cw*	1c
4909.71		4*cw*
4914.34	4c	1
4915.020	100	10
4917.84	6	2
4923.903	200	40
4925.99	2*h*	
4926.893	4	2
4928.585	3*cw*	1*cw*
4932.350	2	
4933.734	30*cw*	5*cw*
4935.842	15	4
4940.53	2*h*	
4943.73	8*cl*	2c
4944.867	7c	2c
4946.72	150	20
4949.82	20	3
4952.270	2	
4955.286	3c	1
4956.765	100	10
4960.42	2*h*	
4961.383	10c	3
4963.065	10*cw*	2*cw*
4969.435	10	3
4972.836	8	2
4976.932	2c	1
4980.677	7c	2c
4981.544	20	3
4984.812	5	3
4985.978	200c	20c
4987.521	5	2
4994.02	3*cw*	
4994.48	1	
4996.22	1	
4997.74	4c	1
5003.60	10	2
5006.68	1	
5008.14	6c .30*Ws*	?
5010.56	4c	1
5014.35	1	
5024.022	2	
5026.432	20	3

Wavelength	Intensity and other characteristics	
	Arc	Spark
A		
5027.943	15	2
5029.75	2c	
5031.57	1*h*	
5031.94	2*h*	
5036.88	1*h*	
5041.40	3*Hw*	
5042.631	7c .26*Ws*	1c*W*
5052.20	2	
5052.365	1	
5054.95	1*h*	
5056.063	10c	2
5058.557	100	9
5060.427	5	1
5063.76	5*cw*	1*cw*
5065.31	3	1
5066.60		1*h*
5067.544	2	1
5068.85	4*cwn*	1c
5070.64		3*h*
5078.423	6	1
5081.573	1	
5087.65	2*h*	
5089.87	1*h*	
5090.57	6	1
5093.19	3c	1
5094.03	3c	1
5095.78	10*cwn*	4*cw*
5096.50	150	10
5098.782	2	
5099.20		5c
5100.70	2	
5104.66	20c .29*Wl*	5c*W*
5105.15	10	3
5108.78	10	2
5112.265	15	3
5113.25	1	
5115.18	1	
5116.90	2	
5117.42	2c	
5120.32	30c	4c
5124.206	2*h*	
5124.597	9c	2
5126.70	20c 6, .52*Wl*	4c*Wl*
5140.058	4	1
5141.288	3	
5142.14	1*h*	
5145.593	6	2
5146.89	15c .28*Ws*	5c*W*
5156.248	15c	2c
5161.650	30	6
5165.198	5	1
5167.860	2c	
5172.370	2	1
5173.92	1*h*	
5178.891	80*cw*	10*cw*
5181.741	20	3
5185.896	3	
5186.149	2	
5186.423	1	
5190.11		2*h*
5198.915	3c .44*Wl*	
5199.89	8*cwl*	2c
5200.82	4*cw*	1c
5202.03	2	
5202.83	1c	
5203.46	2	
5206.74	1*h*	
5209.08	200*cwn*	20*cw*
5209.927	10	2
5210.93	1	
5214.43	5*Hw*	
5214.716	5	1
5217.49	2c	
5218.18	5*h*	
5221.124	5*cw*	2*cw*
5222.124	5	1
5222.733	1	
5223.022	1	
5224.786	10*cwn*	2*cw*
5226.805	2*h*	

Wavelength	Intensity and other characteristics	
	Arc	Spark
A		
5229.087	1	
5231.31	1	
5234.306	20*cwn*	4*cw*
5236.660	10*cwl*	3*cw*
5243.52	2c	
5244.334	10	2
5247.97	1*h*	
5248.856	30	5
5250.085	3*cw*	1c
5252.34	3	1
5255.43	1*h*	
5260.62	3	
5261.88	1	
5262.39	4*cw*	3*cw*
5262.92		5c
5264.416	4	2
5265.12	5*Hw*	2*H*
5270.95	4000c .38*Ws*	2000c*W*
5273.25	2*h*	
5275.56	1000c .50*Ws*	500c*W*
5278.245	200	20
5279.102	2	
5280.54	5c .32*Wl*	
5284.581	5	2
5286.68		5*h*
5287.92	10c .25*Wl*	2c*W*
5289.16	1c	
5292.278	4	1
5299.85	1c	
5300.75	5c	1c
5303.21	1	
5305.56	30c	10*hl*
5306.739	3	1
5309.87	2c	
5311.515	6*cw*	2*cw*
5317.275	30*cwl*	6*cw*
5318.76	1*h*	
5319.23	2*h*	
5321.278	40c	6c
5321.534	2	1
5324.50	2	
5325.00	4c .53*Ws*	
5327.46	200	10
5331.896	50*cwl*	5*cw*
5332.47	2*h*	
5332.76	9c	7*hl*
5333.85	20	5
5338.63	3c	
5339.416	4	
5342.37	3*Hw*	
5343.70	3*Hw*	
5345.221	2	
5349.245	3	
5350.45	4c .39*Wl*	1*cw*
5352.64	1*h*	
5353.35	2*h*	
5353.73	1	
5356.65	1*h*	
5366.664	2	1
5369.480	30	7
5369.797	30	5
5374.720	4	1
5377.10	200c .32*Ws*	30c*W*
5378.163	5c	1c
5379.707	3	1
5390.18	1*h*	
5396.50	9	3
5402.19	2*h*	2*h*
5409.52	1	
5410.01	2*cw*	
5417.78	5*Hw*	
5418.37		5*h*
5423.29	2	1
5423.60	4	1
5423.81	6	2
5431.90	30c	10*hl*
5437.03	10	2
5437.41	3	1
5443.31	2*h*	
5444.50	1*h*	

UNIVERSITY OF MICHIGAN LIBRARIES

TABLE 2. *Arc and spark spectra of rhenium*—Continued

Wavelength	Intensity and other characteristics	
	Arc	Spark
A		
5447.92	15	3
5456.316	4*cs*	1*c*
5458.92	2*h*	
5460.644	30*c*	4
5465.43	7	4*h*
5467.54	3	1
5470.910	3*c*	1*c*
5475.86	1*h*	
5481.003	5	1
5492.19	3*cl*	
5494.34	2*c*	
5495.69	2*cw*	
5499.79	1*h*	
5501.921	5	1
5505.60	3*cw*	
5505.81	1	
5506.492	2	
5514.99	2*cw*	
5519.53	4*cw*	1*c*
5520.05	10*c*	5*c*
5521.10	15	4
5521.83	2*h*	
5523.40	8*c* .35*Ws*	3*cW*
5524.25	2*h*	
5529.96	2*h*	
5532.676	50*cw*	10*cw*
5534.35	1*h*	
5535.94	2*h*	
5545.15	2*h*	
5557.21	7	2
5563.24	100*cwrs*	10*cw*
5564.12	7	2
5570.40	1*h*	
5573.47	30*cw*	5*cw*
5577.69	8*cwrs*	1*cs*
5578.38	3*c* .62*WI*	
5580.77	2	
5582.89	2	
5584.718	30*c*	5*c*
5592.68	2*c*	1
5594.856	6*c*	1
5601.92	3	
5604.15	2*h*	
5607.21	8*c*	2
5607.41	3*c*	
5608.803	3*h*	2*h*
5610.516	3	1
5612.269	10*cwrs*	5*hs*
5614.85	2*c*	
5619.76	4	1
5621.22	1	
5624.625	3*h*	2*h*
5625.441	8*cw*	3*cw*
5635.45	3	2
5644.467	3	1
5653.018	8	2
5658.68	4	1
5662.83	5*c* .33*Ws*	1*cW*
5664.69	3	1
5665.01	3*cw*	1
5667.88	100	20
5671.04	3*c*	?
5672.68	3*cw*	?
5678.34	3*c* .41*Ws*	
5680.92	4*c*	1
5683.40	2*h*	
5684.31	2	1
5686.81	2*cw*	
5689.75	6*c* .20*W*	1*cW*
5692.46	2*cw*	
5706.48	6*h*	3*h*
5711.426	30	3
5714.02	5	1
5716.950	15	2
5725.626	9	2
5727.90	3	1
5730.96	1	
5732.25	2*cw*	
5733.06	5*cwl*	1*c*
5734.26	5*cwrs*	1*c*
5734.79	2	
5736.27	2	
5737.32	2*c*	
5738.17	3*Hw*	
5739.445	7	1
5740.32	10*c* 6, .64*WI*	2*cWI*
5749.86	2*h*	
5752.93	200*cw*	20*cw*
5763.41	3*cw*	
5769.82	2*h*	
5773.32	1*h*	
5776.83	300*c* .47*WI*	20*cW*
5778.16	1	
5778.343	3	
5782.58	7	2
5783.01	2	
5786.10	5	1
5786.27	7	1
5791.595	20	4
5796.262	2	
5805.77	2*cw*	
5806.97	10	2
5807.41	4*cw*	1*cw*
5808.865	8*cw*	2*cw*
5810.82	4*c* .40*WI*	
5815.92	20*c* .25*WI*	2*cW*
5818.07	2	
5818.28	2	
5827.37	1*h*	
5834.31	1000	200
5835.52	5*c* .50*Ws*	
5844.96	2*c*	
5852.02	20*c* .52*WI*	4*cWI*
5852.76	3	
5866.58	3	1
5868.05	8	1
5870.71	2	
5872.557	1	
5885.65	1*h*	
5899.25	8*c* 6, .55*WI*	1*cWI*
5903.99	7*c*	
5908.01	3*Hw*	
5909.99	5*c*	1
5911.14	5*cl*	1
5916.66	4*cwl*	
5919.86	9*cs*	2*c*
5925.08	2*h*	
5927.38	6*cwrs*	1*c*
5938.83	2*h*	
5943.24	100*c*	10*c*
5945.46	2*c*	
5947.57	2*h*	
5950.21	10*cw*	3*c*
5954.308	4*c*	1
5956.10	4*cs*	1*c*
5967.626	5	2
5969.77	20*cwl*	5*c*
5972.58	4*c*	1
5981.65	6*c*	2*c*
5982.67	8	2
5983.14	7	?
5989.99	8*cs*	2
5995.73	20*cw*	5*c*
6021.83	2*h*	
6026.53	3	
6026.60		5*h*
6028.87	2*h*	
6029.16	2	
6030.67	3*cw*	
6036.32	3*c*	
6039.67	10*cwl*	2*cw*
6051.19	5	1
6067.39	2*Hw*	
6068.42	2*h*	
6081.57	2*h*	
6097.20	2*h*	
6114.22	60	6
6125.47	10	2
6132.98	6*cw*	2*c*
6145.81	100*cwl*	15*cw*
6146.82	80*c*	10
6169.51	6	2
6169.20	3	
6176.57	10*cwl*	3*cw*
6181.71	3	1
6187.92	4*c*	1
6191.17	2	
6195.44	15*cwl*	3*c*
6200.734	3	1
6203.24	20*c*	4*c*
6217.97	50*c*	6
6218.74	4*cl*	1
6229.42	60*c* .50*Ws*	10*cWs*
6243.24	80*c* .60*Ws*	15*cW*
6247.44	2	
6247.70	3	1
6252.08	2	
6253.03	5	1
6254.96	1	
6255.21	1	
6260.025	20	2
6260.238	40	4
6265.07	4*cs*	1*h*
6271.37	30*c* .39*Ws*	4*cW*
6272.14	3*cw*	
6278.76	30	4
6286.41	15*cwl*	2*c*
6290.11	6*c*	1*c*
6298.35	2*c*	
6303.42	10	2
6305.97	1*h*	
6306.19	2*h*	
6307.70	400	60
6307.91	200	30
6321.90	800	100
6332.24	2*h*	
6340.65	2*cw*	
6350.64	300	20
6350.87	200	10
6362.69	2	
6362.94	3	
6373.47	10*cs*	2*c*
6374.81	10*c* .48*WI*	2*cW*
6378.60	2	
6382.94	15*c*	3*c*
6401.22	2*cw*	
6402.74	2*h*	
6405.98	20*c* .46*Ws*	2*cW*
6409.14	2*cw*	
6411.47	20	2
6416.13	2*h*	
6420.44	2*h*	
6422.24	2*h*	
6427.88	2*c*	
6436.69	3	
6449.28	8*cs*	
6462.55	2	
6501.17	5	
6502.22	7	
6510.78	3*c*	
6511.47	80*c*	
6515.25	20	
6529.21	7	
6531.11	2*h*	
6544.91	10	
6545.72	8	
6554.66	4	
6557.67	10*cwrs*	
6577.11	70*cwrs*	
6586.21	2	
6592.52	100*c* .48*Ws*	
6603.05	150*c*	
6605.33	100*c*	
6612.53	4	
6623.91	100*c*	
6637.25	30*c* .40*WI*	
6649.02	4*Hw*	
6652.39	200*c* .53*WI*	
6658.74	5	
6665.32	20*c* 6, .74*WI*	

TABLE 2. *Arc and spark spectra of rhenium*—Continued

Wavelength	Intensity and other characteristics	
	Arc	Spark
A		
6675.28	8*cwn*	
6683.28	20*cwn*	
6688.73	7*cw*	
6707.70	5*cw*	
6711.30	10*cn*	
6717.23	2	
6725.19	2	
6725.55	3*h*	
6728.98	6*c*	
6731.22	100	
6761.19	10*cw*	
6791.39	1	
6791.43	1	
6799.59	6*c* .44*Wl*	
6801.66	5	
6805.35	5*cw*	
6811.37	4	
6813.41	300*cwl*	
6816.41	2	
6829.90	300*cwn*	
6835.35	3*Hw*	
6844.06	5	
6844.44	5	
6874.35	8*cw*	
6882.11	3*c*	
6929.12	2*cl*	
6963.50	3*cw*	
6967.67	8*cwn*	
6971.53	200*cw*	
6971.98	7*cw*	
6976.67	2	
6983.20	20*c* 6, .63*Wl*	
7006.63	150*c* .46*Wl*	
7012.56	5*c* .53*Wl*	
7024.15	200*c* .37*Wd*	
7028.47	7*c* .33*Wn*	
7058.24	10*c*	
7059.98	6*c*	
7065.39	3	
7066.47	10	
7093.01	2*cw*	
7119.01	5*Bl*	
7128.98	4	
7129.45	7*c* 6, .70*Wl*	
7135.28	10	
7172.20	10	
7188.04	2	
7198.25	4	
7228.03	20	
7233.90	3*cw*	
7237.26	4*l*	
7246.49	150	
7246.80	100	
7263.86	4	
7265.43	5	
7273.84	150*c* .65*Wl*	
7292.72	300*c* .57*Wl*	
7307.55	5*c*	
7315.91	3	
7324.20	7	
7329.37	6	
7352.04	50*c* 6, .70*Wl*	
7360.95	4*hl*	
7382.67	3*cw*	
7384.07	1	
7386.35	20*c*	
7390.71	4*c* .64*Wn*	
7396.04	2*c*	
7404.28	3*h*	
7409.46	20	
7416.44	3*c*	
7431.93	2	
7437.79	2	
7440.69	4	
7442.75	1	
7447.58	4	
7478.63	5	
7481.15	7*c*	
7488.12	3*c*	
7489.10	2	

Wavelength	Intensity and other characteristics	
	Arc	Spark
A		
7494.02	2	
7524.48	10*Hw*	
7526.49	3*c*	
7536.40	2	
7545.39	5*c* .64*Wl*	
7548.72	30	
7567.80	6	
7578.73	300*c* .40*W*	
7583.26	10*c* 6, .70*Wl*	
7596.30	2	
7611.89	100	
7620.25	200*c* 6, .81*Wl*	
7640.94	400*c* .70*Wl*	
7652.3	5*Bl*	
7656.80	7	
7683.45	2	
7684.83	3	
7693.41	6	
7693.70	10*c*	
7705.92	30*c* .40*W*	
7712.58	2*c*	
7733.61	30	
7743.08	5	
7743.29	4*c*	
7789.75	7	
7789.96	10	
7794.67	5	
7799.58	3	
7801.05	4*c*	
7825.85	20	
7828.13	10	
7844.14	10*c* .40*Wl*	
7861.82	7	
7869.62	100*c* 6, .93*Wl*	
7880.56	2	
7880.78	3	
7882.11	20*c* 6, .60*Wl*	
7888.90	9	
7898.46	40	
7912.94	400*c* .60*W*	
7938.57	9	
7970.87	20	
7971.24	30	
7979.03	10	
7980.77	300*c* 6, .73*Wl*	
7985.26	3	
8004.63	4	
8024.07	2	
8027.50	4	
8052.47	2	
8055.96	5*c*	
8060.10	30*c*	
8098.27	15	
8166.63	6*c* .57*Wl*	
8224.31	3*cw*	
8246.93	4	
8253.24	2	
8253.57	2	
8262.72	5*c*	
8262.98	5*c*	
8273.56	3*h*	
8293.73	20	
8301.01	20*c* .38*Wn*	
8335.44	3	
8354.00	2	
8357.58	40*cwn*	
8399.78	10*c* .42*Wl*	
8403.58	3	
8411.59	3*h*	
8417.13	500	
8433.70	3	
8503.35	3*c*	
8507.73	6*cwn*	
8527.73	500*c* .67*W*	
8537.38	2	
8570.69	15	
8588.50	5*cw*	
8593.60	5	
8603.86	6	
8628.44	5*Hl*	

Wavelength	Intensity and other characteristics	
	Arc	Spark
A		
8630.60	7*Hw*	
8643.59	20*cw*	
8648.98	20*c* 6, 1.25*Wl*	
8675.65	40*c* 6, 1.11*Wl*	
8680.33	3	
8683.74	10	
8686.94	1	
8697.25	20*c* .49*Wl*	
8721.34	4*Hw*	
8721.88	4*Hw*	
8750.44	3*h*	
8772.49	2*h*	
8786.77	40*c* .54*W*	
8792.0	2*h*	
8797.70	30*c* .62*Wl*	
8844.57	2*cn*	
8845.23	3*cw*	
8851.32	3*c* .93*Wl*	
8871.82	1	
8882.95	15*cwn*	
8886.58	15*c*	
8899.2	2*c*	
8901.36	3*cw*	
8927.28	5	
8944.56	2	
8962.07	2	
8966.63	7*cw*	
8969.21	4	
8971.14	2	
8983.55	1	
8988.40	2	
8992.91	1	
8995.26	1	
9003.24	1	
9009.15	2*cw*	
9018.9	1	
9032.46	3	
9044.38	6	
9058.53	3	
9059.85	4	
9063.31	2	
9066.6	2*c*, 1.0*W*	
9070.74	5	
9081.45	4	
9083.03	2	
9102.47	1	
9123.76	1*c*	
9132.08	2*cw*	
9144.86	6*cw*	
9154.52	1	
9165.38	2	
9171.35	1*cw*	
9192.18	1	
9198.04	1	
9205.12	2*cw*	
9209.66	2*cw*	
9213.58	2	
9220.40	1	
9236.50	4	
9250.02	10	
9253.71	1	
9255.71	2*cw*	
9262.28	4	
9268.46	15*cw*	
9278.3	1*cw*	
9298.07	1	
9307.72	1	
9311.59	5	
9325.90	3	
9328.36	1	
9332.47	2*cw*	
9337.73	2*cw*	
9363.13	2*hc*	
9367.59	1	
9370.87	2	
9377.02	1	
9380.24	10*c*	
9383.75	40	
9391.12	2	
9400.27	2*Hl*	

UNIVERSITY OF MICHIGAN LIBRARIES

TABLE 2. *Arc and spark spectra of rhenium*—Continued

Wavelength	Intensity and other characteristics		Wavelength	Intensity and other characteristics		Wavelength	Intensity and other characteristics	
	Arc	Spark		Arc	Spark		Arc	Spark
A			*A*			*A*		
9423.45	15		9955.45	60*c*, 1.2*WI*		10593.74	2*cw*	
9427.53	3		9964.90	2		10599.31	8*cw*	
9468.38	1		9970.87	1*c*		10610.0	2*c*	
9470.15	30		9976.45	4		10618.45	40*c*	
9481.6	1*cw*		9980.9	1*c*		10625.57	8	
9500.49	8		10006.4	1*c*		10639.45	100*cw*	
9504.34	3		10010.29	1*cw*		10654.56	2*c*	
9523.40	6*cw*		10019.21	7*cw*		10725.62	1	
9564.06	1		10026.96	5*c*		10801.55	2*c*	
9571.75	6*cw*		10056.81	1		10804.3	1*c*	
9581.12	8*c*		10059.56	2*cw*		10824.22	10	
9587.0	2*Hl*		10064.02	10*c*, 2.20*W*		10862.25	10*cw*	
9591.32	3*cw*		10127.21	1		10909.5	1	
9600.98	1		10128.78	15		10919.30	1	
9617.78	2*Hl*		10138.24	2		10933.44	2*c*	
9635.30	5*c*		10146.84	1		10942.23	3*cw*	
9685.69	1		10162.75	1		10949.4	2*c*	
9704.94	3		10169.85	100*c*, 1.08*WI*		10962.5	1	
9710.52	50		10175.68	20*cw*		10967.6	1	
9722.76	4		10183.32	4*c*		11004.02	1	
9725.6	1*cw*		10191.57	1*c*		11042.96	2*cw*	
9748.60	3		10197.58	1*c*		11054.29	30	
9749.66	6		10201.86	2*cw*		11065.02	2*cw*	
9752.08	4		10206.32	20		11141.90	1	
9762.65	20		10238.26	4		11278.5	20*c*, 2.2*WI*	
9790.20	1		10242.68	1		11309.97	4*c*	
9813.75	2		10258.42	1		11383.70	8*cul*	
9831.35	9		10262.77	2		11453.12	3*c*	
9842.65	20*c*, 1.32*WI*		10282.46	5*cw*		11474.23	4	
9851.88	1		10287.58	4*cw*		11499.93	5	
9872.38	15*nd*		10329.72	1		11581.4	1*c*	
9884.10	2*cw*		10332.55	10*cw*		11615.8	1*c*	
9901.72	1		10341.3	1		11788.9	1	
9903.30	5*c*		10349.0	4*c*				
9908.97	4*c*		10440.92	3				
9921.7	1*cw*		10464.25	10				
9937.8	1		10492.3	1				
9943.70	20		10556.54	20*c*				
9949.90	20*c*, 1.8*WI*		10579.7	1				
9953.02	3*cw*		10589.7	1				

WASHINGTON, D. C., March 26, 1952.

Journal of Research of the National Bureau of Standards Vol. 49, No. 3, September 1952 Research Paper 2356

Hydraulic Resistance Effect Upon the Dam-Break Functions*

Robert F. Dressler

The dam-break solution, a known centered simple-wave when resistance is neglected, is studied with the Chezy resistance formula added to the nonlinear shallow-water equations. Resistance transforms the wavefront from a characteristic curve into an envelope of characteristics. The flow near the tip differs from the other parts, due to a distinct boundary-layer type of region adjacent to the wavefront envelope. Then a perturbation leads to a system of partial differential equations with variable coefficients. Initial conditions are derived for the singularity at the origin. By studying its characteristic equations, this system is solved explicitly for the correction functions. Except at the tip, resistance raises the water surface and lowers velocities. These functions, no longer simple-waves, possess concurrent straight characteristic lines that map into another set of the same type. The critical flow locus moves downstream, faster for more resistance, and discharge rates are reduced. The method fails in the tip layer because the asymptotic expansions for the first derivatives lose validity there. Estimates are made indirectly for the wavefront velocity by observing where the boundary-layer effect becomes predominant.

1. Introduction

Sudden destruction of a dam results in a highly unsteady flow, with a forward wave (the "positive" wave) advancing over a dry channel, and a back disturbance (the "negative" wave) propagating into the still water above the dam. We consider a two-dimensional problem, a horizontal stream bed, with initially no water below the dam and water at rest above the dam. An explicit solution to this problem was given in 1892 by Ritter [1][1] by applying certain general expressions of Saint Venant [2]. The equations used were the usual approximate ones involving small curvature, due to Saint Venant, often called the nonlinear shallow-water equations.

The problem under consideration possesses genuine practical significance, not merely for the applications involving dynamiting of dams through military action, for example, the destruction in 1941 by Russian engineers of the Dnieprostroy Dam (140 feet high) near Kichkas on the Dnieper River, and the occasional mechanical failure, for example, the St. Francis Dam (205 feet high) in California, which broke in 1928 because of defective geologic foundations, causing the loss of hundreds of lives and immense property damage, but also for the more common occurrences, such as the opening of canal and sluice gates and controls at hydroelectric stations. The problem is most important, however, because of the information desired about the basic question of the behavior of any wave advancing along a dry channel, concerning which very little work has been done so far.

In the case of a wave advancing into still water of appreciable depth, the problem can be handled by approximating the flow with the discontinuity conditions of mass, momentum, and energy for a bore. In that case, one evaluates the relation between hydrostatic forces and rate of change of momentum at the wavefront. For our present case, however, this is not possible; rather, the controlling factor in the propagation of the wave is the hydraulic resistance caused by stream bed friction and turbulence. This effect will predominate especially in the shallow front region of the flow. For this reason the classical solution of Ritter, which neglects resistance, is not realistic. It should, therefore, be significant to initiate some study on the effects of resistance upon this unsteady flow. Forchheimer [3] has presented a summary of most previous work on the dam-break problem.

The experiments of Schoklitsch [4] indicate that actual velocities for the forward wave may be as low as 40 percent of the theoretical result given by Ritter's solution without resistance, whereas the experimental and theoretical results agree for the tip of the negative wave. Thus it is clear that the forward part of the flow is highly sensitive to hydraulic resistance, and it is our present purpose to deduce some approximate quantitative information of this effect by considering the equations containing the resistance term. Experiments of Eguiazaroff [5] likewise confirm the above observations; in his report, the author remarks about the almost complete absence of data concerning the propagation of a wave over dry land.

One can determine analytically the exact wavefront velocity (neglecting resistance) for the case where the bottom is inclined below the horizontal. We will study here, however, only the horizontal case, since the resistance predominates over the slope effect for the usual small slopes occurring in nature. Both effects could be handled simultaneously by the present approach, but since it is only the resistance term that seriously complicates the equations, the slope will be ignored.

In 1946 Ré [6] computed, by a finite-difference calculation on the characteristic equations, the flow to be expected from the destruction of a dam, for one specific value of slope and Chezy resistance coefficient. This was done in anticipation of possible destruction of a dam at the German-Swiss frontier in World War II. Ré's problem included the presence of some water below the dam initially, causing the formation of a bore in his solution.

* The preparation of this paper was sponsored (in part) by the Office of Naval Research.

[1] Figures in brackets indicate the literature references at the end of this paper.

UNIVERSITY OF MICHIGAN LIBRARIES

2. The Basic Equations

We first define the problem in dimensional quantities (denoted by bars) and then transform immediately to dimensionless variables (unbarred). Let $\overline{Y}$ denote the height of the dam, and let the horizontal direction downstream from the dam be measured by $\overline{x}$. Upstream the water is at rest until time $\overline{t}=0$. Let $\overline{y}$ be the vertical distance of the water surface above the bed and $\overline{u}$ the horizontal component of velocity. Introducing $\overline{c}=\sqrt{g\overline{y}}$, the momentum and continuity equations used are

$$\frac{\partial \overline{u}}{\partial \overline{t}}+\overline{u}\frac{\partial \overline{u}}{\partial \overline{x}}+2\overline{c}\frac{\partial \overline{c}}{\partial \overline{x}}+\overline{R}\left(\frac{\overline{u}}{\overline{c}}\right)^2=0,$$

$$\overline{c}\frac{\partial \overline{u}}{\partial \overline{x}}+2\frac{\partial \overline{c}}{\partial \overline{t}}+2\overline{u}\frac{\partial \overline{c}}{\partial \overline{x}}=0, \qquad (1)$$

containing the Chezy resistance term, in which the roughness coefficient $\overline{R}$ has dimensions of acceleration. Neglecting resistance, the well-known Ritter solution is

$$\overline{u}^0=\frac{2}{3}\left(\frac{\overline{x}}{\overline{t}}+\overline{H}\right)$$

$$\overline{c}^0=\frac{1}{3}\left(2\overline{H}-\frac{\overline{x}}{\overline{t}}\right), \qquad (2)$$

where $\overline{H}=\sqrt{g\overline{Y}}$. This defines the parabolic surface profile for any fixed $\overline{t}$, with the negative wave propagating upstream at velocity $-\sqrt{g\overline{Y}}$, and the forward wave advancing at velocity $2\sqrt{g\overline{Y}}$. This profile always intersects the line $\overline{x}=0$ at height $\overline{y}=(4/9)\ \overline{Y}$ with $\overline{u}=(2/3)\ \overline{H}$, giving the constant discharge rate $\overline{Q}=\overline{u}\,\overline{y}=(8/27)\ (\overline{H}^3/g)$. The wave tip at $\overline{c}=\overline{y}=0$ has a horizontal tangent at all times, whereas it is known experimentally that the wavefront is actually vertical.

Transforming to dimensionless notation by the relations

$x=(g/\overline{H}^2)\overline{x}$, $t=(g/\overline{H})\,\overline{t}$, $u=\overline{u}/\overline{H}$, $y=\overline{y}/\overline{Y}$, $c=\overline{c}/\overline{H}$, $R=\overline{R}/g$, $Q=(g/\overline{H}^3)\,\overline{Q}$, and $m=x/t$, the equations become

$$\frac{\partial u}{\partial t}+u\frac{\partial u}{\partial x}+2c\frac{\partial c}{\partial x}+R\left(\frac{u}{c}\right)^2=0,$$

$$c\frac{\partial u}{\partial x}+2\frac{\partial c}{\partial t}+2u\frac{\partial c}{\partial x}=0, \qquad (3)$$

for which the Ritter solution at $R=0$ becomes

$$u^0=\frac{2}{3}\left(\frac{x}{t}+1\right),$$

$$c^0=\frac{1}{3}\left(2-\frac{x}{t}\right). \qquad (4)$$

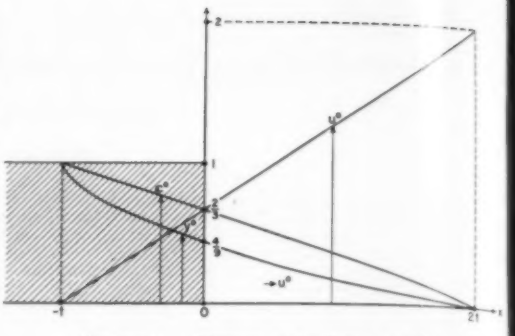

FIGURE 1. *Diagram of the Ritter solution.*

At the site, $x=0$, $y=4/9$, $u=2/3$, and $Q=8/27$ (fig. 1).

The characteristic equations equivalent to system (3), when $R=0$, are

$$I_+: \frac{dx}{dt}=u^\circ-c^\circ,$$

$$I_-: \frac{dx}{dt}=u^\circ+c^\circ,$$

$$II_+: d(u^\circ-2c^\circ)=0, \qquad (5)$$

$$II_-: d(u^\circ+2c^\circ)=0,$$

defining two families γ_+ and γ_- of characteristic curves, along which the corresponding relations given above must hold. A study of these equations produces the Ritter solution by utilizing the solutions for the characteristic curves, which are

$$\gamma_+: x=mt,$$

$$\gamma_-: x=2t-3a^{2/3}t^{1/3}, \qquad (6)$$

where m and a are parameters. The γ_- curves pass through the points $(-a,\ a)$. Since the γ_+ curves are concurrent straight lines through the origin in the x, t plane, the Ritter solution exemplifies what is now commonly called a "centered simple-wave." This simple-wave interpretation of the dam-break solution is discussed in Courant-Friedrichs [7] and Stoker [8]. Figure 2, A, shows the familiar pattern of characteristics for this solution given by (4), (5), and (6). Line OB marks the propagation of the disturbance into the still water, while OF is the trajectory of the forward wavefront, along which $c^\circ=0$. Therefore by (5) the two characteristic directions coincide along OF, which must belong to both the γ_+ and γ_- families. This means the solution of (3) with $R=0$ degenerates from hyperbolic to parabolic type along the boundary defined by the forward wavefront double characteristic.

As the resistence R changes from zero to a positive value, it will distort all the characteristics lying to the right of OB, as shown qualitatively in figure 2, B.

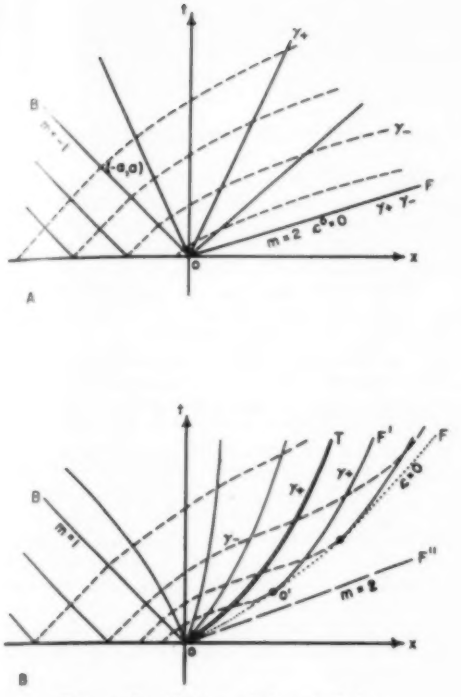

FIGURE 2. *Pattern of characteristics.*
A, Without resistance; B, with resistance.

The characteristic equations for R>0 become

$$I_+: \frac{dx}{dt} = u - c, \qquad I_-: \frac{dx}{dt} = u + c, \tag{7}$$

$$II_+: c^2(u-2c)_\alpha = -Ru^2 t_\alpha, \qquad II_-: c^2(u+2c)_\beta = -Ru^2 t_\beta, \tag{8}$$

introducing characteristic parameters α and β, which vary along γ_+ and γ_-, respectively. Equations (8) can be written in simpler notation as

$$II_+: d(u-2c) = -R\left(\frac{u}{c}\right)^2 dt, \qquad II_-: d(u+2c) = -R\left(\frac{u}{c}\right)^2 dt. \tag{9}$$

The characteristics for this solution in the region of motion are now unknown. In the still-water region upstream where $u \equiv 0$, γ_+ and γ_- have slopes $dx/dt = +1$, respectively; hence they become straight lines here. Because the disturbance emanating from the origin will be carried as a derivative discontinuity along a γ_+ curve from (0, 0), on this curve we still have $u=0$, $c=1$, and therefore OB remains straight with slope -1. Resistance will decrease the forward wave velocity, turning the wavefront curve OF above the straight line $m=2$.

If R has any nonzero value, however small, it is seen in (3) that certain terms must become infinite at the wavefront, where $c=0$, to maintain the equality. It is experimentally known, or can be seen from these equations, that $c_x \to -\infty$ at the tip, that is, a vertical wavefront is maintained. Likewise, $c_t \to +\infty$, while u, u_x, and u_t remain bounded. This singular behavior of these derivatives will cause complications in the subsequent analysis. If the variable hydraulic radius were not present in the denominator of the resistance term, the entire problem would be basically simpler. In a somewhat similar way, it is this variable denominator that produces instability in a uniform flow and creates the possibility of roll-wave formation (see [9] and [10].)

The eq (3) used here are based upon hydrostatic pressure (negligible vertical accelerations or streamline curvature), and the question arises concerning their validity to describe the flow in the tip region. With $c_x \to -\infty$, the profile curvature becomes large, but the depth of water becomes zero, so that their product for the actual flow may stay small. Friedrichs [11] has shown that eq (3) apply when this product is small. Alternatively, one sees from experiment that the wave tip moves along somewhat like a separate mass of nearly fixed shape, with vertical accelerations therefore possibly negligible. In any case we wish to study the mathematical implications of (3) when applied to the dam-break problem.

In order to justify why the characteristic pattern should be as shown in figure 2, B, we will consider the following argument. Let the wavefront OF be defined as the locus, where $c=0$. It is implicit in the basic eq (3) that particles at the tip always remain at the tip, hence the velocity, u, evaluated along OF must always equal the reciprocal slope dx/dt of the line OF. Each of eq (7) is then satisfied by the wavefront curve; and at every point of OF, both characteristic directions γ_+ and γ_- coincide with the direction of OF. This line cannot be a characteristic curve itself, however, since neither of relations (9) can hold along OF for any $R>0$. Therefore, it must be an envelope of γ_+ and γ_- curves (fig. 2, B). Since the reflected γ_+ curves of class O′F′ cannot intersect each other, they must approach some limit line OT as O′→O. Three patterns therefore arise: (a) OT coincides with OB, (b) OT lies in the interior of section BOF, entering O at some intermediate angle between OB and OF, (c) OT is interior to BOF and enters O at the same angle as OF and OF″. Case (c) is shown in figure 2, B, because the following discussion indicates that (a) and (b) are not possible. We assume that the dam-break functions $u\ (x, t, R)$ and $c\ (x, t, R)$ are continuous in R at $R=0$ (but not necessarily so for their derivatives). Then the characteristic directions given by (7) will be continuous in R, and their curves must distort continuously as $R \to 0$.

UNIVERSITY OF MICHIGAN LIBRARIES

If we transform to new variables by $x=x^*/\mathrm{K}$, $t=t^*/\mathrm{K}$ with $u\,(x,t)=u^*\,(x^*,t^*)$, $c\,(x,t)=c^*\,(x^*,t^*)$, defining a radial stretching centered at the origin with constant magnification K, eq (3) transform to

$$\frac{\partial u^*}{\partial t^*}+u^*\frac{\partial u^*}{\partial x^*}+2c^*\frac{\partial c^*}{\partial x^*}+\left[\frac{R}{\mathrm{K}}\right]\left(\frac{u^*}{c^*}\right)^2=0,$$

$$2\frac{\partial c^*}{\partial t^*}+2u^*\frac{\partial c^*}{\partial x^*}+c^*\frac{\partial u^*}{\partial x^*}=0.$$

These equations are identical (in the starred quantities) with (3) except for the resistance coefficient. Hence the effect of letting $\mathrm{K}\to\infty$, R fixed, increasing the stretching, is equivalent to the effect on the original quantities when $R\to 0$. The characteristic pattern for $R>0$ must therefore approach by continuous radial stretching the known limit pattern for $R=0$ (fig. 2, A). This is possible only for case (c). The limit chracateristic OT can now be used as a definition for the beginning of the tip layer TOF and as the separation line for this boundary-layer effect.

To obtain some quantitative results, we let the unknown solutions u and c to eq (3) be represented as asymptotic expressions of form

$$\begin{aligned} u(x,t,R)&\sim u^0(x,t)+U(x,t)R+u^{(2)}R^2+\ \ldots \\ c\,(x,t,R)&\sim c^0(x,t)+C(x,t)R+c^{(2)}R^2+\ \ldots, \end{aligned} \tag{10}$$

where u^0, c^0 is given by (4). Because of the above remarks about $\partial c/\partial x$ and $\partial c/\partial t$ at the wave tip for any $R>0$, whereas $\partial c^0/\partial x$ and $\partial c^0/\partial t$ stay finite, it follows that the derived expansions $\partial c/\partial x\sim\partial c^0/\partial x+\ldots$, and $\partial c/\partial t\sim\partial c^0/\partial t+\ \ldots$, cannot remain valid in the neighborhood of the wave tip. That is, the perturbation procedure based upon (10) becomes singular near the line OF, and from this standpoint also we see that some type of boundary-layer complication must develop there. Therefore these calculations, using the correction functions U and C, cannot be applied directly to the wavefront layer.

Substituting (10) into (3) and equating terms independent of R produce eq (3) with $R=0$ and their solution (4). At the next step, using terms of first degree in R, the equations defining $U(x,t)$ and $C(x,t)$ become, by (4),

$$2\left(1+\frac{x}{t}\right)\frac{\partial U}{\partial x}+3\frac{\partial U}{\partial t}+2\left(2-\frac{x}{t}\right)\frac{\partial C}{\partial x}+\frac{2}{t}U-\frac{2}{t}C+3\left(\frac{1+\frac{x}{t}}{1-\frac{x}{2t}}\right)^2=0 \tag{11}$$

$$\left(2-\frac{x}{t}\right)\frac{\partial U}{\partial x}+4\left(1+\frac{x}{t}\right)\frac{\partial C}{\partial x}+6\frac{\partial C}{\partial t}-\frac{2}{t}U+\frac{2}{t}C=0.$$

In order to solve this nonhomogeneous system with variable coefficients, we will first derive the appropriate initial and boundary conditions and then study the associated characteristic equations.

3. Initial and Boundary Conditions for U, C

At the initial moment of breakage, the water height and the velocity are multivalued at $x=0$. This means that the full solution u, c with resistance has a singularity at the origin; the lowest order approximation u^0, c^0 possesses a singularity there also. Will there likewise be singularities in the higher order terms at (0, 0), or is the entire effect contained in u^0, c^0? In order to get the procedure started in his finite-difference calculations, Ré [6] assumed that the flow could be considered initially as two finite shocks, one positive and one negative. When our problem is considered as defined by (3) with $R>0$, since the velocity starts off discontinuously with nonzero values, the opposing force $-R(u/c)^2$ must become operative instantaneously. Although it has already been indicated that resistance effects on u and c can be ignored in the immediate neighborhood of the origin, a more detailed discussion will also be made now for the behavior of U and C there.

Let the limit values be u_t, c_t for the solutions u, c as we approach the origin along a curve with a limiting slope m_t. By (4),

$$\begin{aligned} u_t^0&=\frac{2}{3}m_t+\frac{2}{3}, \\ c_t^0&=\frac{2}{3}-\frac{1}{3}m_t. \end{aligned} \tag{12}$$

For example, as we approach (0, 0) along OB (fig. 2, A), $c_t^0=1$; along OF, $c_t^0=0$; and intermediate values result for an approach within region BOF. For all such approaches, by (12), $u_t^0+2c_t^0\equiv 2$ through the origin point, consistent with the characteristic relation $d(u^0+2\,c^0)=0$ for γ_- in (5). One may consider this origin point to be stretched out into a γ_- characteristic curve, with c^0 varying continuously from 1 to 0 along this curve from left to right.

Now going over to the full problem with $R>0$ (fig. 2, B), we likewise consider point O to be stretched into the arc MN, shown schematically in figure 3. Interpreting the curve MNF as a γ_- characteristic, the relation holding along it by (9) is

$$d(u+2c)=-R\left(\frac{u}{c}\right)^2dt \tag{13}$$

if $c\neq 0$; but $c=0$ only at N. Hence (13) is applicable on MN, along which $dt=0$. This means $u+2c$ is constant along MN, and so

$$u_t+2c_t=2. \tag{14}$$

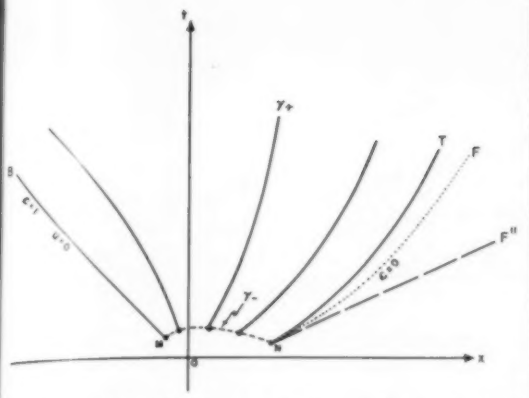

FIGURE 3. *Schematic diagram of characteristics at origin.*

Approaching MN along any γ_+ curve,

$$m_i=\lim \frac{dx}{dt}=u_i-c_i \tag{15}$$

by (7). The solution of (14) and (15) is

$$u_i=\frac{2}{3}\,m_i+\frac{2}{3},$$

$$c_i=\frac{2}{3}-\frac{1}{3}\,m_i, \tag{16}$$

Using (10), $u_i=\lim\ (u^0+U\ R+.\ .\ .)$, we obtain by (12)

$$U_i=0, \qquad C_i=0, \tag{17}$$

which are the desired conditions on U and C at the origin. This result shows that the resistance effects on the main solution can be ignored at the initial instant.

The relations $c(-t,t,R)\equiv 1$, $u(-t,t,R)\equiv 0$, previously discussed, give the necessary data for U and C along line OB. The use of these with (10) yields

$$C(-t,t)\equiv 0, \qquad U(-t,t)\equiv 0. \tag{18}$$

4. The Solution for U and C

To obtain a clue for solving most easily for U and C subject to the conditions just derived, we now study the characteristic equations equivalent to system (11), which are

$$\mathrm{I}_+: \frac{dx}{dt}=u^0-c^0,$$

$$\mathrm{I}_-: \frac{dx}{dt}=u^0+c^0,$$

$$\mathrm{II}_+: d(U-2C)=\left[\frac{4}{3t}(C-U)-\left(\frac{1+\frac{x}{t}}{1-\frac{x}{2t}}\right)^2\right]dt, \text{ if } \frac{x}{t}<2.$$

$$\mathrm{II}_-: d(U+2C)=-\left(\frac{1+\frac{x}{t}}{1-\frac{x}{2t}}\right)^2 dt, \text{ if } \frac{x}{t}<2. \tag{19}$$

The characteristics are the same as (6) for u^0, c^0 (fig. 2, A), but now the relations along them are more complicated. Relation II_- has the right side independent of the unknown, and can therefore be integrated along the γ_- curves, using (6) and (18). The resulting integral along γ_- becomes

$$\frac{U+2C}{a}=\frac{32}{35}-4\left(\frac{t}{a}\right)\left[\frac{3}{7}\left(\frac{t}{a}\right)^{4/3}-\frac{6}{5}\left(\frac{t}{a}\right)^{2/3}+1\right]. \tag{20}$$

This equation used with II_+ of (19) now indicates how to solve explicitly for U and C as follows.

If we move out from the origin along a straight γ_+ characteristic, the value of t at an intersection with a γ_- curve emanating from $(-a,\ a)$ must be proportional to a. This is immediately seen since the equations for the two curves can be written in the form $(x/a)=m\ (t/a)$ and $(x/a)=2(t/a)-3(t/a)^{1/3}$. Now by (20), the quantity $(U+2C)/a$ is a function of t/a, which is constant along each γ_+ ray. Therefore, $U+2C$ is also proportional to a along the ray, and so $U+2C$ must be proportional to t there. Next we observe in the II_+ relation of (19) that $U-2C$ would likewise be proportional to t along a γ_+ ray if the term $(4/3t)\ (C-U)$ were a constant there; then each of the quantities U and C would separately be proportional to t. But this would then be sufficient to make $(4/3t)(C-U)$ constant as required. Therefore the solutions U, C must actually be linear in t along each γ_+ ray, since this will also satisfy the condition (17) at the origin. With this information, the original system (11) can now be solved explicitly, subject to the other boundary condition along OB.

We transform to the new independent variables m and t, putting $C(x,t)=\tilde{C}(m,t)$ and $U(x,t)=\tilde{U}(m,t)$. Then (11) transforms to

$$\frac{2-m}{t}\frac{\partial\tilde{U}}{\partial m}+3\frac{\partial\tilde{U}}{\partial t}+\frac{2(2-m)}{t}\frac{\partial\tilde{C}}{\partial m}+\frac{2}{t}\tilde{U}-\frac{2}{t}\tilde{C}+3\left(\frac{1+m}{1-\frac{m}{2}}\right)^2=0,$$

$$\frac{2-m}{t}\frac{\partial\tilde{U}}{\partial m}+\frac{2(2-m)}{t}\frac{\partial\tilde{C}}{\partial m}+6\frac{\partial\tilde{C}}{\partial t}-\frac{2}{t}\tilde{U}+\frac{2}{t}\tilde{C}=0, \tag{21}$$

with $\tilde{U}(-1,t)\equiv\tilde{C}(-1,t)\equiv 0$ for condition (18). Introduction of $\tilde{U}=h(m)t$ and $\tilde{C}=k(m)t$ leads to the system

$$(2-m)\frac{dh}{dm}+5h+2(2-m)\frac{dk}{dm}-2k+3\left(\frac{1+m}{1-\frac{m}{2}}\right)^2=0,$$

$$(2-m)\frac{dh}{dm}-2h+2(2-m)\frac{dk}{dm}+8k=0. \tag{22}$$

UNIVERSITY OF MICHIGAN LIBRARIES

This possesses the solution, for $h(-1)=k(-1)=0$,

$$h(m)=-\frac{108}{7(2-m)^2}+\frac{12}{2-m}-\frac{8}{3}+\frac{8\sqrt{3}}{189}(2-m)^{3/2},$$

$$k(m)=\frac{6}{5(2-m)}-\frac{2}{3}+\frac{4\sqrt{3}}{135}(2-m)^{3/2}. \tag{23}$$

The desired quantities U, C are then given by ht, kt, respectively.

The characteristic eq (19) have thus furnished an easy method for obtaining the particular solution U, C. It would have been possible, however, to solve the original system (11) first for its general solution, but with much more difficulty. This general solution to (11) is

$$U(x,t)=-\frac{2}{t}\Psi\left(\frac{x}{t}\right)-\left(\frac{108}{7\left(2-\frac{x}{t}\right)^2}-\frac{12}{2-\frac{x}{t}}+\frac{8}{3}\right)t+\Phi(\tau),$$

$$C(x,t)=\frac{1}{t}\Psi\left(\frac{x}{t}\right)+\left(\frac{6}{5\left(2-\frac{x}{t}\right)}-\frac{2}{3}\right)t+$$

$$\frac{\delta}{\tau}+\frac{1}{2}\Phi(\tau)+\frac{1}{2\tau}\int^{\tau}\Phi(\xi)d\xi,$$

where Ψ and Φ are arbitary functions, δ is an arbitrary constant, and $\tau=(2-x/t)t^{2/3}$. In order to keep the corrections finite at the origin, one must select $\Psi\equiv 0$ and $\delta=0$. These expressions for the general solution indicate in an alternative manner the correctness of our conditions (17) at the origin, since we can now see that no other finite values except $U_t=C_t=0$ could be prescribed there. Then conditions (18) along line OB require the selection $\Phi(\tau)=(8\sqrt{3}/189)(2-x/t)^{3/2}t$. The resulting particular solutions are seen to be identical with those previously given by (23).

These particular solutions U and C no longer define a centered simple-wave (as for u°, c° for which the maps of all the x, t characteristics fall on one Γ curve in the u, c plane), but rather define what might be called a "centered seimilinear wave". The map of its characteristics is shown in figure 4. For these solutions it is clear that the γ_+ straight lines in figure 2, A, must map into a pencil of straight lines Γ_+ through the origin (fig. 4). The γ_- family goes over into curves Γ_- (dotted in fig. 4) also concurrent at the origin. The line OB and the origin in the x, t plane map into the single point (0, 0) in the U, C plane. All of the curves remain inside the wedge formed by AO (with slope $-\frac{1}{2}$) and the negative U axis.

The dam-break solution with first order resistance correction is then

$$u(x,t,R)\sim\frac{2}{3}(1+m)+h(m)tR+\ \ldots,$$

$$c(x,t,R)\sim\frac{1}{3}(2-m)+k(m)tR+\ \ldots, \tag{24}$$

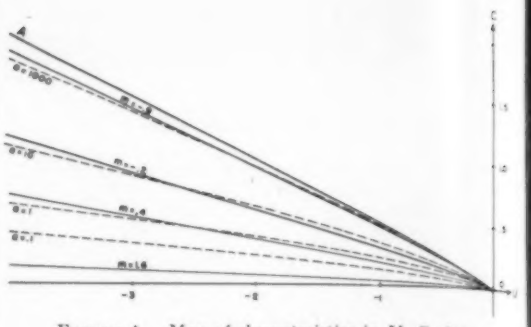

FIGURE 4. *Map of characteristics in U, C plane.*

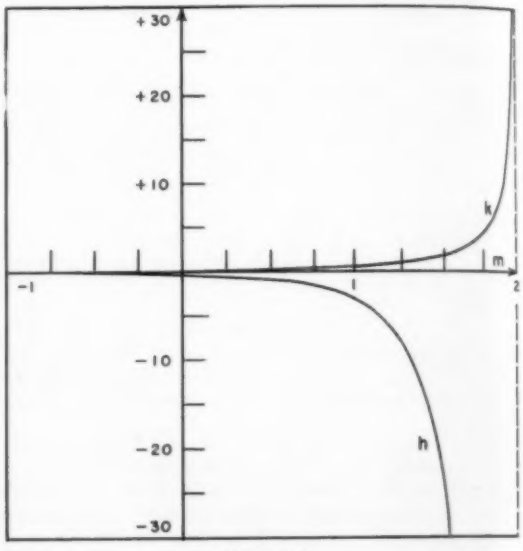

FIGURE 5.

with h, k defined in (23) and $m=x/t$. Up to first-order terms, the solutions depend only upon the product $tR=\sigma$. Both h and k have poles at $m=2$ due to the tip effect; the behavior of these functions is shown in figure 5. It is seen that resistance causes a much greater effect upon the velocity than upon c or the height, since $|h|$ greatly exceeds k.

For a fixed R, (23) implies that the value given by (24) for u must eventually become negative as we go far enough out from the origin along any γ_+ curve. Thus the asymptotic validity of our series weakens with increasing distance from the origin, as the U, C characteristics diverge further from the true characteristics of figure 2, B. For all numerical results presented here, the calculations have been restricted arbitrarily to a region comprising less than one-third the distance to the points where the series would indicate a zero value for u.

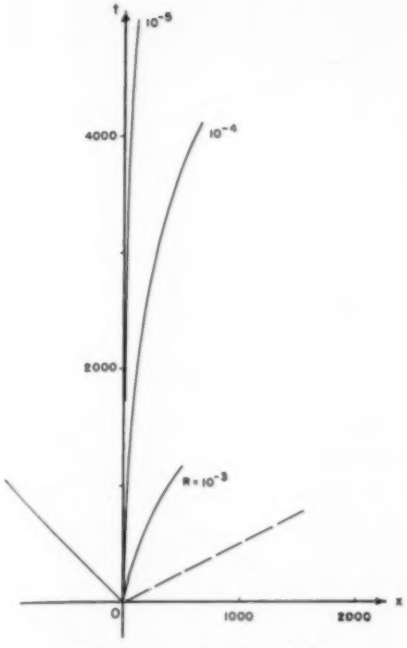

FIGURE 6. *Locus of critical flow.*

5. Locus of Critical Flow

In the u°, c° solution, the flow always remains critical (where $\bar{u}=\sqrt{g\bar{y}}$ or $u=c$) for all $t>0$ at $x=0$, with subcritical flow for $x<0$ and supercritical for $x>0$. The resistance will distort this critical flow locus. To calculate it, we denote the locus where $u=c$ by $x=s(t,R)\sim S(t)R+s^{(2)}(t)R^2+\ldots$, since $s^0(t)\equiv 0$. Using the relation $u(s[t,R],t,R)\equiv c(s[t,R],t,R)$ we obtain

$$u^\circ(s[t,R],t)+U(s[t,R],t)R+\ldots$$
$$\equiv c^\circ(s[t,R],t)+C(s[t,R],t)R+\ldots, \qquad (25)$$

and then expand each function in this identity in a series about $x=0$. Equating terms of first order in the resulting double series gives the result $S(t)=f[C(0,t)-U(0,t)]$. The equation of the locus of critical flow correct to first order is therefore the parabola

$$x=[k(0)-h(0)]Rt^2\doteq 0.395Rt^2. \qquad (26)$$

Figure 6 shows this locus for various values of R within extreme practical limits. We observe that the critical flow position moves continually downstream, and the resistance increases the proportion of the total flow which is subcritical.

We note parenthetically that this double series method cannot be utilized to obtain the locus of the wavefront because of the tip effect. If one designates by $x=z(t,R)$ the locus where $c=0$, with $z\sim 2t+\mathcal{Z}(t)\,R+\ldots$, and $u(z,t,R)\equiv z_t$, one would compute in this manner the formal results

$$\mathcal{Z}(t)=3tC(2t,t)=t^{2/3}\int_0^t U(2\tau,\tau)\tau^{-2/3}d\tau,$$

which are undefined in this case because of the singularities of U and C along the line $x=2t$.

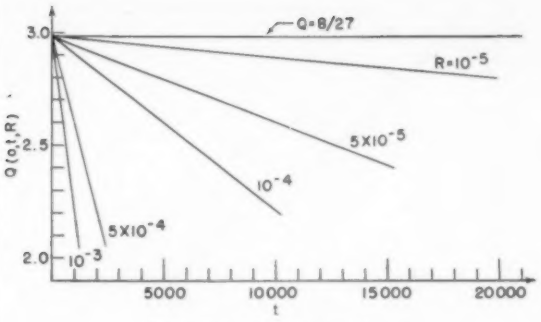

FIGURE 7. *Discharge rates.*

6. The Discharge Rate

From the dimensional discharge rate $\overline{Q}=\bar{u}\ \bar{y}$, we define $Q=(g/\overline{H}^5)\overline{Q}=u\ c^3$, the corresponding dimensionless quantity. For the discharge rate at the site of the dam,

$$Q(0,t,R)\doteq\left[\frac{2}{3}+U(0,t)R\right]\left[\frac{2}{3}+C(0,t)R\right]^3,$$

which becomes, after neglecting terms above first order,

$$Q(0,t,R)\doteq\frac{8}{27}(1-0.239tR). \qquad (27)$$

Figure 7 presents these data for various resistances.

7. Approximations for the Wavefront

We see from the experimental profiles obtained by Schoklitsch [4], converted into dimensionless form by Keulegan [12], figure 8, that the dam-break wave actually governed by resistance has a vertical slope at the tip. As previously discussed here, eq (3) shows that $|c_x|$ and $|y_x|$ become infinite when $c=0$. In the region where $|c_x|$ begins to grow large, our expansions lose validity and the present method of attack breaks down. To handle the tip region accurately, some type of boundary-layer technique would be necessary. This is being investigated at present, but no results are yet available. Figure 9 illustrates schematically this spearation of the two regions, with T marking the transition zone. For present purposes, this point T of transition will be described merely as a point where $|c_x|$ and $|y_x|$ begin to grow large rapidly.

UNIVERSITY OF MICHIGAN LIBRARIES

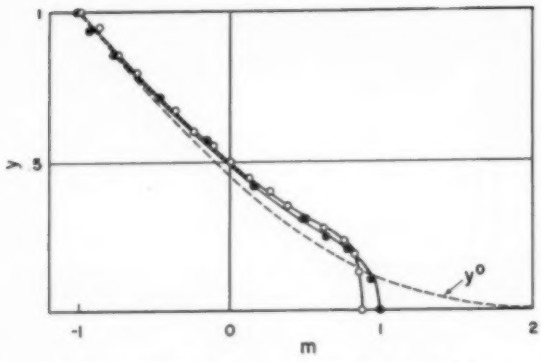

FIGURE 8. *Wave profiles according to Schoklitsch.*
● $t=43$; ○ $t=109$.

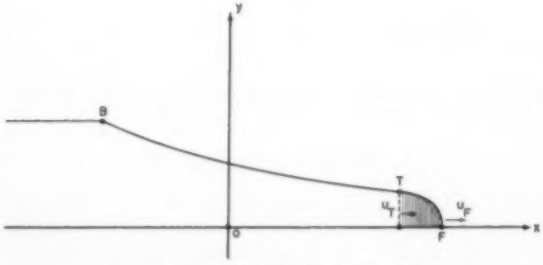

FIGURE 9. *Velocities in the wave tip.*

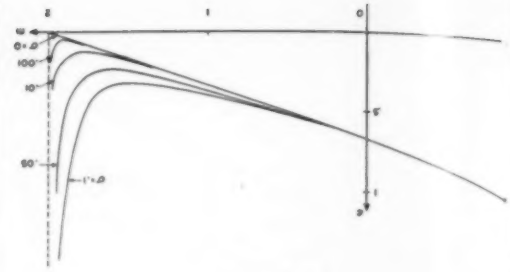

FIGURE 10.

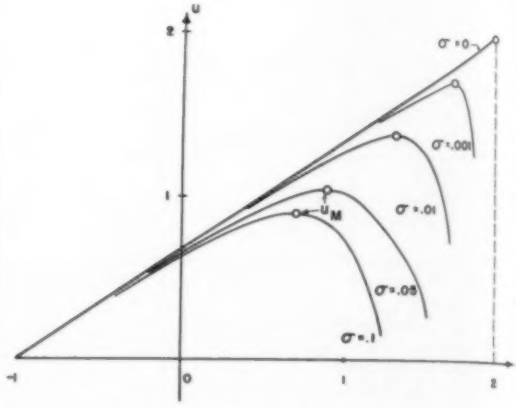

FIGURE 11.

In the absence of any more satisfactory boundary-layer results, we will apply the following approximate considerations to obtain some data about the wavefront. This rough method seems justifiable since there appear to be no other theoretical data and almost no experimental data available on this problem.

We visualize the tip region to be moving somewhat like a separate entity pushed along by the water behind it, and in the tip, u should be changing (increasing) rather slowly toward the front. Hence u_T could be taken as an approximation for u_F.

Next we make the following approximation for u_T. The results in (24) are graphed in figures 10 and 11. Each curve corresponds to a particular value of the parameter $\sigma=Rt$. The c curves, being based upon expressions that lose validity toward the tip, reach a minimum and then turn upward. Analogously, each u curve attains a maximum. Since the true values for c and u should not increase or decrease, respectively, toward the tip, these extremal points must lie already in the tip region. As estimates for u_T we will take u_M, the maximum values of u, indicated by the small circles in figure 11. Actually the tip region will begin before these maximum points are obtained, thus making the approximation too high; but if u_M is now taken as an approximation to u_F, since $u_T<u_F$, these effects will partly compensate for each other to improve the accuracy of the approximation. In figure 11 the locus of maximum points defines a function $\sigma(m)$. Using $\partial u(m,\sigma)/\partial m\equiv 0$, this relation is found to be

$$\sigma(m)=\left(6\left[\frac{54}{7(2-m)^3}-\frac{3}{(2-m)^2}+\frac{\sqrt{3}}{63}(2-m)^1\right]\right)^{-1}. \tag{28}$$

Using (24), the value $u_M=u(m(\sigma),\sigma)$ where $m(\sigma)$ is the inverse function in (28). Applying this as an estimate for the wavefront velocity, these values are graphed in figure 12 as functions of t, with R as a parameter over the limits of the practical range. All the curves must leave the point (2, 0) with vertical tangents.

To obtain the corresponding estimate for the trajectory of the wavefront, the velocity curves of figure 12 are integrated to give the position of the tip in the x,t plane, with R as parameter (fig. 13).

A series of experiments is contemplated here at the National Hydraulic Laboratory to check the validity of the analysis presented and to investigate in more detail the actual behavior of water particles at the tip of a positive wave advancing over a dry channel.

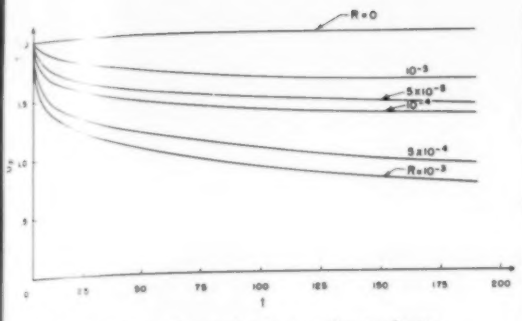

FIGURE 12. *Approximate wave-front velocity.*

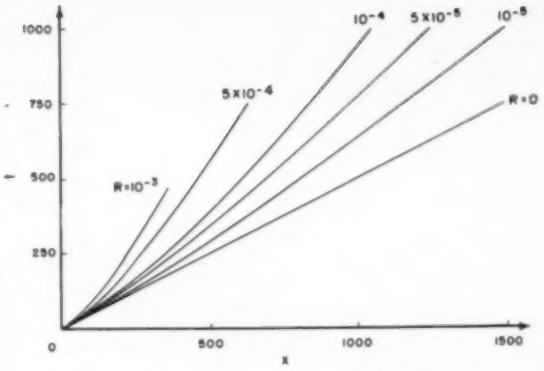

FIGURE 13. *Approximate wave-front trajectory.*

8. References

[1] A. Ritter, Die Fortpflanzung der Wasserwellen, Z. Ver. deut. Ing. **36** (1892).

[2] B. de Saint Venant, Théorie du movement non permanent des eaux, Compt. rend. **73** (1871).

[3] Philipp Forchheimer, Hydraulik, (Teubner, Leipzig, 1930).

[4] A. Schoklitsch, über Dambruchwellen, Sitzber. Akad. Wiss. Wien. **126** (1917).

[5] I. B. Eguiazaroff, Regulation of the water level in the reaches of canalized rivers, XVI International Congress of Navigation, Brussels (1935).

[6] Ré, Étude du lacher instantane d'une retenue d'Eau dans un canal par la méthode graphique, (La Houille Blanche, May 1946).

[7] R. Courant and K. O. Friedrichs, Supersonic flow and shock waves, (Interscience, New York, 1948).

[8] J. J. Stoker, Formation of breakers and bores, Communications on Applied Mathematics **I,** No. 1 (New York University, 1948).

[9] R. F. Dressler, Roll-waves in inclined open channels, Communications on Applied Mathematics **II,** No. 2/3 (New York University, 1949).

[10] R. F. Dressler, Stability of uniform flow and roll-wave formation, Symposium on Gravity Waves, NBS Circular 521 (in press).

[11] K. O. Friedrichs, On the derivation of the shallow-water theory, Appendix to Stoker paper [8].

[12] G. H. Keulegan, Engineering hydraulics, Chapter XI on wave motion (John Wiley & Sons, New York, N. Y. 1950).

Washington, May 28, 1952.

UNIVERSITY OF MICHIGAN LIBRARIES

Journal of Research of the National Bureau of Standards Vol. 49, No. 3, September 1952 Research Paper 2357

Ultraviolet Radiant Energy From the Sun Observed At 11,190 Feet

Ralph Stair

This paper gives the results of some measurements on the ultraviolet and short wavelength visible spectral energy distribution of direct solar radiation, made in September 1951, at Climax, Colo., altitude 11,190 feet. Data are given for wavelengths extending from 535 to 299.5 millimicrons for a number of air masses from 0 to 3.0). A determination of atmospheric transmittance as a function of wavelength results in calculated amounts of ozone approximating 0.21 centimeter (*ntp*) for several days during September. This value is in good agreement with previous determinations by other methods, for the season of the year and the geographical latitude of Climax.

1. Introduction

A preliminary determination of the distribution of radiant energy in the ultraviolet solar spectrum made at Washington, D. C., in 1950 was previously reported [1, 2].[1] This work, having shown great promise for the instruments and method employed, induced the attempt to make similar measurements at a high-altitude station. An invitation from Donald H. Menzel to make use of one of the Harvard high-altitude stations for this work was opportune. After a survey of the expected weather conditions and the available accommodations at possible high-altitude locations, the Climax, Colo. station was chosen for the month of September 1951.

Climax, Colo. is located on the continental divide in the heart of the Rocky Mountains about 100 miles southwest of Denver. A location at the new observatory station on Chalk Mountain, about 2½ miles west of Climax, was assigned for the work. At this point the altitude is approximately 11,190 ft, so that about 35 percent, by pressure, of the atmosphere is below the observer. The longitude and latitude of the station are approximately 106° 12′30″ W and 39°23′45″ N, respectively. Climax was originally chosen by the scientific personnel of Harvard University and the University of Colorado for use as a high-altitude observatory for the study of solar radiation because of its exceptional climatic conditions.

At the temperatures prevailing within the solar body, the atoms are multiply ionized. Only in the outer layers of the solar atmosphere, where lower temperatures prevail, do neutral and singly ionized atoms occur and also small quantities of a few diatomic molecules (for example, NH, OH, CN, etc.). Solar-absorption—Fraunhofer lines—results, therefore, primarily from absorption by hydrogen and by neutral and singly ionized atoms of iron, calcium, aluminum, titanium, chromium, magnesium, and other elements in the solar atmosphere.

According to current concepts of nuclear physics [3], the solar energy is produced through the transformation of hydrogen into helium within the highly heated central nucleus of the sun. The resulting gamma rays are absorbed by the overlying gas layers, which gradually transmit the generated energy to the solar surface. In general, it probably requires thousands of years by this process for a specific bundle of energy to reach the radiating layer, during which time its wavelength distribution has been reduced to that approximating a black body near 6,000° K. At times flares are ejected at terrific velocities from lower solar levels of very high temperature resulting not only in marked changes in the radiating surface but in increased emission by the flares themselves. According to Dodson [18], the emission in these flares is primarily due to atomic hydrogen. In the course of continuous observations during a time of excessive solar activity as many as 83 flares, for which the H_α intensity was estimated to be at least four times the solar background, have been observed within a period of 105 hr [19].

The amount and the spectral quality of the solar radiant energy reaching the earth's surface is also affected by absorption of energy by certain vapors, gases, or dust within the terrestrial atmosphere. One of these, ozone, was suspected [4], at an early stage in astrophysics, because of the fact that the spectra of all the stars, including the sun, terminated at about 300 mμ.

The total solar radiant energy varies slightly from time to time. Furthermore, it can be shown from Planck's law that the variations are more pronounced in the ultraviolet spectrum. But another factor enters the picture; namely, with greater short-wavelength intensity more ozone will be produced in the upper atmosphere. This results in a lower atmospheric transmittance within the spectral region of 300 to 330 mμ. Hence, although more ultraviolet may be emitted, the amount passing through our atmosphere may change but little or actually be less than normal.

2. Instruments and Procedure

The observations on the spectral distribution of the radiant energy from the sun at Climax, Colo., were made with the same Farrand double quartz-

[1] Figures in brackets indicate the literature references at the end of this paper.

UNIVERSITY OF MICHIGAN LIBRARIES

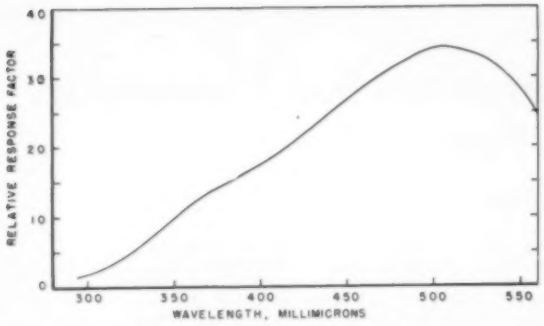

FIGURE 1. *Relative spectral-response factors for the complete spectroradiometer as employed in the Climax measurements.*

935 phototube, slit setting=0.09 mm.

prism spectrometer and auxiliary equipment (consisting of the RCA type 935 phototube, 510-cycle light modulator, tuned amplifier, Ballantine a-c vacuum-tube voltmeter, and Leeds & Northrup type A Speedomax recorder) as previously employed at Washington [1, 2], except that a new type of siderostat (designed to follow the sun) developed by the Optical Division of the Naval Research Laboratory was employed to reflect the sunlight into the spectroradiometer.

The entire equipment, except for the siderostat, was set up in a quonset hut with the entrance slit of the spectrometer toward the south. Through a small opening in one of the windows of the building a beam of sunlight was reflected through the entrance slit of the spectrometer onto the center of the first lithium-fluoride-quartz collimating lens of the instrument.

The siderostat was of simple design, arranged so that a primary (plane aluminized) mirror reflected the beam of light along the polar axis of the instrument. A second stationary mirror reflected the beam horizontally into the spectrometer. Thus each of the mirrors operated at fixed angles relative to the light beam during the day. A synchronous motor-drive provided for the automatic following of the sun during the course of each day's observations.

To assist in the proper alinement of the siderostat and spectrometer and to reduce the amount of sky radiation entering the spectroradiometer to a very low value, diaphragms equivalent to about 2- by 4-in. openings were placed at approximately 2 ft and 5 ft from the entrance slit of the spectrometer. These, together with the relatively extensive distance (about 8 ft) between the primary siderostat mirror (approximately 2 by 4 in.) and the spectroradiometer aided in keeping the solar beam on the optical axis of the instrument.

In accordance with the procedure in the previous work [1], no lens or mirror was employed to produce an image of the sun on the entrance slit of the spectrometer because an integrated solar energy spectrum was desired. Although the spectroradiometer was not used most efficiently, according to general optical principles, because only a small part of the total available aperture was employed, it was expedient to operate it in this manner to eliminate variations in light transmittance through partial cut-off at the edges of some of the optical parts.

The accurate adjustment and calibration of the wavelength scale of the instrument was accomplished through the use of a mercury-arc discharge lamp. After being unpacked and installed, each section of the spectrometer was individually adjusted for highest energy transmittance, and the combination was locked-in for best adjustment at the 313.2 and 405-mμ emission lines. Wavelength settings of the instrument were recorded for each of the intense mercury emission lines between 313.2 and 578 mμ for application to the recorded data on the sun and on a tungsten-filament-in-quartz lamp, which was employed in the radiant energy evaluations. The Fraunhofer lines lend themselves ideally for use as wavelength standards in the measurement of solar spectral radiant energy. However, no such indices are present in the spectrum of the tungsten-filament-in-quartz lamp, so that a precise wavelength calibration, together with a system of chart index marking was highly advantageous. For this purpose, an index pen on the upper part of the recorder chart provided an automatic method of wavelength identification on the chart records. Index marks at regular intervals defined specific wavelengths, so that the three sets of data, that for the mercury arc, the tungsten-filament-in-quartz lamp, and that for the sun, were readily compared for wavelength and relative spectral intensity.

The tungsten-filament-in-quartz lamp, manufactured by the Westinghouse Electric Corporation and described in detail elsewhere [2, 7] was employed in the spectral radiant energy calibration of the entire spectroradiometer, including all the optical and electronic parts from the first siderostat mirror to the recorder. The lamp served both as a standard for relative spectral intensity and for absolute intensity, in microwatts per square centimeter per unit wavelength. This lamp was standardized in terms of color temperature [8], and its spectral radiant energy was evaluated through the application of published spectral emissivity data on tungsten [9 to 12]. The true temperature of 2,805° K, characteristic of the radiation from the lamp, determined on the basis of the observed color temperature and the emissivity values of tungsten, establishes the spectral radiant energy distribution for the lamp.

The reduction of the data on the spectral distribution of the ultraviolet radiant energy from the sun was accomplished in a manner similar to that previously reported [1, 2]. Most of the essential data employed in this evaluation are given in table 1, illustrating the various steps involved in obtaining the instrumental spectral response factors (see fig. 1).

In the present work the entrance and middle slits of the spectrometer were set at about 0.09 mm—a value that gave a resolution of about 1 mμ at 300 mμ (to 2 to 3 mμ at longer wavelengths). The final

TABLE 1. *Relative spectral-energy data on standard tungsten-filament-in-quartz lamp and its application in the calibration of the spectral-response factor of the spectroradiometer*

Wave length	Relative energy black body $T=2805°K$ $C_2=14,380$	Emissivity of tungsten	Relative spectral energy from lamp	Absolute energy from lamp in $(\mu w/cm^2)/m\mu$ at 1 meter	Recorder response reduced to amplifier sensitivity 1	Instrumental spectral response factors (col. 6÷5)
1	2	3	4	5	6	7
$m\mu$						
300	66.2	0.422	27.9	0.048	0.00087	0.0181
310	97.4	.427	41.6	.072	.00215	.0299
320	139	.433	60.2	.104	.0043	.0413
330	195	.438	85.4	.148	.0087	.0588
340	264	.443	117.0	.202	.0155	.0767
350	351	.447	156.9	.271	.0268	.0989
360	459	.448	205.6	.356	.0429	.1205
370	588	.450	264.6	.457	.0613	.1341
380	741	.451	334.2	.577	.0849	.1471
390	920	.452	415.8	.719	.1150	.1599
400	1126	.452	509.0	.880	.153	.1739
410	1361	.453	616.5	1.066	.203	.1904
420	1624	.452	734.0	1.269	.264	.2080
430	1917	.451	864.6	1.495	.343	.2294
440	2241	.449	1006.2	1.740	.435	.2500
450	2595	.448	1162.6	2.010	.543	.2701
460	2978	.447	1331	2.302	.663	.2880
470	3381	.445	1505	2.603	.791	.3039
480	3830	.444	1701	2.942	.937	.3185
490	4296	.442	1899	3.283	1.083	.3299
500	4787	.441	2111	3.651	1.233	.3377
510	5301	.441	2338	4.043	1.380	.3413
520	5837	.440	2568	4.440	1.495	.3367
530	6392	.440	2812	4.863	1.584	.3257
540	6964	.439	3057	5.286	1.626	.3076

slit was then set at the minimum value such that most of the radiant energy passing through the first two slits reached the phototube at all wavelength settings between 300 and 600 mμ.

For operation of the equipment, commercial 110-v., 60-cycle alternating current was available. Frequency control was assured through interpower connections, but voltage fluctuations were very large, probably partly because of heavy and irregular power consumption at the nearby plant of the Climax Molybdenum Co. The voltage changes, however, usually remained within the control limits of a 1,000-va voltage regulator that had been incorporated into the equipment. It was only during a single temporary power failure that measurements were interrupted because of power difficulties.

Measurements of the spectral radiant energy from the sun were made at Climax over a period of about 3 weeks during September 1951. On each day, except when clouds interfered, data were taken between about 7.30 a. m. and 4.30 p. m. Trees and mountains prevented observations at earlier or later hours. These limitations, together with the season of the year, confined the measurements to solar angles (zenith distances) corresponding to air masses between about 1.25 and 3.00.[2] Snow and the accompanying cloudiness interrupted the work on several days. During the 3 weeks (September 6 to 27) there were three snowfalls, totaling approximately 7 in. These not only rendered the air more free of haze and smoke but kept down much dust occasioned by temporary public and private road construction and by heavy traffic over nearby unpaved roads.

Usually the data were recorded in the general order illustrated in figure 2, except that each curve was

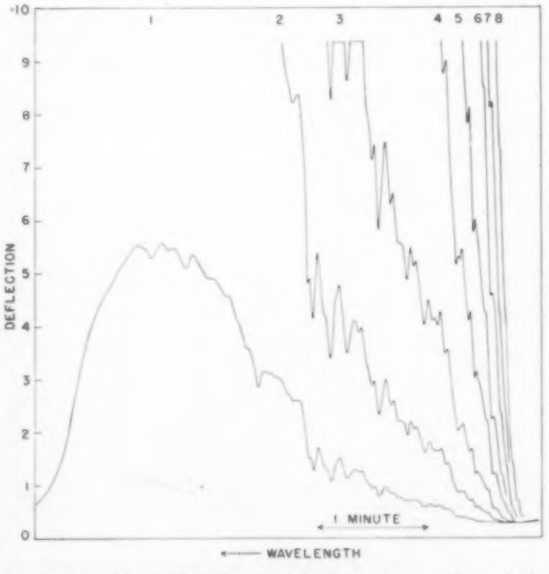

FIGURE 2. *Representative data taken from a section of the recorder chart.*

September 26, 1951, approximately 10:30 a. m., air mass 1.40.

[2] "Air mass" as employed here refers to the amount of atmosphere traversed by the solar rays. It is numerically equal to the secant of the zenith angle of the sun.

UNIVERSITY OF MICHIGAN LIBRARIES

repeated before passing on to the next amplifier setting. Ordinarily the amplifier was first set at a high sensitivity (sensitivity 8) so that only the spectral intensities for the shorter wavelengths appeared on the chart. Successively lower amplifier sensitivity settings (7 to 1) were made so that different parts of the solar spectrum appeared on the upper portion of the chart, the previously recorded values being compressed on the lower part of the record. Usually the small interval of time (about 1 to 2 min.) between records reflected the change in solar intensity resulting from the small change in the sun's zenith distance, or in the air mass. An appreciable range of the solar ultraviolet spectrum was thus automatically plotted within a very short interval of time. This rapid scanning speed, made possible by the high sensitivity of the detecting and amplifying equipment, was many times faster than that obtainable through the photographic or the point-by-point radiometric methods previously employed by other observers [4, 21, 25].

Except for a few days during the early part of the work, the temperature within the building surrounding the spectroradiometer and recording equipment was maintained at 70° F (plus or minus a few degrees). Ordinarily the electronic equipment was placed in operation about 30 min or more before data were recorded and was left in continuous operation until measurements were concluded for the day. As a further check on the sensitivity of the electronic equipment throughout each day, numerous checks were made through the use of a secondary standard lamp that could be momentarily placed in front of the spectrometer entrance slit.

Since in a lens-prism spectrometer there are a number of reflecting surfaces (on the lenses and prism faces) where the transmitted beam is incident at angles differing from the normal, a certain amount of polarization of the transmitted energy necessarily occurs. Furthermore, since there are two mirror reflections of the light beam by the siderostat before it enters the spectroradiometer, there is a varying amount and direction of polarization in the incident beam. As a result of the combined polarizations, the amount of radiant energy reaching the phototube varies as some function of the relative angles of the optical elements of the system. In the case of all the optical components, except the primary siderostat mirror, there was little change in the angle orientations during the measurements at Climax. A study was made therefore to determine the amount by which the transmitted radiant energy was affected by the combined polarization effects of the siderostat and spectroradiometer as functions of both the wavelength and the primary mirror angle. The results of this investigation indicated that for wavelengths shorter than about 550mμ the polarization effects were independent of wavelength of incident radiation within 1 percent. An over-all change approximating 10 percent in the transmitted energy occurred between an angular setting of 30° and 150°, that is between positions of the sun corresponding to air mass 2.0 in the morning and air mass 2.0 in the afternoon. These data are summarized by the curve in figure 3.

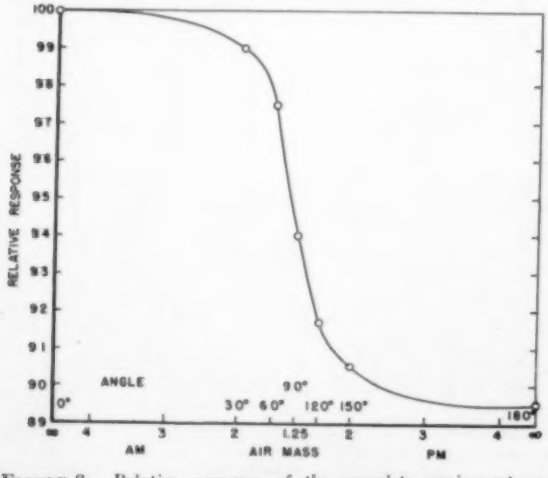

FIGURE 3. *Relative response of the complete equipment as affected by light polarization by the siderostat and the spectrometer.*

Polarization factor versus air mass.

3. Spectral Solar Energy Curve

The observations of the solar spectral energy distribution requires measurements on a source that is rapidly changing in intensity and spectral quality. The small (sometimes large) fluctuations resulting from variations in the transmission characteristics of the terrestrial atmosphere are largely eliminated through making the measurements at a high-altitude station above most of the dust and smoke commonly present in the lower terrestrial atmosphere.

Data on the spectral solar radiant energy are given in table 2 for a single solar zenith angle corresponding to air mass (secant Z)=1.40 for four of the days during which extensive series of measurements were made. Mean values for a number of selected air masses are given in table 3. Data on other days during the investigation, and not included in these tables, differ but little from those employed in the preparation of the tables. Data for selected air masses fall approximately on a straight line (see fig. 4) when plotted in terms of the logarithm of the deflection (intensity) as a function of air mass. Extrapolating these lines to air mass 0 gives the logarithms of numbers representing the spectral solar intensity outside the earth's atmosphere. From determinations at about 25 separate wavelengths between 300 and 540 mμ for each of the 4 days (approximately 100 determinations) the M_0 factor in column 7 of table 2 was determined from a smooth curve passing through a plot of the wavelength against the multiplying factors required to give the values of the intercepts at air mass 0. Most of the data for one day (September 26) employed in this evaluation are shown in figure 4. The slopes of these lines define the atmospheric transmission coefficients discussed in greater detail below.

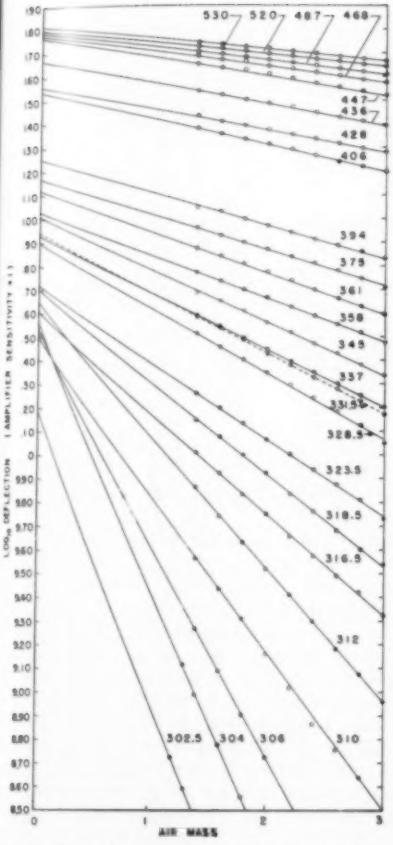

FIGURE 4. *Determination of the solar intensity outside the atmosphere through graphing the logarithm of the observed data as a function of the solar angle (air mass).*
Climax, Colo., September 26, 1951.

TABLE 2. *Spectral distribution of radiant energy from the sun, Climax, Colo., September 1951*

Altitude of station, 11,190 ft. Air mass 1.40 and outside the atmosphere, air mass 0.
Energy in microwatts per square centimeter per 10 $m\mu$.

1	2	3	4	5	6	7	8
Wavelength	Sept. 16. Air mass 1.40	Sept. 17. Air mass 1.40	Sept. 19. Air mass 1.40	Sept. 26. Air mass 1.40	Mean. Air mass 1.40	M_0 factor	I_0 Air mass 0
$m\mu$							
299.5	7.1	6.1	6.3	7.2	6.7	100	670
302.5	9.3	14.0	14.7	15.0	13.3	55.7	741
304	46.9	40.9	43.0	41.7	43.1	28.9	1246
306	72.3	65.2	71.1	73.1	70.4	16.7	1176
309.2	128.3	120.1	124.5	130.4	125.8	10.2	1283
310	124.7	114.6	120.0	126.7	121.5	8.60	1045
312	223	208	215	222	217.0	6.38	1384
314.9	267	255	261	269	263.0	5.05	1328
315.8	280	267	275	283	276	4.64	1282
316.5	269	247	256	266	260	4.30	1116
317.9	378	350	360	375	366	3.87	1415
318.5	353	325	338	350	342	3.85	1315
321.1	435	408	413	429	421	3.48	1466
321.7	418	389	396	410	404	3.40	1372
322.8	404	380	384	397	391	3.25	1272
323.5	388	360	366	377	373	3.15	1174
325.5	469	422	451	461	451	2.97	1339
327.5	622	567	581	592	591	2.78	1642
328.5	589	542	553	565	562	2.69	1512
330.3	682	645	659	667	663	2.57	1705
331.5	610	578	587	602	594	2.50	1486
332.9	614	575	591	606	597	2.45	1461
333.6	603	566	580	592	585	2.42	1416
335.3	619	593	596	609	604	2.36	1426
337	542	510	526	526	526	2.30	1210
340.8	652	615	638	634	635	2.33	1415
341.7	626	589	614	605	609	2.21	1345
343.5	642	604	628	621	624	2.18	1360
345	540	505	527	523	524	2.15	1126
348.6	586	550	569	613	580	2.09	1211
351.5	636	601	619	606	616	2.04	1256
352.6	593	565	584	574	579	2.02	1170
355.1	684	646	669	648	662	1.97	1304
358	500	470	486	484	485	1.92	931
360	620	594	625	625	616	1.89	1164
361	604	567	581	595	587	1.87	1097
363.8	676	626	638	660	650	1.84	1196
367.1	806	772	799	818	799	1.80	1438
368.6	773	744	773	770	765	1.79	1369
371	803	774	801	795	793	1.76	1396
375	649	623	645	645	641	1.72	1101
379.4	870	846	873	871	865	1.69	1462
380.7	815	799	828	820	816	1.68	1370
385	575	554	573	574	569	1.66	945
387.7	710	694	710	706	705	1.64	1156
391.5	891	874	894	898	889	1.62	1441
394	665	633	659	657	654	1.60	1046
396.1	778	740	768	776	766	1.58	1209
397.0	759	716	748	757	745	1.57	1170
403.3	1355	1254	1294	1276	1295	1.52	1968
406	1301	1202	1244	1240	1247	1.50	1870
410	1333	1228	1290	1310	1290	1.47	1897
416.8	1410	1331	1362	1355	1365	1.43	1951
421	1396	1315	1348	1343	1351	1.40	1891
424	1362	1297	1320	1325	1326	1.38	1830
428	1197	1137	1156	1159	1162	1.35	1569
432	1363	1306	1322	1348	1335	1.34	1789
436	1408	1346	1361	1374	1372	1.33	1825
441	1552	1513	1505	1540	1528	1.31	2001
447	1647	1591	1594	1617	1613	1.29	2080
455.7	1672	1630	1630	1641	1643	1.28	2103
468	1561	1518	1522	1535	1534	1.26	1933
482	1612	1571	1569	1577	1582	1.25	1978
487	1501	1473	1463	1473	1478	1.24	1832
497	1566	1547	1532	1547	1548	1.23	1904
500	1549	1527	1516	1533	1531	1.22	1868
509	1578	1558	1545	1555	1559	1.21	1886
520	1518	1491	1481	1491	1495	1.20	1794
526	1612	1573	1569	1579	1583	1.195	1892
530	1643	1621	1598	1618	1620	1.19	1928
535	1583	1566	1541	1591	1570	1.185	1861

UNIVERSITY OF MICHIGAN LIBRARIES

TABLE 3. *Spectral distribution of radiant energy from the sun for selected air masses, Climax, Colo*

Altitude 11,190 ft. Mean for 4 days in September 1951. Radiant energy in microwatts per square centimeter per 10 mμ.

1	2	3	4	5	1	2	3	4	5
Wavelength	Air mass 0	Air mass 1	Air mass 2	Air mass 3	Wavelength	Air mass 0	Air mass 1	Air mass 2	Air mass 3
mμ					mμ				
299.5	670	25.1	0.9	0.0	367.1	1438	946	622	409
302.5	741	41.9	2.4	.1	368.6	1369	904	597	395
304	1246	112.7	10.2	.9	371	1396	933	623	416
306	1176	157.4	21.1	2.8					
309.2	1283	245	46.9	8.9	375	1102	749	509	346
					379.4	1462	1005	692	476
310	1045	225	48.7	10.5	380.7	1370	947	655	453
312	1384	370	98.7	26.4	385	945	658	459	320
314.9	1328	419	132.1	41.7	387.7	1156	813	571	401
315.8	1282	429	142.5	48.1					
316.5	1116	395	138.8	49.6	391.5	1441	1021	724	513
					394	1046	748	535	383
317.9	1415	540	206	78.6	396.1	1209	873	631	456
318.5	1315	504	193	73.4	397.0	1170	848	615	446
321.1	1466	621	263	111.3	403.3	1968	1461	1084	804
321.7	1372	574	240	100.5					
322.8	1272	549	224	91.2	406	1870	1401	1050	786
					410	1897	1441	1095	832
323.5	1174	519	229	101.2	416.8	1951	1513	1173	909
325.5	1339	617	284	130.7	421	1891	1488	1171	921
327.5	1642	793	383	185	424	1830	1454	1156	919
328.5	1512	747	369	182					
330.3	1705	870	444	226	428	1569	1267	1023	826
					432	1789	1452	1179	957
331.5	1486	773	402	209	436	1825	1489	1215	992
332.9	1461	772	408	216	441	2001	1651	1362	1124
333.6	1416	754	402	214	447	2080	1735	1447	1209
335.3	1426	773	419	227					
337	1210	668	369	204	455.7	2103	1764	1479	1241
					468	1933	1639	1390	1178
340.8	1415	799	451	255	482	1978	1677	1441	1226
341.7	1345	765	435	247	487	1832	1591	1349	1157
343.5	1360	780	448	257	497	1904	1643	1417	1223
345	1126	653	379	220					
348.6	1211	717	423	251	500	1868	1621	1406	1219
					509	1886	1647	1438	1255
351.5	1256	754	453	272	520	1794	1575	1384	1215
352.6	1170	709	429	260	526	1892	1666	1467	1292
355.1	1304	804	496	306	530	1928	1703	1505	1329
358	931	585	366	231					
360	1164	740	470	298	535	1861	1648	1461	1294
361	1097	703	450	288					
363.8	1196	774	502	325					

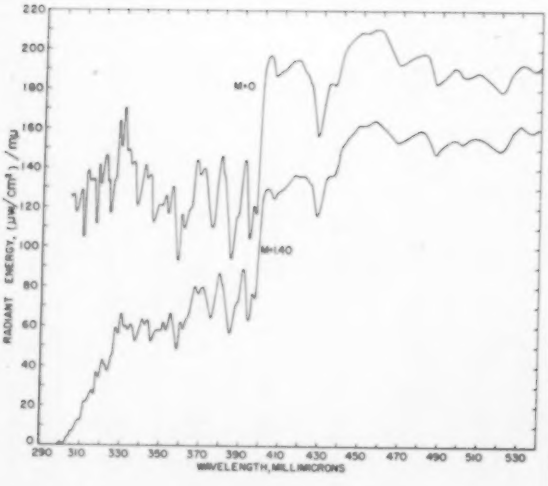

FIGURE 5. *Spectral distribution of the radiant energy from the sun.*

Climax, Colo., September 1951. (Mean of 4 days.)

Some of the data from table 2 (mean for air mass 1.40 and 0 are shown in figure 5. In order to simplify the illustration of these data, the wavelengths in table 2 for air mass 1.40, were chosen so that they included maxima and minima as well as the points of inflection on the solar energy curve. The data (tables 2 and 3) are nominally tabulated in microwatts per square centimeter per 10 mμ. They might better be represented in terms of 1-, 2-, or 3-mμ intervals because the effective slit widths were within this range.

The solar-energy curves shown contain numerous absorption bands varying in magnitude both in spectral width and in intensity of absorption. If reference is made to the Rowland maps and wavelength data [5, 22] and to the Utrecht photometric atlas of the solar spectrum [6], it is found that each band results from one or more groups of intense Fraunhofer lines. In table 4, which lists the approximate wavelengths of the principal absorption bands as recorded in the present investigation, are also listed the principal elements and diatomic molecules responsible for the observed absorption. The wavelength positions of these absorption bands are in close agreement with those of the main concentrations of the winged lines [15] in the solar spectrum.

TABLE 4. *[illegible]sation of principal Fraunhofer absorption regions of the ultraviolet and short-wavelength visible portion of the solar spectrum, and (from the Rowland and Utrecht maps) the elements in the solar atmosphere primarily responsible for the various bands.*

Very strong lines result from absorption by the elements marked in boldface type.

Wavelength	Principal absorbing elements
mμ	
310	Fe I, Ni I, Mn I, Al I, OH.
316.5	Fe I, Fe II, Cr II, Ni I, Ti II, OH.
318.5	Ca II, Fe I, Ti I, V II.
323.5	Fe I, Fe II, Ti II, Ni I.
328.5	Fe I, Fe II, Ti I, Ti II, Co I.
331.5	Fe I, Fe II, Zr II, Na I, Ti II, Ni I, Mg I, Co I.
337	NH, Ti II, Ni I, Cr II, Co I.
345	Fe I, Mn II, Ti II, Ni I, Co I.
358	**Fe I,** Ni I, V II, Sc II, Co I, Ti II, Cr II.
375	**Fe I,** Ni I, Ti I, Ti II.
385	**Fe I,** Mg I, **CN**.
394	**Ca II,** Al I, Hε.
397	**Ca II.**
406	Hδ.
428	Fe I.
436	Hγ.
447	Fe I, Ti I, Ti II, Ca I, Mn I.
468	Mn I, Fe I, Ti II, Ni I.
487	Hβ, Fe I.
500	Fe I, Fe II, Ti I.
520	Mg I.
535	Fe I, Fe II, Ca I, Cr I.

Iron appears to be the principal ultraviolet absorbing material in the solar atmosphere. In spectral regions where some of the other important absorbing materials have superimposed Fraunhofer lines—in particular, the region between about 340 and 397 mμ, where Ca II, NH, CN, and possibly the Balmer continuum of hydrogen, show strong absorption—there results a spectral region departing significantly from the normal black-body curve. There appears to be little absorption due to Fraunhofer lines and bands near 330 mμ, and at shorter wavelengths much less than in the 336- to 394-mμ region, because the envelope of the part of the solar spectrum at wavelengths shorter than 330 mμ is much closer to that of the expected 6,000° K black-body curve.

4. Atmospheric Transmittance and Ozone

The atmospheric transmission curve, depicted in figure 6 represents the average data for the 4 days (September 16, 17, 19, and 26) covered by tables 2 and 3. In this illustration the logarithm of the observed transmittances of unit atmosphere (at Climax) for the different wavelengths are plotted as a function of the wavelength, which in turn is expanded [21] according to the function $-(\mu-1)^2\lambda^{-4}$ of the Rayleigh law of molecular scattering, $\log T_R = -32\pi^3 (3N)^{-1}(\mu-1)^2\lambda^{-4} H \log e$. Since for the zenith position the atmospheric depth, H, and the molecular density, N, are constant, the resulting plot of the logarithm of the atmospheric transmittances becomes a straight line in those spectral regions wherein the Rayleigh law of pure molecular scattering is applicable. In the present case, any scattering, other than molecular was small and simply has been combined with the molecular scattering in giving a straight line of possibly slightly lesser ordinates. At wavelengths shorter than about 340mμ ozone absorption enters the picture. This results in transmission data that drop below the straight line representative of scattering alone. The difference in ordinates for any wavelength in this region between the straight line and the observed data is a measure of the ozone absorption for that particular wave length.

In order to translate optical absorption data in the ultraviolet spectral region into specific amounts of ozone, absorption coefficients of the pure gas are required. In the present case, data given by Fabry and Buisson [16] were employed in the calculations of the two curves (fig. 6) representing amounts of ozone required for a similar amount of optical absorption. On the basis of these data, about 0.21 cm of ozone (*ntp*) was present at the time this solar investigation was in progress (September 1951). This value is in close agreement with the average for the same season of the year as obtained for a similar latitude, Washington, D. C. [17].

The multiplicity of Fraunhofer absorption bands (as observed with a prism instrument) in the ultraviolet solar spectrum suggests the need of great care in using a double-prism instrument such as an ozone meter, unless a reasonable region of the spectrum is scanned to assure that intensity settings are being made on specific wavelengths. A very small change, or error, in wavelength calibration may result in the shift of the spectrum setting from a Fraunhofer minimum to a maximum, or vice versa, between two absorption regions. On the other hand, a scanned spectrum, such as that obtained in the present work, offers an ideal method for evaluating ozone, because a definite pair of wavelengths may be chosen with a definite assurance that no error in wavelength setting can be made.

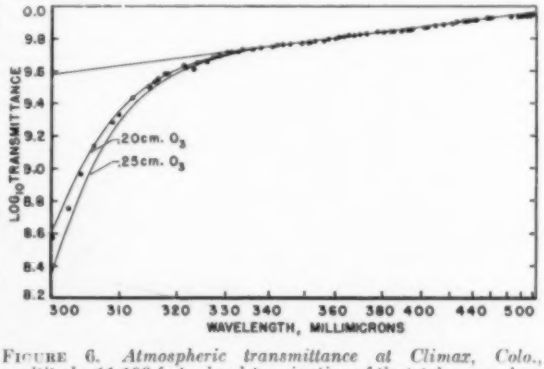

FIGURE 6. *Atmospheric transmittance at Climax, Colo., altitude, 11,190 feet; also determination of the total ozone above the observing station.*

Upper curve, scattering; lower curves, ozone; ●, atmospheric transmission; air mass 1.0, Climax, Colo.; wavelength scale as function of $-(\mu-1)^2\lambda^{-4}$.

UNIVERSITY OF MICHIGAN LIBRARIES

5. Summary and Conclusions

This work, although performed under the expected difficulties of transporting about 1,200 lb of delicate electronic and optical equipment to a more or less isolated mountain station and setting it up and operating it in a temporary building, demonstrates the relative ease with which the ultraviolet spectral distribution of the radiant energy from the sun may be measured with this equipment. From the data obtained, the spectral distribution of the ultraviolet (also part of the visible) radiant energy from the sun has been determined for various air masses at the earth's surface (altitude 11,190 ft) and for outside the earth's atmosphere. From the changes in spectral intensity as a function of air mass (solar angle) the atmospheric transmission coefficients and the total atmospheric ozone content have been determined. These determinations are in good agreement with the best published values. The spectral-energy distribution curve shows much greater Fraunhofer structure than previously reported data for prism instruments. The rapidity of recording assures a complete spectrum before marked changes can occur in intensity as the result of air-mass change.

The relative ease with which the ultraviolet spectral distribution of the radiant energy from the sun may be measured suggests the use of this type of instrument and method for routine use in weather and ozone studies and in the determination of the radiant-energy spectra of some of the brighter stars [23]. Photoelectric equipment of this type is at least a thousand times as sensitive as the best radiometric apparatus presently available. As limited amounts of spectral data have been obtained radiometrically for some of the brighter stars, there appears to be no question regarding the feasibility of using a photoelectric spectroradiometer in conjunction with a large telescope on some of the stars or possibly brighter nebulas.

The author expresses his deep appreciation and gratitude to Walter O. Roberts and other members of the High Altitude Observatory staff for placing the facilities of the Climax station at our disposal and otherwise rendering assistance to us while there; to Norton Baron for helpful assistance in the operation of the equipment in the field; to Russell Johnston for carrying out many of the tedious calculations involved; and to the personnel of the Optics Division of the Naval Research Laboratory for their intense interest and other cooperation in the investigation.

6. References

[1] Ralph Stair, Ultraviolet spectral distribution of radiant energy from the sun, J. Research NBS **46**, 353 (1951) RP2206.

[2] Ralph Stair, Photoelectric spectroradiometry and its application to the measurement of fluorescent lamps, J. Research NBS **46**, 437 (1951) RP2212.

[3] H. A. Bethe, Energy production in stars, Phys. Rev. **55**, 434 (1939).

[4] Ch. Fabry and H. Buisson, L'absorption de l'ultra-violet par l'ozone et la limite du spectre solaire, J. Phys. radium (5) **3**, 196 (1913).

A. Fowler and R. J. Strutt, Absorption bands of atmospheric ozone in the spectra of sun and stars, Proc. Roy. Soc. (London) [A] **93**, 577 (1917).

Ch. Fabry and H. Buisson, Étude de l'extrémité ultraviolette solaire, J. Phys. radium (6) **2**, 197 (1921).

Charles Fabry and H. Buisson, A study of the ultraviolet end of the solar spectrum, Astrophys. J. **54**, 20 (1921).

H. Buisson and Ch. Fabry, Mesures de longueurs d'onde dans l'extrémité ultra-violette du spectre solaire, J. Phys. radium (6) **2**, 297 (1921).

[5] Rowland's map of the solar spectrum. For Rowland's wavelengths, see Astrophys. J. **1, 2, 3, 4, 5** (1895-97). For revised wavelengths, see Revision of preliminary table of solar spectrum wavelengths, etc., by Charles E. St. John, et al., Carnegie publication No. 396 (1928).

[6] M. Minnaert, G. F. W. Mulders, and J. Houtgast, The Utrecht photometric atlas of the solar spectrum (J. Schnabel, Amsterdam 1940).

[7] R. Stair and W. O. Smith, A tungsten-in-quartz lamp and its applications in photoelectric radiometry, J. Research NBS **30**, 449 (1943) RP1543.

[8] Deane B. Judd, The 1949 scale of color temperature, J. Research NBS **44**, 1 (1950) RP2053.

[9] W. E. Forsythe and A. G. Worthing, The properties of tungsten and the characteristics of tungsten lamps, Astrophys. J. **61**, 146 (1925).

[10] F. Hoffman and H. Willenberg, Das Emissionsvermögen des Wolframs in ultraviolett bei hohen Temperature, Physik. Z. **35**, 1, 711 (1934).

[11] H. C. Hamaker, Reflectivity and emissivity of tungsten, Inaug. Diss. (Utrecht, Holland, 1934).

[12] L. S. Ornstein, Tables of the emissivity of tungsten as a function of wavelength from 0.23 to 2.0 μ in the region of temperature 1600° to 3000° K, Physica **3**, 561 (1936).

[13] H. T. Wensel, D. B. Judd, and W. F. Roeser, Establishment of a scale of color temperature, BS J. Research **12**, 527 (1934) RP677.

[14] Deane B. Judd, The 1931 I. C. I. standard observer and coordinate system for colorimetry, J. Opt. Soc. Am. **23**, 360 (1933).

[15] Charlotte E. Moore and Henry Norris Russell, On the winged lines in the solar spectrum, Astrophys. J. **63**, (1926).

[16] C. Fabry and H. Buisson, Data on ozone absorption, Compt. rend. **192**, 457 (1931).

[17] Ralph Stair, Seasonal variation of ozone at Washington, D. C., J. Research NBS **43**, 209 (1949) RP2022.

[18] Helen W. Dodson, Solar flares, Astrophys. J. **110**, 382 (1949).

[19] Helen W. Dodson and E. Ruth Hedeman, The frequency and positions of flares within three active sunspot areas, Astrophys. J. **110**, 242 (1949).

[20] Helen W. Dodson and Robert W. Donselman, The eruptive prominence of August 7, 1950, Astrophys. J. **113**, 519 (1925).

[21] Edison Pettit, Spectral energy-curve of the sun in the ultraviolet, Astrophys. J. **91**, 159 (1940).

[22] Harold D. Babcock, Charlotte E. Moore, and Mary F. Coffeen, The ultraviolet solar spectrum, 2935–3060A, Astrophys. J. **107**, 287 (1948).

[23] C. G. Abbot and L. B. Aldrich, Energy spectra of some of the brighter stars, Smithsonian Misc. Collections **107**, No. 19 (Pub. No. 3914, 1948).

[24] Joel Stebbins and A. E. Whitford, Six-color photometry of stars. The colors of extragalactic nebulae, Astrophys. J. **108**, 413 (1948).

[25] F. W. Paul Götz and Ernst Schönmann, Die spektrale Energieverteilung von Himmels-und Sonnenstrahlung, Helv. Phys. Acta **21**, 151 (1948).

[26] Heinz Reiner, Die Struktur des Sonnen Spectrums Zwischen 400 und 600 mμ, Garlands Beitr. Geophys., **55**, Heft 2, 234 (1939).

WASHINGTON, May 5, 1952.